



# Introduction to Karst Aquifers

Eve L. Kuniansky, Charles J. Taylor,  
John H. Williams, Frederick Paillet

# *Introduction to Karst Aquifers*

*The Groundwater Project*

***Eve L. Kuniansky***

*Emeritus Scientist  
United States Geological Survey  
Norcross, Georgia, USA*

***Charles J. Taylor***

*Head, Water Resources Section  
Kentucky Geological Survey  
University of Kentucky  
Lexington, Kentucky, USA*

***John H. Williams***

*Groundwater Specialist  
United States Geological Survey  
Troy, New York, USA*

***Frederick Paillet***

*Emeritus Scientist  
United States Geological Survey*

*Adjunct Professor of Geosciences  
University of Arkansas  
Fayetteville, Arkansas, USA*

# ***Introduction to Karst Aquifers***

*The Groundwater Project  
Guelph, Ontario, Canada  
Version 4, March 2023*

All rights reserved. This publication is protected by copyright. No part of this book may be reproduced in any form or by any means without permission in writing from the authors (to request permission contact: [permissions@gw-project.org](mailto:permissions@gw-project.org)). Commercial distribution and reproduction are strictly prohibited.

GW-Project (The Groundwater project) works are copyrighted and can be downloaded for free from [gw-project.org](http://gw-project.org). Anyone may use and share [gw-project.org](http://gw-project.org) links to download GW-Project's work. It is not permissible to make GW-Project documents available on other websites nor to send copies of the documents directly to others. Kindly honor this source of free knowledge that benefits you and all those who want to learn about groundwater.

Copyright © 2022 Eve L. Kuniansky, Charles J. Taylor, and Frederick Paillet (The Authors)

Published by the Groundwater Project, Guelph, Ontario, Canada, 2022.

Kuniansky, Eve L.

Introduction to Karst Aquifers/(Eve L. Kuniansky, Charles J. Taylor, John H. Williams, and Frederick Paillet) - Guelph, Ontario, Canada, 2022.

216 pages

ISBN: 978-1-77470-040-2

DOI: <https://doi.org/10.21083/978-1-77470-040-2>

Please consider signing up for the GW-Project mailing list to stay informed about new book releases, events, and ways to participate in the GW-Project. When you sign up for our email list it helps us build a global groundwater community. [Sign-up](#).

APA (7<sup>th</sup> ed.) Citation: Kuniansky, E. L., Taylor C. J., Williams J.H., & Paillet F. (2022). [Introduction to karst aquifers](#). The Groundwater Project. [doi.org/10.21083/978-1-77470-040-2](https://doi.org/10.21083/978-1-77470-040-2).



*Domain Editors:* John Cherry and Eileen Poeter

*Board:* John Cherry, Paul Hsieh, Ineke Kalwij, Stephen Moran, Everton de Oliveira and Eileen Poeter



*Steering Committee:* John Cherry, Allan Freeze, Paul Hsieh, Ineke Kalwij, Douglas Mackay, Stephen Moran, Everton de Oliveira, Beth Parker, Eileen Poeter, Ying Fan, Warren Wood, and Yan Zheng.

*Cover Images:* Images of karst features around the globe as follows:

*Top row, left to right:* Example of forest karst towers from Li River, China near Guilin (Eve Kuniansky, November, 2006), Waterslide Cave, Stephens Gap Callahan Cave Preserve, Southeastern Cave Conservancy, Jackson County, Alabama, Mississippian Age Pennington Formation (Alan Cressler, November 22, 2014), Putai Blowholes and Pancake Rocks, stylobedding, Dolomite Point, Paparoa National Park, Buller District, West Coast, New Zealand (Alan Cressler, January 3, 2013), Deer Cave, West Entrance Area, Gunung Mulu National Park, Borneo, Sarawak, Malaysia (Alan Cressler, November 25, 2009).

*Middle row, left to right:* Conduits formed along fractures and bedding planes in the middle portion of the Glen Rose Limestone as seen along the channel of Canyon Gorge, Texas- (Bob Morris, U.S. Geological Survey, May 18, 2017), Sinkhole lakes near Carlsbad, New Mexico (Eve Kuniansky, U.S. Geological Survey 2014), Upper Cueva Ventana, Ventana Entrance, Municipio de Arecibo, Puerto Rico, overlooking the Rio Grande de Arecibo valley (Alan Cressler, January 8, 2005), unnamed West Virginia spring (Eve Kuniansky, U.S. Geological Survey, August 22, 2002).

*Bottom row, left to right:* Blue Hole Spring vent, Ichetucknee Springs State Park, Suwannee County, Florida (Alan Cressler, November 21, 2011), Spring that flows out of base of cliff and forms a creek that flows into the Buffalo River, Arkansas (Patrick Tucci, retired U.S. Geological Survey, April 28, 2011), Ocala Limestone, Eocene Age, Ozello Archipelago, Gulf of Mexico, Citrus County, Florida (Alan Cressler, March 17, 2016).

All photographs used with permission. U.S. Geological Survey photographs taken while on duty are in the public domain. All photographs by Alan Cressler used with permission and under copyright by Alan Cressler.

# Table of Contents

<b>TABLE OF CONTENTS.....</b>	<b>V</b>
<b>THE GROUNDWATER PROJECT FOREWORD .....</b>	<b>IX</b>
<b>FOREWORD .....</b>	<b>X</b>
<b>PREFACE .....</b>	<b>XI</b>
<b>ACKNOWLEDGMENTS.....</b>	<b>XII</b>
<b>1 INTRODUCTION .....</b>	<b>1</b>
<b>2 KARST CONDUIT FLOW DEVELOPS BY GEOCHEMICAL AND FLOW PROCESSES .....</b>	<b>5</b>
2.1 FORMATION OF KARSTIC CONDUIT FLOW SYSTEMS.....	6
2.2 DEEP CHEMICALLY AGGRESSIVE WATER FORMS INTERCONNECTED CONDUITS .....	7
2.3 WATER TABLE DECLINE AND FLUCTUATION FORMS INTERCONNECTED CONDUITS.....	8
2.4 SUMMARY OF FORMATION OF CONDUIT FLOW .....	10
<b>3 HYDROGEOLOGIC CHARACTERISTICS OF KARST AQUIFERS .....</b>	<b>11</b>
3.1 KARST DRAINAGE SYSTEM.....	11
3.2 KARST OCCURRENCE WHERE SOLUBLE AND LESS SOLUBLE UNITS OCCUR TOGETHER .....	18
3.3 MULTIPLE POROSITY AND PERMEABILITY STRUCTURE .....	20
3.4 VARIANCE IN SURFACE-WATER AND SPRING DISCHARGE IN KARST AQUIFERS .....	28
3.5 CONDUIT DRAINAGE PATTERNS .....	34
3.6 SUBSURFACE PIRACY AND KARST DRAINAGE BASINS .....	39
3.7 VULNERABILITY OF KARST AQUIFERS TO CONTAMINATION.....	44
3.8 KARST AQUIFER FLOW CHARACTERISTICS COMPARED WITH AQUIFERS COMPOSED OF OTHER ROCK TYPES.....	49
<b>4 FLUID MECHANICS CONSIDERATIONS FOR KARST AQUIFERS.....</b>	<b>52</b>
4.1 LIMITATIONS OF DARCY'S LAW FOR APPLICATION TO KARST AQUIFERS .....	52
4.2 REYNOLDS NUMBER AS AN INDICATOR OF FLOW REGIME.....	55
4.3 INVESTIGATION OF ONSET OF TURBULENT FLOW IN ROCK SAMPLES .....	58
4.4 FLUID MECHANICS OF PIPES AND OPEN CHANNELS.....	59
<b>5 METHODS OF KARST CHARACTERIZATION .....</b>	<b>63</b>
5.1 HYDROGEOLOGIC MAPPING .....	66
<i>Enhancing Mapping with Subsurface Data .....</i>	<i>68</i>
<i>Enhancing Mapping with Geophysical Data .....</i>	<i>70</i>
<i>Surface Geophysics Useful to Karst Aquifer Characterization .....</i>	<i>71</i>
5.2 BOREHOLE TESTING .....	75
<i>Borehole Geophysical Tools Commonly Applied to Any Aquifer Type .....</i>	<i>75</i>
<i>Borehole Geophysical Tools Particularly Useful for Characterizing Karst Aquifers .....</i>	<i>78</i>
5.3 WATER TRACING TESTS.....	82
5.4 AQUIFER TESTS.....	88
5.5 USE OF WATER CHEMISTRY DATA .....	94
<i>Basic Water Quality Data.....</i>	<i>95</i>
<i>Use of End Member Mixing to Estimate Groundwater Contribution to Surface Water.....</i>	<i>98</i>
<i>Use of Natural Stable Isotopes.....</i>	<i>101</i>
<i>Water Quality Issues for Water Supply .....</i>	<i>102</i>
<b>6 MATHEMATICAL MODEL APPLICATIONS IN KARST .....</b>	<b>103</b>
6.1 FITTING MODELS .....	107
<i>Example Application of Complex Fitting Model Using Stable Isotopes .....</i>	<i>109</i>
6.2 LUMPED PARAMETER MODELS .....	112

	<i>Example Application of a Lumped Parameter Model</i> .....	112
6.3	DISTRIBUTED PARAMETER MODELS .....	114
	<i>Single-Continuum Porous-Equivalent Models</i> .....	118
	<i>Dual-Continuum Porous-Equivalent Models</i> .....	121
	<i>Hybrid Models</i> .....	121
	<i>Discrete Single and Multiple Fracture or Conduit Network Models</i> .....	124
	<i>Example Comparisons of Single-Continuum and Hybrid Models</i> .....	125
7	SUMMARY .....	137
8	WHAT IS ON THE HORIZON FOR KARST AQUIFER KNOWLEDGE? .....	139
9	EXERCISES .....	141
	EXERCISE 1 .....	141
	EXERCISE 2 .....	141
	EXERCISE 3 .....	142
	EXERCISE 4 .....	142
	EXERCISE 5 .....	143
	EXERCISE 6 .....	144
	EXERCISE 7 .....	145
	EXERCISE 8 .....	145
	EXERCISE 9 .....	146
	<i>Part 1</i> .....	146
	<i>Part 2</i> .....	146
	EXERCISE 10 .....	147
	<i>Part 1</i> .....	147
	<i>Part 2</i> .....	147
	EXERCISE 11 .....	148
	EXERCISE 12 .....	149
	EXERCISE 13 .....	149
	EXERCISE 14 .....	150
	EXERCISE 15 .....	151
	EXERCISE 16 .....	151
	EXERCISE 17 .....	152
	EXERCISE 18 .....	152
	EXERCISE 19 .....	152
	EXERCISE 20 .....	153
	EXERCISE 21 .....	153
	EXERCISE 22 .....	153
10	REFERENCES .....	154
11	BOXES .....	185
	BOX 1 STAGES FROM FRACTURE FLOW TO CONDUIT FLOW .....	185
	<i>Stage 1</i> .....	185
	<i>Stage 2</i> .....	185
	<i>Stage 3</i> .....	186
	<i>Stage 4</i> .....	186
	<i>Stage 5</i> .....	187
	<i>Stage 6</i> .....	187
12	ABBREVIATED GLOSSARY OF KARST AND GROUNDWATER TERMINOLOGY .....	189
	<i>Allogenic Recharge</i> .....	189

<i>Autogenic Recharge</i> .....	189
<i>Capillary Fringe</i> .....	189
<i>Carbonates</i> .....	190
<i>CO<sub>2</sub> Partial Pressure</i> .....	190
<i>Diagenetic Processes</i> .....	191
<i>Dissolved Solids (or TDS—Total Dissolved Solids)</i> .....	191
<i>Eogenetic Karst Aquifer</i> .....	191
<i>Epigene Karst Aquifer</i> .....	191
<i>Epikarst</i> .....	191
<i>Estavelle</i> .....	191
<i>Evaporites</i> .....	192
<i>Geomorphic Period</i> .....	192
<i>Hydraulic Conductivity</i> .....	192
<i>Hypogene Karst Aquifer</i> .....	192
<i>Hyporheic Zone</i> .....	192
<i>Hysteresis</i> .....	193
<i>Karst Window</i> .....	195
<i>Mesogenetic Karst Aquifer</i> .....	195
<i>Newtonian Fluid</i> .....	195
<i>Non-Point Source</i> .....	195
<i>Phreatic Zone (Zone of Saturation or Saturated Zone)</i> .....	195
<i>Point Source</i> .....	195
<i>Post-Depositional Structural Deformation</i> .....	196
<i>Sinkhole</i> .....	196
<i>Swallet (Throat or Swallow Hole)</i> .....	196
<i>Stream Discharge Hydrograph</i> .....	196
<i>Telogenetic Karst Aquifers</i> .....	197
<i>Thermodynamically Saturated</i> .....	197
<i>Thermodynamically Undersaturated</i> .....	197
<i>Vadose Zone</i> .....	197
<i>Water Salinity</i> .....	197
<b>13 EXERCISE SOLUTIONS</b> .....	<b>199</b>
EXERCISE 1 SOLUTION .....	199
EXERCISE 2 SOLUTION .....	199
EXERCISE 3 SOLUTION .....	200
EXERCISE 4 SOLUTION .....	201
EXERCISE 5 SOLUTION .....	201
EXERCISE 6 SOLUTION .....	202
EXERCISE 7 SOLUTION .....	202
EXERCISE 8 SOLUTION .....	202
EXERCISE 9 SOLUTION .....	203
<i>Part 1</i> .....	203
<i>Part 2</i> .....	203
EXERCISE 10 SOLUTION .....	205
<i>Part 1</i> .....	205
<i>Part 2</i> .....	205
EXERCISE 11 SOLUTION .....	207
EXERCISE 12 SOLUTION .....	207



EXERCISE 13 SOLUTION .....	208
EXERCISE 14 SOLUTION .....	208
EXERCISE 15 SOLUTION .....	209
EXERCISE 16 SOLUTION .....	209
EXERCISE 17 SOLUTION .....	210
EXERCISE 18 SOLUTION .....	210
EXERCISE 19 SOLUTION .....	210
EXERCISE 20 SOLUTION .....	211
EXERCISE 21 SOLUTION .....	211
EXERCISE 22 SOLUTION .....	211
<b>14 NOTATION .....</b>	<b>212</b>
<b>15 ABOUT THE AUTHORS .....</b>	<b>213</b>
<b>MODIFICATIONS TO ORIGINAL RELEASE .....</b>	<b>A</b>

## The Groundwater Project Foreword

The Year 2022 marks as an important year for groundwater because the United Nations Water Members and Partners chosen the theme of this year's March 22 World Water Day to be: "Groundwater: making the invisible visible". The goal of the Groundwater Project (GW-Project) is in sync with this theme.

The GW-Project, a registered charity in Canada, is committed to contributing to advancement in education and brings a unique approach to the creation and dissemination of knowledge for understanding and problem solving. The GW-Project operates the website <https://gw-project.org/> as a global platform for the democratization of groundwater knowledge, founded on the principle that:

*"Knowledge should be free and the best knowledge should be free knowledge." Anonymous*

The mission of the GW-Project is promoting groundwater learning. This is accomplished by providing accessible, engaging, high-quality, educational materials, free-of-charge online in many languages, to all who want to learn about groundwater. In short, providing essential knowledge tools for developing groundwater sustainably for humanity and ecosystems.

This is a new type of global educational endeavor in that it is based on volunteerism of professionals from different disciplines and includes academics, consultants and retirees. The GW-Project involves many hundreds of volunteers associated with more than 200 hundred organizations from over 27 countries and six continents, with growing participation.

The GW-Project is an on-going endeavor and will continue with hundreds of books being published online over the coming years, first in English and then in other languages, for downloading wherever the Internet is available. An important tenet of the GW-Project books is a strong emphasis on visualization via clear illustrations that stimulate spatial and critical thinking to facilitate absorption of information.

The GW-Project publications also include supporting materials such as videos, lectures, laboratory demonstrations, and learning tools in addition to providing, or linking to, public domain software for various groundwater applications supporting the educational process.

The GW-Project is a living entity, so subsequent editions of the books will be published from time to time. Users are invited to propose revisions.

We thank you for being part of the GW-Project Community. We hope to hear from you about your experience with using the books and related material. We welcome ideas and volunteers!

The GW-Project Steering Committee

January 2022

## Foreword

Karst is of great importance to humanity and ecological systems because karst terrain makes up about 10 percent of the Earth's surface, provides fresh drinking water to an estimated 10 percent of the world's population and by some estimates supplies up to 25 percent of groundwater withdrawn for agricultural and industrial water use. Karst occurs in more than 100 countries, hence there is an immense scientific literature in many languages about karst. Many karst books are planned for publication by the Groundwater Project to cover many aspects of karst. This book: *Introduction to Karst Aquifers* in the topic domain: *Introduction to Physical and Chemical processes* is the first of the karst books.

Previous books published by the GW-Project and most of those yet to be published are about groundwater flow represented by Darcy's law with flow concepts founded on porous media flow theory and *hydraulic conductivity* of granular or fractured media. In contrast, flow in karst is often non-Darcian. Karst systems have focused outlets, mostly at springs, and the hydraulic conductivity is dominated by solution channels and cavities. Understanding karst systems is a multidisciplinary endeavor aimed at unlocking the mysteries of this most majestic part of the Earth's subsurface to underpin water use and management. This introductory book provides a brief discussion of: karst-aquifer features; genesis of karst; water flow in karst and pertinent fluid mechanics; many types of investigative methods for characterizing and understanding karst; and mathematical modeling applied to karst. This lays the foundation for other karst books being written by the GW-Project and is aimed at introducing readers to groundwater flow in karst with recognition of key differences from other types of aquifer systems.

The authors of this book are senior researchers of Geological Surveys. In combination, they have broad experience in applying diverse methods to understanding a variety of karst systems. In her 35-year career at the United States Geological Survey (USGS) where she attained the level of Regional Groundwater Specialist, Eve Kuniansky provided technical assistance to groundwater projects throughout the southeastern USA, Puerto Rico, the Virgin Islands, and in China, Israel, Cyprus, Ethiopia, Kenya, and South Africa through the USGS International Water Resources Branch, and led the USGS Karst Interest Group. Chuck Taylor heads the Water Resources Section of the Kentucky Geological Survey (KGS) where his primary research is in karst hydrogeology and aquifer characterization. John Williams has advised many government agencies in multiple nations (including the United States, Canada, United Arab Emirates, and Iraq) on issues related to contaminated fractured-bedrock aquifers. Fred Paillet was Chief of the USGS Borehole Geophysics Research Project for many years and has held visiting appointments at universities throughout the world, improving characterization of karst aquifers through advanced analysis of geophysical well logs that are key to determining flow in karst.

John Cherry, The Groundwater Project Leader

Guelph, Ontario, Canada, January 2022

x

## Preface

*Introduction to Karst Aquifers* is designed for upper-level undergraduate science and engineering students (that is, students in geology, earth science, hydrology, hydrogeology, water resources management, or civil and environmental engineering), but will be of interest to all readers with some science and math background who want to know more about karst. The topic of karst is extremely broad. However, the focus of this book is narrow, addressing groundwater flow in karst aquifers.

An aquifer is a geologic formation, a group of formations, or a part of a formation that contains enough saturated permeable material to yield significant quantities of useable water to wells and springs. Thus, the focus of a karst aquifer book is on water supply in formations composed of rocks that can dissolve (aquifers composed predominantly of carbonate and evaporite rocks). The study of carbonate and evaporite sedimentary rocks is a complex field in geology involving physical, chemical, and biological processes along with an understanding of sedimentation in fluvial and marine environments. Thus, the study of karst aquifers is interdisciplinary because investigating them involves geologic mapping, geophysics, geochemistry, fluid mechanics, geomorphology, hydrology, numerical modeling, and microbiology. Most hydrogeologists develop their skills related to karst aquifers on the job or through study for an advanced degree and continue learning throughout their careers. The purpose of this introductory book is to expose readers to the complexity of flow in karst aquifers and the many methods from various disciplines that have been applied to study and characterize karst aquifers for water supply.

Sections 1 through 3 present the important topics pertaining to groundwater flow in karst aquifers in a general way. The rest of the book provides details about the methods of characterization mentioned in the first section. Section 6 describes mathematical models to provide a general understanding of the types of models applied in Karst settings. The extensive Section 10, *References*, provides hyperlinks to the original articles, when possible, for interested readers who have access to them. Additionally, an abbreviated glossary of terms is provided after the references section. Most terms in the glossary are often defined within the text at their first introduction with italicized text. However, a few terms, such as hysteresis or stream hydrograph, are too complex to adequately describe within the text so the definition is included in the abbreviated glossary.

For readers interested in pursuing a career specializing in karst hydrogeology, we recommend becoming proficient in basic mathematics (algebra, geometry, calculus, differential equations and statistics with probability); inorganic chemistry; physics at a level requiring knowledge of calculus; and computer programming. Programming skills are important because many commercial packages for simulating groundwater flow in karst often lack some functionality such that customization is required. Also, programming knowledge helps one understand how data are manipulated by software which is vital to using the software wisely.



## Acknowledgments

We deeply appreciate the thorough and useful reviews of and contributions to this book by the following individuals:

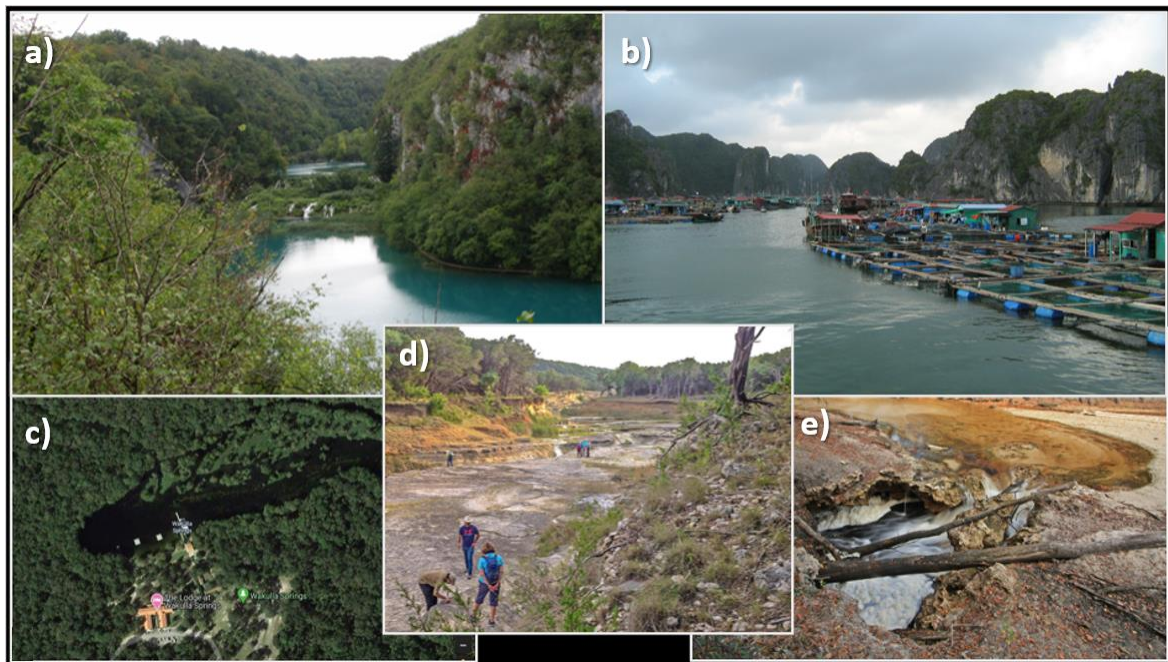
- ❖ Dr. Eileen Poeter, Professor Emeritus, Colorado School of Mines, United States;
- ❖ Dr. Ineke M. Kalwij, President, Principal Hydrogeologist, Kalwij Water Dynamics Inc.;
- ❖ Earl Greene, Director, Water Resources Research Act Program, USGS, United States;
- ❖ David Nelms, Retired Groundwater Specialist, USGS, United States;
- ❖ Dr. Thomas D. Byl, Hydrologist USGS and Assistant Professor, Tennessee State University, United States;
- ❖ Dr. Warren Wood, Emeritus, Groundwater Hydrologist, USGS, United States;
- ❖ Dr. John Cherry, Adjunct Professor, University of Guelph; Professor Emeritus, University of Waterloo, Canada;
- ❖ Dr. Patryk Quinn, Research Scientist, Engineering Department, University of Guelph, Canada;
- ❖ Dr. Jack Sharp, Professor Emeritus, Department of Geological Sciences, University of Texas at Austin, United States;
- ❖ Everton de Oliveira, President of Hidroplan, Brazil, Director-President of the Instituto Água Sustentável (Sustainable Water Institute), Brazil; and,
- ❖ Dr. Hugh Whiteley, Adjunct Professor, Engineering, University of Guelph, Canada.

We are grateful for Amanda Sills and the Formatting Team of the Groundwater Project for their oversight and copyediting of this book. We thank Eileen Poeter (Colorado School of Mines, Golden, Colorado, USA) for reviewing, editing, and producing this book.

# 1 Introduction

The term “karst” is often interchangeably used in areas underlain by soluble bedrocks (*carbonates* and *evaporites*) to describe:

- a landscape, known as karst terrain, characterized by distinctive surface features such as sinkholes, caves, sinking streams, and springs, whose formation is attributable in part to the process of chemical dissolution, with examples shown in Figure 1;
- a hydrogeologic setting, called a karst terrane, in which the surface and subsurface hydrology is largely influenced by the presence of underlying karstified bedrocks and karst aquifers; and,
- a groundwater flow system, known as a karst aquifer, in which water storage and movement occurs mainly through subsurface openings created or modified by dissolution, including unique voids known as “solution conduits”.



**Figure 1** - Karst terrain varies depending on the physiographic and geohydrologic setting as can be seen in both the cover collage and these photos. The photographic images on the cover of this book and this figure present only a few of the many appearances of karst terrain. a) Tufa rimmed lakes at Plitvice Lakes World Heritage karst, Croatia<sup>1</sup>. b) Aqua culture village in drowned karst in the South China Sea, Vietnam<sup>2</sup>. c) Satellite view of Wakulla Springs, Florida, USA<sup>3</sup>. d) Outcrop of the middle portion of the Glen Rose limestone in Canyon Gorge, Texas, USA<sup>4</sup>. e) Alapaha River, river sink, Jennings Bluff-Avoca Tracts, Suwannee River Water Management District Lands, Hamilton County, Florida, USA<sup>5</sup>.

<sup>1</sup> Photo by Kuniansky, 2008a.

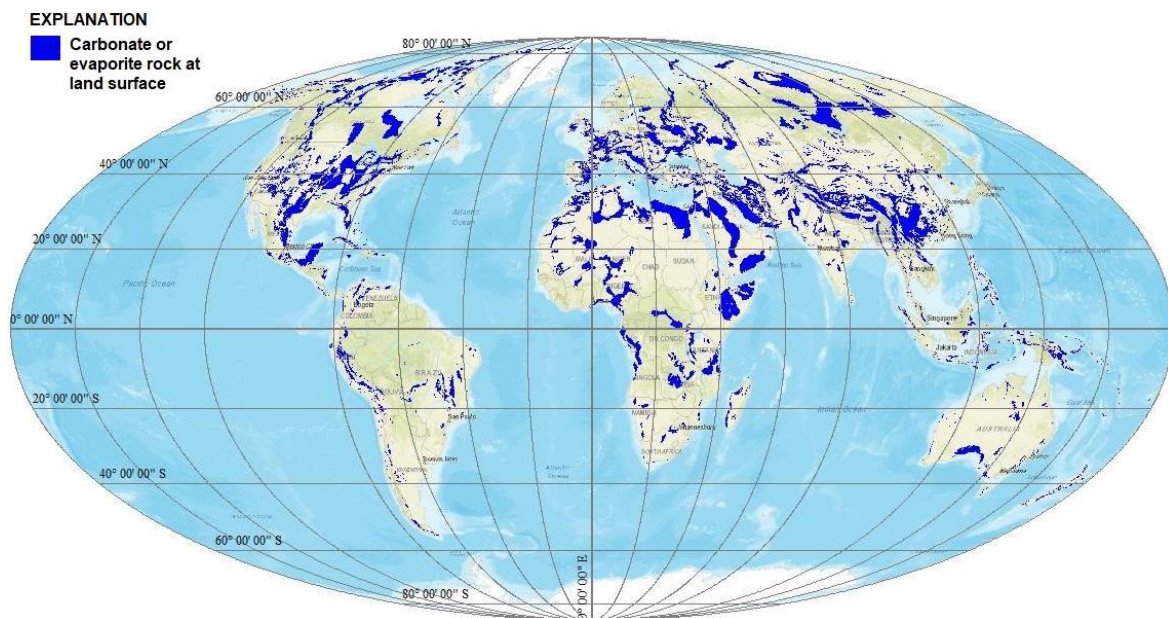
<sup>2</sup> Photo by Kuniansky, 2012.

<sup>3</sup> Public domain image clipped from Google maps (Kuniansky, 2020).

<sup>4</sup> photo by Morris, 2017.

<sup>5</sup> Photo by Allan Cressler taken November 25, 2010, used with permission.

The term karst comes from the Slovenian word “Kras” because the Slovenian Kras region has characteristic karst rocks. This region is in southwestern Slovenia and extends across the border into northeastern Italy. Karst occurs throughout the globe (Figure 2) in a variety of physiographic areas: on islands and in coastal regions, in prominent mountain ranges and massifs, and throughout interior continental regions. In many, perhaps most locations, karst’s presence is easily recognizable by the occurrence of caves, sinkholes, disappearing or losing streams, and the distinctive grooved, scalloped, and fluted erosional features that develop on exposed soluble bedrock surfaces that are called *karren*. In other locations however, the surficial expression of karst is subtle and less easily recognized.



**Figure 2** - Outcrop of carbonate and evaporite rocks forming karst terrains and aquifers around the world indicates the unconfined parts of karst aquifers not the total extent as many of these formations dip underground with confined extents often greater than unconfined extents (created from the World Karst Aquifer Map spatial data set Chen and others (2017) on the Mollweide map projection WGS-84 Datum and Spheroid).

Many geological, topographical, climatological, and hydrological factors influence the formation and physical manifestations of karst; not all karst develops in the same way, or exhibits the same types of surface and subsurface features. However, where karst occurs, its development and physical manifestation is influenced by a combination of groundwater flow and the hydrogeological characteristics and geochemical evolution of the soluble rocks. In areas underlain by limestone rocks, for example, the formation and characteristics of karst are influenced by the original depositional environment, lithologic and stratigraphic variability, diagenetic processes, post-depositional structural deformation, geomorphological evolution of the landscape, as well as variability and changes in precipitation and geochemical weathering processes over both short and long geological time scales.

The focus of this book is on karst aquifers. Karst aquifers serve as vital water resources for a large population, providing fresh drinking water to an estimated 10 percent

of the world's population (Stevanović, 2018) and accounts for up to 25 percent of all groundwater withdrawals (Ford and Williams, 2007). Thus, karst aquifers are important components of local and regional hydrologic and hydrogeologic systems. In karst areas, groundwater and surface water are highly interconnected, with karst aquifers and springs serving as headwaters and major tributaries to surface streams and rivers.

Karst aquifers help to sustain important biological and bio-geochemical systems in, for example, the *hyporheic zone* of surface streams and in subterranean aquatic ecosystems, including habitats for threatened and endangered cave species. In recent years, concerns about effects of global climate change have increased and carbon cycling in karst areas and aquifers has become a topic of greater scientific interest. Hydrogeochemical processes associated with karst areas involve reactions that both generate and sequester carbon and the effects of karstification in areas underlain by carbonates may be one of the larger variables that remain relatively unaccounted for in global carbon budgets and climate-change models (Fong et al., 2013; Cao et al., 2012, 2018).

Flow in karst aquifers is unique (Worthington et al., 2017). Aquifers are comprised of either granular material in which water moves through small pores, and/or fractured material where water moves through cracks and interconnected fractures. Some aquifers have both pores and fractures. Pores and fractures occur in karst aquifers, but in some karst aquifers so much rock has dissolved that the openings form large and interconnected conduits. In these cases, water moves not only through cracks and pores, but also through conduits of large aperture (greater than 0.1 m) or submerged caverns where subsurface flow is similar to flow in open channels and pipes. In some places, subsurface conduits occur in insoluble rocks such as lava tubes that form in volcanic rocks when molten lava solidifies and is called pseudokarst. Where conduits are interconnected, locations of water inflow and outflow are more localized than in granular and fractured aquifers, and flow moves more rapidly. At times the flow is turbulent.

In contrast to porous media flow and small fracture flow, conduit flow can have very high velocities and provide rapid transit of water from its entry into the subsurface to its discharge location. In some locales, conduits may exist, but their entry and/or exit points may be clogged such that the rate of groundwater movement is similar to aquifers composed of granular rocks, such as sandstone or alluvium. The potential for conduit flow in karst aquifers leads investigators to supplement standard aquifer investigation methods with mapping of surficial karst features, dye tracing, and more elaborate monitoring of the volume of groundwater discharge and water chemistry at springs.



The complexities presented by karst aquifers are among the most fascinating and challenging in hydrogeologic sciences. For example, karst aquifers present extreme forms of heterogeneity, including multi-scale porosity and permeability structures and groundwater flow dominated by networks of solutional openings that are fed by a combination of surface runoff and water leaking from the rock matrix. Groundwater flow



in karst conduits can occur under high velocities (greater than 10 to 100 meters per day [m/d]) under both laminar and turbulent conditions. Hydrologic, hydraulic, and geochemical (for example, water-quality) characteristics in karst aquifers are typically among the most spatially and temporally variable in hydrogeology. These and other notable hydrogeologic complexities contribute to a widespread perception that groundwater resources provided by karst aquifers are difficult to develop, sustain, and protect. The likelihood of this perception being true increases where karst data collection and interpretation, as well as understanding of karst hydrogeology concepts, are insufficient to enable effective characterization of the aquifer and resource-management decisions.

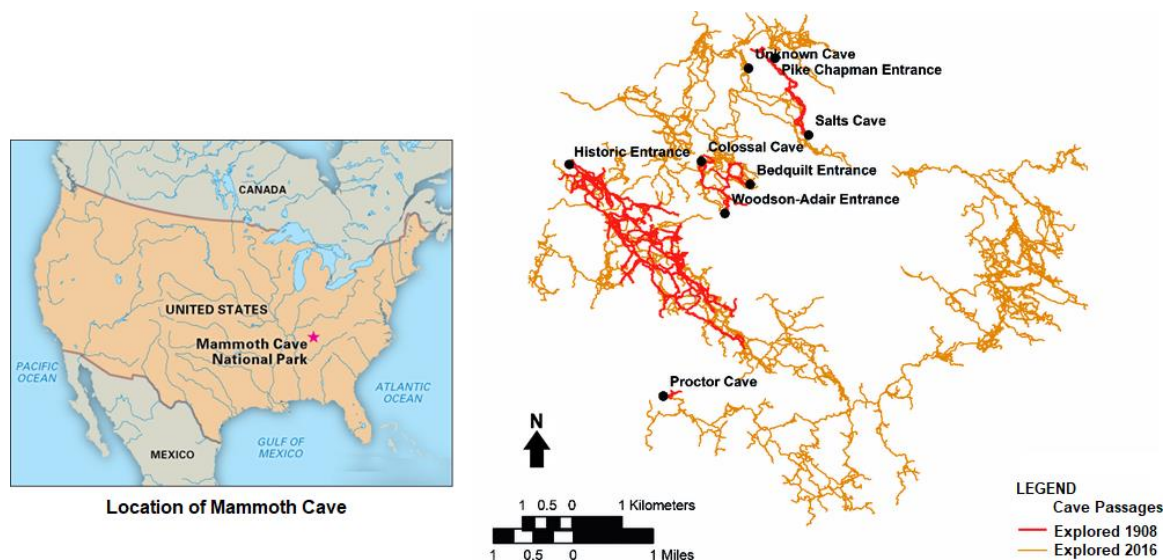
This book reviews and highlights important basic hydrogeological characteristics of karst aquifers and summarizes investigative methods useful in their study and characterization. One key aspect to the investigation of karst aquifers is the realization that traditional methods of groundwater investigation developed and used successfully to characterize granular and many fractured-rock aquifers are often less successful, or must be modified and interpreted differently, when applied to karst. For example, mapping of water levels—a fundamental practice used to determine groundwater flow directions and rates in most aquifers—is often problematic in karst for reasons that will be discussed later. In addition, the hydrogeological complexities presented by karst generally require a multidisciplinary investigative approach that incorporates the use of several highly-specialized techniques such as water-tracing tests, spring-discharge monitoring, and various borehole and surface geophysical methods that often are not taught in traditional groundwater course curricula. Many of these techniques are the subject of additional books planned for the Groundwater Project.

The vast range of specialized topics related to karst are beyond the scope of this introductory book. After reading this introductory book, readers may want to consult other publications that provide overviews of karst hydrogeological concepts and investigative techniques, such as Goldscheider and Drew (2007), Taylor and Greene (2008), and Taylor and Doctor (2017). Textbooks authored by White (2019, 2016, 1993, 1999, 1988), Ford and Williams (2007), Milanovic (1988) are highly recommended resources for anyone interested in areas related to karst hydrogeology and water resources.

Readers who are not familiar with groundwater flow are encouraged to read other introductory books of the Groundwater Project including the overview book [“Groundwater in Our Water Cycle”](#)  and the basics presented in [“Hydrogeologic Properties of Earth Materials and Principles of Groundwater Flow”](#) .

## 2 Karst Conduit Flow Develops by Geochemical and Flow Processes

Karst is formed in soluble rocks especially limestone and to a lesser extent in dolomite but can develop in gypsum or salt. Karst is the most dramatic evidence of the ability of groundwater to alter the form of the earth's surface and subsurface as illustrated on the cover of this book and in Figure 1. More than one episode of karst development can occur as geological conditions change, which adds complexity to the karst system. Formation of substantial-sized openings in rocks requires chemical dissolution operating over geologic time scales. For example, Mammoth cave in the state of Kentucky in the USA includes multiple bedrock formations and several levels of conduits that extend over an estimated 200 km<sup>2</sup> (Figure 3). It is believed that groundwater began interacting with the uppermost cave-forming limestone formation—about 10 million years ago and that the upper levels of the cave system were fully formed by 3.2 million years ago, based on radiometric dating of quartz pebbles (Quinlin and Ewers, 1989; USGS website, 2021). Mammoth cave is the longest known cave system in the world with mapped passages extending more than 600 km. Personnel of Mammoth Cave National Park estimate there may be as much as 1000 km of unmapped caves (Toomey et al., 2017).

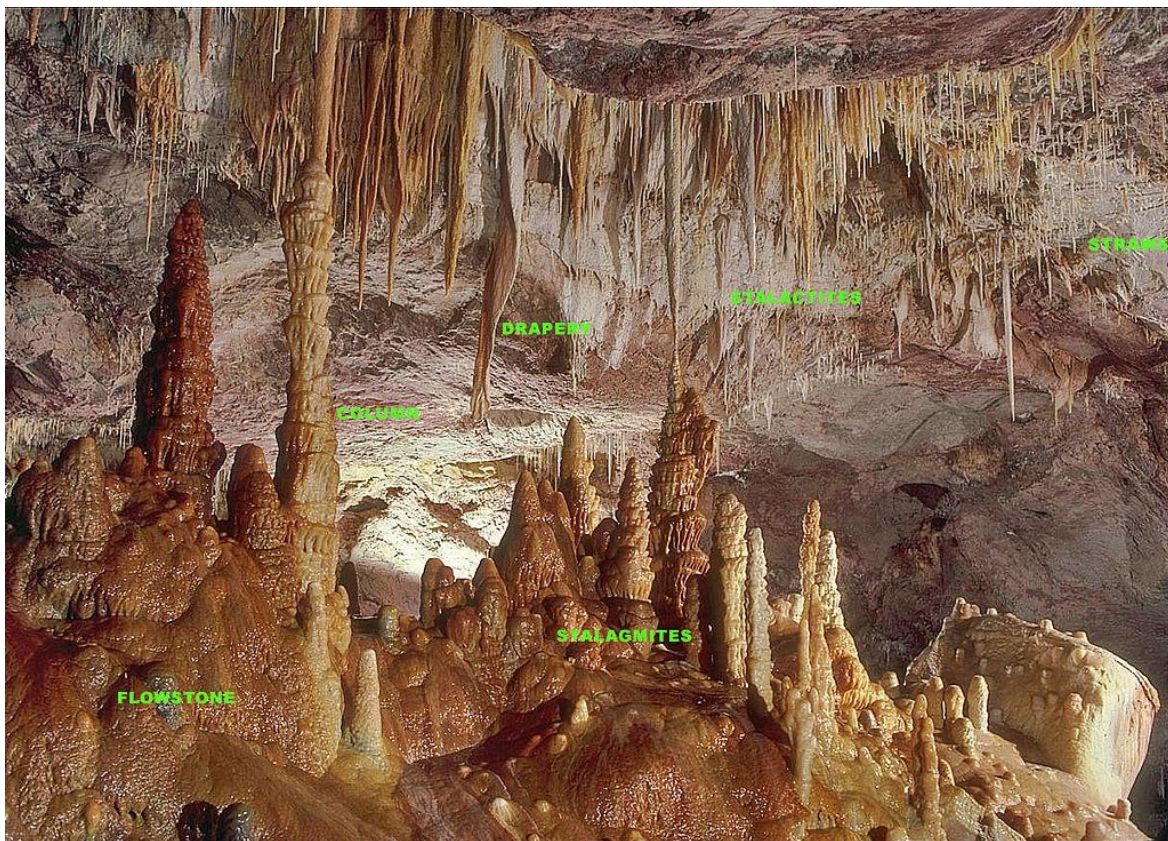


**Figure 3** - Systems of cave networks that constitute karst terrane can be extensive and can require decades of mapping as evidenced from this map of the known passages in the Mammoth Cave system and the adjacent caves from those known in 1908 and those explored as of 2016. Modified from Toomey and others (2017).

Karst openings result from the combination of water flow and mineral dissolution that removes rock mass to create and/or enlarge openings. However, much of the beauty observed in karst results from the creation of mineral mass by chemical precipitation that forms striking cave structures (Figure 4). Most karst aquifers are formed as a consequence of the infiltration of precipitation, subsurface diversion of stormwater runoff and surface stream flow, and the subsequent movement of groundwater. These are *epigene* karst



aquifers and are active components of the meteoric water system and the critical zone, and are the topic of this book. The critical zone is Earth's permeable near-surface boundary layer where rock, soil, water, air, and living organisms interact. Another type of karst, *hypogene* karst, develops by deep-sourced corrosive waters or gases upwelling through fault zones and fractures and/or following the geologic dip of permeable and soluble bedrock strata. Hypogene karst is generally located in, or near, regions of tectonic, volcanic, or high-temperature geothermal activity past or present, such as Carlsbad Caverns, New Mexico, USA. Depending on the depth and hydrogeological isolation, geological strata altered by hypogene karst may or may not interact with shallow meteoric waters to store and transmit fresh groundwater. Thus, they may or may not be identified as aquifers, and may or may not play a role in the occurrence of near-surface karst geomorphic features.



**Figure 4** - Underground cave photograph showing common structures formed by precipitation of minerals from groundwater (Dave Bunnell, 2006. "Photo by Dave Bunnell showing the most common speleothems" by Dave Bunnell is licensed under [CC BY-SA 2.5](https://creativecommons.org/licenses/by-sa/2.5/)).

## 2.1 Formation of Karstic Conduit Flow Systems

The formation of karst begins with flow in a network of connected fractures, such as open joints or along bedding plane openings (fractures) originating from rock stresses during crustal movements (for example, as shown in the middle-left photo on the cover of Glen Rose Limestone as seen along the channel of Canyon Gorge, Texas and notice fracture joints with vegetation). There are interconnected fractures with groundwater flow in other

types of rock such as granite, but karst does not form because granite and most other igneous rock formations do not contain minerals soluble enough for substantial dissolution. After some time, the enlarged fractures in soluble rocks become connected to form solution channels and caves, which then provide the main paths for groundwater flow.

Before any solution enlargement has occurred in a fractured limestone, fresh groundwater originating from rainfall infiltrates through surficial soils then flows through a network of fractures, joints and bedding planes, as is the case in all fractured sedimentary rock. In order to dissolve rock, the water must be chemically aggressive, that is, *thermodynamically undersaturated* with respect to the mineral calcite ( $\text{CaCO}_3$ ). Carbon dioxide ( $\text{CO}_2$ ) is continually produced in the *vadose zone* from microbial decay of organic matter and from respiration of plant roots. That  $\text{CO}_2$  combines with water to form carbonic acid ( $\text{H}_2\text{CO}_3$ ) which dissolves calcite. This process is well established in soil science.

Given the presence of chemically aggressive water, karst development proceeds by hydrogeochemical processes that involve complex interactions through time and space. Comprehensive discussions of the processes of fracture enlargement and cave genesis are provided by Holland and others (1964), Howard (1964a, 1964b), Thraikill (1968), Ford and Cullingford (1976), and Palmer (1999).

Long periods of time are required for solution channels to form a conduit flow system because, although recharge water is chemically aggressive, it quickly dissolves calcite and loses its chemical aggressivity, *unless* conditions change such that the water becomes undersaturated with respect to calcite. There are two ways that conditions may change: 1) chemically aggressive water may form at depth, or 2) the water table may decline allowing unsaturated zone processes to be active deeper in the system.

## 2.2 Deep Chemically Aggressive Water Forms Interconnected Conduits

Occurrence of water undersaturated in calcite at large depth and distance into the subsurface system requires the presence of carbon dioxide gas which can develop when groundwater transports organic carbon into the system that is then oxidized to form carbon dioxide gas. Both aqueous and gaseous carbon dioxide ( $\text{CO}_2$ ) play a role in development of karst because  $\text{CO}_2$  produces carbonic acid that results in dissolution of calcite.

The six mechanisms for instigation of calcite dissolution are:

1. variation in groundwater temperature because calcite solubility decreases with rising temperatures unlike most rock forming minerals;
2. production of sulfuric acid along groundwater flow paths, as suggested by Moore and Nicholas (1964) during which oxidation of small amounts of sulfide minerals, especially pyrite, results in sulfuric acid ( $\text{H}_2\text{SO}_4$ );



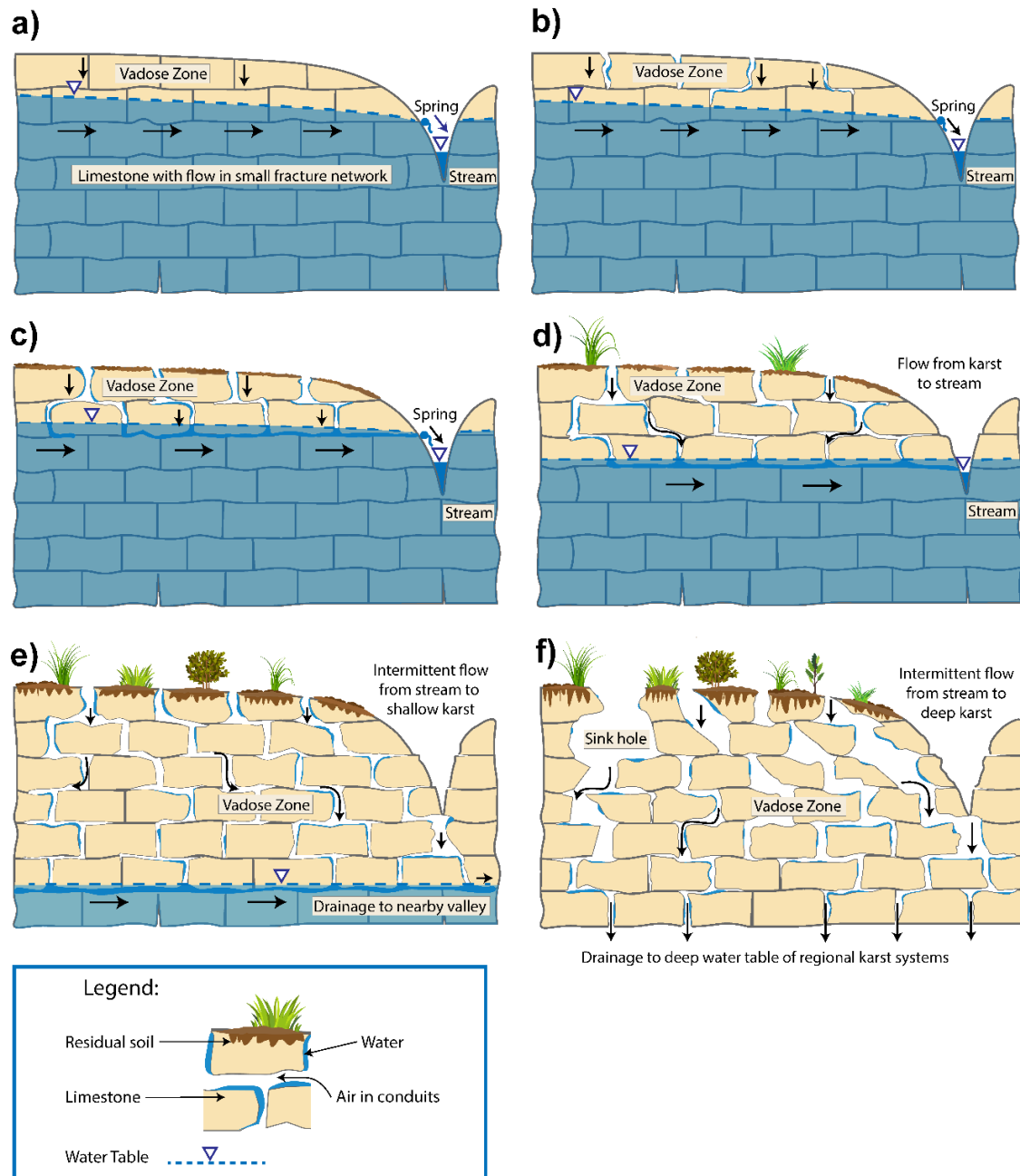
3. floods in surface streams or rapid snowmelt causing exceptionally large rapid recharge of undersaturated water;
4. mixing of dissimilar waters at fracture/joint intersections, because when waters of different chemistry (each saturated in calcite but with different  $\text{CO}_2$  *partial pressure* or temperatures) mix, the mixed water can be slightly undersaturated in calcite (Wigley and Plummer, 1976; Thraikill, 1968);
5. in-situ formation of  $\text{CO}_2$  deep in the vadose zone by particulate and dissolved organic transport (Wood and Petraits, 1984); Wood, 1985); and,
6. degassing of groundwater that is *thermodynamically saturated* with calcite as it reaches caves (Cao et al., 2021) resulting in precipitation of calcium carbonate and formation of stalactites and stalagmites.

Another less common source of  $\text{CO}_2$  or  $\text{SO}_4$  at depth occurs near magmatic areas or oil fields and can create chemically aggressive water.

Once chemically aggressive water is present at depth, karst openings are enlarged by dissolution of rock surrounding permeable openings which then become more permeable, thus higher flow volumes and velocity bring more aggressive water in contact with the soluble rocks and the karstification process proceeds.

## 2.3 Water Table Decline and Fluctuation Forms Interconnected Conduits

When the water table drops during short-term drought or longer-term minor changes in climate, the *vadose-zone* karstification processes function at greater depth and when the water table rises, groundwater flows in solution openings formed under the earlier saturated and unsaturated conditions. Additionally, as the water table rises and falls seasonally, this results in more mixing of water. Figure 5 illustrates the stages of karst aquifer evolution from a fractured flow system to a conduit flow system as a result of water table decline and rise. In the first stage (Figure 5a) the limestone has normal small fractures before chemical weathering, followed by a second stage in which chemically aggressive water dissolves calcite along the fracture walls. In this second stage (Figure 5b), some fractures have been enlarged but are insufficient to form a network of enhanced hydraulic conductivity and therefore the rock does not yet have conduit flow. In the third stage (Figure 5c), further dissolution has connected the enlarged fractures so that conduit flow begins. In the fourth stage (Figure 5d) enlargement and interconnection has increased the hydraulic conductivity of the interconnected paths so much that flow can be driven by a lower gradient, thus the water table declines and vadose-zone karstification processes occurs at deeper levels. This lowering of the water table may be increased if it is accompanied by down cutting of streams in the area. In the fifth stage (Figure 5e) a wetter period occurs, raising the water table and resulting in active conduit flow through what was the deep part of the vadose zone when the water table was lower.



**Figure 5** – Illustrations (a-f) show the evolution of a karst hydrologic system over geologic time in six stages from a barren limestone landscape (no soil) with a fracture network with groundwater flow in connected fractures connecting to a nearby hillslope and ending with a fully developed karst hydrologic system that drains the local precipitation through the bottom to discharge at faraway places not within the topographic watershed:

- Stage 1: Barren limestone with small fractures that contribute a small flow from the spring to the stream;
- Stage 2: Soil develops causing generation of  $\text{CO}_2$  and organic matter that generates more  $\text{CO}_2$ , both creating larger fractures and dissolution channels;
- Stage 3: Connected dissolution channels form to cause lowering of the water table and spring flow from conduits formed along fractures increases, soil development continues;
- Stage 4: Channel network deepens in the vadose zone as  $\text{CO}_2$  and organic matter are driven downward maintaining chemically aggressive water at deeper levels, and the stream is fed by karst drainage;
- Stage 5: Channel network deepens below the stream bottom so that the stream feeds karst system; and,
- Stage 6: Channel network drops below the local flow system with karst flow draining to a distant exit.

The enlargement of karst channels is driven by chemically aggressive subsurface water with its aggressivity continually renewed by production and dispersion of  $\text{CO}_2$  in the subsurface through the synergistic combination of hydrologic flow, downward erosion along surface stream channels, and hydrogeochemical processes. If limestone extends far and deep, then given sufficient geologic time, the karst system will extend far and deep. Modified from Wood and Cherry (2021).

The sixth stage (Figure 5f) is a mature karst with no overland flow, the water table below the image area, unknown distant discharge areas and dry caves. These stages can occur within a single *geomorphic period*. If crustal uplift or a major climate change occurs, then a different era of karstification can begin as is typical in the evolution of most karst systems. More detailed descriptions of the stages of karst aquifer evolution from a fractured flow system to a conduit flow system are provided in [Box 1](#) ↓ along with a repeat of Figure 5 for the readers convenience.

Underlying horizontal beds of mudstones, sandstones, dolostones, or any rock that are both less soluble than limestone and less transmissive of water will restrict the downward movement of water resulting in conduits forming in the limestone directly above and along the dip of the less soluble formation. If the water encounters vertical fractures through these less soluble rocks and is still undersaturated with calcite, another deeper more soluble limestone layer will begin to dissolve. This occurs in both the unsaturated zone and saturated zone as changes in the rock facies focus water movement through the more permeable rock. These units of karst aquifers are called preferential flow units or zones (Williams and Kuniansky, 2016; Cunningham et al., 2006; Rose, 1972). If present, these facies changes result in a complex three-dimensional karst network as compared to a system with no facies changes, as in the stages of karst development shown in Figure 5.


Inland areas, such as in southwest China along the Li River (as shown in cover collage), dissolution of limestone often occurs over time at the level of the alluvial valley. In the karst areas of southwest China, Laos, and Vietnam, inland caves are common at the level of the current rivers and along alluvial plains and sunken valleys between karst towers (haystacks) or mountain ridges. Often these caverns have rivers running through them under the large haystacks or mountains. Foot trails follow and boats move between the villages in these sunken alluvial valleys (Khang, 1985). Additionally, there are many dry caverns far above the current river valleys. Worthington (2005) discusses how base level lowering results in the upper dry caves and the dissolution processes creating conduits and cave formation.

## 2.4 Summary of Formation of Conduit Flow

In summary, the evolution of karst development is a function of the availability of chemically aggressive water over time. The availability of chemically aggressive water depends on the volume of recharge water and CO<sub>2</sub>, as well as varying water table elevation, dissolved and particulate organic content, sulfide mineral content, temperature, and mixing of different waters at depth. Once chemically aggressive water is present at depth, karst openings are enlarged by dissolution of rock surrounding permeable openings which then become more permeable, thus higher flow volume and velocity bring more aggressive water in contact with the soluble rocks and the karstification process proceeds. This is a

simplified discussion as the formation and depositional environment of carbonates is complex and results in extreme variability in the resulting rock formations. Post-depositional structural changes may also affect how and where fractures occur that allow aggressive water to begin to move through the rocks. The changing geologic structure and climate over the millennia are collaborators in the creation of the dissolution features.

Coastal karst aquifers form by complex processes involving mechanical weathering, and biological and geochemical processes creating dissolution and formation of sea caves. While seawater is generally saturated with calcite, dissolution occurs under a variety of conditions, and not all the conditions understood (Taborski and Kazmer, 2013). The extremely complex processes involved in speleogenesis and karst geomorphology occur over geologic time scales, and are not the focus of this book.

[Exercise 1](#)  invites the reader to consider the composition of carbonate and evaporite rocks.

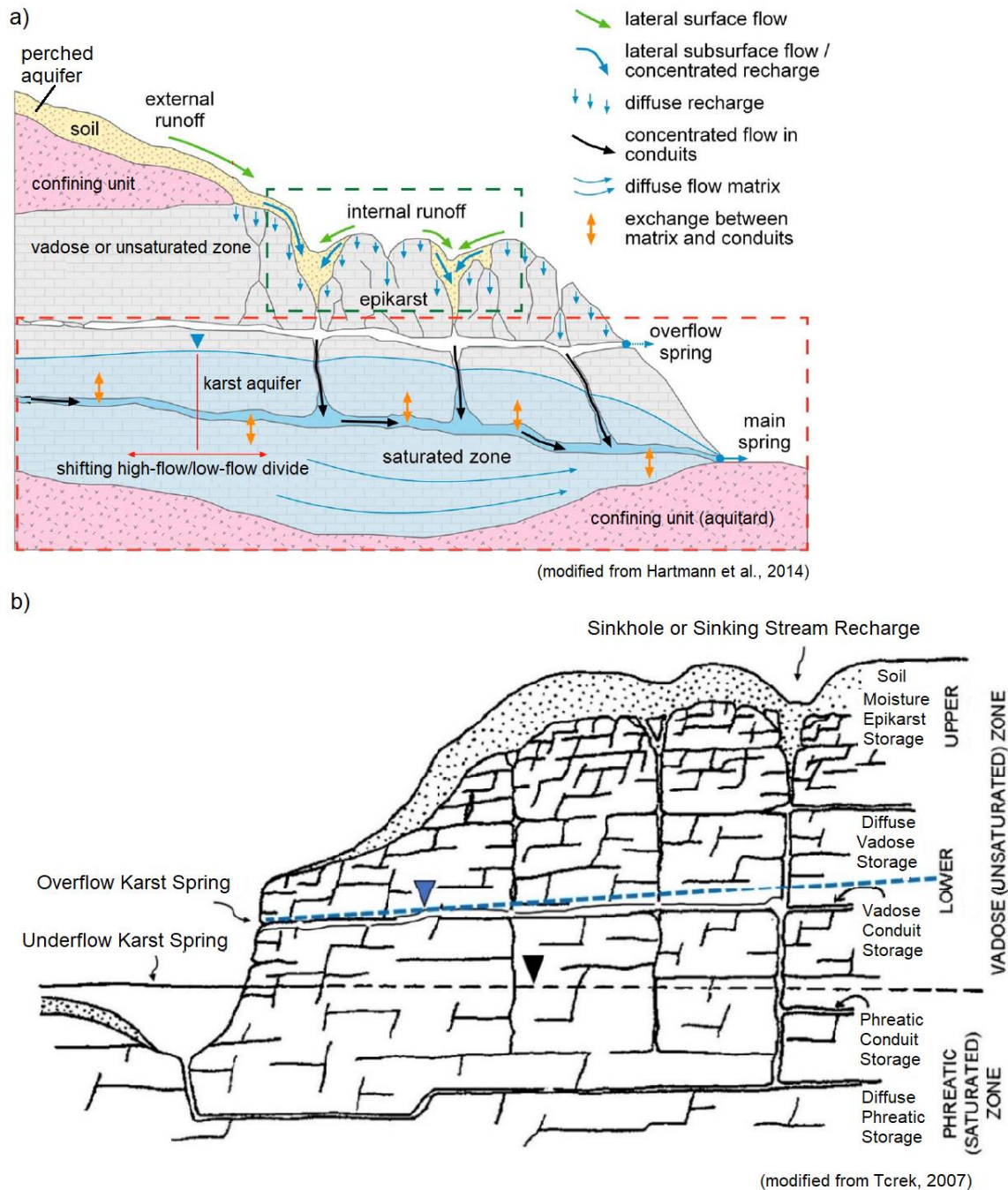
## 3 Hydrogeologic Characteristics of Karst Aquifers

In general terms, a karst aquifer can be identified as an aquifer in which permeability, flow, recharge, and storage characteristics have been created or modified as a result of dissolution by naturally occurring acidic fluids, such as rainwater that combined with carbon dioxide to form a weak carbonic acid. To many, the term “karst aquifer” is virtually synonymous with limestone aquifer due to the latter’s susceptibility to dissolution and widespread geographical occurrence, but other carbonate rocks such as dolostone, chalk, marble, and soluble non-carbonates (evaporites) such as gypsum and anhydrite, are also subject to varying degrees of karstification and may exhibit hydrogeological characteristics typical of karst aquifers.

### 3.1 Karst Drainage System

Karst aquifers are one major component of a complex natural drainage system composed of many surface and subsurface hydrologic components (Figure 6). Early on, groundwater professionals recognized that the prevalence and hydrologic significance of recharge from surface runoff draining rapidly into a karst aquifer from point sources (for example, open sinkholes and sinking/disappearing streams) required conceptualizing the aquifer in a non-traditional way. That is, not focusing exclusively on the saturated zone, but also considering the role of the unsaturated zone and its interrelationship with the saturated zone. This led to conceptualizing groundwater flow in the context of the karst drainage system as a whole. Figure 6 illustrates the hydrological zones of a typical karst aquifer, and the major recharge, storage, and flow components within the zones. All of the features contribute to the water budget of a karst aquifer, some being more significant seasonally and/or during and after storm events.





**Figure 6 - a)** Karst drainage system showing relationship between the karst aquifer (blue-shaded area) and the many different surface and subsurface hydrologic components of recharge, storage, and flow. The dark green box indicates the soil/epikarst area and the dark red box the main karst aquifer subsystems (Modified from Hartmann et. al. 2014). **b)** Cross-sectional diagram showing distribution of unsaturated (vadose) and saturated (phreatic) zone components. The interface between the two zones is defined by the position (or elevation) of the water table which may rise or fall significantly depending on flow conditions and influx of storm recharge. It is also dependent on the presence of overflow springs and relative vertical distance between overflow and underflow springs. Black dashed line and triangle indicate base-level water table elevation, blue dashed line and triangle indicate raised water table elevation under high- or flood-flow conditions. Vertical scale exaggerated. Modified from Terek (2007).

Flow paths and water fluxes in karst drainage systems are complex, being controlled by the distribution and interconnection of zones of higher and lower permeability and higher and lower flow velocities; driven by relative differences in

hydraulic heads and corresponding hydraulic gradients within and among these zones. In both the unsaturated and saturated zones, flow components exist that may be broadly characterized as “diffuse”. In diffuse flow zones, permeability is widely distributed throughout the rock matrix, micro-to-small-aperture fractures and pores, as well as small conduits and solutional openings, in which laminar, low-velocity flow occurs. In contrast, flow zones described as “conduit” include large solutional voids, pipe-like or channel-like solutional openings, and solution-widened fractures in which the volumetric flow rate is larger than in other types of aquifers. Both laminar and turbulent flow regimes, occur in conduits. In many karst aquifers, conduits are large horizontal dissolution features along bedding planes in soluble formations. These can be less than a meter to multiple meters thick and generally occur where a more soluble formation overlies a less soluble formation.

Flow paths and fluxes vary greatly across spatial and temporal scales, changing seasonally as well as during and after storms. Therefore, it is often necessary to sample and characterize karst aquifer hydrology under designated low-flow, average-flow, and high-flow conditions. In the saturated zone, water levels (potentiometric heads) measured in wells in highly-developed karst aquifers may exhibit significant spatial and temporal differences depending on the spatial variability of permeability zones, antecedent and existing flow conditions (low flow, base flow, or high flow), as well as the timing and variability in recharge that occurs during individual storms.

During seasonal increases in recharge, or after intense and/or prolonged storms, water levels may rise in the aquifer and flow paths may be temporarily re-activated in higher-elevation fractures and conduits that are in the unsaturated zone during low-to-base flow conditions. This mechanism is one cause of the oft-noted phenomenon of changes in groundwater flow directions and shifts in the position and configuration of groundwater divides during higher-flow conditions. Worthington (1991) proposed the term “overflow” routes for storm re-activated flow paths and “overflow springs” to identify the discharge from intermittent spring outlets re-activated during high-flow conditions. Conversely the term “underflow springs” identifies the perennial spring outlets that discharge the base flow of the karst drainage system (Figure 7). Other spring classification systems exist and are frequently used, such as the Meinzer classification (Meinzer, 1927) which is based on discharge and descriptive physical characterizations (for example, artesian versus gravity flow). Other classifications rely on geomorphologic or hydrogeologic descriptors, such as, thermal, bedding plane (or contact), geyser, vent, artesian and seepage, perched and seepage, seep, cave or tubular, offshore, onshore, karst, resurgence (river rise), *estavelle* (transitions between resurgence (or exsurgence) to a sink depending on ambient hydrologic conditions), instream, headwater, and so on (Copeland, 2003, Mathey, 1989). For karst springs, the advantage of the characterizing springs as underflow or overflow outlets is that it describes each spring’s hydrologic function for groundwater discharge and helps one develop a better conceptual model of the structure and functioning of the entire karst drainage system and its conduit flow.






**Figure 7** - Photos showing discharge from overflow and underflow springs in a shallow karst aquifer (limestone) after a storm event: a), multiple small overflow springs discharging from outlets located at slightly higher elevations than the larger, underflow spring in the center of the photo; and b) view from downstream showing additional overflow spring outlets discharging from limestone bedrock in the wall of the ravine. Field photographs provided by Taylor (2021a).

The elevation of underflow springs has much control on the elevation of the water table at the outflow boundary of the karst aquifer, whereas the matrix hydraulic conductivity and the hydraulic capacity of conduits determines the slope of the water table and its fluctuation under varying hydrologic conditions (Ford and Williams, 2007). Underflow springs typically occur at a local or regional groundwater discharge boundary, in the vicinity of the lowest hydraulic heads in the aquifer, which is usually close to the elevation of a nearby base-level stream (White, 1988). Convergent tributary flow through the conduit network to a trunk conduit that discharges through a single large underflow spring is common (White, 1999), but many karst aquifers discharge via a conduit network with multiple underflow spring outlets.

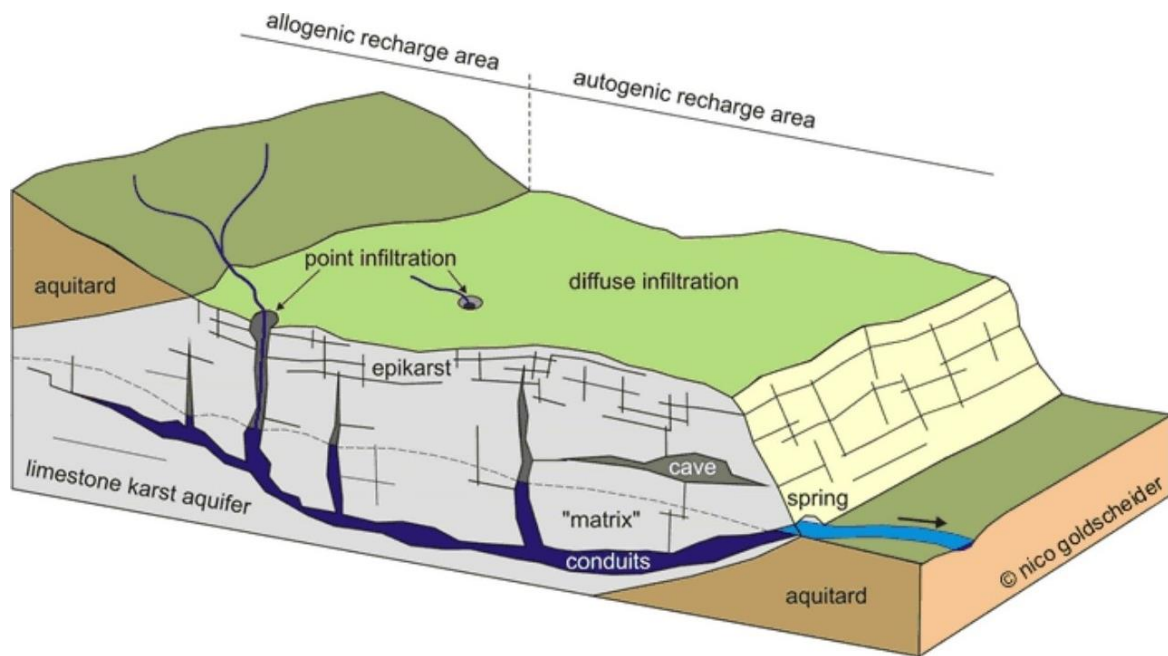
Unsaturated zone hydrology is of critical importance to the investigation and characterization of most karst aquifers. As with other kinds of unconfined aquifers, karst aquifers are recharged by diffuse infiltration of precipitation. However, unique to karst is concentrated recharge of surface runoff through sinkholes and joints derived from surface streams that are diverted underground (as shown in Figure 1c where water flows from the Alapaha River into a river sink at Jennings Bluff-Avoca Tracts, Suwannee River Water Management District Lands, Hamilton County, Florida, USA). These are commonly called disappearing, sinking, or losing stream channels. Sinkholes (also known as dolines) exhibit a variety of shapes and sizes, but are simply closed surface depressions that collect and drain surface runoff into underlying fractures and conduits. Sinkholes may be part of the unsaturated zone, or, where they intersect the water table, part of the saturated zone.

In terms of the surface hydrology, sinkholes may appear to function as isolated or disconnected surface catchments or basins (“zero” order basins). However, it is important to recognize that the runoff collected and drained by a sinkhole is flowing somewhere via

underground conduits, either within the basin defined by surface topography or to another topographic basin, spring or stream. When a sink (a losing stream reach or a sinkhole) moves water from one topographically defined basin to another, this is called stream piracy. It is erroneous to consider sinkholes as “non-contributing” drainage areas (Taylor and Doctor, 2017) because during and after storms, sinkholes that are normally dry can act as rapid natural drains that divert surface runoff to underground conduits. It is this type of concentrated recharge that renders karst aquifers more vulnerable to non-point-source pollutants, and other contaminants that spill or leak into the environment. Rates of drainage from sinkholes vary greatly depending on whether the depressions have open “throats” called *swallets*. The hydraulic capacity of *swallets* increases with size of the opening and decreases if filled with overlying soil or sediment. In some karst aquifers the rate of sinkhole drainage is impacted by the elevation of the water table or water that is backed-up in karst conduits. Additionally, some sinkholes or openings to the underground network (*karst window*) reverse the direction of flow depending on the rise or fall of the groundwater table and are called *estavelles* or a sinkhole flood.

[Exercise 2](#)  explains the types of sinkholes and invites the reader to consider how they influence recharge and flow.

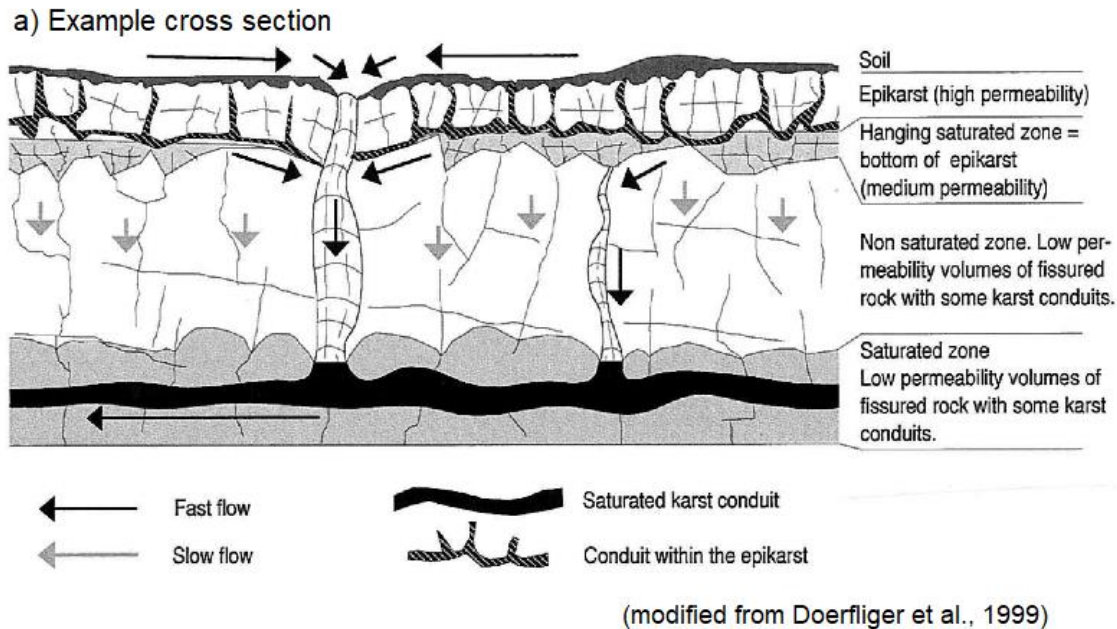
Infiltration or recharge to karst aquifers is sometimes identified by the terms *autogenic* and *allogenic*. Autogenic recharge originates from infiltration of precipitation that falls on the area directly underlain by the karst aquifer, or from underground diversion of surface runoff that accumulated within the geographic boundaries of the area underlain only by the karstified bedrock (Figure 8). Allogenic recharge is contributed by surface runoff carried into the karst aquifer by sinking or disappearing streams, but which originates through precipitation falling on areas underlain by non-karstic bedrocks. Allogenic recharge contributions and the catchment areas they derive from must be included in the water budget for karst aquifers even though they are geographically and geologically outside the physical boundaries of the karst system. Mixing of allogenic waters with autogenic waters, and the timing and proportions of those recharge fluxes, often profoundly alters karst water chemistry. This hydrochemical signature can provide a useful set of parameters that serve as natural tracers for investigation of the internal conduit structure and hydraulic functions of karst aquifers. Section 5.3 “Water Tracing Tests” presents an example of using natural hydrochemical properties with end member mixing models to understand the groundwater contribution to surface-water streamflow.



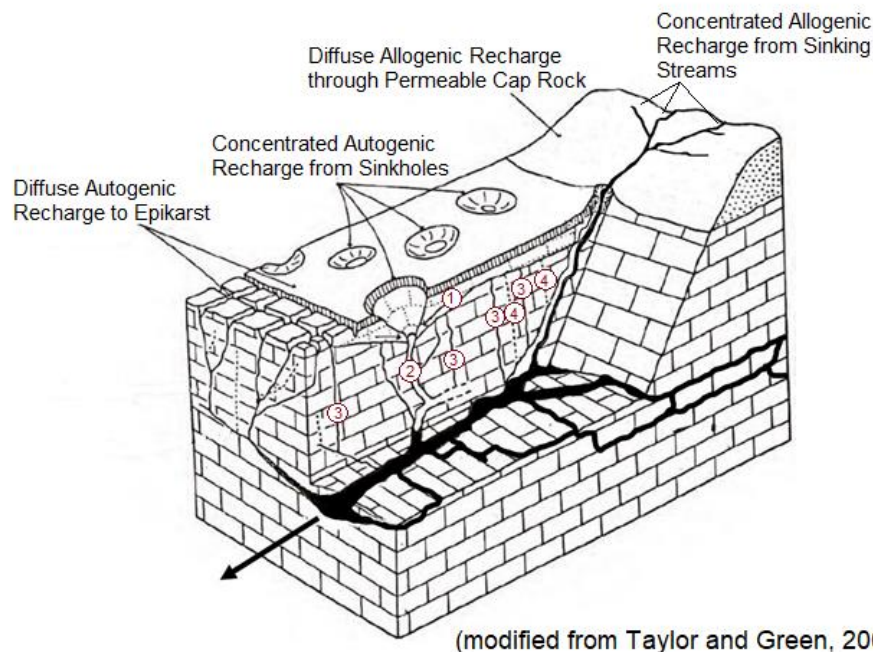
**Figure 8** - Geological block diagram illustrating the difference between allogenic and autogenic recharge to epikarst and conduits. Modified from Goldscheider and Drew (2007).

Another unique source of recharge, storage, and flow in the unsaturated zone of the karst drainage system is the *epikarst* (Mangin, 1975; Per Klimchouk, 2015). Epikarst is the uppermost weathered zone of carbonate rocks that possesses substantially enhanced porosity and permeability relative to the deeper parts of the rock mass. Epikarst stores and intermittently distributes infiltrated recharge water to the underlying karst aquifer's unsaturated zone. Epikarst is an important storage zone that functions as a perched leaky aquifer. Some studies suggest that water storage in the epikarst can be more significant than storage in the saturated zone of the karst aquifer. The enhanced shallow porosity and permeability facilitates considerable lateral flow within epikarst, and, depending on its thickness, decreasing permeability with depth causes flow to converge towards solution-enhanced, deeply penetrating, vertical fractures, conduits, and sinkhole drains (Figure 9). Recharge percolation from the epikarst to the deeper unsaturated zone occurs as diffuse seepage.





## b) Block diagram



**Figure 9** - Illustrations of the epikarst zone and its hydrologic function: a) Cross section showing recharge, storage, and flow characteristics within the epikarst zone (Modified from Doerfliger et. al., 1999). b) Geologic block diagram showing relationship between diffuse recharge from epikarst and concentrated recharge from sinkholes and sinking stream drainage and the underlying conduit network. The epikarst or unsaturated zone can have some perched water tables on top of less permeable sediments, such as a mudstone layer or chert layer within the epikarst-usually composed of highly weathered sediment or loess or sometimes the remaining clay and sand minerals post dissolution of all of the limestone (sometimes called residuum). Water flows through the unsaturated zone via:

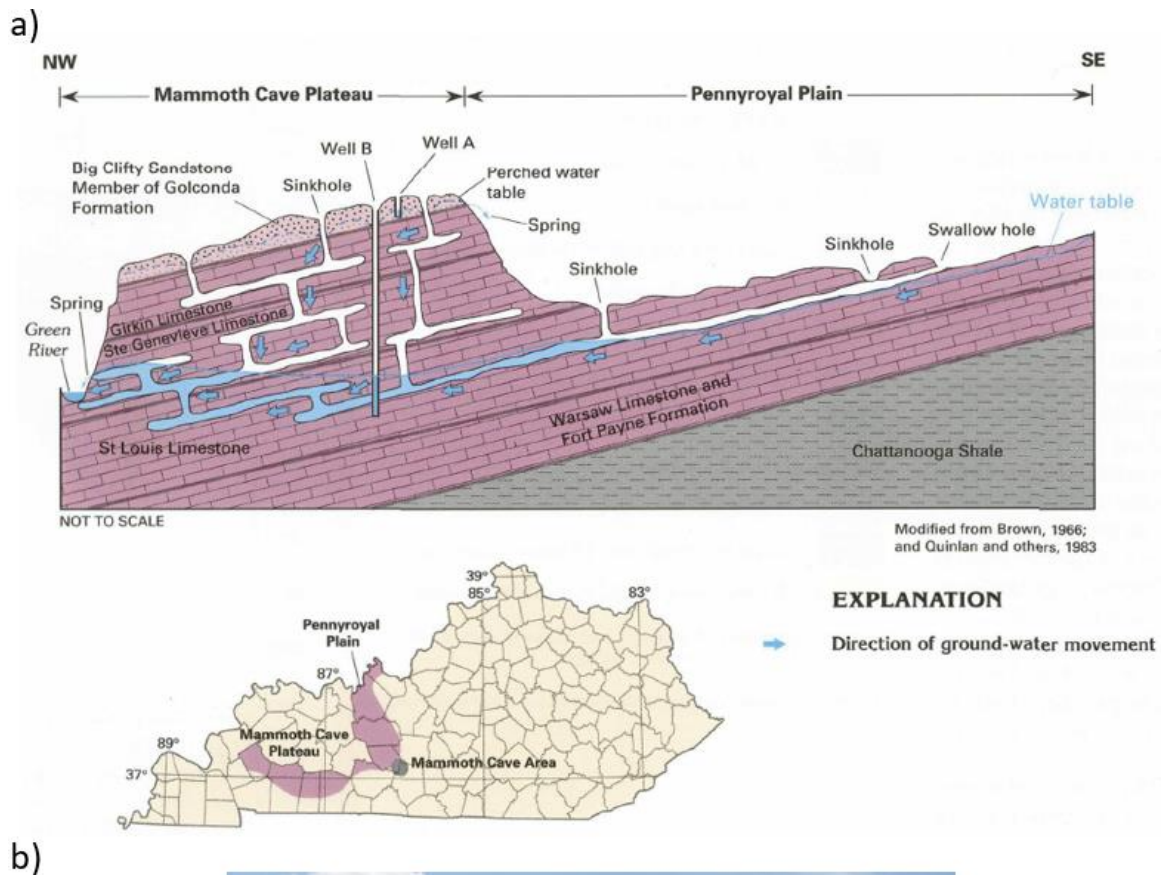
- (1) diffuse flow through soil or unconsolidated surface materials,
- (2) concentrated flow through solution-enlarged sinkhole drains,
- (3) diffuse percolation through vertical fractures, and
- (4) diffuse percolation through permeable rock matrix.

Subterranean conduits shown as solid black are filled with ground water. Vertical scale exaggerated. Modified by Gunn (1986), from as it appears in Taylor and Greene (2008).

### 3.2 Karst Occurrence where Soluble and Less Soluble Units Occur Together

Carbonate and evaporite rocks are sedimentary rocks that accumulate from shallow tidal flats to deep-water basins in coastal or marine environments. Because carbonates are a product of precipitation of limestone or biological activity rather than being a sediment that is transported from elsewhere, some carbonates can form far from a coastline such as a reef or atoll. Carbonates can form by calcite precipitation from inland waters into rocks called tufa. Often in coastal environments near large rivers where large quantities of sand and gravel are available, karst aquifer systems form within layered sequences of sandstones, mudstones, shales, and carbonates. Many major karst aquifer systems are composed of carbonate and sandstone or are adjacent to other aquifers composed of unconsolidated sediments. Where carbonate and sandstones are interbedded, the carbonate rocks generally yield more water than the sandstones.

If sandstones, shales, or less soluble and less permeable rock overlie the carbonates, they can form caprocks that protect the limestone beneath from dissolution and serve as an area of slow, diffuse recharge. The Mammoth Cave system is within a Mississippian age carbonate and sandstone aquifer. The sandstone caprock overlies the cavern system within the Mammoth Cave Plateau, which overlooks the dissolved limestone plain called the Pennyroyal Plain (Figure 10).

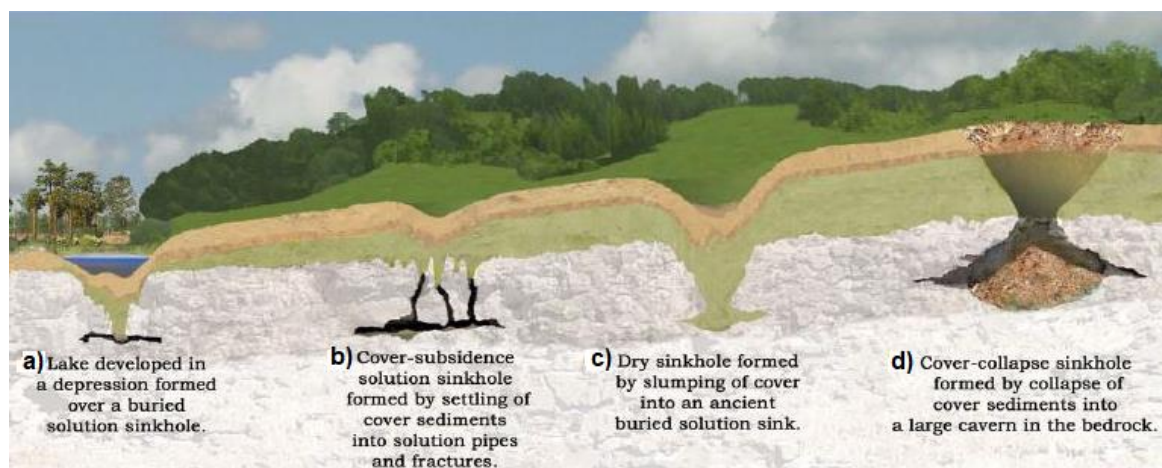


**Figure 10** - a) Karst aquifers commonly occur between strata of other types of sedimentary rocks such as sandstone and shale as shown in this cross-section from the Mammoth Cave Kentucky region. Large volumes of water move rapidly from sinkholes and swallow holes through a well-developed network of solution cavities in the St. Louis and Ste. Genevieve Limestones to discharge at springs or to the Green River. The openings were formed by dissolution of the limestones as water moved along bedding planes and fractures. The sandstone that remained intact protected the upper formations forming the Mammoth Cave Plateau. The Chattanooga Shale forms a confining unit below the Warsaw Limestone and Fort Payne Formation (Miller, 1999). b) East looking view of the Pennyroyal Plain from overlook on Mammoth Cave Plateau at Mammoth Cave National Park with Rick Toomey discussing hydrogeology of the area. Photograph by Kuniansky (2008b).

In some parts of the world sediments of gravel, sand, silt, and clay have been deposited on top of older karstified limestones and fill in the conduits. This occurs frequently in the confined parts of the Floridan aquifer system in peninsular Florida where in some cases the sediment plugs up all the older solution features and lakes form (Figure 11a), or the process is ongoing with sediments gradually filling in the solution features. In both cases, recharge occurs slowly as in a traditional porous media aquifer



(Figure 11b and c). The dangerous, rapid form of sinkhole collapse makes the news when there is a sudden cover-collapse sinkhole where the sediment falls into a large underground cavern within a period of hours or over several days (Figure 11d). In Canada and northern areas of the central United States, glaciers deposited sediment over many areas of limestones. When both the inlets and outlets of the conduits are clogged with sediment, the flow system reverts to behaving like a fractured-rock or granular flow system because there is no longer rapid inflow to and outflow from interconnected conduits. Sinkhole lakes in Canada and the northern United States are similar to the circular sinkhole lakes of Florida, but were filled in by glacial unconsolidated sediments rather than alluvial and coastal unconsolidated sediments.

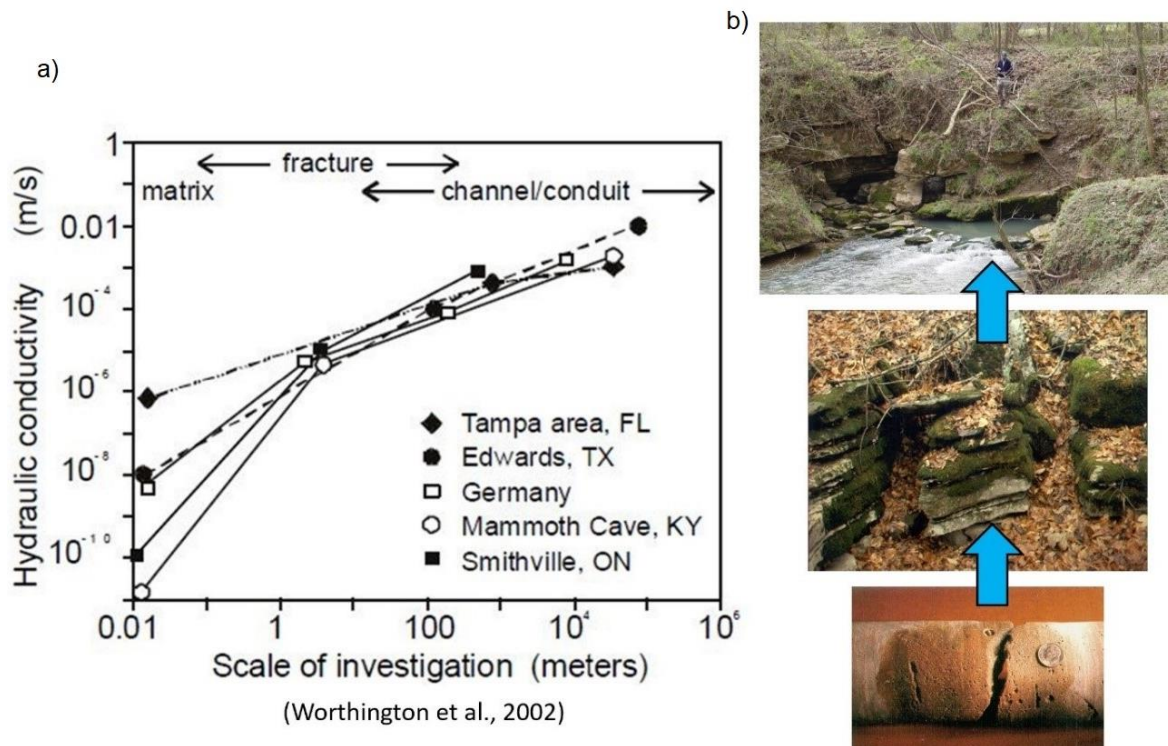


**Figure 11** - In some areas, historically exposed karst terrain has been covered with unconsolidated sediments that fill in the dissolution features: a) sediment infilling over a completely clogged sinkhole; b) sediment slowly settling into solution openings forming a gradual depression in land surface and plugging the karst, but not enough to create a lake; c) a dry depression where sediments have completely plugged the solution openings at an elevation where rainwater moves slowly into the subsurface; and d) a sudden cover-collapse sinkhole. All of these are typical types of sediment filled sinkholes in Florida. In Canada and the northern parts of the USA, unconsolidated sediments from glacial deposits overlie many older limestone systems and similar circular lake features occur. Modified from Rupert and Spencer (2004).


### 3.3 Multiple Porosity and Permeability Structure

Heterogeneities within an aquifer affect the timing, velocity, direction, and amount of groundwater transmitted through an aquifer. Therefore, one of the most important concepts in karst hydrogeology is the recognition of the spectrum of heterogeneity created by the existence of multiple, or more precisely triple, porosity and permeability components and their influence on the hydraulics and hydrologic behavior of the aquifer. The porosity and permeability structure of a karst aquifer include 1) matrix (intergranular), 2) fracture, and 3) solutional (conduit) components. For some karst aquifers, solutional components include macro-porosity features from biologic activity at the time of formation. This triple porosity structure is sometimes described as “nested hydraulic discontinuities”, with each component contributing its own range of hydraulic conductivities, groundwater flow velocities, storage, and residence times to a portion of the aquifer. This nested

structure is, in large part, the source of the “scaling effect” observed in hydraulic conductivity measurements (Halihan et al., 1999; 2000). The scaling effect is that different magnitudes of hydraulic conductivity are obtained when different volumes of the aquifer are sampled. Smaller samples of the aquifer generally include only matrix material. These samples have lower magnitude and a wider range of hydraulic conductivity values than larger samples that include fractures and conduits. The larger samples tend to have higher magnitude and a narrower range of hydraulic conductivity values (Figure 12).



**Figure 12** - a) Graph showing typical range in hydraulic conductivities measured in matrix, fracture, or conduit porosity components in various karst aquifers; and b) photographs depicting typical karst matrix, fracture and conduit permeability components to illustrate scale effect created by these “nested” hydraulic discontinuities. Photographs by Taylor (2021b).

[Exercise 3](#)  invites the reader to look up the definition of porosity, permeability, and hydraulic conductivity and describe how hydraulic conductivity is related to permeability and porosity.

The occurrence of turbulent flow is one of the identifying characteristics of a karst aquifer. The Reynolds number is used to indicate whether flow is laminar, turbulent or in the transition zone between the two regimes. Critical Reynolds numbers for turbulence can occur within fractures or conduit openings on the scale of millimeters given the normal range of flow velocities common in karstic bedrocks (White, 1988). Sections 4.1 and 4.2 of this book describe the Reynolds number and how this applies to karst aquifers.

Conduit permeability contributes to the highest equivalent hydraulic conductivities, fastest flow velocities, and shortest residence times, but conduits typically occupy a relatively small volume of the karst aquifer and contribute relatively little to the

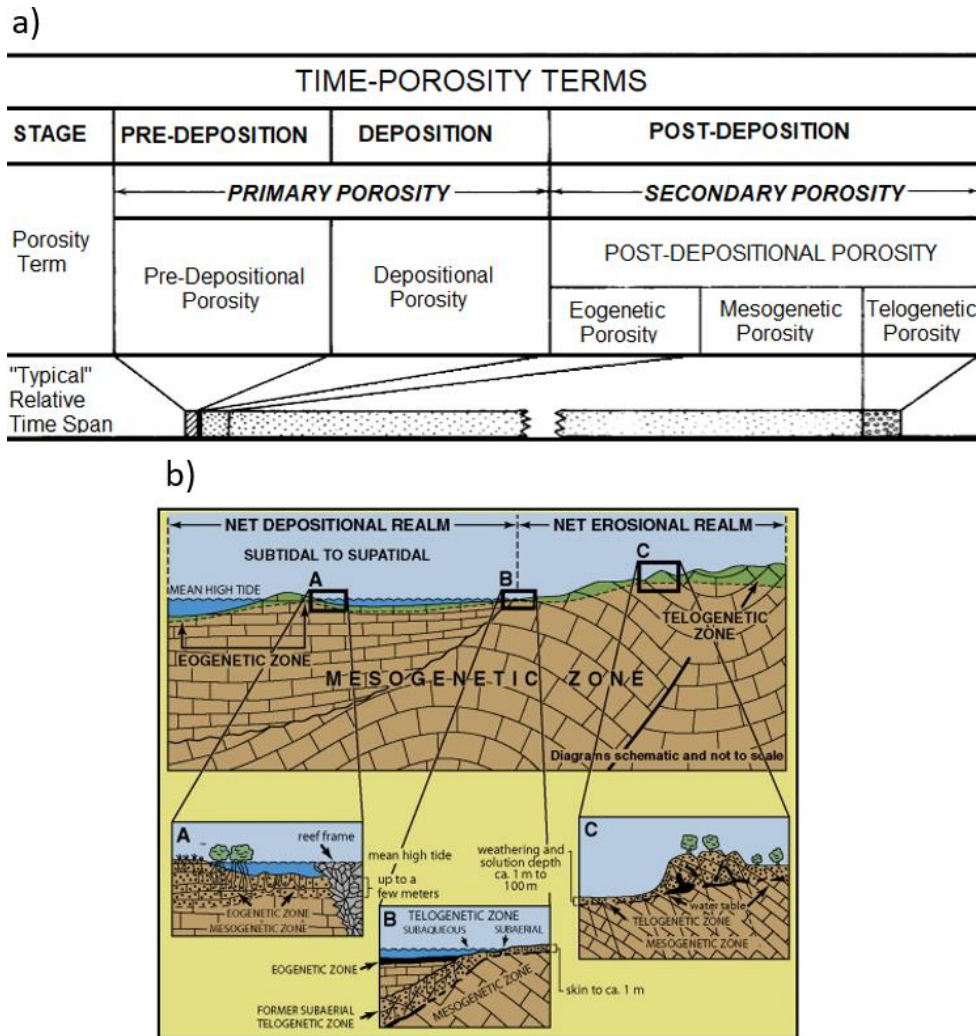
storage of groundwater (Worthington et al., 2000). Section 4 of this book discusses fluid mechanics providing a foundation for better understanding of the hydraulics of large flow features in karst.

Fractures might occupy a greater aquifer volume than conduits, but their contribution to aquifer hydraulic properties depends on their apertures, frequency, distribution, and especially their interconnection with each other, with sources of recharge, and with water stored in the matrix. Fractures that are not well interconnected hydraulically may store and yield groundwater to nearby conduits, but are not influential in transmission of groundwater throughout the aquifer. Poorly interconnected fractures may function as either low velocity or hydraulic “dead” zones with long groundwater residence times.

While intergranular matrix porosity and permeability constitutes the largest volumetric proportion of water in the aquifer, their hydraulic influence on aquifer properties is variable. Carbonate rocks undergo changes in porosity over time and under different conditions. Choquette and Pray (1970) subdivided temporal porosity changes of karst into three stages:

- *eogenetic* changes occurring at deposition and early exposure to the surface;
- *mesogenetic* changes that occur during deep burial; and,
- *telogenetic* changes occurring after the rock has been re-exposed and eroded.

Most karst aquifers occur near the land surface because near-surface processes create karst. Thus, typically karst aquifers are subdivided into *eogenetic* (generally composed of younger near surface carbonates) and *telogenetic karst aquifers* (generally composed of uplifted older carbonate rocks). Figure 13 diagrams *eogenetic*, *telogenetic*, and *mesogenetic* time-porosity zones.



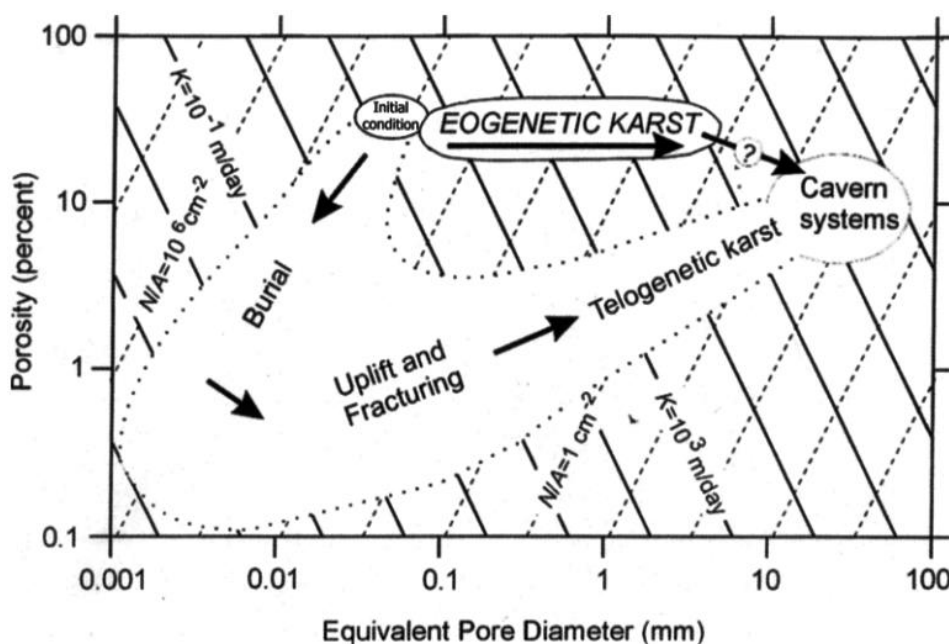
(modified from Choquette and Pray, 1970 and Moore and Wade, 2013)

**Figure 13** - Time-porosity terms and zones of creation and modification of porosity in sedimentary carbonates. a) Interrelation of major time-porosity terms. Primary porosity either originates at time of deposition (depositional porosity) or was present in particles before their final deposition (predepositional porosity). Secondary or postdepositional porosity originates after final deposition and is subdivided into eogenetic, mesogenetic, or telogenetic porosity depending on stage or burial zone in which it develops as shown in (b). The bar at the base of (a) depicts our concept of "typical" relative durations of stages. b) Schematic representation of major surface and burial zones in which porosity is created or modified. Two major surface realms are those of net deposition and net erosion. Upper cross section and enlarged diagrams A, B, and C depict three major postdepositional zones. The eogenetic zone extends from surface of newly deposited carbonate to depths where processes genetically related to surface become ineffective. The telogenetic zone extends from erosion surface to depths at which major surface-related erosional processes become ineffective. Below a subaerial erosion surface, the practical lower limit of telogenesis is at or near water table. The mesogenetic zone lies below major influences of processes operating at surface. The three terms also apply to time, processes, or features developed in respective zones. From Choquette and Pray (1970).

From field data collected over decades, karst hydrologists have begun to distinguish significant differences in the hydraulic characteristics of eogenetic and telogenetic karst aquifers because matrix porosity and permeability is reduced in the latter relative to the former due to increased diagenetic alteration usually associated with increased age and depth of burial (Florea and Vacher, 2006). For example, in the United States, the



geologically younger and less diagenetically altered Floridan aquifer in the coastal southeastern states of Florida and Georgia, and the Edwards Aquifer in Texas, exhibit greater overall matrix porosity and permeability compared to the older Paleozoic Mississippian karst aquifers in the mid-continental states of Kentucky and Tennessee. The range of matrix hydraulic conductivities, spanning several orders of magnitude, as shown in Figure 12, reflects the differences in hydraulic conductivity between eogenetic and telogenetic karst. The Tampa, Florida, and some of the Edwards Aquifer, Texas samples represent eogenetic karst while the Mammoth Cave, Kentucky and Smithville, Ontario, Canada samples represent telogenetic karst. In contrast, the range of hydraulic conductivity values depicted for fractures is greater than for conduits, but conduits have a far greater hydraulic conductivity overall than matrix or fracture porosity. Vacher and Mylorie (2002) developed a schematic diagram indicating the evolution of porosity and equivalent pore diameter for eogenetic to telogenetic karst; as porosity and pore diameters increase, hydraulic conductivity increases (Figure 14).

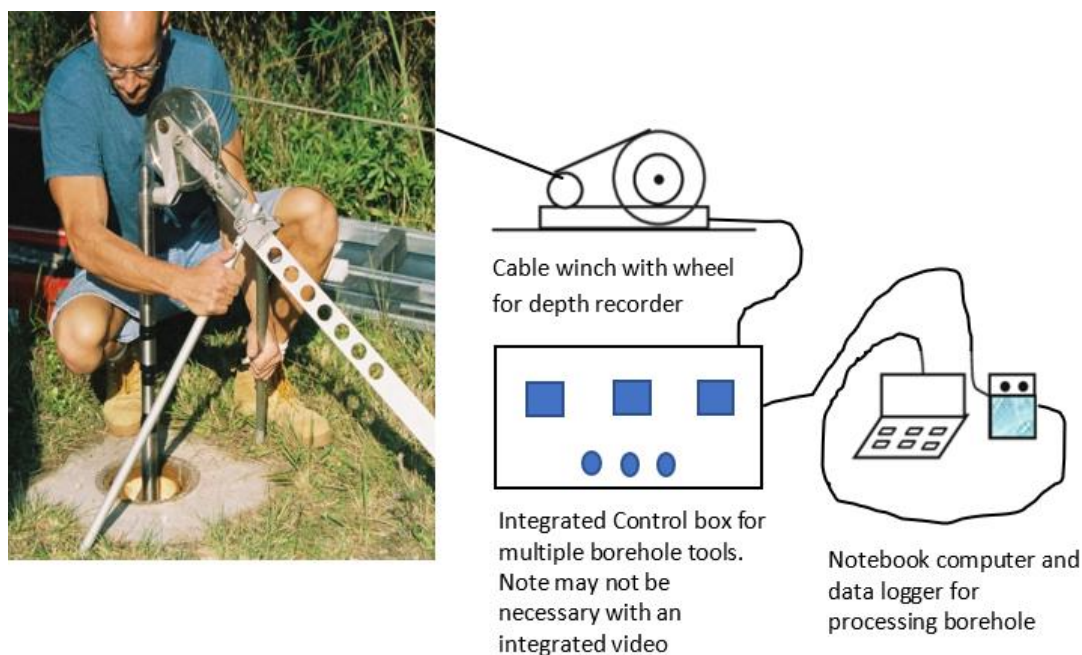


**Figure 14** - Schematic diagram showing the evolution of porosity and pore diameter with progression from eogenetic to telogenetic karst. As karst is buried, both porosity and pore size decrease. After uplift, fracturing and exposure to geochemically aggressive water, dissolution may create caverns within the telogenetic karst, increasing hydraulic conductivity,  $K$ . Modified from Vacher and Mylorie (2002).

In practical terms, eogenetic karst aquifers are generally capable of supporting larger and more reliable withdrawals of groundwater than telogenetic karst aquifers because of their greater accessible storage and interaction between matrix and conduits (Florea and Vacher, 2006). In contrast, the low matrix permeability of most telogenetic karst aquifers render the largest volume of the aquifer body essentially impermeable, with little to no groundwater held in storage in the matrix, and little to no hydraulic interaction between the matrix and fractures and conduits.

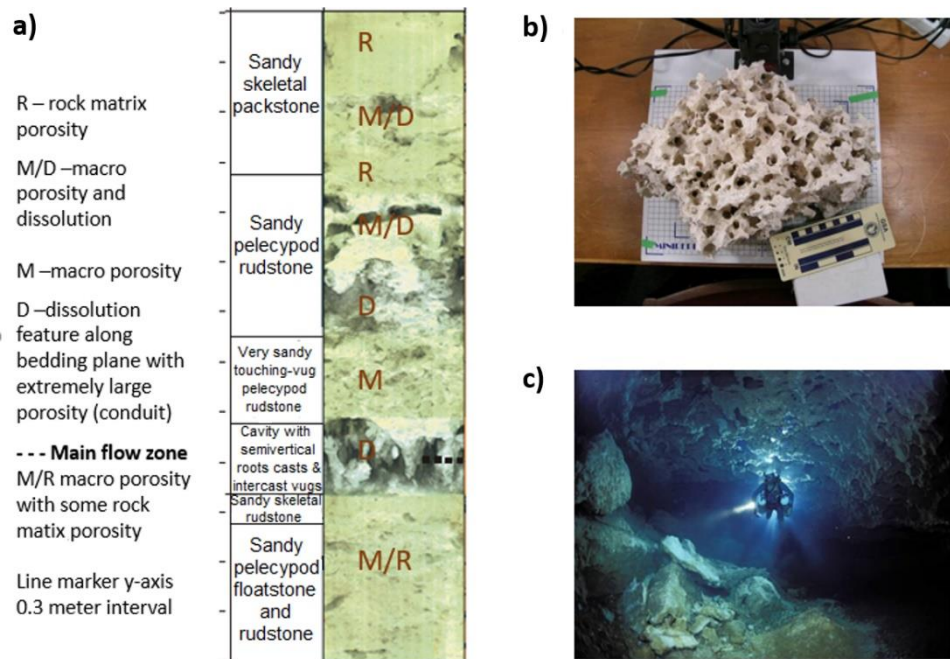
Aquifer heterogeneities and preferential flow can be extreme in telogenetic karst, whereas groundwater flow in eogenetic karst aquifers can approach that of granular aquifers although preferential flow paths and turbulent flow may exist in localized zones where conduits and solution-enhanced intergranular permeability are more pronounced. Groundwater occurrence within telogenetic karst is dominated almost entirely by flow through highly localized and preferential flow paths created by the integrated network of fracture and conduit components. Consequently, development of higher-yielding and reliable water supply wells will depend significantly on the ability to locate and successfully drill into interconnected, transmissive fractures and/or water-bearing conduits.

Some studies of karst aquifers include digital borehole images acquired by lowering a camera into a well (Figure 15) to create a video of either the borehole wall (side-looking camera) or a downhole view. Figure 16 shows porosity types from eogenetic karst aquifers in Florida and Figure 17 shows borehole images from a telogenetic karst aquifer.

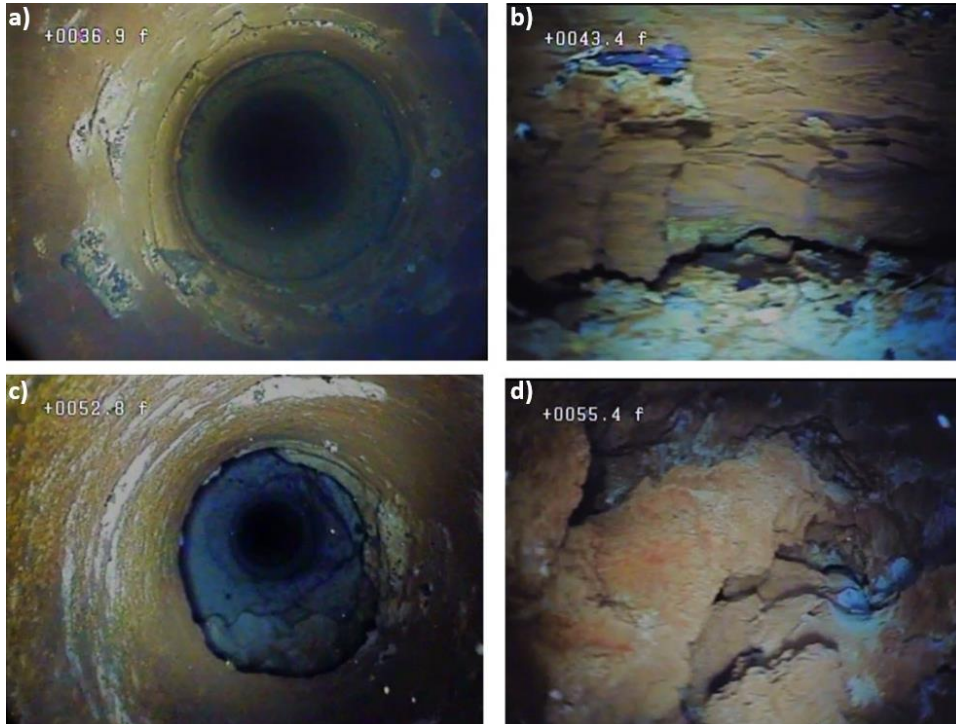


**Figure 15** - Photograph of borehole tool lowered from a tripod into the well taken near Miami, Florida, USA (photograph by Johnson (2008)). The technician sets the borehole tool, such that the depth of the information is set at zero for land surface and the depth below land surface is known from the amount of cable lowered down the well from a winch system that is either a dedicated device directly connected to a data logger and computer or part of a suite of borehole tools connected to a controller box that can support different communications cables and winch systems. The controller box connects different data loggers and computers to different borehole tools that employ different communication systems. The schematic shows possible configuration of equipment that might be in a borehole logging truck. Note it is critical to keep these cables from kinking as this can damage the signal. Additionally, a logging truck may have multiple winch systems as different borehole tools require different communications cables and data loggers. Geophysicists and their technicians generally have some good electronics repair skills along with computer technology skills for repairing cables and connections and electronic communications between devices in the field. For simple borehole video and less depth, plumbing inspection cameras work great and often are simple dedicated devices that record length of cable with the video and encode that length date and time on the video.





**Figure 16** - Illustration of porosity and permeability components in an eogenetic karst aquifer: a) digital borehole image from Biscayne Aquifer in southern Florida, USA showing multiple porosity types; b) sample of rock also from the Biscayne Aquifer showing macro porosity created by burrowing shrimp before the carbonate sediment solidified; and c) a scuba diver within a conduit in the Floridan aquifer that transmits water to Wakulla Springs near Tallahassee, Florida, USA. Photographs a and b by Cunningham (2008). Photograph c obtained from Suwanee River Water Management District (2008) and used with permission.





**Figure 17** - Borehole camera photographs illustrating permeability features typical of a telogenetic karst aquifer. a) Intergranular matrix porosity is essentially nonexistent in this Paleozoic limestone, and porosity and permeability are provided by solution-enhanced vugs (downhole view); b) and c) solution modified fractures and brecciated zones (b) side view and (c) downhole view); and d) conduit like voids (side view). Borehole diameter is approximately 8 inches (20.3 cm). Photographs by Taylor (2021c).


A complicating form of porosity is the macro porosity created by biological activity. Martin and Scream (2001) define three types of karst porosity: 1) intergranular matrix porosity, 2) fracture porosity, and 3) cavernous porosity (conduit porosity), but they define a two-component flow system because they include the smaller fracture porosity with intergranular porosity and larger fractures with cavernous porosity. However, the larger biogenic interconnected macro porosity units are considered a fourth form of porosity by Vacher and Mylroie (2002) and by Cunningham and others (2006), thus creating a triple porosity flow system.


The Edwards Aquifer and Biscayne Aquifer in south Florida have formations with macro porosity layers formed by burrowing animals along with larger conduit features (Figure 16). The Floridan aquifer occurs in rocks of Tertiary Period (approximately 66 to 2.6 million years ago) and are older than the Biscayne Aquifer that occurs in rocks of the Quaternary Period (2.6 million years ago to the present). Some of the large horizontal voids and higher-permeability, relatively-horizontal planar features in the Floridan aquifer may have been burrowed units in pure limestone. In the younger Biscayne limestone, interconnected shrimp burrows have not had time to dissolve into large horizontal openings although, as revealed in Figure 16, larger openings are beginning to form in some of these layers (Cunningham and Aviantara, 2001). The Edwards Aquifer (in rocks of the lower Cretaceous 145 to 100 million years ago) in Texas contains mudstone units that do not dissolve readily so the small, interconnected, biologically-formed, macro porosity remains intact and this zone was named the burrowed unit by Rose (1972). These burrowed units of macro pores can be found in older and younger rocks because the burrows form at the time of deposition. Depending on the amount of clay, sand, and dolomite, these burrowed units may retain their void shape regardless of exposure (telogenetic or eogenetic karst). These units have large water transmitting properties and are considered preferential flow layers because typically they are laterally extensive layers within the carbonate rock strata. Additionally, in buried burrowed units of pure limestone, the voids left by biological activity may be infilled with clastic materials that become cemented and do not dissolve, while the surrounding limestone disappears over time. These casts remain, also creating a layer of macro porosity.

Figure 16 and Figure 17 reveal a huge range in water transmitting properties of the relatively horizontal layers shown in the borehole images of the carbonate aquifers. It is not uncommon for *hydraulic conductivity* to range over 5 orders of magnitude in karst systems.

[Exercise 4](#)  invites the reader to download materials showing borehole images and compare the character of the dissolution features.

[Exercise 5](#)  illustrates how hydraulic conductivity contrasts between layers effects flow parallel to (that is, horizontal flow if layers are relatively flat) or perpendicular to (that is, vertical flow in relatively flat layers) layers of contrasting hydraulic conductivity, thus has a significant influence on the magnitude of flow in horizontal and vertical direction.

[Exercise 6](#)  invites the reader to explore how the scale of heterogeneity effects advective transport in aquifers.

[Exercise 7](#)  invites the reader to consider the difference between hydraulic conductivity ( $K$ ) and intrinsic permeability ( $k$ ).

### 3.4 Variance in Surface-Water and Spring Discharge in Karst Aquifers

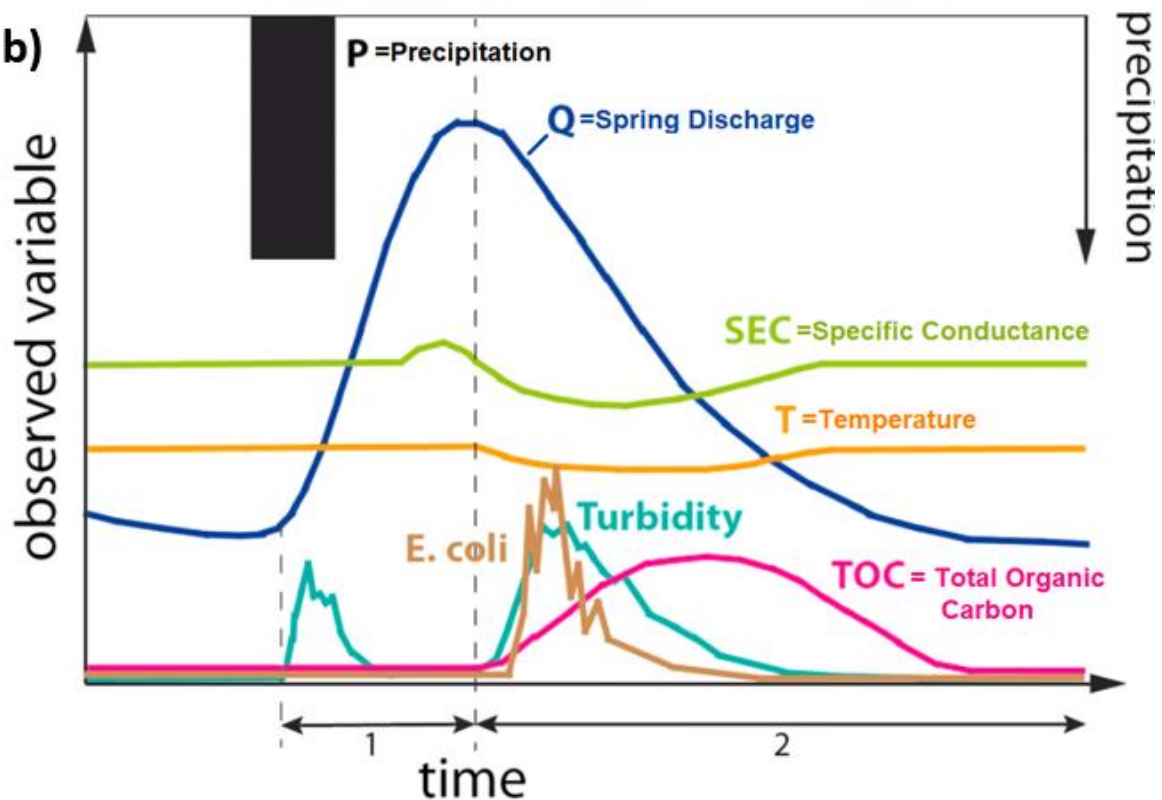
Spring discharge monitoring is one of the most insightful tools used by karst hydrogeologists. Monitoring of variability of spring flow (discharge) and selected water-quality characteristics such as water temperature, pH, specific conductance, and turbidity, provides much of the most useful and important information about the hydrologic characteristics and internal functioning of karst aquifers that can be acquired by field studies (Taylor and Greene, 2008). Modern technological advancements in electronic sensing probes and data-logging equipment have greatly aided and simplified the collection of continuous spring discharge data (Figure 18). Analysis of continuous, high-frequency (short-intervals between individual measurements) spring discharge and water-quality data provides amazing insight into karst aquifer recharge, storage, and discharge functions, and how these change under short-term specific storm events. Long-term continuous monitoring and analysis is used for understanding seasonal changes in weather and annual-to-decadal climate change. A great variety of analytical methods have been devised and used in the analysis of *hydrograph* plots of spring discharge characteristics. Analyses of peak flow and discharge recession has long been used to assess water-supply potential and sustainability, and to attempt to evaluate the relative contributions of water stored in karst matrix or fracture networks versus water transmitted through conduits. Because of the number and diversity of methods and publications that have been devoted to these topics over many decades, a more detailed and comprehensive review of spring discharge analysis is beyond the scope of this introductory book. Summaries provided by Taylor and Greene (2008) and Goldscheider and Drew (2007), and textbooks by Kresic (2007), Milanovic (1981), and Stevanovic (2015) contain more detailed information.



a)



b)

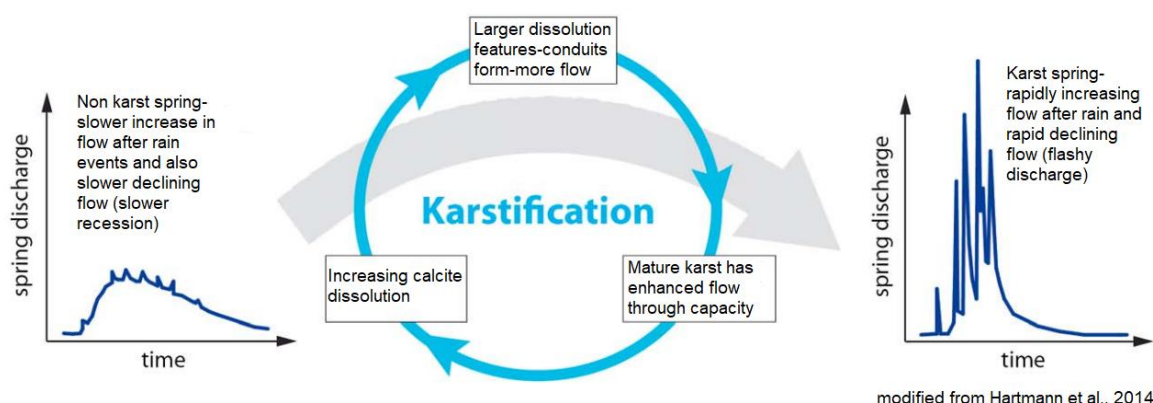


(modified from Hartmann et al., 2014)

**Figure 18** - Deployment of continuous multi-parameter probes and data-logging equipment at karst spring sites is one of the most useful investigative tools available in the study of karst aquifers. a) Charles Taylor inspecting a multi-parameter water quality sonde at a karst spring (photo provided by Taylor, Kentucky Geological Survey, 2021). b) Example of hydrograph plotting of continuous discharge and water-quality data collected from a karst spring, showing trends and relationships between discharge or flow (Q), specific conductance (SEC), water temperature (T), turbidity, total organic carbon (TOC), and bacterial counts (*E. coli*), following a storm event (denoted by precipitation (P)). Modified from Hartmann and others (2014).

Variability in discharge and water-quality hydrograph plots from continuously monitored springs generally falls between two end members described by the terms “diffuse or slow flow” and “conduit or rapid flow”. Rapid, high-amplitude changes, sometimes described as “flashiness”, in discharge and water chemistry parameters such as

turbidity, pH, temperature, or specific conductance have been interpreted as representing a karst aquifer system dominated by conduit flow, whereas gradual, buffered or muted patterns of change are interpreted as indicating dominance of diffuse, non-conduit flow. Most karst aquifers possess a combination of slow-velocity (diffuse) and rapid velocity (conduit) permeability components. Consequently, patterns in hydrochemistry and/or discharge hydrographs, and *hysteresis* plots sampled across storm events (during rise, peak, and recession periods) are best interpreted as reflecting temporal changes caused by changes in timing, proportions, and mixing of recharge contributed from matrix, fracture, and conduit sources. The water fluxes that generate these changes are head dependent and often driven by recharge events (Figure 19).

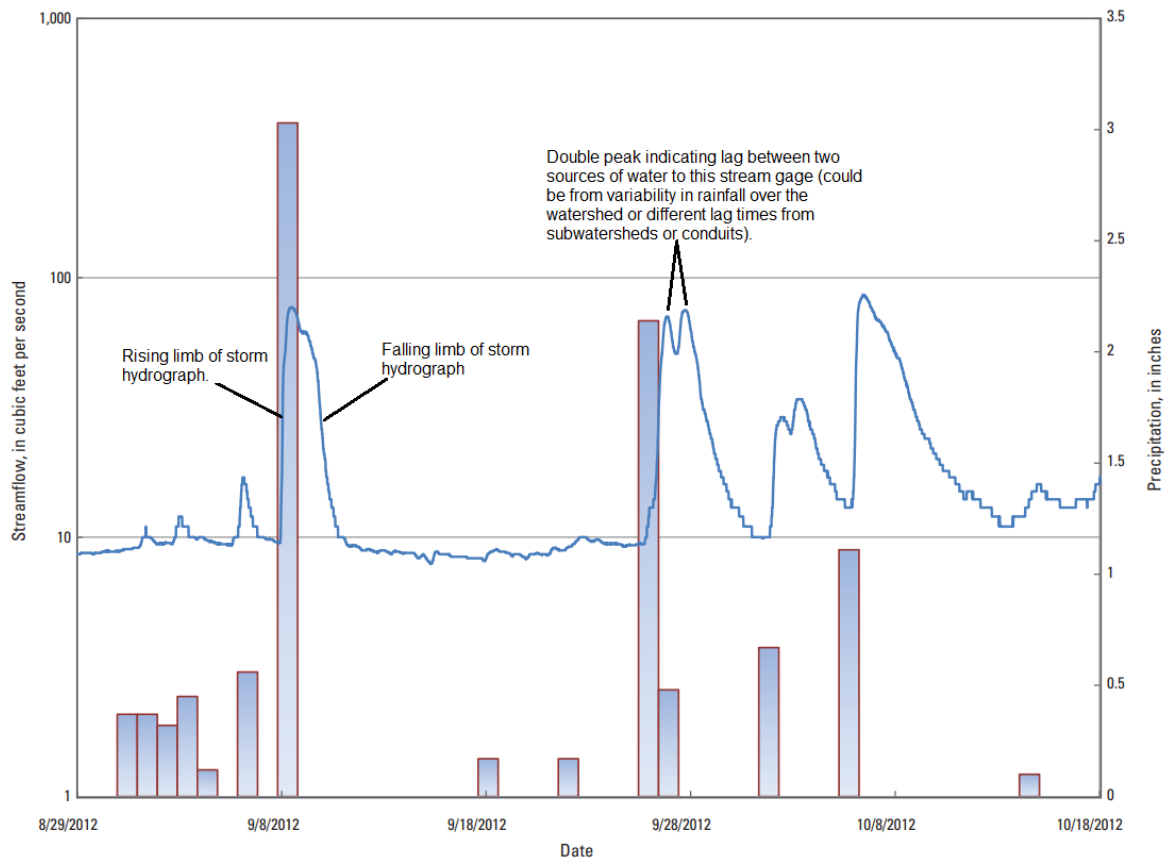


**Figure 19** - Generic example of the spring discharge behavior from a non karst spring and a mature karst spring. Non karst springs have slower rise and fall in discharge from rain events. A mature karst spring is flashy owing to the rapid movement of rainwater underground through large dissolution features to the spring and into surface streams.

Groundwater and surface-water are almost inseparable in a well-developed karst watershed. The streamflow gaging station for the Orangeville Rise in Indiana, USA, provides an example of a streamflow hydrograph that represents a stream predominantly fed by karst conduits (Figure 20). With the 15-minute unit-value stream discharge data plotted with the daily precipitation the very short time lag between storm event and the peak discharge indicates rapid flow to the gage through conduits. Additionally, for some storm events, a double peak indicates two distinct sources of discharge with differing lag times from the storm to the peak discharge. These double peaks show that the two sources of rapid flow from a storm event are out of phase. These out of phase peaks require further investigation as they could be the result of uneven rain distribution over various sub watersheds, differing antecedent conditions resulting in water moving in different elevation conduit systems, or water moving from sub watersheds with different times of travel. The lag times for the peaks varies from storm to storm and may also be influenced by antecedent conditions, such as, activation of a higher elevation conduit system (overflow conduits). For the hydrograph of Figure 19, it appears that the velocity of diffuse flow (water moving slowly through the system) is approximately 9 to 20 ft<sup>3</sup>/s (cubic feet per

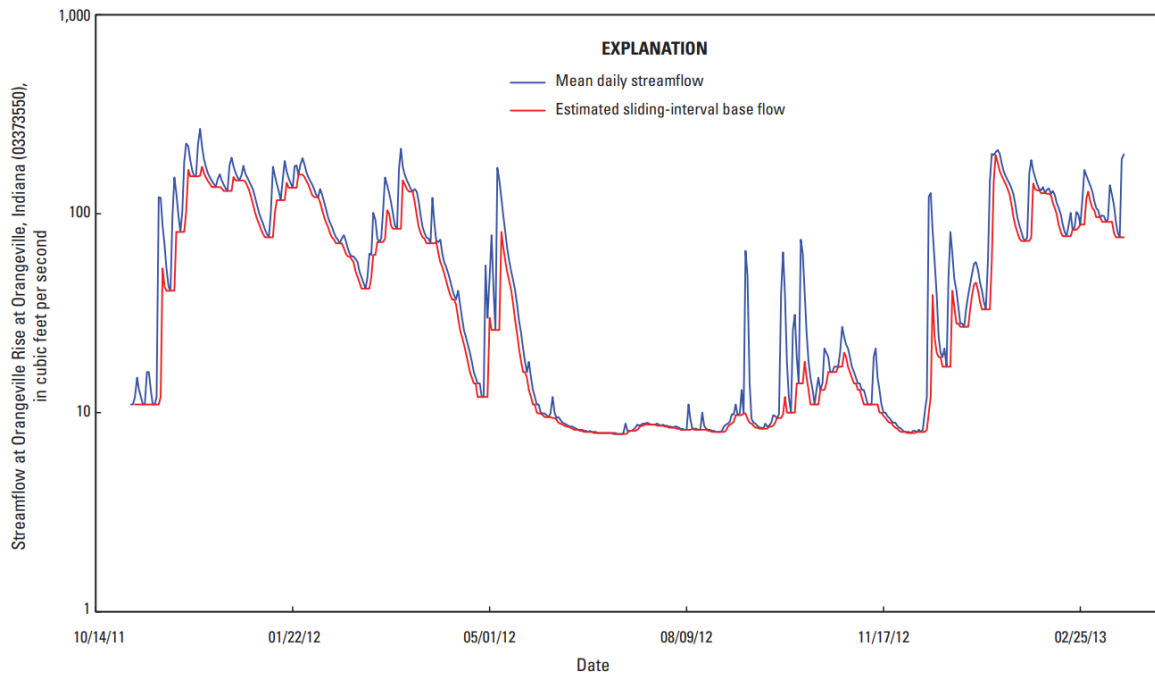


second) ( $\sim 0.3$  to  $0.6 \text{ m}^3/\text{s}$ ) based on the horizontal portion of the hydrograph between storm events. The streamflow is also dependent on antecedent conditions.



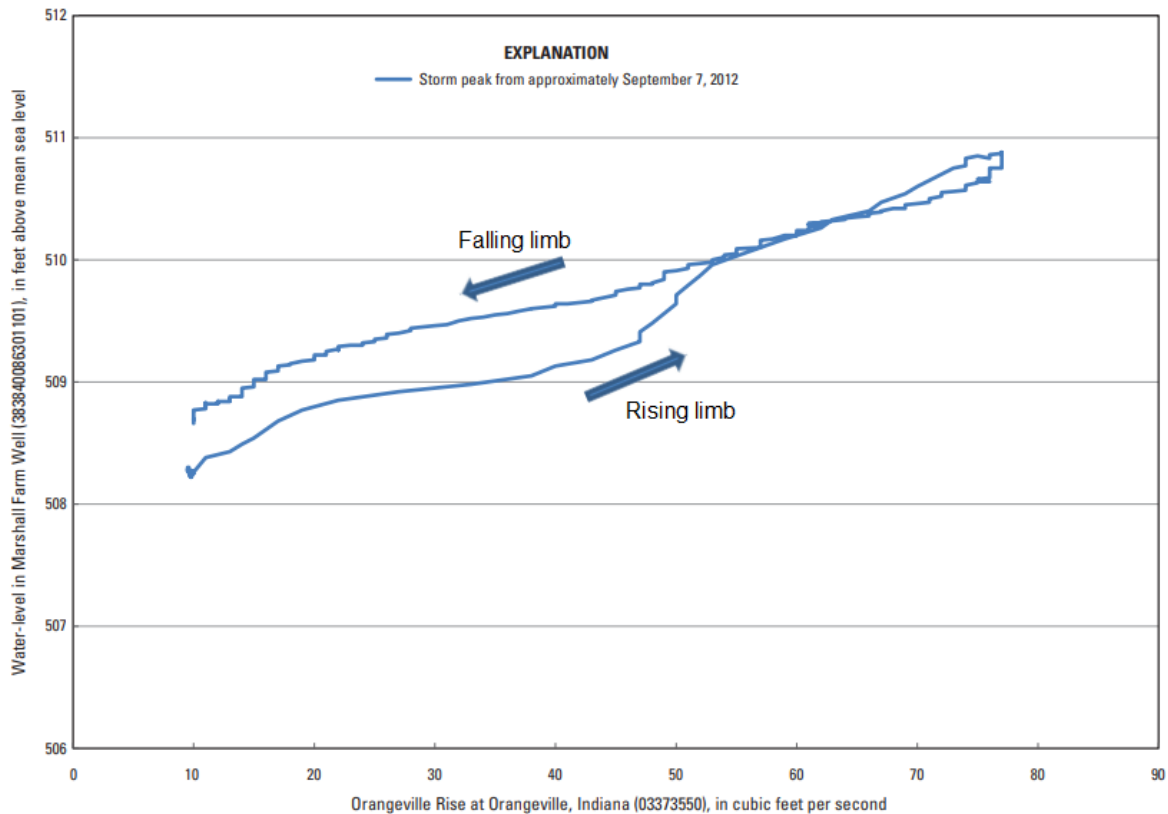
**Figure 20** - Daily precipitation (vertical bars) and 15-minute unit-value stream discharge data for U.S. Geological Survey streamflow-gaging station 03373550 (Orangeville Rise at Orangeville, Indiana, USA), showing double-peak nature of storm peaks and the lag time between rainfall and discharge from the spring. Modified from Bayless and others (2014).

Hydrograph separation is a method by which overland runoff is separated from stream base flow. Base flow can be dominated by groundwater discharge; however, watersheds vary, and base flow can have contributions from bank storage, or slow snow melt, or in flat terrain very slow surface-water drainage, thus may not be predominantly groundwater discharge. Continuous monitoring of discharge at the spring itself is best but not always possible. At the Orangeville Rise gage, daily streamflow hydrographs were processed using an automated hydrograph separation program with the assumption that most of the base flow is groundwater discharge from the karst basin (Figure 21). The daily streamflow hydrograph at Orangeville Rise does not exhibit double peaks as are visible in the 15-minute unit-value discharge data. Use of graphical hydrograph separation methods to estimate groundwater discharge is greatly improved by using water quality data as demonstrated in Section 5.5 of this book. The Orangeville Rise stream gage is within a well-developed karst area where base flow represents between 53 to 98 percent of the flow as estimated using monthly data for station 03373550 (Orangeville Rise at Orangeville, Indiana), November 1, 2011 to February 28, 2013 (Bayless et al., 2014, Table 8).



**Figure 21** - Estimated base flow, following Sloto and Crouse (1996, page 4), for U.S. Geological Survey streamflow-gaging station 03373550 (Orangeville Rise at Orangeville, Indiana), November 1, 2011 to February 28, 2013. From Bayless and others (2014).

The Indiana study site provides an example of hysteresis. For this example, a plot of water level in a well in the basin versus 15-minute discharge data for a storm event at the Orangeville Rise gage indicates a looping pattern (Figure 22). The hysteresis plot is created by plotting the pairs of unit values and connecting these as a line between adjacent points in time and noting the rising limb and falling limb of the stream gage hydrograph. As streamflow increases on the rising limb, the groundwater level also rises. The graph line created by this time series loops over itself and the falling limb of the graph line is above the rising limb line with groundwater level on the y-axis and stream discharge on the x-axis (both linear axes). This indicates that the groundwater level peak lags behind the streamflow peak. The analysis of data for Orangeville Rise gage, shows how examination of 15-minute discharge data indicates possible networks of conduits at different elevations and the flashiness of base flow indicates multiple porosity within the karst aquifer.



**Figure 22** - Fifteen-minute unit-value water levels in the Marshall Farm Well, Indiana (383840086301101), versus 15-minute unit-value streamflow from the Orangeville Rise, Indiana gage station (03373550), showing a counterclockwise hysteresis that is indicative of the groundwater peak lagging slightly behind the surface-water peak for a storm peak starting on September 7, 2012. From Bayless and others (2014).

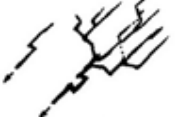









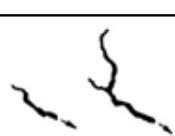

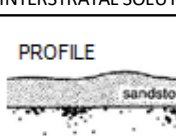
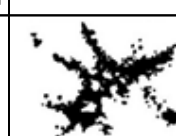
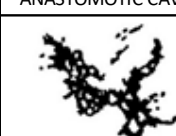
Wong and others (2012) report that telogenetic karst systems tend to reflect flow through the conduit networks and fractures with flashy spring discharge as there is little flow or storage in the rock matrix. Whereas in eogenetic karst systems, which tend to have some storage and interconnected voids in the rock matrix, the spring discharge can be dampened by this storage. Florea and Vacher (2006) note several significant differences in apparent hydraulic/hydrologic behavior between eogenetic and telogenetic karst aquifer types:

- the flashiness or ratio of maximum to mean ( $Q_{\max}/Q_{\text{mean}}$ ) discharge is smaller in springs of eogenetic karst than springs of telogenetic karst;
- aquifer inertia (system memory) is larger in eogenetic karst because:
  - eogenetic karst aquifers have a buffered or longer response time to recharge inputs; and,
  - high-frequency storm events affect discharge less in eogenetic karst, basically reflecting differences in interaction between the matrix and conduits because of differences in matrix porosity and permeability between eogenetic and telogenetic karsts.

### 3.5 Conduit Drainage Patterns

Speleogenesis, the origin and development of caves and by extension karst conduits, is a dynamic hydrogeologic process and is the primary mechanism by which conduit flow systems evolve and acquire more “karstic” characteristics and complex organization (Klimchouk, 2015). Speleogenesis results in the most universally-recognized feature of karst aquifers—the networks of linked underground conduits that meander among bedding units, join as tributaries, and increase in size and order in the downstream direction (Palmer, 1991). Conduits act as master drains for a karst aquifer and do not form at random but rather form along groundwater paths of greatest discharge and solutional aggressiveness (Palmer, 1991). Thrailkill (1968) suggested that conduit development is most active in the mixing zone created at or near the water table (the unsaturated/saturated interface). Palmer states that *“Solutional caves form where there is enough subsurface water flow to remove dissolved bedrock and keep undersaturated water in contact with the soluble walls. This is possible only where a pre-existing network of integrated openings connects the recharge and discharge areas.”* Bakalowicz (2005) theorizes that conduit formation is often initiated by, and approximately follows, the pattern created by existing fractures. He envisions that hydraulic conductivity increases as a result of hydraulic and geochemical feedback between flow through the larger, more permeable fractures and the upper, near-surface, densely fractured, permeable part of the bedrock mass.

The geospatial pattern of conduit network formation may be extremely complex in plan-view and in three dimensions, influenced by stratigraphy and geological structure, as well as by locations of recharge. Common cave network patterns, shown in Figure 23 include branching-dendritic, which in plan-view resembles surface stream tributary systems; network or anastomotic mazes, often prevalent in karst aquifers with extensive fracture permeability and frequent episodic low-velocity flooding, respectively; and spongework, typical of eogenetic karst aquifers dominated by extensive matrix permeability. As described by Palmer (1991), *“Their patterns depend on the mode of groundwater recharge. Sinkhole recharge forms branching caves with tributaries that join downstream as higher-order passages. Maze caves form where (1) steep gradients and great undersaturation allow many alternate paths to enlarge at similar rates or (2) discharge or renewal of undersaturation is uniform along many alternate routes. Flood water can form angular networks in fractured rock, anastomotic mazes along low-angle partings, or spongework where intergranular pores are dominant. Diffuse recharge also forms networks and spongework, often aided by mixing of chemically different waters. Ramiform caves, with sequential outward branches, are formed mainly by rising thermal or H<sub>2</sub>S-rich water.”*

		TYPES OF RECHARGE				
		VIA KARST DEPRESSIONS		DIFFUSE		HYPOGENIC
		SINKHOLES (LIMITED DISCHARGE FLUCTUATIONS)	SINKING STREAMS (GREAT DISCHARGE FLUCTUATIONS)	THROUGH SANDSTONE	INTO POROUS SOLUBLE ROCK	DISSOLUTION BY ACIDS OF DEEP-SEATED SOURCE OR BY COOLING OF THERMAL WATER
		BRANCHWORKS (USUALLY SEVERAL LEVELS) & SINGLE PASSAGES	SINGLE PASSAGES AND CRUDE BRANCHWORKS USUALLY WITH THE FOLLOWING FEATURES SUPERIMPOSED	MOST CAVES ENLARGED FURTHER BY RECHARGE FROM OTHER SOURCES	MOST CAVES FORMED BY MIXING AT DEPTH	
DOMINANT TYPE OF POROSITY	FRACTURES					
		ANGULAR PASSAGES	FISSURES IRREGULAR NETWORKS	FISSURES NETWORKS	ISOLATED FISSURES AND RUDIMENTARY NETWORKS	NETWORKS SINGLE PASSAGES FISSURES
	BEDDING PARTINGS					
		CURVILINEAR PASSAGES	ANASTOMOSES, ANASTOMOTIC MAZES	SHAFT AND CANYON COMPLEXES, INTERSTRATAL SOLUTION	SPONGEWORK	RAMIFORM CAVES RARE SINGLE PASSAGE AND ANASTOMOTIC CAVES
	INTERGRANULAR					
		RUDIMENTARY BRANCHWORKS	SPONGEWORK	RUDEMENTARY SPONGEWORK	SPONGEWORK	RAMIFORM & SPONGEWORK CAVES

**Figure 23** - Common cave network patterns and their relationship to different types of recharge (in plan-view unless specified as profile) and generalized to represent typical caves in each category. From Palmer (1991).

Stratigraphic contacts and the relative position and stability of the water table influence lateral distribution of conduit development. In carbonate rock sequences, individual stratigraphic units may contain considerable amounts of non-soluble, erosion-resistant siliceous mineral, particularly chert, or relatively less soluble dolomite and mudstones. These strata may act as bounding units that confine conduit and sinkhole development to one or more distinctive horizons (Figure 24).





**Figure 24** - Example of stratigraphic control on sinkhole and conduit development as seen in Silurian-Devonian carbonates exposed in a roadcut outcrop near Louisville, Kentucky, USA. Note the enlarged bedding-plane fracture, horizontal plane of conduit development, and termination of sinkhole drains. The karst features are formed in coarse-grained dolomitic limestone that overlies less soluble and finer-grained cherty limestones. Photograph by Taylor (2021d).

Multilevel conduit networks are typical of karst terranes where the base-level of main surface streams is actively or episodically lowered due to stream downcutting in response to tectonic uplift, isostatic (glacial) rebound, or other causes. Multiple levels of formerly active higher-elevation conduits may be preserved, especially if protected from erosion under non-karstic caprock, as for example demonstrated in the internationally renowned Mammoth Cave-Flint Ridge Cave system in central Kentucky (USA), where several levels of horizontally extensive conduit networks are preserved under overlying sandstone conglomeratic caprock. In such multilevel conduit systems, the high-level conduits may be dry and part of the vadose-conduit zone as depicted in Figure 6, or, if they are located at elevations within the range of fluctuation of the water table, they may be reactivated as overflow routes.

The size and shape of individual conduits or conduit segments are likewise influenced by lithologic, stratigraphic, and structural conditions, as well as hydrologic conditions that occurred both when the conduit development was initiated and subsequently. Klimchouk (2015) states *“Passages influenced by bedding-plane partings are sinuous and curvilinear ... Closely spaced joints within favorable beds may produce a similar pattern (Powell, 1976). Solutionally enlarged joints and high-angle faults tend to produce fissure-like passages with lenticular cross sections and angular intersections. Where joints are prominent, they can determine the pattern of nearly every passage in a cave ... Faults usually exert only local control of cave passages and determine the overall trend of relatively few caves (Kastning, 1977).*

*Intergranular pores are significant to cave origin only in reef limestones and poorly lithified carbonates."*

Again, quoting Palmer (1991) and noting his use of the term phreatic refers to the saturated zone: *"Phreatic passages originate along routes of greatest hydraulic efficiency (least expenditure of head per unit discharge). Such a passage enlarges solutionally over its entire perimeter and usually acquires a rounded or lenticular cross section. Most are tubular passages ... although some phreatic caves are irregular and room-like ... A passage along the water table may be water filled only during high flow and still meet the criteria for phreatic origin ... Passages of vadose origin are formed by gravitational flow and trend continuously downward along the steepest available openings ... Most vadose passages are canyon-like with floors entrenched below the initial route by free-surface streams ... They may be tubular where entrenchment is limited by resistant beds or insufficient time. Water descending vertically along a fracture or a cluster of intersecting fractures may form a shaft, a well-like void with nearly vertical walls ... A typical vadose passage consists of inclined canyons or tubes interrupted in places by shafts."* Examples of a tubular and a canyon-like conduit passage are provided in Figure 25 and Figure 26, respectively.



**Figure 25** - Example of slightly curving elliptical tube conduit typical of formation at a bedding plane contact and at or below the water table from Rumbling Falls Cave, Van Buren County, Tennessee, USA. Photograph courtesy of Christopher Anderson, [Darklight Imagery](#)<sup>↗</sup>, used with permission. The photo shows a large deposit of sediment on the right bank.





**Figure 26** - Canyon-like conduit passage, created by downcutting of cave stream, and illustrating the irregular profile of sidewalls created by stratigraphic variability in lithology and resistance to dissolution and erosion at Webster Cave Complex, Breckinridge County, Tennessee, USA. Photograph courtesy of Christopher Anderson, [Darklight Imagery](#), used with permission.

Depending on their diameters (that is, their hydraulic capacities) and organization (interconnection), conduit networks are capable of discharging large volumes of water and sediment rapidly through a karst aquifer (White, 1993). Flow velocities in well-developed and well-integrated conduit networks that range on the order of 100's to 1000's of feet per day (10's to 100's of meters per day) are not uncommon (White, 1988). *"Sediment loads discharged by karst aquifers is a largely unrecognized and unappreciated process. Huge volumes of sediment are mobilized and transported in many karst conduits during and after storms when turbulent flow exceeds the critical shear stress of sediments. The mobilization and deposition of sediments in karst aquifers often affects the quality of karst groundwater resources and may have significant influence on transport and fate of subsurface contaminants."*

Flow discontinuities that occur within or between conduits, or between conduits of the unsaturated and the saturated zones, is an under-recognized characteristic of karst aquifers that differentiates them from other aquifer types. Horizontal discontinuities (for example, breaks in flow manifested as waterfalls or cascades) are common within and between horizontal conduit segments where flow is perched by a resistant or insoluble bed (chert for example). Vertical flow discontinuities are commonly observed as seeps and drips from fractures and permeable zones in conduit passage roofs, and as waterfalls or laminar sheet-flows on the walls in shafts and domes (Figure 27).

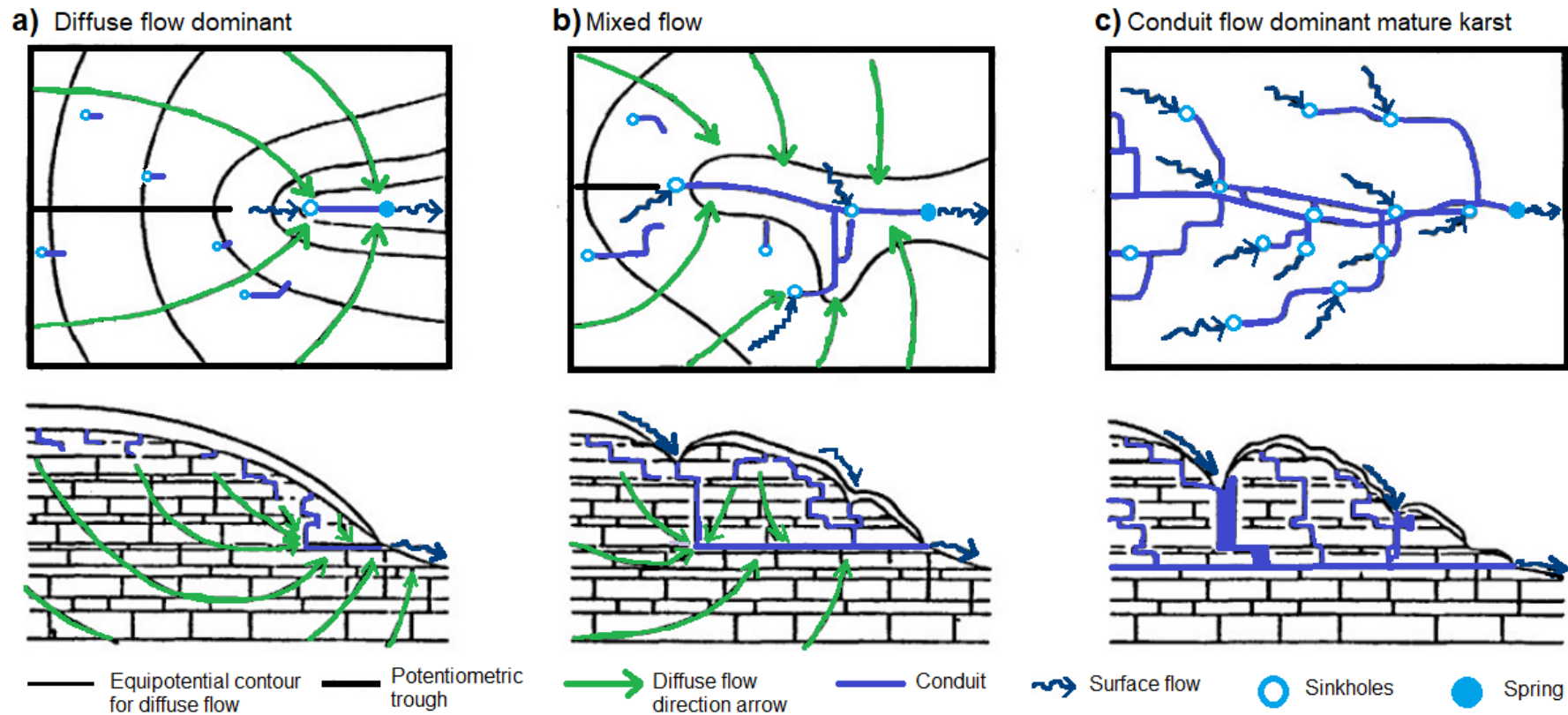


**Figure 27** - Examples of common types of flow discontinuity in conduits: a) waterfall at junction between two levels of conduits (upper level perched on resistant bed at Hawkins River, Mammoth Cave, Edmondson County, Kentucky, USA); b) waterfall in canyonlike conduit passage; c) vertical shaft, open to surface runoff. The glistening, moist sidewalls are indicative of laminar sheet flow in the shaft at Freeman's Pit, Indiana, USA). The vertical grooves and flutes in sidewalls of the canyon b) and shaft c) indicate preferential dissolution and erosion by vertical flow. Photographs courtesy of Christopher Anderson, [Darklight Imagery](#)<sup>7</sup>, used with permission.

### 3.6 Subsurface Piracy and Karst Drainage Basins

The conduit networks of many karst aquifers are characterized by a hierarchical tributary pattern of underground drainage. In simple terms, these conduit networks develop and continuously evolve by a process of subsurface piracy. The growth and propagation of conduits occurs by way of a complex flow-and-dissolution feedback mechanism. The larger initial conduit flow paths, having greater hydraulic capacity, develop preferentially and enlarge most rapidly. The largest conduits act as master drains that create localized zones of greater discharge and lower hydraulic head in the aquifer. Consequently, this alters the hydraulic flow field (changes the hydraulic heads) so as to increasingly capture ground water from the surrounding aquifer matrix, fractures, and smaller nearby conduits (Palmer, 1991, 1999; White and White, 1989). As the process continues over geological time with hydraulic gradients continually changing, discrete conduit flow paths link together. The larger, more efficient conduits capture flow from nearby incipient and developed small conduits and enhanced fractures, forming the characteristic branching drainage networks that converge in the downgradient direction, diverging and propagating in the headward (upgradient) direction (Figure 28).





**Figure 28** - Diagrams showing plan view (top panel) and cross-sectional view (bottom panel) of hypothetical stages in conduit network development by the alteration of hydraulic gradients and subsurface conduit piracy. Open light blue circles indicate sinkholes where water is recharged. Lines extending from them represent the beginning formation of conduits along fractures. Filled light blue circles are springs where water is discharged. Wavy dark blue lines are surface streams. Heavy purple lines are conduits. For diffuse flow, the thin black lines are equipotential contours of a typical potentiometric map and the thick black line is the groundwater trough. a) Early-stage development with one master conduit connecting drainage from a surface stream into a sinkhole to the discharge from a karst spring with multiple small inputs of concentrated recharge from other sinkholes and incipient conduits. Flow is predominantly diffuse with equipotential and flow lines indicating the diffuse flow field. b) Growth of master conduit and linking of smaller nearby conduits results in a mix of diffuse and conduit flow that alters the equipotential field such that potentiometric trough shifts. c) Late-stage linking of all conduits into a subsurface tributary drainage network such that concentrated-conduit (*alternatively*: conduit-controlled) flow dominates the aquifer. Diffuse flow is negligible and occurs as local leakage from the rock matrix into conduits with only intermittent overland flow during storm events. Modified from Mull and others (1988a).

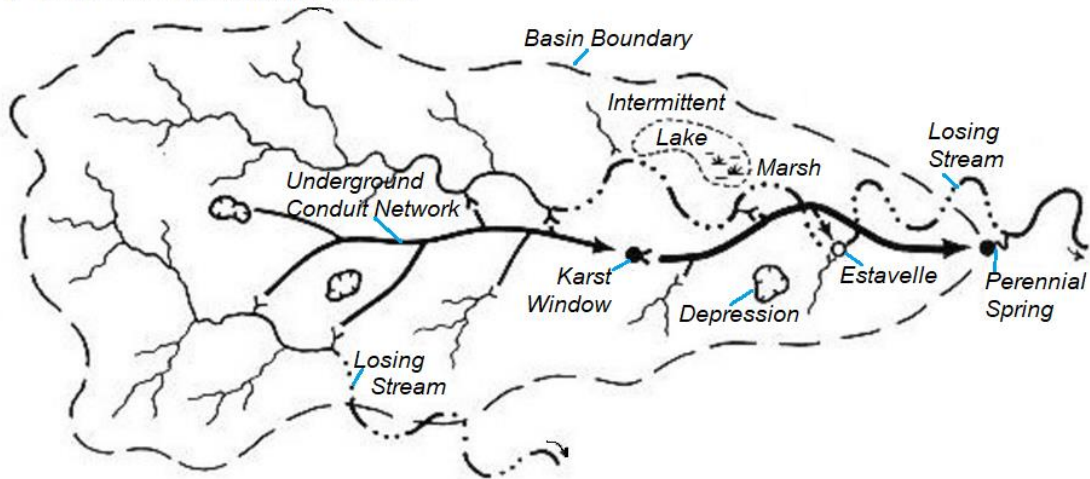
Palmer (1999) notes that in many karst-aquifer systems, flow convergence is present even in the pre-conduit openings because of differences in hydraulic efficiency created by zones of enhanced intergranular porosity and fractures, and that the branching pattern that develops as conduits grow is largely inherited. The dynamics of this process have been simulated repeatedly using both physical and numerical models, and recent advances in numerical models have been able to effectively simulate the development and linking of conduits to form complex drainage networks that are representative of karst aquifers as delineated by field data, and to forecast their continued evolution in response to projected changes of hydrologic conditions (Perne et al., 2014; de Rooij and Graham, 2017).

In many karst areas, conduit development short-circuits surface stream drainage by providing alternative subsurface flow paths (White, 1999). Conduit piracy of surface stream flows often initiates the formation of sinking or disappearing streams, whose flows abruptly end via subsurface diversion into a streambed swallow hole, terminal cave, sinkhole, losing stream reach, or “dry” stream channels (Brahana and Hollyday, 1988; Ray, 2012). In “dry” stream channels, surface flows occur intermittently during seasonally-high water-table conditions or when storm events overwhelm the drainage capacities of streambed swallow holes and underlying conduits. This hydrologic mechanism is sometimes responsible for localized, often damaging, recurrent flooding in karstic watersheds (Bayless et al., 2014).

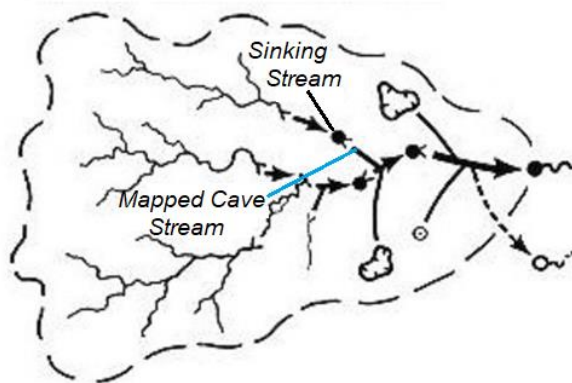
From field observations in the Mammoth Cave area, Kentucky, USA, where conduit drainage originated by leakage or base-flow piracy beneath stream channels, Ray (1999) hypothesized that the hydrologic characteristics of stream valleys in karstic watersheds change along an evolutionary sequence as erosion progressively exposes more limestone bedrocks to weathering and karstification, and as conduit piracy of surface drainage progressively increases. He described three significant phases of development by classifying watersheds as either: overflow allogenic (type 1), underflow allogenic (type 2), or local autogenic (type 3) as shown in Figure 29. In the overflow allogenic basin, the drainage capacity of subsurface conduits is initially too limited to capture and discharge more than low-to-base flow runoff from the entire watershed. Storm flows and higher runoff are discharged from the watershed through streambeds of downstream surface reaches that are usually dry or losing streams. These intermittent higher surface flows continue to erode and maintain the downstream surface channels. As the conduit networks evolve over time and increase their drainage capacity and piracy, more of the surface flow is diverted underground, upstream surface tributaries disconnect from downstream reaches, becoming sinking streams, and all watershed runoff, including storm runoff, is discharged through conduits and karst springs. These characteristics define an underflow allogenic basin. Eventually, as all or the majority of surface runoff is diverted underground, sinkhole catchments increase in number and grow in size, surface stream channels and intervening topographic divides erode, and internal drainage through conduits and karst

springs dominate the hydrology of the watershed. These are the characteristics that define a local autogenic basin.

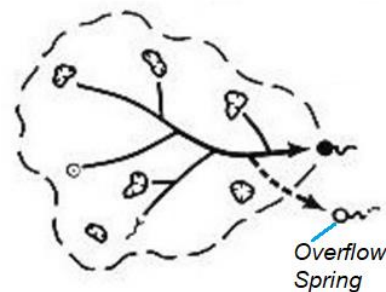
a) *Overflow Allogenic (Type I Basin)*



b) *Underflow Allogenic (Type II Basin)*



c) *Local Autogenic (Type III Basin)*



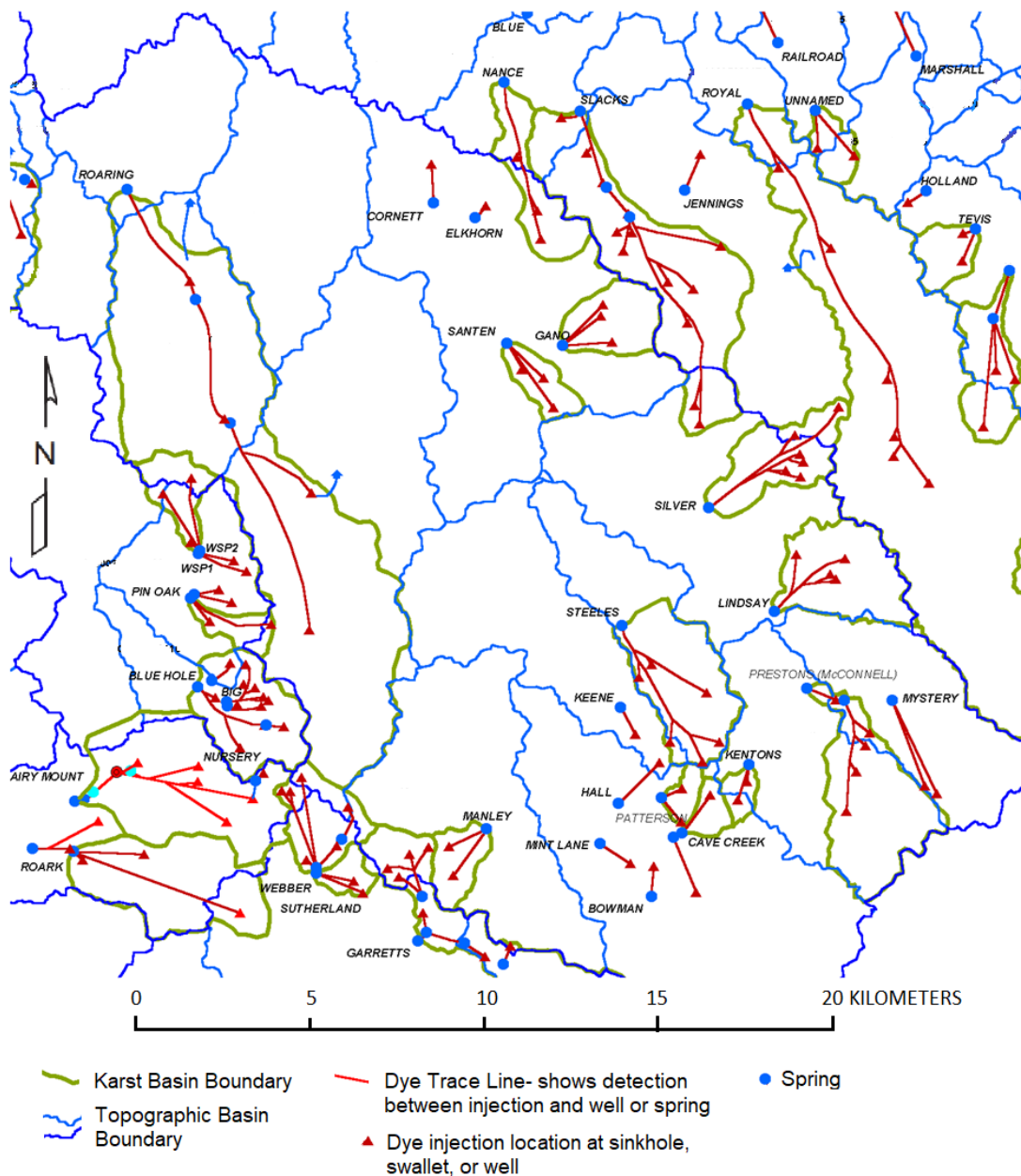
**Figure 29** - A conceptual model of the evolution of some karstic watersheds, resulting from progressive piracy of surface drainage by subsurface conduits. a) Overflow allogenic (type 1) where nearly all outflow from the basin occurs via surface stream channels. The karst window is an opening in the stream where some of the surface-water flow may move underground. If the karst window is not large there is an upper limit to the amount of flow diverted underground, but here the arrow indicates all surface flow goes underground. The estavelle is an open ground orifice that can either be a sinking stream (like a karst window), but under conditions when the groundwater table rises high enough, flow will reverse (so flow goes either direction). The main difference between the losing stream and sinking stream is that all the flow is not lost in a losing stream and the sinks aren't specifically known, whereas at a sinking stream usually the sink is a known karst window and all flow moves underground into the conduit network. b) Underflow allogenic (type 2) where conduit networks have evolved to the extent that nearly all outflow is from conduits and karst springs in lower portions of the basin. Note the now three karst windows that divert surface-water flow underground towards the springs. c) Local autogenic (type 3) where outflow is from conduits and karst springs at the lowest part of the basin. The surface is devoid of perennial streams and most of the rainfall moves underground through surface depression sinks. Modified from Ray (2001).

Within a karst aquifer or aquifer system, multiple discrete karst groundwater basins are often present. Each basin receives recharge from a specific area of land surface through infiltration and point sources such as sinkholes and sinking streams and drains to a specific spring or group of springs, by way of an integrated network of subsurface conduits (White,

1993). Identification and delineation of karst basins is challenging because their characteristics differ considerably from conventional conceptual models of porous media aquifers and cannot be determined using only conventional methods that rely on water-level data from wells and topographic mapping to identify recharge and discharge boundaries and groundwater flow directions (Groves, 2007; Taylor and Doctor, 2017). Moreover, the term “groundwater basin” is somewhat of a misnomer in that it misrepresents both the highly interconnected nature of surface and groundwater in most karst aquifers and the role of concentrated stormwater runoff as a significant, often dominant, source of recharge. The boundary of a karst basin includes surface catchments for all contributing sources of allogenic recharge and sinkholes (sinkholes usually provide autogenic, but may provide allogenic, recharge).

Karst basins differ from conventional groundwater basins as defined by Toth (1963) in major ways. Karst basin boundaries may not coincide with topographic drainage divides that define the hydrologic boundaries of surface water drainages. Groundwater recharge at karst basin divides may flow in multiple directions, following conduits in a radial or semiradial pattern and flow into one or more adjacent basins. Moreover, the position of recharge areas and basin divides may shift under different hydrologic conditions, for example under flood or storm conditions groundwater levels rise and flow follows higher level conduits. Subsurface conduits and karst basin boundaries may extend well beyond boundaries indicated by topographic drainage divides (Figure 30), giving rise to so-called “misbehaved” drainage patterns in karstic watersheds (Ray, 2001). Often, discharge from a karst basin does not occur over a widely distributed seepage zone along a surface stream channel but is concentrated at local points, for example, at one or more springs that form major headwaters that are perennial tributaries of nearby surface streams. Finally, because water movement is largely concentrated within discrete conduit-controlled flow routes or preferential flow layers, groundwater flow directions and discharge locations at springs do not always conform with those anticipated or predicted from hydraulic gradients inferred by water-level measurements in wells. The concept of a karst water table has been debated and considered problematic, in part because of the extreme heterogeneities, discontinuities of flow and hydraulic head fields in the aquifer (White, 1993; Ewers, 2006; Taylor and Doctor, 2017).





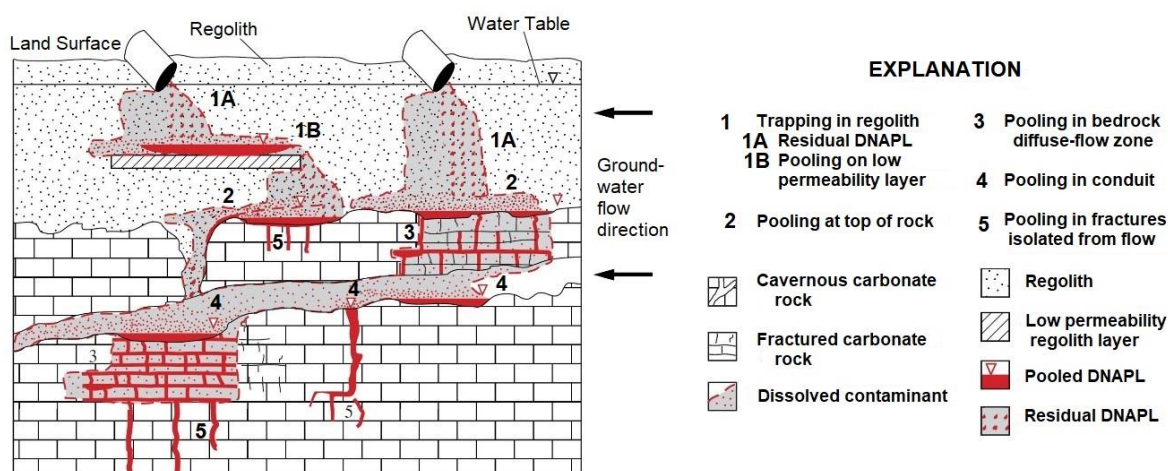
**Figure 30** - Section of a map showing examples of so-called “misbehaved” drainage patterns in karstic watersheds where surface water divides and groundwater divides do not coincide. These are indicated where karst basin boundaries (green polygons) as determined by dye tracer tests (red lines link from injection to detection of dye) extend across topographic basin boundaries (blue polygons). Blue dots represent karst springs, red triangles represent sinkholes, swallets, or wells used for dye-tracer injection sites. Modified from Currans and others (2002).

### 3.7 Vulnerability of Karst Aquifers to Contamination

Karst aquifers are recognized as being especially vulnerable to contamination. Contaminants sourced from above-ground human activities and land uses, such as accidental chemical spills or releases, agricultural chemical applications and livestock waste disposal easily and rapidly reach the aquifer via surface runoff entering sinkholes and sinking streams. Contaminants that infiltrate soils or are released from subsurface sources such as buried wastes, landfill leachate, and underground storage tanks and

pipelines, may move rapidly and/or slowly through the epikarst into deeper parts of the aquifer. Once contaminants reach the saturated zone, they may move rapidly and/or slowly throughout the aquifer depending on the distribution of zones of higher and lower hydraulic conductivities in the bedrock matrix, and the hydraulic properties of fractures and conduits.

Heterogeneities created by the multiple porosity and permeability of karst aquifers, and especially by multiple discrete conduit and fracture flow paths, are the major factor contributing to the overall higher vulnerability of karst aquifers to contamination, and to the difficulties encountered in detecting, assessing, and remediating contaminant occurrences (Field, 1993). Contaminant transport, storage, fate, and remediation are especially complicated where the karst aquifer is extremely heterogeneous and/or the contamination involves mixtures of contaminants having different physio-chemical characteristics, such as a combination of non-aqueous-phase liquid (NAPL) and dissolved contaminants (Figure 31). The conventional conceptual model of a single contaminant plume defined by concentration gradients and spreading gradually through an aquifer by advection and diffusion does not represent contaminant transport in karst. Contaminant transport through conduits occurs rapidly, often over long distances, and contaminants within them may be dispersed into multiple “plumes” of varying concentration that take unpredictable or unknown pathways to the aquifer’s discharge boundaries at wells, springs, or surface waters. Contaminants may be rapidly diluted within or flushed from conduit systems, but residual contaminants may be stored and released gradually or effectively immobilized within lower-permeability, slower-velocity zones of the karst aquifer matrix (Green et al., 2006). Contaminant flow paths, flow velocities, residence times, travel times and concentrations may change significantly under different hydrologic conditions.



**Figure 31** - Hypothetical representation of multiple storage and transport pathways following two spills of dense non-aqueous phase liquid (DNAPL) into a heterogeneous karst aquifer showing migration and pooling of free-product (i.e., DNAPL that is not mixed with water) and the associated zones of dissolved DNAPL that form as groundwater flows around the free-product. Modified from Wolfe and others (1997).

Vesper and others (2001) broadly summarize the factors involved in contamination of karst aquifers by:

- inorganic and organic water-soluble compounds;
- LNAPLs - Light Non-Aqueous Phase Liquids that are slightly soluble organic liquids, such as gasoline, that are less dense than water;
- DNAPLs - Dense Non-Aqueous Phase Liquids that are low to slightly soluble organic liquids, such as chlorinated solvents like trichloroethylene (TCE), that have a higher density than water;
- pathogens including microbes and viruses;
- metals; and,
- trash.

Their key points are concisely highlighted in this excerpt:

*“Transport of the contaminants through the aquifer is by a variety of mechanisms depending on the physical and chemical properties of the contaminant...Water soluble compounds...move with the water. But rather than forming a plume spreading from the input point, the contaminated water forms linear stringers migrating down the conduit system toward the discharge point. LNAPLs...float on the water table and can migrate down the water table gradient to cave streams where they tend to pond behind obstructions. DNAPLs...in contrast, sink to the bottom of the aquifer. In the conduit system, DNAPLs pond in low spots at the bottom of the conduit and infiltrate sediment piles. Transport of both LNAPL and DNAPL is dependent on storm flow which can force LNAPL through the system as plug flow and can move DNAPLs by mobilizing the sediment piles. Pathogens...are transported through the karstic drainage system because of the absence of filtration and retain their activity for long distances. Metals (i.e. chromium, nickel, cadmium, mercury, and lead) tend to precipitate as hydroxides and carbonates in the neutral pH, carbonate rich water of the karst aquifer. Metal transport is mainly as particulates and as metal adsorbed onto small particulates such as clays and colloids...”.*

Trash and sediment are relatively underrecognized contaminants uniquely associated with environmental and water-quality degradation in karst (Mahler and Bennett, 1999; Mahler et al., 2007). Often introduced directly into the conduit system by storm-induced runoff entering open sinkholes and swallow holes, these contaminants may be transported by turbulent flow far into the karst aquifer system where they may act as subsurface sources of leachable chemical and microbial pollutants. High concentrations of suspended sediment or turbidity, especially during storm events, is a hallmark of sinkhole-dominated karst recharge, and is a surrogate indicator of karst water vulnerability to contamination by surface runoff. In many karst aquifers, even those unaffected by anthropogenic contaminants, groundwater quality is naturally degraded by suspended

sediment. It is often a factor limiting groundwater resource development, affecting the water quality of water-supply wells and springs, and is a recurrent or ongoing problem contributing to higher costs for water treatment and water well maintenance. The mineralogical composition and grain-size of the sediment are important co-factors in the transport, storage, and fate of many contaminants in karst aquifers. For example, in areas undergoing increasing urbanization, high organic carbon content and high specific surface area increases the potential of sediments to transport metals and organic chemical contaminants (Mahler et al., 1999). Core samples of layered sediment deposits in conduits provide useful data to track temporal and spatial changes in karst water quality and pollutant loading and provide a record of changing anthropogenic activity in a karst basin (Feist et al., 2020).

The article “Threat Down Below: Polluted Caves Endanger Water Supplies, Wildlife” by Streater (2009) highlights a number of fascinating cases of contamination in karst and their impacts on caves, groundwater, and karst ecosystems. Historically, in rural areas sinkholes have been used to dispose of: trash; industrial and agricultural liquid wastewaters and slurries; highway stormwater runoff; and household septic wastewater. In the United States, wells categorized as Environmental Protection Agency Class V, inject non-hazardous fluids underground and have been drilled in many karst areas to enhance drainage from soil-mantled sinkholes, dispose of highway runoff, or mitigate karst-related flooding (Zhou, 2007). In conduit systems that have free air space, volatile gases may exsolve from contaminated water or LNAPL and migrate to the upper parts of the aquifer, through the vadose zone to the soil or surface, creating hazardous explosive or noxious conditions. An example of this was documented by White and others (2018). Karst areas are notable for higher concentrations of radioactive, carcinogenic radon gas ( $\text{Rn}^{86}$ ), a naturally-occurring element generated by decay of uranium-containing minerals. Radon gas is often detectable in spring waters and at high concentrations in the air of limestone caves as well as buildings underlain by karstic carbonate rocks (Hakl et al., 1997; Peano et al., 2011).

Point-source (for example, sewage or industrial plant outfall) and non-point source (for example, diffuse contamination from cattle field) contaminant releases in karst terranes may result in rapid and devastating affects to drinking-water supplies (Field, 2004). One widely-reported, tragic incident involved microbial contamination of public water-supply wells in Walkerton, Ontario, Canada, in the spring of 2000, in which over 2,300 people were sickened, and seven died, as a result of groundwater contamination by *Escherichia coli* (*E. coli*) and *Campylobacter jejuni* bacteria. Subsequent investigations revealed that the source of the contamination was livestock waste entering the karstic limestone aquifer through rapid infiltration of surface runoff. Field testing using dye-tracing methods demonstrated the occurrence of flow velocities greater than 300 m/d and contaminant travel times of 5 to 26 hours in an area that conventional groundwater model applications had been delineated as having a 30-day time-of-travel. The groundwater model simulations did not include



karst features, thus did not represent the flow system. Obviously, conventional groundwater modeling mis-represented the time require for contaminants to reach points of contact because karst features were not included in the model (Worthington et al., 2002).

This type of outcome—where groundwater simulation fails to accurately represent karst flow and contaminant transport characteristics—should be expected if the karst flow system is poorly conceptualized and the mathematical model does not properly represent the potential multiple porosity and permeability scale effects created by preferential flow paths within conduits or thick macro-porosity preferential flow layers. Conventional groundwater flow models typically use values reflecting total porosity of the rock matrix to represent effective porosity. Effective porosity represents only the porosity of interconnected conduits and preferential flow layers which is generally a much smaller value than total porosity. Contaminant travel time is linearly related to effective porosity, so over estimation of porosity increases calculated travel time. Effective porosity is most accurately determined from tracer testing (Kuniansky et al., 2001; Davis et al., 2010).

Ewers (2006) discusses the importance of properly collecting and interpreting hydrogeologic mapping data needed to determine conduit flow and contaminant transport characteristics, and the use of special techniques such as dye-tracing tests to identify groundwater flow directions, and connections between potential sources and receptors of contaminants. Field (2004) advocates for the use of multiple quantitative tracer tests initiated from potential source locations to obtain dye-breakthrough curves. These estimated solute-transport parameters that are needed to predict the fate of contaminant releases. In karst aquifers, quantitative groundwater tracing is the single-most demonstrably reliable method of obtaining information about hydraulic geometry of conduits, groundwater flow velocities and residence times, as well as other insights into contaminant transport characteristics that cannot be acquired using conventional methods such as potentiometric-surface mapping and aquifer tests (Mull et al., 1988a; Field and Nash, 1997). Dye-tracer tests are an effective method of estimating the behavior of soluble conservative contaminants (and to lesser extent non-soluble and reactive contaminants) whose transport characteristics are dependent on groundwater flow velocities. However, other tracer agents are needed, and are available, to simulate transport of bacteria, colloids, non-soluble and particle contaminants. Examples are provided by Benischke (2021) and Bandy and others (2016). Tracer properties should be carefully evaluated and matched to the known or anticipated type of contaminant transport under investigation. More discussion of water tracing is provided in Section 5.3, *Water Tracing Tests*.

[Exercise 8](#) invites the reader to read about poluted caves and consider the types of contaminants found in the caves.

### 3.8 Karst Aquifer Flow Characteristics Compared with Aquifers Composed of Other Rock Types

The main rock types for aquifers include sand and gravel; sandstone; sandstone and carbonate; carbonate; igneous; and metamorphic rocks. Sand and gravel and sandstone aquifers are considered granular porous media. Shallow aquifers composed of sand and gravel are considered unconsolidated sediments, whereas sandstone is considered an indurated sedimentary rock. Igneous and metamorphic rocks tend to form fractured rock aquifers. In igneous and metamorphic rock aquifers, the rock itself is not very permeable so water flows through cracks in the rock, but there are exceptions such as lava tubes in some basalts, which may behave as conduits. The uniqueness of karst aquifers is the solubility of the aquifer rock such that the aquifer continuously evolves over geologic time as a result surface and groundwater flowing through them and dissolving the rock.

Table 1 provides a list of flow characteristics for the three basic types of aquifers. Characteristics unique to karst aquifers are extreme heterogeneity, multilevel porosity and permeability, conduit-dominated groundwater flow, point-source recharge, and large temporal variability in flow and chemistry due to rapid recharge and to mixing of water from multiple recharge sources. Table 2 is a compilation of hydraulic conductivity data for aquifer and confining unit rock types or specific aquifer systems within a rock type. The enormous heterogeneity of karst aquifers is revealed by hydraulic conductivity,  $K$ , spanning eight orders of magnitude for some of the karst aquifers, whereas unconsolidated sediments have a range on the order of four orders of magnitude and fractured rock aquifers have roughly a six order of magnitude range in hydraulic conductivity. Additionally, for many of the karst aquifers the hydraulic conductivity of a conduit or preferential flow layer would be underestimated as aquifer tests estimate transmissivity and to estimate hydraulic conductivity, transmissivity is divided by either the length of the open interval of the well or total aquifer thickness which are larger than the actual thickness of the flow zone. The need for field investigations to account for the rapid flow through conduits resulting in large discharges from complex conduit networks cannot be overstated.

**Table 1** - Comparison of various hydrogeologic properties of granular porous media, fractured rock, and karst aquifers (Modified from ASTM, 2002).

Aquifer Characteristics	Aquifer Type		
	Granular Porous Media	Fractured Rock	Karst
Effective porosity	Mostly primary, through most of the intergranular pore space of the sediment matrix	Mostly secondary, through joints, fractures, and bedding plane partings-not the rock matrix	Mostly tertiary (secondary porosity modified by dissolution within large conduits) with primary if rock matrix permeable as with reefs or shell mixtures, through pores, bedding planes, and fractures
Isotropy	Generally isotropic in a formation	Often anisotropic related to fracture direction related to structure	Frequently anisotropic as fractures form along joints related to calcite mineral or in formation units oriented along bedding planes in units that dissolve more readily than adjacent units
Homogeneity	Generally homogeneous in a formation	Often heterogeneous	Extremely heterogeneous
Flow	Generally slow and laminar; exception are large clean gravels with large pore diameters	Slow and laminar when fracture apertures are less than 1 centimeter, but can be rapid under laminar and turbulent conditions if fracture aperture over 2 centimeters	Often rapid flow under laminar and turbulent conditions in large pipe like conduits greater than 0.5 m wide
Storage	Unconsolidated sediment has large specific storage. Indurated sedimentary rocks have smaller specific storage.	Generally small specific storage as rocks have little elasticity and storage mainly related to the porosity and elasticity of water.	Generally small specific storage as rocks have little elasticity and storage mainly related to the porosity and elasticity of water.
Temporal head and chemistry variations	Generally, less variations than the other aquifer types	Head variations can be large owing to small storage properties, but chemistry changes generally moderate variations	Both head and chemistry can have moderate to large temporal variations.

**Table 2** - Hydraulic conductivity of rock types and karst aquifers (Modified from Halford and Kuniansky, 2002).

<b>Rock Hydraulic Conductivity Ranges, values in meters per day</b>					
<b>Aquifer Material</b>	<b>Extreme Minimum</b>	<b>Likely Minimum</b>	<b>Likely Maximum</b>	<b>Extreme Maximum</b>	<b>References</b>
<b>Unconsolidated Sedimentary Rock</b>					
Gravel	30	90	900	900	1,5
Sand and Gravel Mixes	0.3	9	90	90	1
Coarse Sand	10	20	90	90	1
Medium Sand	0.3	6	20	60	1,5
Fine Sand	0.01	0.9	6	6	1,5
Gulf Coast Aquifer Systems, USA	0.6	9	60	200	2
Stream Terrace Deposit, Texas, USA	0.003	0.3	30	90	3
Fine sand and silt, Florida, USA	0.003	0.03	9	10	4
Silt, Loess	$9 \times 10^{-5}$	0.0003	0.03	2	5
Till	$9 \times 10^{-8}$	0.0009	0.09	0.2	1,5
Clay soils (surface)	0.003	0.003	0.3	0.3	1
Clay	$3 \times 10^{-7}$	$3 \times 10^{-6}$	$3 \times 10^{-5}$	0.0003	5,7
<b>Indurated Sedimentary Rock</b>					
Fine-Grained Sandstone	$3 \times 10^{-5}$	0.0003	0.3	2	1,6
Medium-Grained Sandstone	0.0003	0.3	3	20	6,9
Siltstone	$3 \times 10^{-7}$	$3 \times 10^{-6}$	0.001	0.01	6
Claystone	$9 \times 10^{-10}$	$3 \times 10^{-7}$	$3 \times 10^{-6}$	$9 \times 10^{-6}$	6,7,10
Anhydrite	$3 \times 10^{-8}$	$3 \times 10^{-8}$	0.002	0.002	5
<b>Metamorphic or Volcanic Rock</b>					
Shale	$3 \times 10^{-9}$	$3 \times 10^{-8}$	$3 \times 10^{-5}$	0.3	7
Permeable Basalt	0.03	0.3	30	2000	5
Fractured Igneous/Metamorphic Rock	0.0003	0.02	3	30	1
Weathered Granite	0.03	0.3	3	6	6
Weathered Gabbro	0.03	0.03	0.3	0.3	6
Basalt	0.0003048	0.009	0.03	0.03	5
Unfractured Igneous/Metamorphic Rock	0.0304785	$3 \times 10^{-9}$	$2 \times 10^{-5}$	$2 \times 10^{-5}$	1,5
<b>Carbonate Rocks</b>					
Unweathered Marine Clay	$6 \times 10^{-8}$	$6 \times 10^{-8}$	0.0002	0.0002	5
Karst	0.0002	3	300	10,000	4,5,8,11
Reef Limestone	0.09	3	300	300	5
Limestone, Dolomite	$9 \times 10^{-5}$	0.001	0.03	0.6	5
Upper/Unspecified Floridan Aquifer, USA	0.002	3	200	10000	11
Middle/Lower Floridan Aquifer, USA	0.0002	0.01	40	8,000	11

**References:** 1) Bouwer, 1978 (order of magnitude in m/d); 2) Prudic, 1991; 3) Sonia A. Jones, USGS, Written communication, 1998; 4) Kinnaman, 2002, Slug Test Results 1998-2001, USGS, Orlando, Florida; 5) Domenico and Schwartz, 1990; 6) Morris and Johnson, 1967; 7) Wolff, 1982; 8) Reese and Cunningham, 2000; 9) Kuniansky and Hamrick, 1998; 10) Neuzil, 1994.

This book illustrates the underlying causes of complex flow fields in karst aquifers. The Minnesota Department of Agriculture developed an excellent animation of flow in karst systems to help the public understand how water moves through karst aquifers (Figure 32).



How Groundwater Moves in the Karst Landscape (A Short Animation)

**Figure 32** - This animation, portraying groundwater movement in a karst landscape, was created by the Minnesota Department of Agriculture as part of a series that highlights the geology and complex movement of groundwater in southeast Minnesota. The animation “brings to life” many of the concepts presented in this book and enhances one’s ability to conceptualize the hydrology that is typical of many karst aquifers.

## 4 Fluid Mechanics Considerations for Karst Aquifers

Two basic fluid mechanics topics are useful to address when considering flow in karst as compared with porous/granular and fractured aquifers. These are the conditions for laminar and turbulent flow for which the Reynolds number offers insight, and the character of flow in pipes and open channels.

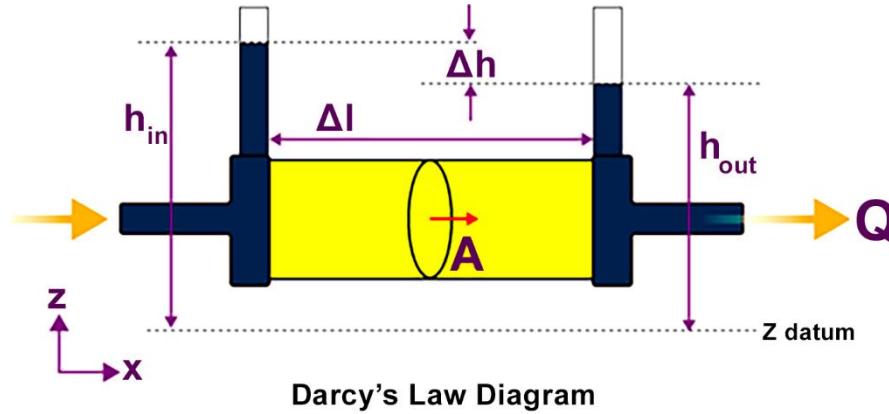
This brief section provides basic fluid mechanics information important to concepts of flow in karst. It is not intended to provide the complete knowledge of fluid mechanics required for working on karst aquifers. The textbook most often cited on elementary fluid mechanics is authored by Vennard and Street (1975), whose first edition was published in 1940. It was the most popular fluid mechanics textbook used in the United States for many decades.

### 4.1 Limitations of Darcy’s Law for Application to Karst Aquifers

Darcy’s law was derived empirically (Figure 33). Laboratory studies undertaken by Darcy (1856) for one-dimensional laminar flow through a known cross-sectional area,  $A$ , of porous media, indicated a constant of proportionality between discharge,  $Q$ , and the



hydraulic gradient,  $\frac{dh}{dl}$ , for water flow through a material comprised of small pores (less than 10 mm). The constant of proportionality is called hydraulic conductivity,  $K$ , as presented in Equation 1.



**Figure 33** - Schematic diagram for experimental permeameter determination of hydraulic conductivity based on Darcy's Law. The porous material (yellow) is within a circular tube of cross-sectional area,  $A$ , of known length  $\Delta l$ . The volumetric rate of flow through the porous material,  $Q$ , is measured as head in the water reservoirs remain constant ( $h_{in}$  and  $h_{out}$ ) in order to have a constant head gradient,  $\frac{\Delta h}{\Delta l}$ . The reservoir elevations are modified, and a new equilibrium established and a new flow,  $Q$ , and new gradient,  $\frac{\Delta h}{\Delta l}$ , recorded. This is repeated several times to determine the slope of a line fit through the points created with  $Q/A$  values on the x-axis and  $\frac{\Delta l}{\Delta h}$  on the y-axis. The slope of that line is the hydraulic conductivity,  $K$ .

$$Q = -KA \frac{\Delta h}{\Delta l} \quad \text{and rearranging, produces:} \quad K = -\frac{Q}{A} \frac{\Delta l}{\Delta h} = -q \frac{\Delta l}{\Delta h} \quad (1)$$

where:

$Q$  = volumetric flow through the system ( $L^3T^{-1}$ )

$K$  = hydraulic conductivity of the porous medium ( $LT^{-1}$ )

$A$  = cross-sectional area perpendicular to flow ( $L^2$ )

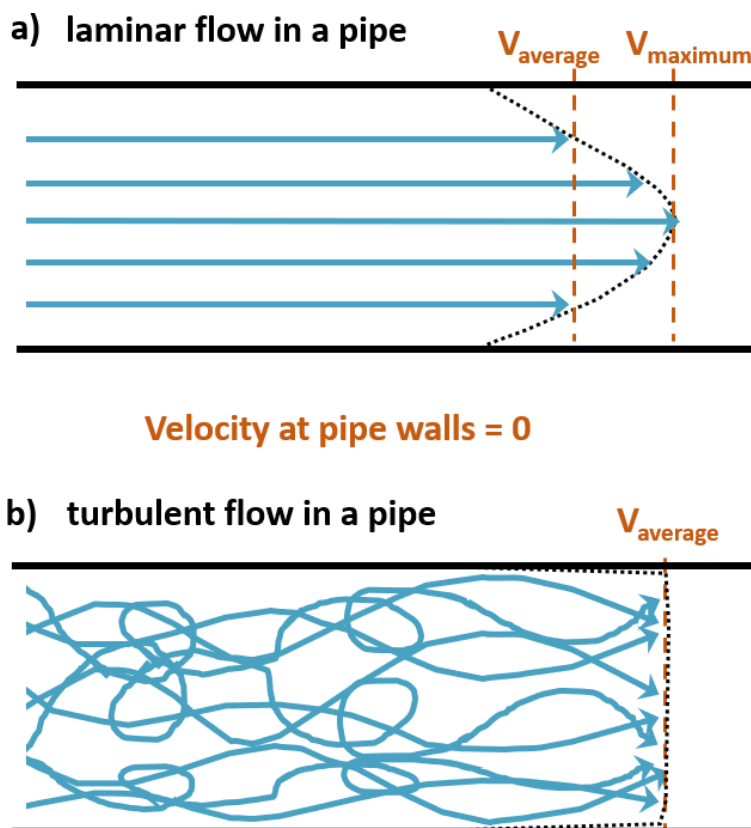
$\Delta h$  = measured head difference (L)

$\Delta l$  = length over which the head difference is measured (L)

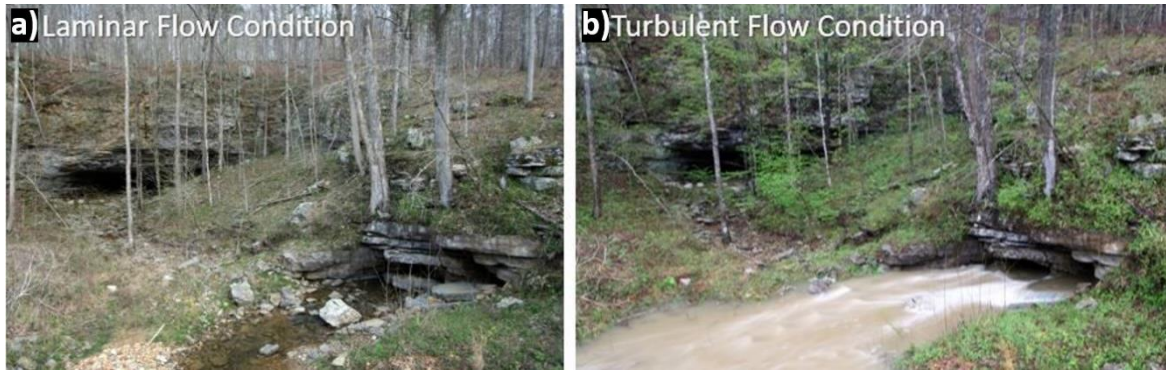
$q$  = specific discharge ( $LT^{-1}$ )

Darcy's law is valid for laminar flow conditions. Laminar flow occurs when water particles flow in smooth, parallel path lines no matter the shape of the conveyance. For laminar flow, the velocity along a path line is constant. If the conveyance shape changes, obstacles are present in the flow channel, or wall roughness changes, the smooth path lines may begin to cross each other. Initially, it is the change in geometry of the flow path that causes flow lines to cross, then the fluid behavior begins to transition away from Darcian flow, however, this initial deviation from Darcian flow has nothing to do with turbulence, instead it is the flow path geometry that causes the water to change direction even at relatively low velocities. In the 1970s, researchers studying flow through rock fractures

(Sharp, 1970; Maini, 1971) reported that when they observed the onset of non-Darcian flow in experiments (that is, larger head change per unit increase in flow), flow was still laminar based on the linear behavior of dye injected into the flow stream. They termed this initial deviation from Darcian flow as nonlinear laminar flow. As velocity increases, the viscous forces are gradually overcome by increasing inertial forces. At full turbulence, path lines cross each other, eddies form, the *average* forward velocity along the direction of the conveyance is relatively constant and flow is less orderly. For most porous media, water cannot move through the rock fast enough for turbulence to occur because of the large gradient required to reach the velocity that results in turbulence. Figure 34a shows path lines under laminar flow and at the onset of turbulent flow in a smooth straight pipe. In a smooth circular pipe, the velocity is zero at the wall and is maximum at the center, forming a three-dimensional, parabolic, cone-shaped profile (Figure 34a). For a given pipe diameter, a smoother and straighter pipe can support higher velocities before flow transitions to turbulent conditions (Figure 34b). Figure 35a shows laminar flow (Figure 35a) and turbulent steady flow (Figure 35b) from a spring in Alabama, USA.



**Figure 34** - Water path lines in a pipe showing a) laminar flow where the velocity profile is parabolic and the average velocity is 50 percent of the maximum velocity in the center; and b) turbulent flow where the velocity profile across the pipe is constant and equal to the average velocity.



**Figure 35** - Photographs of spring discharge from Dry Spring cave in Jackson County, Alabama, USA: a) discharge on April 2, 2006 showing laminar flow conditions; and b) discharge on April 8, 2006 showing turbulent steady flow conditions. Photographs by Alan Cressler (2006), used with permission.

For most porous media, water cannot move through the rock fast enough for turbulence to occur. With typical porous media, the pore size is generally so small that the gradient required to cause turbulent flow is extremely large thus flow tends to be slow and remain laminar. However, laboratory flow experiments through optically smooth channels with a separation distance of 200 to 500 mm used a water pump capable of producing 250 pounds per square inch ( $250 \text{ psi} = 1,700,000 \text{ N/m}^2$ ) of pressure and these achieved the entire flow range from laminar through turbulent (Acosta et al., 1985). An exception to the condition of laminar flow in porous media occurs in rare situations in aquifers near the wall of a well that is pumped at an extremely high rate because a large rate of flow converges on a small area as defined by the surface of the cylindrical wellbore. This turbulence can occur in any aquifer type if the hydraulic conductivity is large enough that the high pumping rate can be maintained.

The main difference between karst aquifers and most other aquifers is that the rocks have dissolved along fractures creating large water conveyances of high hydraulic conductivity and turbulent flow occurs during major recharge events, such as large storms or near areas of focused recharge such as sinking streams. In any rock type with interconnected pores greater than approximately 10 mm, hydraulic conductivity can be extremely large and turbulent flow can occur.

[Exercise 9](#) invites the reader to consider what other aquifer types may have extremely large pores and high hydraulic conductivity, where flow can be laminar or turbulent. A second part of the exercise invites the reader to consider converging flow to a production well for different radial distances and aquifer types.

## 4.2 Reynolds Number as an Indicator of Flow Regime

The Reynolds number,  $Re$ , is a dimensionless number used in fluid mechanics to indicate whether flow is laminar or turbulent (Reynolds, 1883). The original experiments conducted by Reynolds used straight smooth glass pipes. He injected a small dye stream into the center of the clear water stream while temperature was held constant and the flow

rate through the tube could be controlled and measured (Reynolds, 1883). The experiments started with very low velocities and a stable single line of colored water passing through the tube as a distinct straight line of color, then velocity was increased in small increments until turbulence was reached and subsequently velocity was gradually reduced until laminar flow was again achieved. Numerous experiments with the same diameter tube confirmed the same velocity for the onset of turbulence from the laminar to turbulent state and a different velocity for the transition from turbulent back to laminar flow. Reynolds then conducted experiments with different diameter pipes and at different temperatures.

The Reynolds number,  $Re$ , represents the ratio of fluid inertial to viscous forces. It is a similarity law such that the onset of turbulence in any size of smooth, straight pipe will be relatively the same (typically,  $2100 < Re < 2300$ ). The critical Reynolds number,  $Re_c$ , is the value of  $Re$  when flow begins to deviate from linear flow and below which flow is laminar.  $Re$  is computed and defined as shown in Equation 2.

$$Re = \frac{VD\rho}{\mu} = \frac{VD}{\nu} \quad (2)$$

where:

$Re$  = Reynolds number (dimensionless)


$V$  =  $Q/A$  and is the mean flow velocity ( $LT^{-1}$ ) across a cross sectional area (also called Darcy velocity), which is equal to the volumetric flow,  $Q$  ( $L^3T^{-1}$ ), divided by the cross-sectional area perpendicular to the direction of flow,  $A$  ( $L^2$ )

$D$  = mean pore size diameter for porous media or the pipe diameter ( $L$ )

$\rho$  = density of the water ( $ML^{-3}$ )

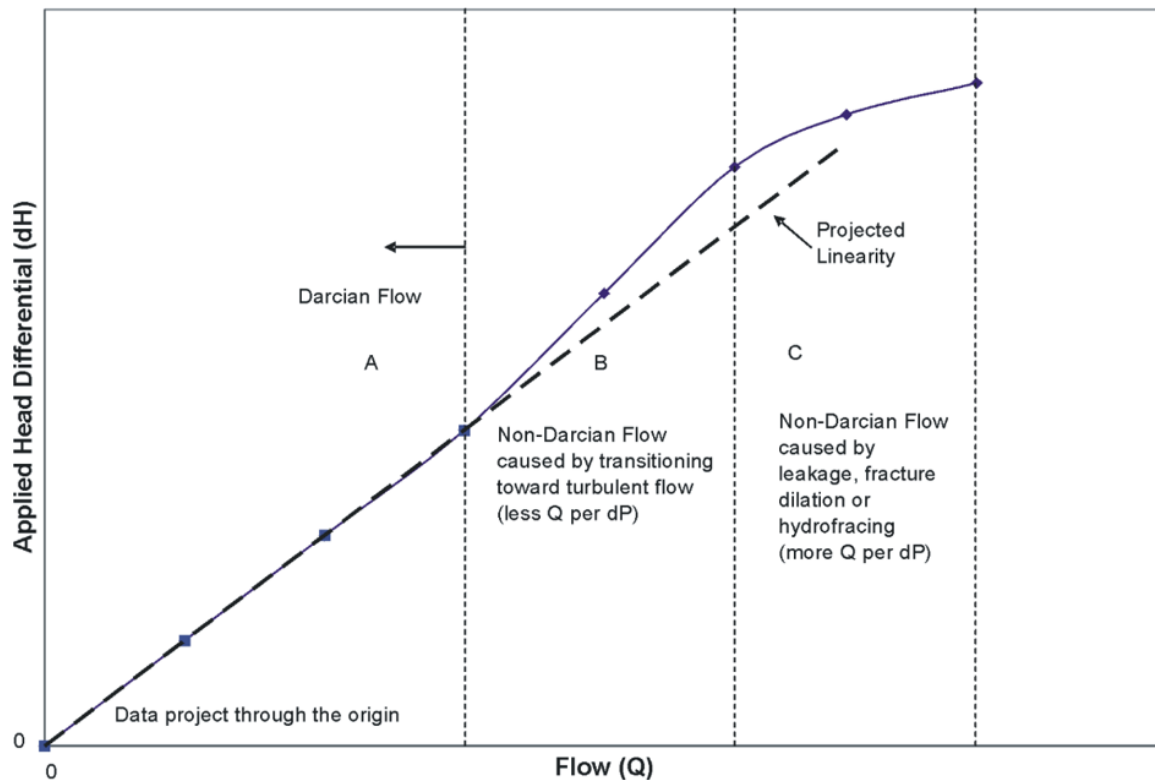
$\mu$  = absolute or dynamic viscosity of water ( $ML^{-1}T^{-1}$ )

$\nu$  = kinematic viscosity of water ( $L^2T^{-1}$ )

[Exercise 10](#)  invites the reader to consider why Reynolds tried experiments with different temperatures of water with each pipe. A second exercise uses the results from Exercise 6 (average velocity at different radial distances from a pumping well) to calculate the  $Re$  at each radial distance.

For porous media, the Darcy velocity ( $V=Q/A$ ), not the pore velocity (which is the Darcy velocity divided by effective porosity), is used to define the Reynolds number. Porous media flow tends to remain at low velocity and laminar under many natural gradients because of the small pore diameters and the effect of surface tensional forces between the water and rock. For most porous media, the  $Re_c$  ranges from 1 to 60, and is dependent on smoothness of the grains, tortuosity of the connected pore spaces, average pore diameter, temperature, as well as other properties of the aquifer and fluid. When flow becomes turbulent, some of the flow energy is lost by the movement of water in eddies, which results in specific discharge not increasing as rapidly as the head gradient increases. Thus, in turbulent conditions, flow is no longer a linear function of head gradient

(Figure 36), as is the case for Equation 1, thereby limiting the applicability of Darcy's law. Limitations to the applicability of Darcy's law for very low permeability media is also expected, but this has not been thoroughly tested (Ingebritsen and Sanford, 1998).



**Figure 36** - Data from many field tests in fractured rocks reveal Darcian flow at low gradients as indicated by a linear relationship between gradient and flow (zone A of this graph). At higher gradients (zone B of this graph), an increase of gradient results in a smaller increase in flow because flow paths change direction and some flow energy is lost to the crossing flow paths as shown in Figure 34b (Lage and Antohe, 2000). Eventually, larger increases of gradient cause larger increases in flow because the higher gradient causes one of the following that increase the hydraulic conductivity of the material: short circuiting around testing seals; dilation of the fractures/pores; or new fracturing, as shown in zone C of this graph. From Quin and others (2011b). In pipes and porous media there is also a transition from laminar to turbulent flow where the flow rate begins to drop with increasing gradient, but once fully turbulent, the flow drop is a function of the velocity squared as opposed to the Darcy velocity as discussed in Section 4.4.

It is not possible to know the exact value of  $Re_c$  for a specific aquifer or porous medium, but  $Re_c$  can be estimated through laboratory experiments. Many researchers have measured discharge under different gradients to estimate the  $Re_c$  by noting the point at which discharge becomes a nonlinear function of the gradient. The larger the pore diameter and smoother the grain surfaces, such as might occur in a well-sorted gravel, point-bar deposit, the higher the  $Re_c$ . For porous media, various representative lengths are used for  $D$  in order to calculate  $Re$ , such as a representative grain size (frequently  $d_{10}$  or  $d_{50}$  is used, which is the diameter of the sieve size at which 10 or 50 percent, respectively, of the grains pass in a standardized geotechnical sieve analysis). Many textbooks report the range of  $Re_c$  for porous media from 1 to 10 (for example, Bear, 1979; Freeze and Cherry, 1979). Schneebeli (1955) used glass spheres and found flow became turbulent at a range of  $Re$  from 5 to 60,



which is consistent with our expectation that the transition to turbulence occurs at a higher  $Re$  for smooth surfaces with relatively uniform geometry.

### 4.3 Investigation of Onset of Turbulent Flow in Rock Samples

Bulk density, total porosity, effective porosity, constant head, and permeameter test data were published for 13 cubes of Key Largo Limestone from southern Florida (DiFrenna et al., 2007). This limestone is denser and has smaller pores than the Biscayne Aquifer rock specimen shown in Figure 16b. Seventy percent of the permeameter tests conducted on the Key Largo Limestone samples remained under laminar flow, even with extreme gradients imposed during the permeameter experiments. Kuniansky and others (2008) fit the data for flow measurements along three orthogonal axes of the Key Largo Limestone cube number 6, one of the samples which exhibited a nonlinear relation between hydraulic gradient and discharge (DiFrenna et al., 2007). This nonlinear relation is indicative of non-Darcian flow. Cube number 6 measures 0.2 m on an edge with bulk density of  $1.38 \text{ g/cm}^3$ , total porosity of 0.49, effective porosity of 0.34, and a representative pore diameter of 0.01 m (DiFrenna et al., 2007). The range of laminar hydraulic conductivity,  $K$ , was 36 to 61 meters per day and  $Re_c$  for all axes was 1.44 (Kuniansky et al., 2008). Thus, this carbonate exhibits the onset of non-Darcian flow at small  $Re_c$ . The sample has an average pore diameter at the upper limit of typical porous media, most of the samples had smaller pores and thus behaved as porous media.

Cunningham and others (2009) published hydraulic conductivity values for samples of the Biscayne Aquifer in south Florida, which is predominantly layers of secondary macro porosity limestone created by a large macropore network resulting from biologic activity. These samples of aquifer rock have pore diameters generally greater than 10 mm with the largest diameter being 300 mm. Laboratory determination of hydraulic conductivity was not always possible. For four samples,  $K$  ranged from 4 to 3,000 m/day from smallest to largest macro porosity. The impermeable and 300 mm pore size samples were omitted from the study. Sukop and others (2013) wrote about non-Darcian flow for models of these samples using lattice-Boltzmann simulations and found that flow begins to be non-Darcian at  $Re > 0.1$  and is most likely turbulent between  $Re$  of 1 to 10.

In fractured rock systems, where flow occurs predominantly within the fractures between surfaces of less permeable rock, Quinn and others (2011a, b) conducted numerous short-interval borehole hydraulic tests and determined non-Darcian flow occurred at  $Re_c$  values between 0.1 and 6 for a fractured dolostone, which was in agreement with critical  $Re_c$  from laboratory experiments of single fractures in unidirectional flow where  $Re_c$  ranges between 1 to 10 (Konzuk and Kueper, 2004; Nicholl et al., 1999; Zimmerman et al., 2004).

To summarize, for most porous media, turbulent flow cannot be induced even with imposing unnaturally large gradients. For karst aquifers with layers that do not have dissolution features but have interconnected macropores without dissolution conduits,

turbulence is possible and occurs at small Reynolds numbers more typical of large-pore, granular aquifers. The onset of turbulence in large dissolution conduits that behave more like pipes, is discussed briefly in Section 4.4 of this book.

#### 4.4 Fluid Mechanics of Pipes and Open Channels


When a pipe is full, flow within the pipe can be assumed to be one dimensional along the axis of the pipe. Flow velocity at the pipe wall is zero and increases towards the center of the pipe. Experiments of the late 1850s on flow of water in straight cylindrical pipes indicated that the head loss along the pipe varied “*directly with velocity head and pipe length, and inversely with pipe diameter*” (Vennard and Street, 1975). Owing to the parabolic shape of the velocity distribution across the center of a circular pipe during laminar flow (Figure 34a), flow through the pipe can be approximated from the pressure gradient (that is, the difference in pressure on each end of a pipe, divided by its length) by using the Hagen-Poiseuille equation (Vennard and Street, 1975).

Equation 3 describes the relationship between pressure gradient and specific velocity based on the Hagen-Poiseuille equation for laminar flow in a full pipe.

$$\frac{\Delta p}{L} = \frac{8Q\mu}{\pi r^4} = \frac{8\pi\mu Q}{A^2} = \frac{8\mu V}{r^2} \quad (3)$$

where:

- $\Delta p$  = pressure difference between two ends of the pipe ( $\text{ML}^{-1}\text{T}^{-2}$ )
- $L$  = pipe length (L)
- $r$  = pipe radius (L)

[Exercise 11](#)  invites the reader to visit the Wikipedia page discussing the Hagen-Poiseuille equation and the Poiseuille law and then consider the relationships and associated assumptions.

For turbulent flow in full pipes, an empirical equation developed by Henry Darcy and Julius Weisbach (the Darcy-Weisbach Equation) indicates that the pressure gradient is proportional to the square of the mean velocity ( $V=Q/A$ ) and a dimensionless friction factor as shown in Equation 4.

$$\frac{\Delta p}{L} = f_D \frac{\rho V^2}{2D} \quad (4)$$

where:

- $f_D$  = Darcy friction factor (dimensionless)
- $D$  = hydraulic diameter of the pipe (L) (for circular pipe it is the pipe diameter, but for a non-circular pipe  $D \approx 2\sqrt{\frac{A}{\pi}}$  ; where  $A$  is the cross-sectional area in  $\text{L}^2$ )

The friction factor in Equation 4 is a function of the Reynolds number and the relative roughness of the pipe. The relative roughness of a pipe is usually defined by the

ratio of roughness of the pipe wall and the mean height of the pipe. Under laminar flow conditions for a smooth circular pipe,  $f_D = 64/Re$ .

[Exercise 12](#) invites the reader to substitute  $64/Re$  and the equation for the Reynolds number into Equation 4 to confirm that this results in the Hagen-Poiseuille equation for a circular pipe.

The density and viscosity of water change with temperature. If density and viscosity are constant, many fluid flow problems can be solved with water level gradients rather than pressure gradients as shown in Equation 5.

$$\frac{\Delta p}{L} = \rho g \frac{\Delta h}{L} \quad (5)$$


where:

$g$  = local acceleration due to gravity or gravity constant ( $LT^{-2}$ )

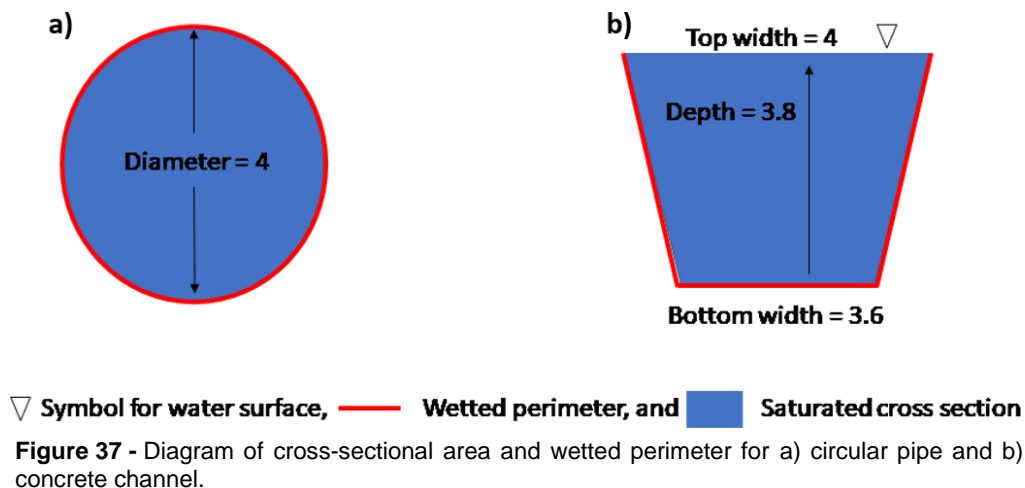
The original Reynolds experiments were conducted with smooth glass pipes (Reynolds, 1883). By running multiple experiments with different diameter pipes and at different temperatures, he discovered that there was an upper and lower critical Reynolds number for all straight pipes and all fluids. Due to conservation of momentum, flow in a laminar state tends to stay laminar and flow in a turbulent state tends to stay turbulent. Thus, when the velocity of laminar flow gradually increases the flow becomes turbulent at a higher  $Re$  than the value at which flow becomes laminar when the velocity of turbulent flow gradually decreases. That is, a lower  $Re$  is required before the flow goes back to a laminar state. These are called the upper and lower critical Reynolds numbers ( $U_R$  and  $L_R$ , respectively).

It has been observed that between the  $U_R$  and  $L_R$ , the discharge in pipes is a function of mean velocity to a power greater than 1 but less than 2 (Vennard and Street, 1975). The  $U_R$  for smooth glass pipes in the original experiment was between 12,000 and 14,000 but has little practical use as most water pipes are manufactured from rougher material and/or are not straight. For more common pipes, the  $U_R$  value is smaller and depends on the roughness and shape of the pipe. A rougher pipe surface results in the onset of turbulence at smaller velocities and thus a smaller  $U_R$  and a curve or bend in a pipe also results in a lower  $U_R$ . According to Vennard and Street (1975) for practical purposes, the  $U_R$  likely falls between 2700 and 4000 for common pipe materials. The  $L_R$  denotes flow is in a laminar state. For circular pipes, if  $Re$  is less than 2100, flow is likely laminar and if  $Re$  is greater than 4000 flow is likely turbulent. Differently shaped conveyances result in different critical  $Re$ . For example, for flow between parallel plates, using plate spacing instead of pipe diameter, the  $Re$  below which flow is laminar is 1000; for wide, open channels using flow depth instead of pipe diameter, the  $Re$  for which flow is laminar is 500; and for flow around a sphere using sphere diameter instead of pipe diameter, the  $Re$  for laminar flow is generally

close to 1. As with groundwater, the actual critical Reynolds number for pipes and natural channels is determined through experiments.

[Exercise 13](#)  invites the reader to consider how the irregularities of dissolution features impacts the onset of turbulent flow.

Most naturally occurring conduits in karst aquifers are not circular in cross-sectional shape (Figure 16, Figure 17, Figure 25, and Figure 26). In fluid mechanics some approximations are used to allow estimates based on equations for circular pipe geometry. Two important terms in open channel flow hydraulics are wetted perimeter and hydraulic radius. The terms are defined in the same manner whether they are used for a fully submerged pipe, an open stream channel or a karst aquifer conduit. The wetted perimeter is the length of conveyance wall on a cross-section perpendicular to flow that is fully wet from flow (Figure 37). The hydraulic radius is the ratio of the cross-sectional area to the wetted perimeter (for example, for each item of Figure 37 the area of the blue shape divided by the length of the red line). For karst conduits, estimates of  $Re$  are conducted using the equations for circular pipe that would have the same hydraulic radius as the conduit and this radius is used to calculate the diameter. The wetted perimeter and the effective hydraulic radius of karst conduit passages vary substantially as shown in Figure 38.







**Figure 38** - The wetted perimeter and the effective hydraulic radius of conduit passages vary substantially as shown here in photographs from caves in Kentucky, USA. Natural conduits may have relatively smooth surfaces as on the left or scalloped and rough surfaces as on the right, in addition to curves that cause changes in flow direction. Increased roughness and curves both lower the critical Reynolds number for the onset of non-Darcian flow. Photographs by Christopher Anderson, [Darklight Imagery](#), used with permission.

[Exercise 14](#) invites the reader to calculate the hydraulic radius of the circular pipe and the concrete channel of Figure 37.

Open-channel flow is dependent on gravity and the slope, shape, and roughness of the conveyance. Flow in open channels can be laminar or turbulent, steady or unsteady. Steady flow is defined as when the velocity, pressure, and kinematic viscosity (density and temperature) of the flowing fluid remain constant through time at a cross-section. Unsteady or non-steady flow indicates that the fluid properties at a point change with time. Steady flow is like laminar flow, but not the same in that in laminar flow each particle moves along the same line at a constant velocity and no streamlines cross each other (Figure 34a). Thus, laminar open-channel flow would always be considered steady flow. Often stream flow can be turbulent, but if the average velocity remains constant with no change in pressure, density and viscosity of the water then this is steady-turbulent flow. It is beyond the scope of this section and even elementary fluid mechanics to cover the topic of unsteady flow.

Flow in a full pipe is different from open-channel streamflow or flow in partially full pipes. The primary difference is that the water surface in a stream or partially full pipe is exposed to atmospheric pressure over the entire water surface. Thus, flow is not related to pressure at the ends of the pipe and the friction factor of the pipe wall, because the pressure is the same across the entire surface. Flow in a full pipe can be laminar or turbulent. Figure 39 links to a video showing laminar flow in large karst conduits.



**Figure 39** - This video of scuba divers exploring the deepest part (over 400 feet, ~122 m, below land surface) of the saturated zone karst conduit network of the Weeki Wachee and Twin Dees springs network near Spring Hill, Florida within the Floridan aquifer system on March 23, 2019 was made publicly available by Andrew Pitkin [Weeki Wachee: Mount Doom & Deeping Stream](#). There are huge conduit features as well as extensive and large bedding plane voids. Under laminar flow, large volumes of water move through these aquifers. Near the end of the video the bubbles from the scuba divers gently rise indicating flow is laminar. Almost all scuba diving to map these submerged conduit systems occurs during laminar flow conditions. Average and low flow is laminar most of the time in the large, first-magnitude springs and becomes turbulent during storm events.

[Exercise 15](#) invites the reader to consider, how wetted perimeter and the effective hydraulic radius for the two conduit passages of Figure 37 would be calculated under varying flow conditions, and how flow velocities would vary as the conduits fill.

[Exercise 16](#) invites the reader to consider why we define three types of karst porosity, particularly with respect to the occurrence of laminar and turbulent flow.

## 5 Methods of Karst Characterization

Characterization of the unique hydrogeologic features in karst aquifers require more data to achieve an understanding similar to what can be attained for granular and fractured aquifer systems, and the nature of the required data makes it more difficult to obtain (Teutsch and Sauter, 1991; Kiraly, 2003). Groundwater professionals working in karst need to anticipate the presence of heterogeneities and non-Darcian conditions that may limit analysis by conventional hydrogeologic methods. An understanding of open-channel flow and pipe flow is necessary when describing flow in karst conduits. Field investigations must provide the data that is necessary to properly conceptualize the recharge, storage, and throughflow components of the karst aquifer system.

Karst aquifer studies need to have greater focus on the identification of hydrologic boundaries and preferential subsurface flow paths created by the integrated network of conduits and solution-enhanced fractures. Acquisition of these data typically requires a multidisciplinary study approach that includes using more specialized investigation

methods such as water-tracing tests and the analysis of variations in spring discharge and water chemistry (White, 1993; Ford and Williams, 2007). Multiple hydraulic, hydrologic, and geophysical investigative methods have been successfully developed and employed to probe the subsurface karst environment. However, many of these technologies and methods have not obtained widespread usage due to technical challenges, cost, and labor requirements. Some technologies and methods are only capable of evaluating part of the karst environment and must be used in combination with other complementary methods to provide a complete picture of the aquifer.

Applicability of a karst-aquifer investigation method is dependent on 1) the volume of the aquifer sampled or tested and 2) the proportion of conduit-dominated flow in the volume of the aquifer sampled or tested. Additionally, the selection of investigative methods requires a good understanding of the question that is to be answered or problem to be solved.

Basic geologic mapping and understanding of the depositional environment of the carbonate or evaporite rock type is applicable to all scales of investigation. Readers who want to know more about carbonate geology and karst geomorphology may want to read Folk (1981), Scoffin (1987), White (1988) and Ford and Williams (2007).

At a *local scale* (small study areas less than 1 km<sup>2</sup>), karst-aquifer investigation methods rely on the use of single wells and application of borehole tests at single wells for sampling or measuring small volumes of the aquifer. Surface geophysics may also prove useful. Unless a well penetrates one or more conduits, data obtained by these methods are influenced by the diffuse-flow component (non-conduit permeability) of the aquifer. If data can be obtained at multiple wells, sometimes geophysics along with reliable lithologic and geologic information can be used for understanding which local units transmit and store water at the basin and regional scales.

At the *basin scale* (~20 to 3,000 km<sup>2</sup>), conduit-flow may be the most significant component of flow in a karst aquifer. A karst basin is usually controlled by the number, distribution, and interconnection of conduits (White, 1988). Methods of well testing that are applicable at the local scale may not be capable of characterizing the karst aquifer's properties at the basin scale. Basins are typically drained by spring(s), which integrate flow from individual conduits along with water contributed from diffuse-flow components of the aquifer. Therefore, a spring is the most appropriate natural sampling point for basin scale investigation. Water-tracing tests, spring hydrographs and spring chemograph analyses are the most useful techniques for investigating the hydrologic and hydraulic behavior of the karst aquifer at the basin scale. Quantitative tracer tests and chemograph analyses are some of the better tools for understanding the character of a karst aquifer within the diffuse-versus-conduit-flow continuum.

At the *regional scale*, (> 25,000 km<sup>2</sup>) karst aquifers consist of multiple groundwater basins. Water-level (or potentiometric surface) mapping, water-tracing tests with natural

or artificial tracers, and water-quality or geochemical sampling, field mapping of faults and joints, and geophysical methods (borehole and surface) are all appropriate methods of investigation and are used to understand the hydrogeologic framework of the karst aquifer.

The selection and use of a karst groundwater investigative method and the proper interpretation of the resulting data requires careful consideration of the appropriate scale for applying each method (Table 3).

**Table 3** - Applicability of research techniques to investigation of karst aquifers. Spaced dashes indicate greater difficulty in application due to effects of heterogeneity.

Method	Scale of Applicability		
	Local (Site) <1 km <sup>2</sup>	Basin > 25,000 km <sup>2</sup>	Regional
Hydrogeologic Mapping (surface geology, potentiometric surfaces, location of karst features, well inventories, and compilation of all existing data sets and reports on the site)	-----		
Surface Geophysics (seismic, gravity, ground-penetrating radar, electromagnetics)	-----		
Single Borehole Geophysics (including flowmeter tests, tomography, packer tests, etcetera)	-----		
Multiple borehole geophysical logs and surface geophysics (combined with stratigraphic and lithologic information)	-----		
Airborne Geophysics (electromagnetics, aerial infrared photography)	-----		
Well hydraulic (aquifer) tests	-----		
Qualitative and Quantitative Water-Tracing Tests (artificial tracers-dyes, solutes, or microspheres)	-----		
Natural Tracers (isotopes, naturally occurring dissolved solutes)	-----		
Well Hydrograph/Chemograph Analysis	-----		
Spring Hydrograph/Chemograph Analysis	-----		
Mathematical Modeling (Distributed Parameter, Lumped Parameter, and Fitting Models)	-----		

In general, multiple methods of investigation provide a better understanding of groundwater flow in karst aquifers. Different mathematical models are used at all scales of study: for hydrograph and chemograph analyses; or to approximate the entire physical flow system with a groundwater flow simulation. Thus, it is best to have multiple investigators or advisors with multi-disciplinary backgrounds for investigations of karst aquifers. This introduction describes some of the more useful technologies and approaches to the investigation of karst aquifers. Application of these methods improve our ability to manage the effect of human activities in karst areas and manage water resources.

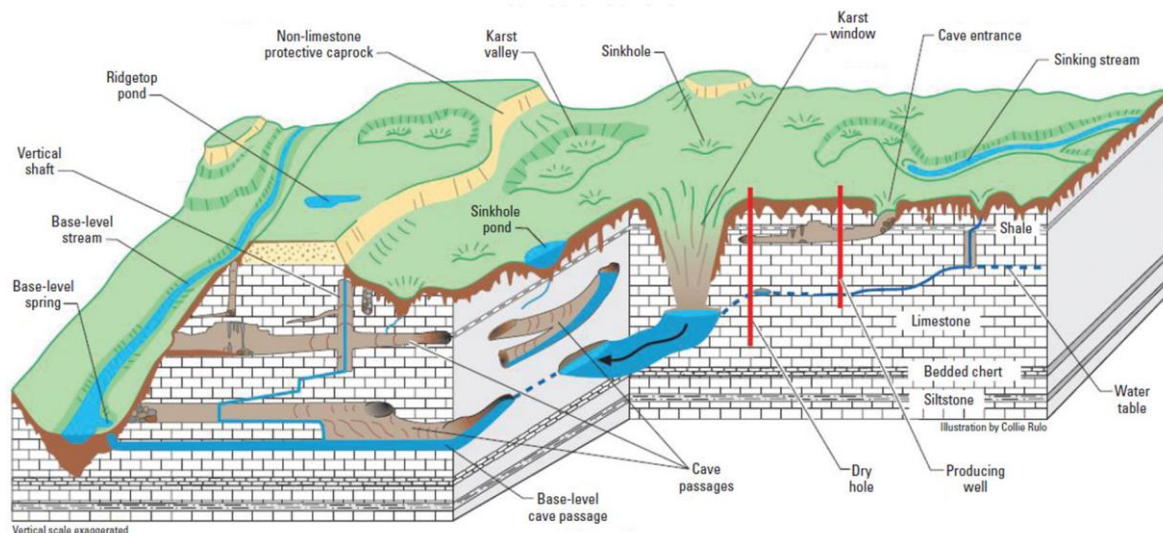
[Exercise 17](#) invites readers to ask themselves, what is a hydrograph or chemograph?



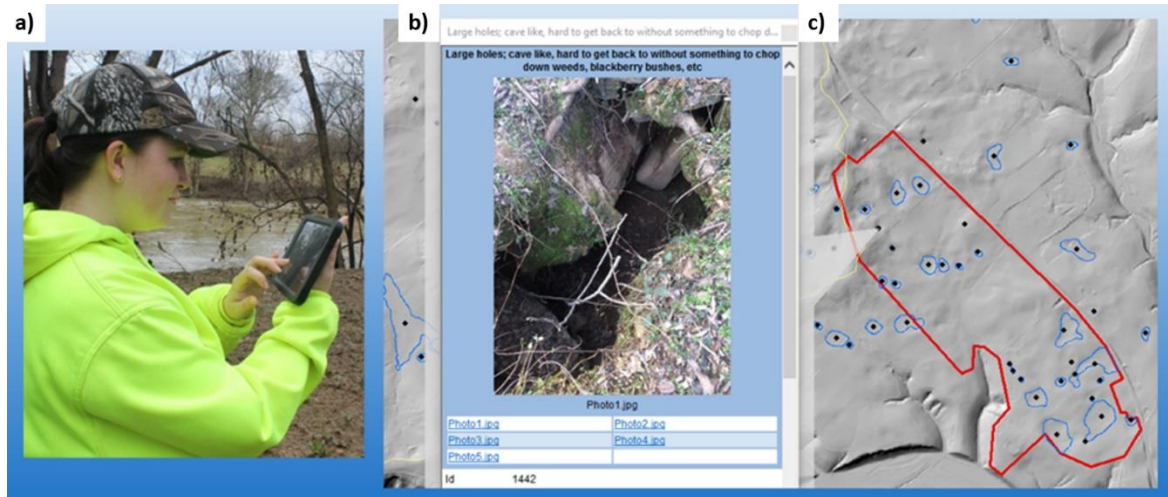
## 5.1 Hydrogeologic Mapping

Hydrogeologic mapping is the identification of physical boundaries of aquifer systems and their hydrologic/hydraulic characteristics. An important distinction is that while hydrogeologic mapping incorporates conventional geologic mapping techniques—such as identifying and mapping the various stratigraphic or bedrock units present and their structural characteristics (geologic strike and dip, presence of faults and fractures, and so on)—it is focused on mapping the storage and transmitting properties of the rocks rather than strictly mapping the geologic stratigraphic units. In fact, in karst and many fractured rock aquifer systems, the aquifer “boundaries” may include multiple distinctive bedrock units or strata, and the aquifer may be defined physically as the interconnected networks of fractures and karst conduits that transmit water throughout a specific volume of rock. Hydrogeologic mapping is the first step in developing an understanding of the aquifer geometry and the locations where water enters and exits the aquifer. Compiling this information leads to the creation of a conceptual model of the aquifer—also called the hydrogeologic framework. This basic understanding is critically important for investigations and analysis of all types of aquifers.

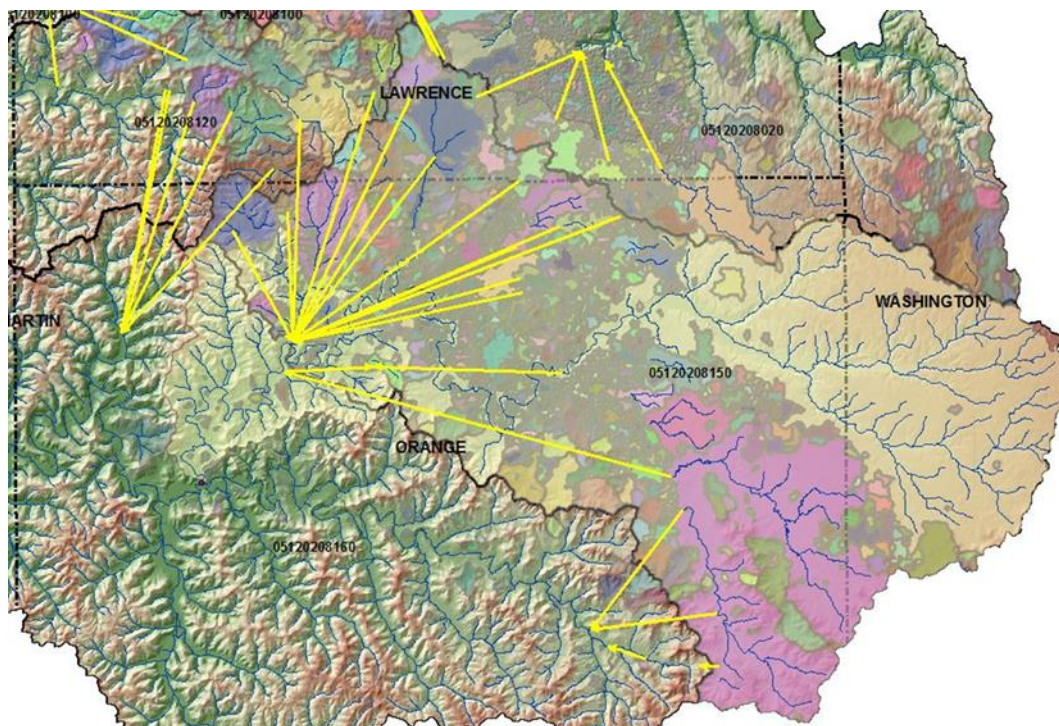
Karst aquifers present unusual challenges as many of the rules for typical porous media do not apply. For example, groundwater flow in karstic watersheds and their subsurface basins may not be inferred from the surface topography. A first step is to identify and characterize the distribution of some of the surface and underground features of karst landscapes in the study area (Figure 40). Mapping the occurrence and distribution of surface karst features (springs, sinking streams, sinkholes) in relationship to the general topography, bedrock stratigraphy, and geological structure (bedrock dip, and visible fault and joint patterns) is critical for karst aquifer studies. Advances in technology have improved field mapping as internet, cell phone and geospatial technology allow real time collection of the location of karst features (Figure 41 and Figure 42).



**Figure 40** - Generalized features in many karst landscapes. Modified from Taylor and Greene (2008).



**Figure 41** - Modern internet and cellphone-based geospatial technology greatly help expedite and enhance collection of karst-hydrogeologic mapping data. a) Antonia Bottoms, a geologist at Kentucky Geological Survey, uses a portable tablet equipped with GIS (Geographic Systems Information) and geocaching software capabilities to verify sinkhole locations identified and delineated using processed LIDAR topographic data, and collect additional field data, such as b) geotagged photographs, needed to characterize their visible physical and hydrologic characteristics. c) On the LiDAR-based topographic map image, sinkhole depressions are delineated by blue polygons and potential swallets (open-throat sinkhole drains) are identified by black dots. The red polygon delineates the boundaries of a farm property which was the site of the field investigation. Photographs and graphics provided by Taylor (2021).



**Figure 42** - Use of modern GIS technology greatly facilitates the task of compiling, visualizing, and analyzing karst geospatial data needed for hydrogeologic mapping. Here GIS is used to visualize the relation between surface streams, watersheds and catchments (surface basins) of sinkholes as well as sinking streams (multicolored polygons) in the upper Lost River basin, south-central Indiana, USA. Dye-trace flow vectors (yellow lines) are added to help identify general directions of subsurface flow through conduits and point-to-point connections between sinkholes or sinking streams and mapped karst springs. Modified from Taylor and Nelson (2008).



## Enhancing Mapping with Subsurface Data

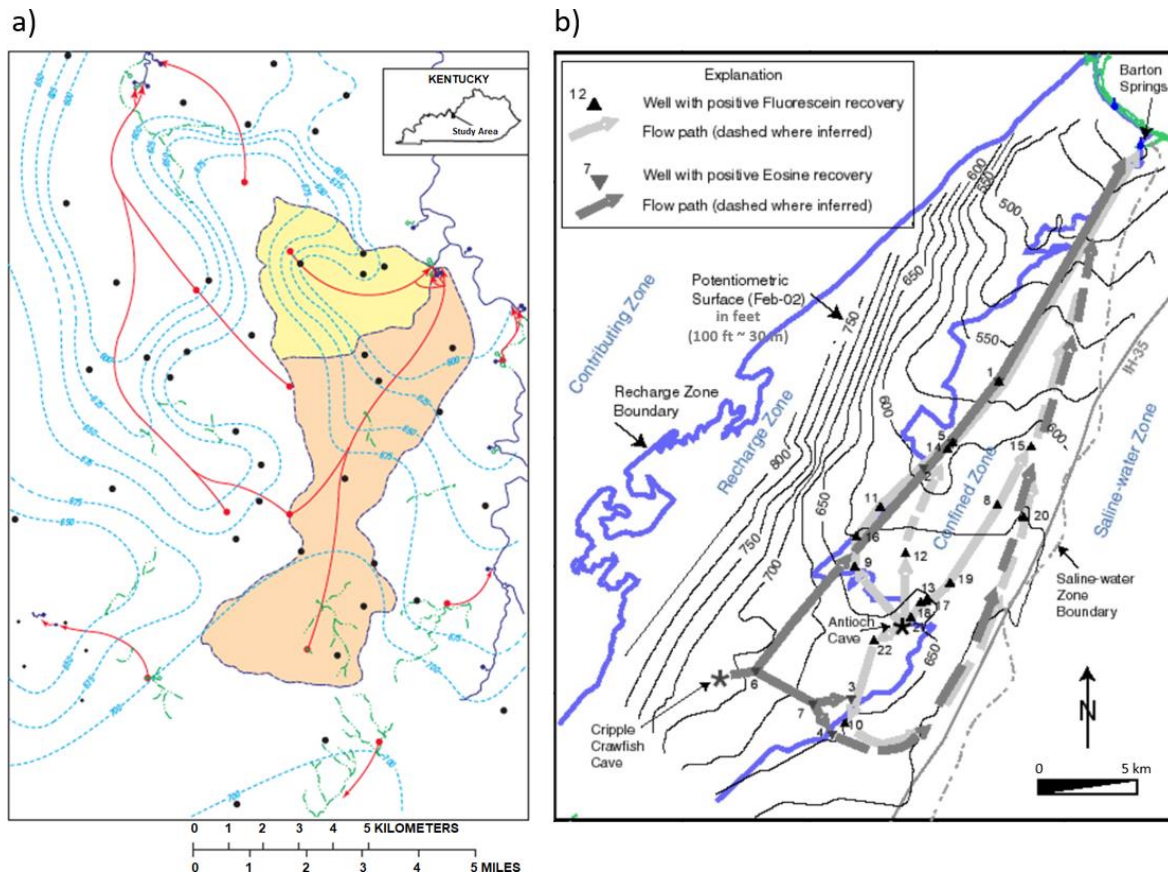
Surficial karst-feature mapping needs to be enhanced with subsurface data including: water well construction and static water level measurements; groundwater withdrawal information; information from aquifer tests in the study area; and surface or borehole geophysics studies. These are the more conventional types of hydrogeologic methods used to investigate aquifers in many types of aquifer settings. They are useful and may provide critical information in the investigation of karst aquifers if the data are applied within the framework of a karst conceptual model (Taylor and Greene, 2008).

In karst terranes, an emphasis must be placed on delineation of karst basin boundaries; subsurface flow paths; contributions of water from localized recharge sources; and the geometric and hydraulic properties of conduits. The acquisition of these data requires a multidisciplinary study approach that includes combining conventional hydrogeological mapping methods with specialized investigation methods such as water-tracing tests and spring monitoring including the analysis of variations in spring discharge and water chemistry (White, 1993; Ford and Williams, 1989). By far, the most valuable single source of information is obtained using properly designed qualitative or quantitative water-tracing tests, usually conducted with non-toxic, fluorescent dyes. Applications of these tests are discussed in detail by Mull and others, 1988a; White, 1993; Goldscheider and Drew, 2007; and Taylor and Greene, 2008. Water tracing tests are discussed in Section 5.3.

The combination of water-level (potentiometric-surface) mapping and dye-tracing tests (Figure 43) has been extensively and successfully employed for decades to:

- determine groundwater flow directions;
- infer approximate locations of conduit-dominated flow paths;
- identify or confirm hydrologic connections between specific sinkholes and other sources of recharge and karst springs;
- identify and delineate karst basin boundaries; and,
- investigate and characterize other physical hydrogeologic characteristics of the karst aquifer system.

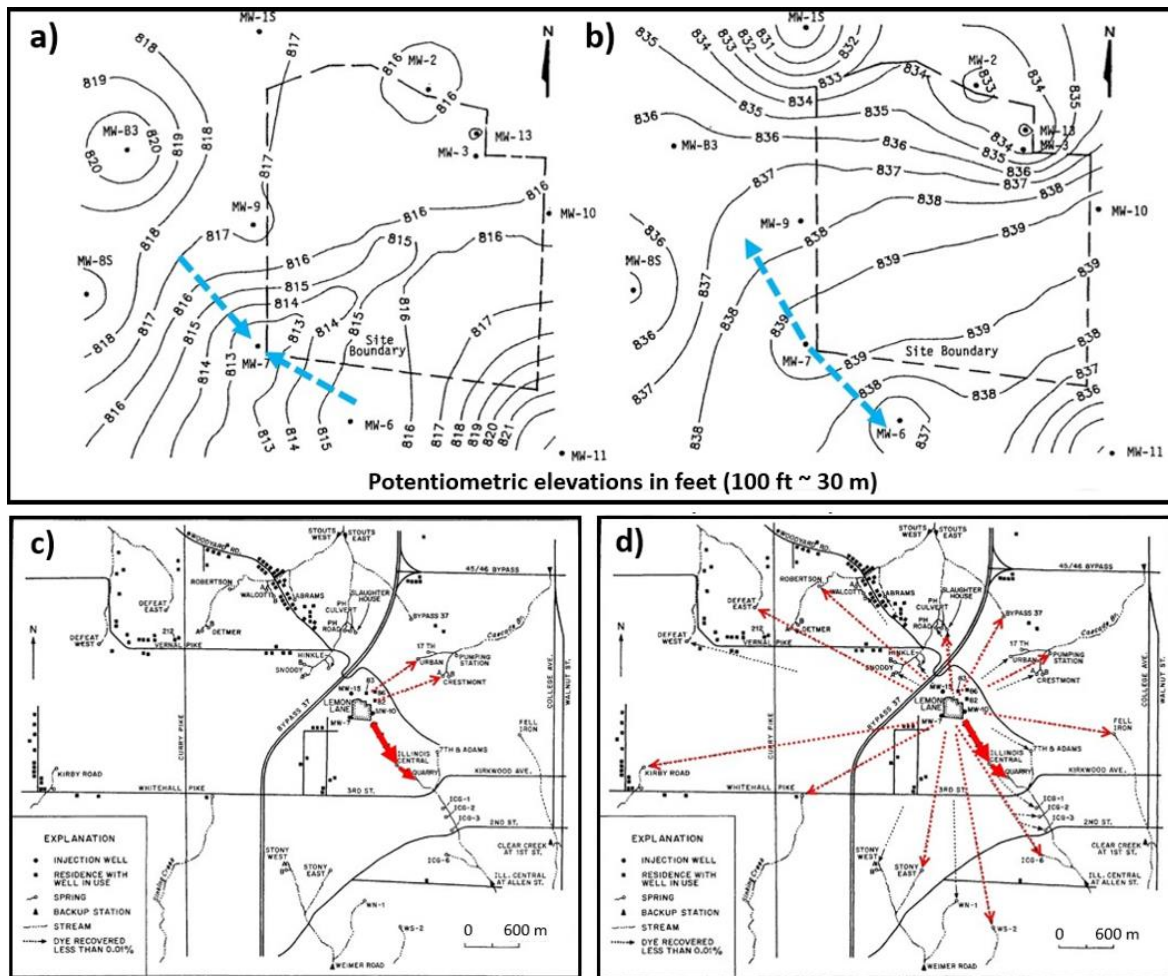
Dye-tracing or water tracing tests conducted with other appropriate types of water tracing agents are the only reliable methods of confirming whether flow inferred by potentiometric or water-table contours indicate the groundwater flow direction, and of accurately assessing karst groundwater velocities and other important hydraulic parameters critical to wellhead protection as well as contaminant characterization and remediation efforts (Quinlan et al., 1995; Field and Nash, 1997; Ewers, 2006).



**Figure 43** - Potentiometric and dye tracing tests for delineation of karst spring boundaries. a) Example of combined use of potentiometric data and dye-tracing tests to delineate karst spring basin boundaries in Kentucky, USA. The “U”-shaped troughs or depressions in the contoured potentiometric surface often indicate the presence (and general but not precise location) of major karst conduits (Modified from Taylor and McCombs, 1998). b) Example demonstrating combined use of potentiometric data and dye tracing tests for hydrogeologic mapping in the Barton Springs karst basin, Edwards Aquifer system, Texas, USA. From Hunt and others (2005).

The hydrology of karst is dynamic and temporally variable, such that water levels, flow directions, groundwater velocities, basin boundaries, spring discharge locations and other downstream receptors of flow may change with changing hydrologic conditions. Thus, it is important to consider whether tracing tests and potentiometric mapping should be repeated under differing hydrologic conditions in order to accurately investigate and assess the range of hydrogeologic variation (Figure 44).






**Figure 44** - Examples of changes in configuration of the mapped potentiometric surface near monitoring well MW-7 at the southwest corner of a landfill which is outlined by a dashed line: a) under low flow conditions; and b) under high flow conditions with blue arrows indicating direction of groundwater flow inferred from the potentiometric surface with respect to MW-7. Showing a larger area surrounding the landfill, dye traced karst groundwater flow paths through probable conduits or enhanced fractures are indicated with red arrows: c) under low flow conditions; and d) under high flow conditions. Modified from McCann and Krothe (1992).

## Enhancing Mapping with Geophysical Data

Geophysical studies can provide a wealth of information that is critical to gaining a better understanding of subsurface conditions needed for groundwater and environmental studies. Geophysical methods of investigation involve studying the earth by measuring its physical properties, with either passive methods such as, changes in gravity; electromagnetic field; or natural radiation; or active methods such as measuring the response of the earth to mechanical; electromagnetic; radioactive; or sound sources. Surface geophysical methods are applied from the earth's surface or from the air. Borehole methods record and analyze measurements of physical properties made in wells or test holes. Probes that measure different properties are lowered into the borehole to collect continuous or point data that are graphically displayed as a geophysical log.

Successful application of a geophysical method requires an understanding of the general principal of the method, how the measuring tool works, the physical property that is measured, and what could be interpreted from the method. Table 4 summarizes this

information and lists some studies that have applied surface geophysics to karst systems. Even in the most well-funded karst studies, there is unlikely to be enough drilling to characterize the hydraulic conductivity variations and the location of conduits. Using a combination of flow logging, stratigraphic correlation, and cross-borehole flow testing can be beneficial for smaller site studies, but it is too expensive to conduct enough of these to characterize a large area. Combining borehole measurements with surface geophysical soundings can provide the area-wide coverage needed to better characterize the subsurface.

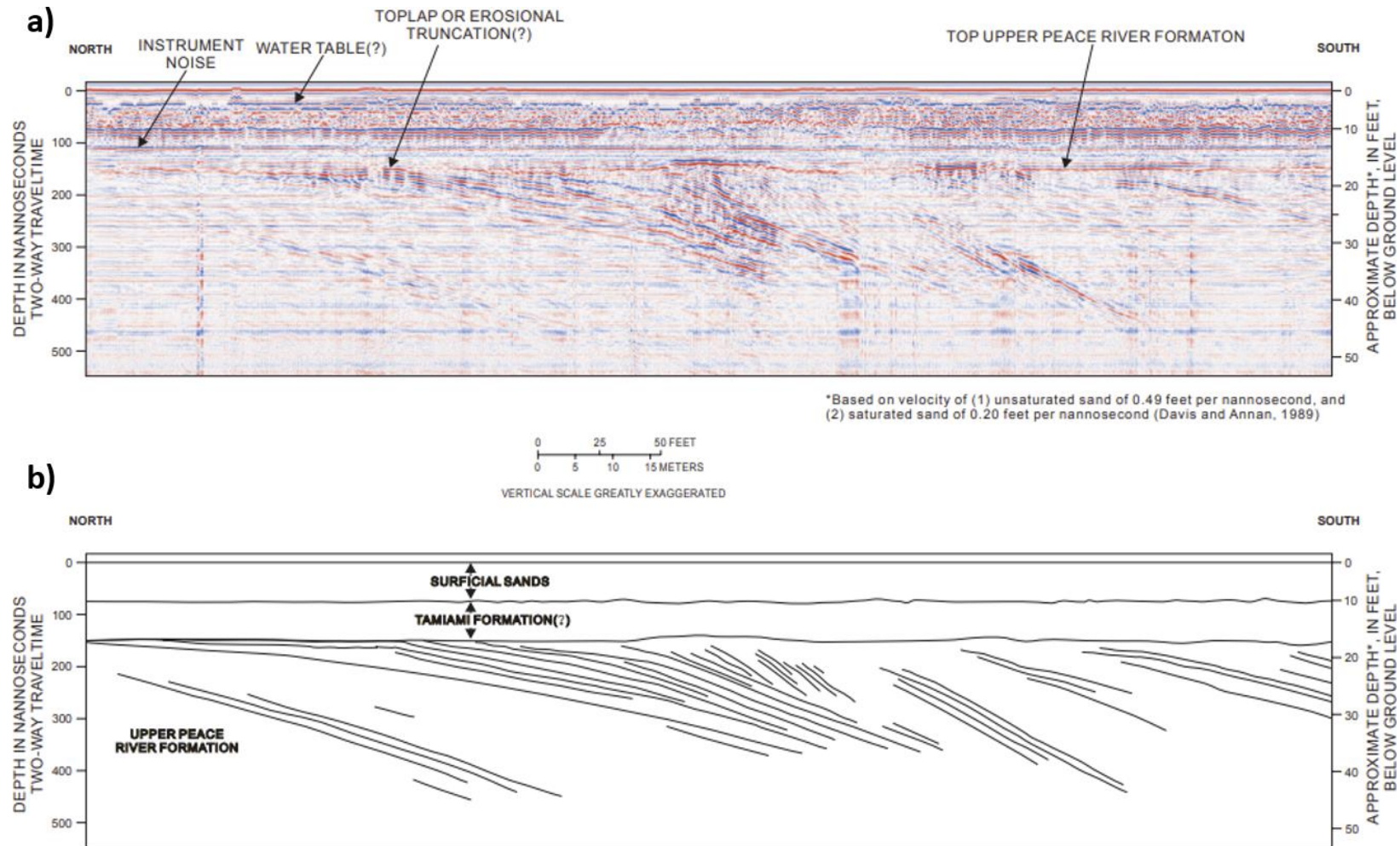
The information in Table 4 is useful whether considering surface or borehole geophysical techniques. [Exercise 18](#)  invites the reader to learn about more about the terms used in Table 4.

### Surface Geophysics Useful to Karst Aquifer Characterization

Some of the most effective surface geophysical tools commonly applied to karst for defining subsurface features are ground-penetrating radar and seismic methods (Cunningham and Aviantara, 2001; Cunningham et al., 2001; Kindinger et al., 1999, 2000, 2001; Kraemer et al., 2001; Steeples and Miller, 1987). Ground-penetrating radar is useful for shallower depths than seismic (Figure 45). Marine reflection seismic data are far easier to collect and interpret and can be run in rivers and lakes. This has been done throughout most of the waterways in Florida and used to define sinkholes (Figure 46).

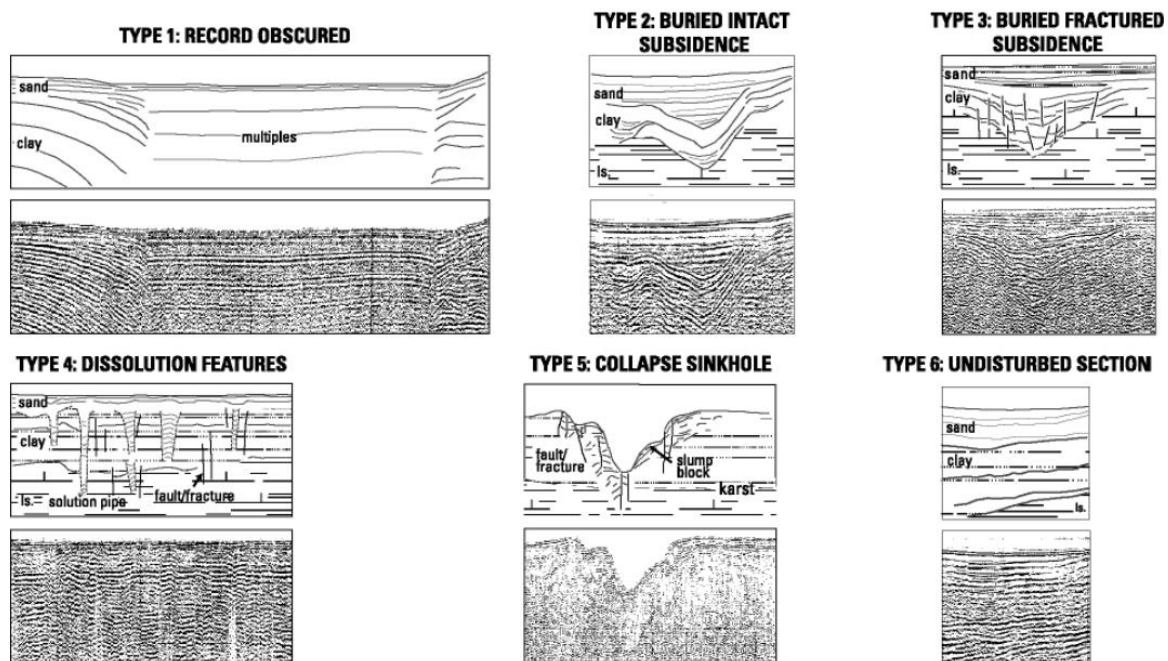
**Table 4 - Surface geophysical tools and what they can detect (Modified from National Research Council, 2000).**

Method	How it works	What property is measured	What is detected	Example Karst applications
<b>Gravity</b>	Detects variations in the gravitational field of the earth caused by mass variation	Density	Depth, geometry, and density of local subsurface features; cavity detection	Butler, 1984
<b>Magnetic</b>	Detects variations in the earth's magnetic field caused by local variations in magnetic properties of subsurface materials	Magnetic properties	Depth, geometry, and magnetic susceptibility of localized subsurface features	Stanton and Schraeder, 2001 Smith et al., 2003, 2005 Gary et al., 2013
<b>Seismic</b>	Sends vibrations (elastic waves) through the subsurface and analyzes changes in velocities (property dependent) and reflections or refractions as waves pass through heterogeneities	Compressional, shear, and surface waves; seismic velocities; and elastic moduli	Interface depths, layer velocities, geometry, or structure, elastic moduli, porosity	Kindinger et al., 1999, 2000, 2001 Kraemer et al., 2001 Steeple and Miller, 1987
<b>Electrical resistivity and electromagnetic (EM) Induction</b>	Detects natural or induced electrical current flow through subsurface materials; electrical properties controlled by material properties of the subsurface along with porosity and pore fluid compositions	Electrical resistivity, magnetic susceptibility	Depth, thickness, electrical resistivity, porosity, inferred fluid chemistry (for example, location of saltwater/freshwater interface)	Fitterman and Deszcz-Pan, 1998 Stanton and Schraeder, 2001
<b>Ground Penetrating Radar (GPR)</b>	Sends high-frequency radar waves through the subsurface; analysis similar to seismic reflection and refraction (velocities are property dependent)	Dielectric permittivity, electrical resistivity, magnetic susceptibility	EM wave speed, depths, thicknesses, geometry	Cunningham and Aviantara, 2001 Cunningham et al., 2001.
<b>Thermal (land based or remote)</b>	Qualitative using thermal images to spot thermal contrasts or quantitative using fiber optic methods or time series of temperature with various devices	Temperature over area in an image or survey or time series temperature at a point or along a line. Often used for groundwater- surface water interactions in karst terrain	Qualitative temperature contrast usually used to note where groundwater enters surface water. Quantitative time series of temperature changes and can calculate flow	Anderson, 2005
<b>Integrated interpretation of multiple methods</b>			Soil and rock type (lithology), structure and stratigraphy, porosity, permeability, fluid content	Cunningham and Aviantara, 2001 Cunningham et al., 2001



**Figure 45** - Ground-penetrating radar profile and interpretation from the Indian Mound site in Glades County. a) Radar profile showing parallel, oblique prograding reflections that are b) interpreted to be images of low angle, accretionary foreset beds. This geophysical technique profiles a unique view into the internal geometry of the subsurface, producing information that can be used for interpretation of depositional environments and hydraulic conductivity. A deep sand pit is located about 500 feet north of the profile, which suggests the entire profile is imaging a quartz sand lithology. From Cunningham and others (2001).





**Figure 46** - Line-drawn interpretations shown above their associated marine seismic profile explaining six types of features beneath lakes of northeastern Florida, USA. Note: Multiples are multiplicative events seen in seismic sections. These events have undergone more than one reflection. They are produced in the data gathering process when the signal does not take a direct path from the source to the geologic feature and back to the receiver on the surface. Multiple events occur in the example labeled "Type 1: Record Obscured" where a large area is indicated as "multiples". From Kindinger and others (2001).

Ground-based magnetic surveys are often used to locate metallic objects such as abandoned wells and have been applied in karst aquifers over small areas (Stanton and Schraeder, 2001). Areal magnetic surveys combined with ground surveys, such as direct current resistivity have proven useful in identification of large features and lithologic changes near the surface over larger areas (Smith et al., 2003, 2005; Gary et al., 2013).

Temperature contrasts have been used to identify groundwater inflow to surface water (springs) using infrared cameras at the local level and areal infrared imaging for examination of temperature contrasts over larger areas (Anderson, 2005). Such surveys must be conducted at a time of year when there is a significant difference between surface-water and groundwater temperature. Additionally, electrical resistivity surveys have been conducted in marine environments from boats to find submarine groundwater discharge in many depositional environments including karst (Henderson et al., 2010). Airborne electromagnetic methods were used to map *salinity* in the shallow coastal Biscayne Aquifer (Fitterman and Deszcz Pan, 1998).

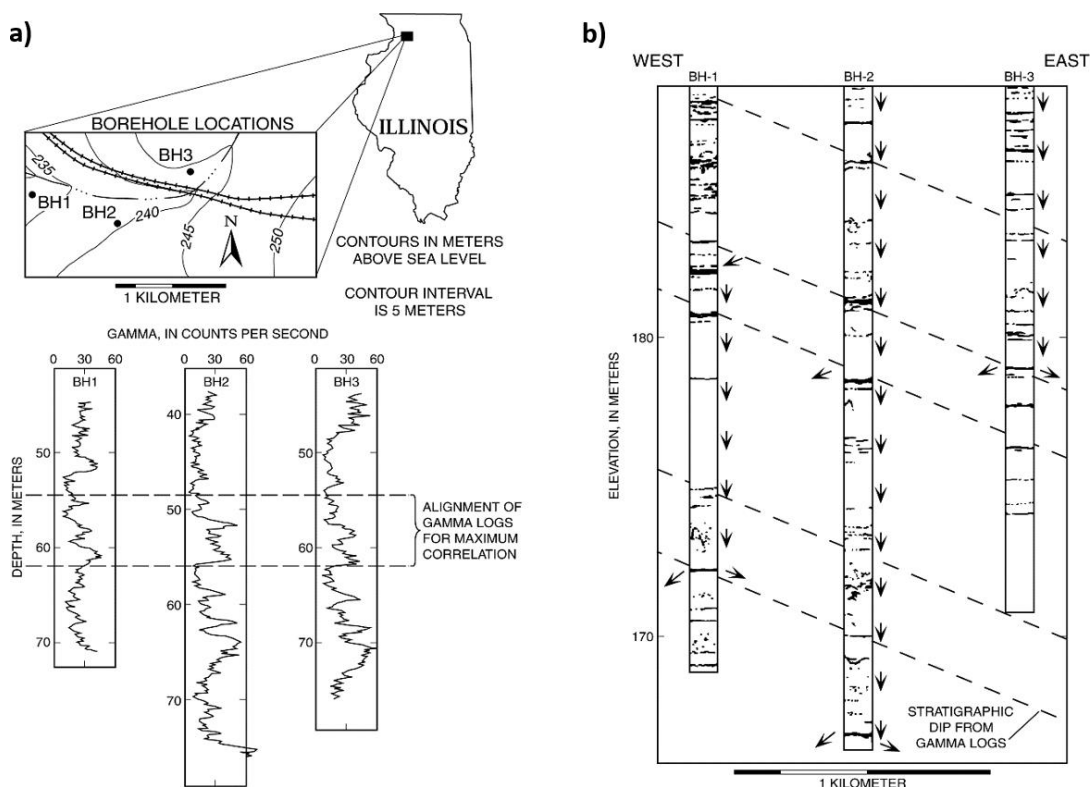
## 5.2 Borehole Testing

Borehole testing in karst systems differs from investigation in other aquifer types because connected conduit networks need to be identified and delineated. Tests used in other types of aquifers have some application in karst with respect to identifying strata that tend to contain conduits and control their connections, but additional tests are needed to specifically find conduits and evaluate their connectivity. These tests include: borehole geophysical techniques that acquire images of borehole walls and measure flow to/from specific zones; water tracing tests that determine connectivity of conduits over short and long distances; and aquifer tests (often using packers to isolate sections of the borehole) that provide information on the distribution of transmissivity and storativity in the aquifer.

### Borehole Geophysical Tools Commonly Applied to Any Aquifer Type

Often borehole measurements at a single well provide minimal information in karst aquifer studies because randomly drilled boreholes are unlikely to intersect conduits that are important to karst systems, especially if the rock matrix porosity is small and conduits are sparse. Measurements of the transmissivity or permeability of fractures and solution openings intersecting boreholes represent formation properties that apply to, at most, a few borehole diameters around the measurement point. This is an inherent property of the radially convergent or divergent flow regime where most flow dissipation occurs in the immediate vicinity of the borehole wall. Therefore, geophysical well logs are mostly of use in characterizing the general hydrogeologic context of the formation containing karst features. In the example shown in Figure 47, conduits are unlikely to be detected; however traditional natural gamma logs from several wells are used to determine the subsurface dip of the sedimentary rocks. Borehole logs can indicate the continuity or offset of bedding plane horizons, or the pattern of fracture connectivity related to joints and large-scale stress patterns influencing the geometry of solution openings.

Borehole geophysics is generally used in groundwater and environmental investigations to: delineate hydrogeologic units; define water quality; and determine well construction and condition. These generalized applications of logs are discussed in a separate GW-Project book describing borehole geophysics.



**Figure 47** - a) Horizontal alignment of gamma logs along an east west profile was used to identify stratigraphic dip in a dolomite aquifer in northern Illinois. The gamma profile along with borehole lithologic logs are used to distinguish a geologic unit that has a similar gamma signal (marker). This marker is shown within the dashed lines and used to align the logs. b) Televiwer logs, stratigraphic correlation, and flowmeter information were used to identify continuous bedding planes and aquifer flow zones where arrows indicate direction of ambient flows measured in boreholes and locations of inflow and outflow (Paillet and Crowder, 1996). Inflow or outflow was associated with solutional-enlarged bedding plane openings. Many such bedding planes intersected each borehole, but only a few conducted most of the flow. The correlation of these conductive bedding planes was established over borehole separations of about a kilometer by correlating gamma logs. The gamma correlation established the strike and dip of bedding so that borehole elevation and the regional dip could be used to define the precise stratigraphic position of the bedding planes in each borehole. This structural correlation showed that sets of bedding planes served as regional conduits, but that the most transmissive bedding plane within groups of closely spaced bedding planes varied from one borehole to the next.

Common borehole geophysical logs include caliper, gamma, single-point resistance, spontaneous potential, normal resistivity, electromagnetic induction, fluid resistivity, temperature, flowmeter (ambient and pumping), television, and acoustic and optical televiwers provide continuous and in-situ data (Table 5). Multiple logs are typically collected to take advantage of their synergistic nature--much more can be learned by the analysis of a suite of logs as a group than by the analysis of the same logs individually.

**Table 5** - Borehole geophysical tools that record properties with depth and what they measure.

Method	What it measures
Caliper	Records borehole diameter. Changes in borehole diameter are related to well construction, such as casing or drilling-bit size, and to fracturing or caving along the borehole wall. Because borehole diameter commonly affects log response, the caliper log is useful in analysis of other geophysical logs, including interpretation of flowmeter logs.

Method	What it measures
Gamma	Records the amount of natural gamma radiation emitted by the rocks surrounding the borehole. The most significant naturally occurring sources of gamma radiation are potassium-40 and daughter products of the uranium- and thorium-decay series. Clay- and shale-bearing rocks commonly emit relatively high gamma radiation because they include weathering products of potassium feldspar and mica and tend to concentrate uranium and thorium
Single-point resistance	Records the electrical resistance from points within the borehole to an electrical ground at land surface. Resistance is a function of both resistivity and the geometry of the material being measured. In general, resistance increases with increasing grain size and decreases where the borehole is enlarged, fracture frequency increases, and dissolved-solids concentration of the water decreases. Single-point resistance logs are useful in the determination of lithology, water quality, and location of fracture zones.
Spontaneous potential	Records electric potential or difference in voltage between the borehole fluid and the surrounding rock and fluid. Spontaneous-potential logs can be used in the determination of lithology and water quality. Collection of spontaneous-potential logs is limited to water- or mud-filled open holes.
Normal resistivity	Records the electrical resistivity of the borehole environment and surrounding rocks and water as measured by variably spaced potential electrodes on the logging probe. Normal-resistivity logs are affected by bed thickness, borehole diameter, and borehole fluid and can only be collected in water- or mud-filled open holes.
Electro-magnetic induction	Records the electrical conductivity or resistivity of the rocks and water surrounding the borehole. Electrical conductivity and resistivity are affected by the porosity, permeability, and clay content of the rocks and by the dissolved-solids concentration of the water within the rocks. The electromagnetic-induction probe is designed to maximize vertical resolution and depth of investigation and to minimize the effects of the borehole fluid.
Fluid resistivity	Records electric resistivity of water in the borehole. Changes in fluid resistivity reflect differences in dissolved-solids concentration of water. Fluid-resistivity logs are useful for delineating water-bearing zones and identifying vertical flow in the borehole.
Radar	Can be used in a single-hole reflection mode or in a cross-hole tomography mode. In the reflection mode, radar provides an image of discontinuities in the bedrock surrounding a borehole, including bedding planes, lithologic contacts, fractures, and cavities. The measurements are either directional or omni-directional, depending upon the type of equipment and antennas. In the tomography mode, where the transmitter and receiver are in separate boreholes, radar provides an image of the planar section between the boreholes. The radius of investigation depends on the antenna frequency and the electrical conductivity of the bedrock. (Haeni, 2002)
Temperature	Records the water temperature in the borehole. Temperature logs are useful for delineating water-bearing zones and identifying vertical flow in the borehole between zones of differing hydraulic head penetrated by wells. Borehole flow between zones is indicated by temperature gradients that are less than the regional geothermal gradient, which is about 1 degree Fahrenheit per 100 feet (~30 m) of depth.
Flowmeter	Records the direction and rate of vertical flow in the borehole. Borehole-flow rates can be calculated from downhole-velocity measurements and borehole diameter recorded by a caliper log. Flowmeter logs can be collected under non-pumping and/or pumping conditions. Impeller flowmeters are the most widely used but they generally cannot resolve velocities of less than 5 feet/minute (~1.5 meters/minute). Flowmeters using heat-pulses or electromagnetic signals named Heat-pulse and Electromagnetic flowmeters can resolve velocities of less than 0.1 feet/minute (~0.03 meters/minute).
Television	Records a video of the borehole wall. Well construction, lithology and fractures, water level, cascading water from above the water level, and changes in borehole water quality (chemical precipitates, suspended particles, and gas) can be viewed directly with the camera.
Acoustic or Optical viewer	Records a magnetically oriented, photographic image of the acoustic reflectivity of the borehole wall. Televue logs indicate the location and strike and dip of fractures and lithologic contacts. Collection of televue logs is limited to water- or mud-filled open holes.



## Borehole Geophysical Tools Particularly Useful for Characterizing Karst Aquifers

Borehole geophysics provides several tools that can make significant contributions to characterization of karst systems. Image logs (Figure 16 and Figure 17) and flow logs provide detailed information about the nature of hydraulically active zones intersected by boreholes that can be used to infer how these zones fit into regional hydrogeology. Geometric correlation of logs from different boreholes can indicate connections of features between boreholes. Water-chemistry and hydraulic-head data derived from logs can be used to identify possible connections of flow paths in the subsurface. Cross-borehole flow experiments can be used to infer the properties of hydraulic connections among subsurface conduits. Geophysical measurements can be made at local, intermediate, and large scales to infer the relation between scale and hydraulic conductivity (Paillet, 2001).

Most geophysical logs provide precise information about the in-situ properties of subsurface formations in the form of measurements such as gamma activity or electrical conductivity that are indirectly related to the hydraulic properties of interest. Generally, the transmissivity of bedding planes, fractures, and solution openings cannot be inferred from the appearance of those features on borehole image logs or the apparent aperture of those features on caliper logs (Paillet, 1998). High-resolution flow logging equipment such as the heat-pulse (Hess, 1986) and electromagnetic (Molz et al., 1994) flowmeters add the important ability to tie borehole hydraulics to geophysical log data.

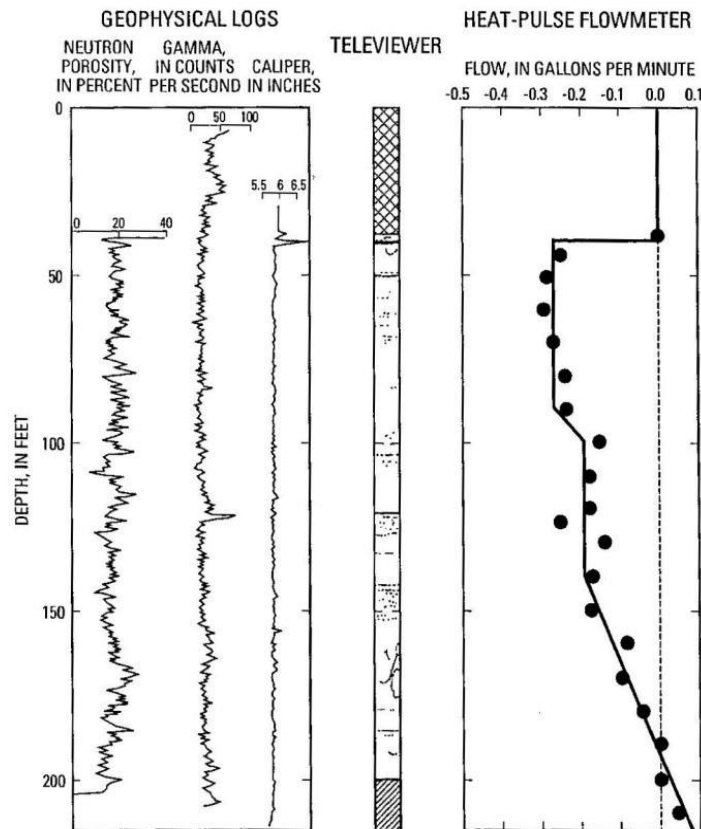
Paillet (1998) illustrates the application of logs to karst aquifers, by comparing gamma, short-normal resistivity, fluid column resistivity, caliper, and televiwer logs with a borehole flow profile obtained with a heat-pulse flowmeter during injection in a borehole that was drilled into fractured and bedded limestone in northern Arizona. The logs indicate the precise depths where water exits the borehole during steady injection. The outflow points can be associated with features on the other logs that represent the hydraulically conductive features in the vicinity of the borehole, including fractures, bedding planes, and a small cavern. Although the full set of logs from one well provides no information about how far these features extend away from the borehole, the flow log indicates where flow enters or exits the borehole. Patterns from all the logs associated with the flow feature may represent a useful vertical marker for comparison with borehole logs from adjacent wells. These marker patterns in specific units can be used to find similar zones in other wells where flow logs have not been recorded. Similar to the use of the gamma-log marker pattern in Figure 47. This is an important step beyond simply identifying the fractures and solution features that intersect a single borehole.

One possible approach to understanding how hydraulically conductive fractures, bedding planes, and solution openings identified in boreholes are connected to form conduit flow systems is to project these features into the regions between boreholes. This seems simple in principle, but is difficult in practice when there are many features that may be permeable in each borehole and boreholes are located far apart. Spatial correlation based on the appearance of features in image logs and their occurrence at similar depths is

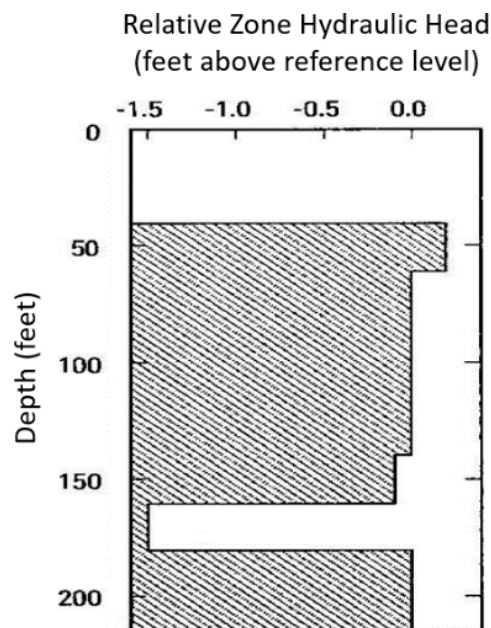
generally not effective. An effective approach is to locate permeable openings with respect to sedimentary structure and potential marker units (parts of the formation with a distinct geophysical log pattern that are associated with flow). The combination of structural correlation and flow log analysis can be useful in identifying how solution openings are organized into continuous flow paths even when large-scale aquifer-test data are not available.

Geophysical measurements made in boreholes apply to the immediate vicinity of the measurement point, however, hydraulic head measurements made at discrete points in a borehole can be related to the large-scale flow field in the formation and, therefore, to the possible presence and location of interconnected conduits supporting active flow. Such discrete head measurements have traditionally been made with straddle-packer equipment that isolate short sections of borehole to provide a direct measurement of hydraulic head in openings connected to that interval. Use of straddle packer technology is equipment- and time-intensive and is especially cumbersome in boreholes that are intersected by many potentially separate flow zones. For this reason, the US Geological Survey developed a wireline-operated packer system as a simple extension of a typical geophysical logging program (Paillet et al., 1990). The equipment was designed to measure the hydraulic head above and below a single packer dividing the borehole into two separate compartments, and then data analysis converted a series of such measurements into hydraulic head values for the intervals between individual packer stations.

An example of the borehole-packer head-measurement application is given in Figure 48 and Figure 49 for a karst site in eastern Illinois, USA. This study investigated a site where heavy-metal contamination was detected at shallow depths in bedded limestone overlying a municipal aquifer with production wells completed below 1000 feet (~300 m) in depth. In planning the study, it was assumed that a steep vertical hydraulic head gradient was present in the shallow subsurface. Heat-pulse borehole flowmeter logs indicated strong downward flow under ambient conditions in response to that gradient. However, flow logs indicated an unexpected reversal to upward flow near the bottom of the boreholes (Figure 48). The wireline packer was used to investigate the hydraulic head distribution along the borehole and showed that very little vertical head gradient was present. Instead, the packer analysis showed a nearly constant hydraulic head along the borehole with lower head in a single zone about 165 feet (~50 m) deep. Although no obvious karst features were indicated at that depth on the televiewer or caliper logs, the head data showed that flow in the shallow part of the formation was being conducted along one or more bedding planes at that depth, probably to a vertical conduit located at an undetermined distance.



**Figure 48** - Neutron, gamma, caliper, televiewer and heat pulse flowmeter logs for borehole T-6 located in eastern Illinois karst. Unit conversions: 100 feet ~30.5 m; 1 inch ~2.54 cm; 1 gallon per minute ~3.8 L/min (liters per minute). From Paillet and others (1990).

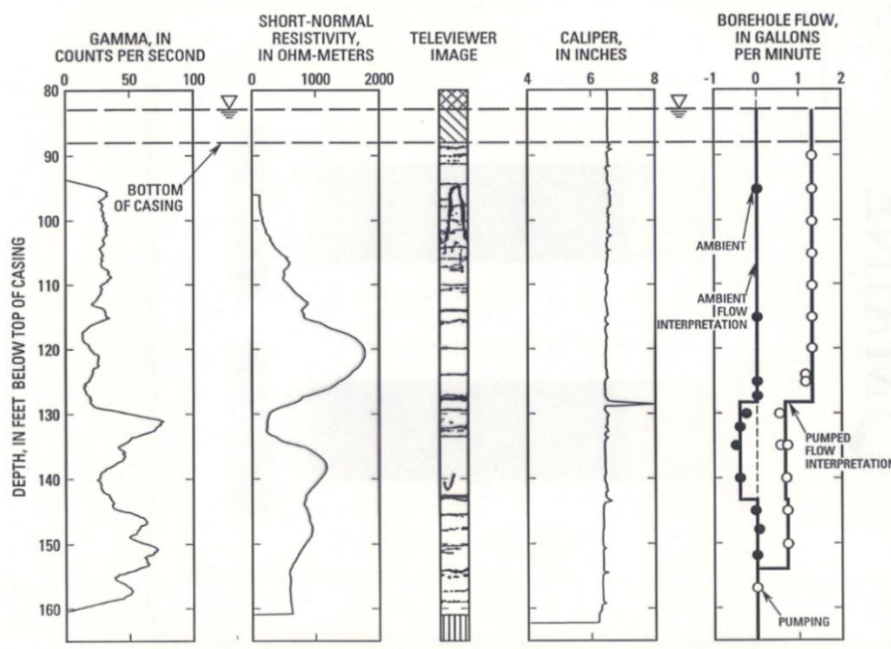


**Figure 49** - Estimates of in situ hydraulic head made with an experimental wireline-operated packer for borehole T-6 in karst in eastern Illinois karst. Unit conversions: 100 feet ~30.5 m; 1 foot ~0.305 m. From Paillet and others (1990).

At the time of the wireline packer study, there was no alternative for interval head measurements. Since then, methods for estimating the hydraulic head directly from borehole flowmeter measurements have been developed (Paillet, 2000; Day-Lewis et al., 2002). The analysis starts where a pair of steady flow profiles obtained under two different conditions (usually ambient and pumping) are simultaneously modeled to estimate transmissivity and hydraulic head for each inflow or outflow zone. An example of this technique applied to a karst aquifer in north-central Tennessee is shown in Figure 50. The borehole site was located a fraction of a kilometer from a ravine with known karst discharge from a small cavern. The ambient flow profile showed downflow entering at about 128 feet (~39 m) and exiting at about 143 feet (~50 m). Pumping at about 1.3 gallon per minute changed the flow regime to upward flow entering at about 154 feet (~47 m) and exiting at 128 feet (~39 m). Flow log modeling showed three equally transmissive zones with the lowest hydraulic head at 143 feet (~50 m), highest head at 128 feet (~39 m), and an intermediate head at 154 feet (~47 m). This distribution indicated that the bedding plane at 143 feet (~50 m) was connected to the discharge point in the nearby ravine and that flow was directed downward towards that horizon from above, and upward from below.

It is important to note the significance of conducting both ambient and pumping flow measurements in this situation. The ambient and pumping flow profiles in Figure 50 show that the central flow conduit in this karst study would not have been identified if only a pumping profile had been obtained. The ambient flow log indicates, there is no flow above and below the fracture zone (from approximately 128-143 feet (~39-44 m) below top of casing) and all measurements indicate small downward flow (Figure 50). From the pumping flow log, there is still no flow at the bottom of the well, some flow is detected slightly below the main fracture and enters in the fracture zone (a constant and low upward flow rate), then just above the main fracture (note large opening in caliper log at approximately 129 feet below top of casing; the flow rate exhibits an abrupt increase and stabilizes. Thus, with only a pumping flow log a much longer vertical zone would appear to be contributing flow to the borehole. The combination of the ambient and pumping flow logs and the caliper log help identify the fracture where most of the water enters the borehole.





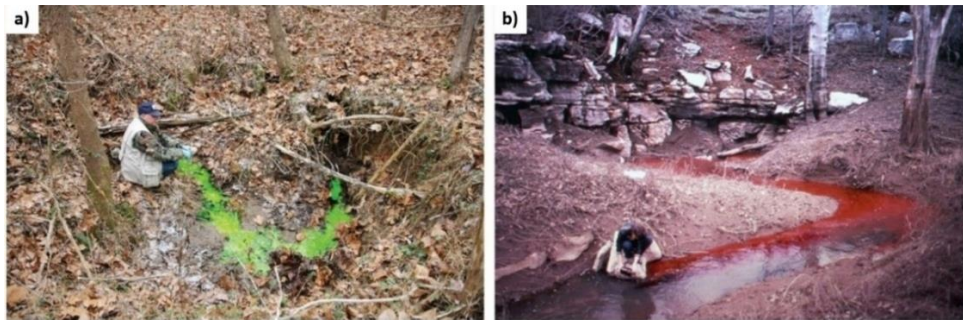
**Figure 50** - Geophysical log composite for a karst well at Fort Campbell, Tennessee using flowmeter logging. Unit conversions: 100 feet ~30.5 m; 1 inch ~2.54 cm; 1 gallon per minute ~3.8 L/min (liters per minute). From Paillet (2000) and Day Lewis and others (2002).

Many hydrologists still rely on straddle packer measurements to determine hydraulic head distributions in karst formations. Televiewer and caliper logs often indicate several potential flow zones that would have to be treated with individual tests. Even when packer work is included in a study, the use of flow log profiling as part of the geophysical log suite can identify the specific flow zones that take part in flow to enhance the efficacy of packer work or piezometer installation. Also, once the initial pair of flow logs has been analyzed, zone transmissivity is determined, and subsequent monitoring of zone hydraulic head variation can be conducted with repeat ambient flow logs in an open borehole without use of packers or elaborate completions.

### 5.3 Water Tracing Tests

Water-tracer tests are perhaps the most cost- and scientifically-effective method employed in the investigation of karst aquifers. Although naturally-occurring chemicals and isotopes are often, and increasingly, used as tracer agents, especially for studies of recharge and mixing dynamics, many tracer tests are conducted by injecting an artificial tracer—a substance that does not occur naturally in the water or occurs at negligible concentrations—and using various techniques to detect its presence and/or concentration, as it moves through the karst aquifer and resurges from the subsurface (Taylor and Doctor, 2017). The artificial tracer introduced can be a dye (usually a non-toxic fluorescent dye as shown in Figure 51), a dissolved chemical (generally a harmless salt), or particles (size and properties dependent on the nature of the aquifer and the property of interest). Any artificial tracer introduced must be considered toxicologically safe and sometimes a permit

is required to introduce a tracer into the natural system and for access to place measurement devices to determine when and if the tracer arrived from the injection location to the monitoring location (Table 6).



**Figure 51** - Photographs showing injections of two commonly used fluorescent dye tracers: a) injection of sodium fluorescein into storm runoff drained by an open sinkhole throat; and, b) injection of rhodamine WT into the perennial flow of a disappearing stream. Photographs provided by Taylor (2021e).

**Table 6** - Summary of artificial tracers. Tracers classified as toxicologically “safe” by Behrens and others, (2001) are marked with an asterisk; the others were either not assessed or have associated toxicological concerns. Chemical Abstracts Service Registry Numbers (CAS RN) allow unambiguous identification. DOC: dissolved organic carbon, ICP MS: inductively coupled plasma mass spectrometry, IC: ion chromatography. From Goldscheider and others (2008).

Group	Tracer name (CAS RN)	Detection Limit	General Problems	Specific Problems
Fluorescent dyes	Uranine (518-47-8)	10 <sup>-3</sup> µg/L	Sensitive to light and strong oxidants. Analytical interferences between fluorescent dyes of similar optical properties.	-
	Eosin (17372-87-1)	10 <sup>-2</sup> µg/L		-
	Amidorhodamine G (5873-16-5)			-
	Sulforhodamine B (3520-42-1)			Ecotoxicological concerns
	Rhodamine WT (37299-86-8)			Genotoxic
	Pyranine (6358-69-6)			Biodegradable
	Naphthaionate (130-13-2)	10 <sup>-1</sup> µg/L		Analytical (optical) interference with DOC
	Tinopal CBS-X (27344-41-8)			
Salts	Sodium	Using Inductively Coupled Plasma-Mass Spectrometry (only cations) 10 <sup>-3</sup> to 0.1 µg/L and using Ion Chromatography 0.1 mg/L	Sorption of cations (Sr>K>Na>Li)  Variable and sometimes high natural background, particularly for Na and Cl	-
	Potassium			-
	Lithium			-
	Strontium			-
	Chloride			-
	Bromide			Can form toxic compounds
				Bio-chemically unstable
	Iodide			
Particles	Fluorescent microspheres	Detection	Analysis is relatively time consuming.  Prone to filtration.	-
	Bacteria	of single		Limited stability (inactivation) Analysis within 24 hours
	Bacteriophages	particles		

There are two main types of tracer tests, one is called a qualitative, or point-to-point tracer test, and the other a quantitative tracer test. Qualitative, point-to-point, tracer tests, are typically conducted using a variety of fluorescent dyes and have been the mainstay of karst hydrologic studies for many decades because of their relatively low cost and ease of implementation. These types of tests are generally conducted to determine karst groundwater flow directions and basin boundaries by helping identify the presence of one or more subsurface flow path connections between a dye-injection site (usually a sinkhole, sinking stream, or well), and downstream monitoring sites, such as a spring, surface stream, or water well. These tests are also commonly employed within caves to identify hydraulic connections and flow paths between cave segments or levels (Goldscheider and Drew, 2007). Hydraulic connections can be verified with visual confirmation if using colored fluorescent dyes or through the deployment of passive detectors, often informally called dye “bugs”. Bugs are composed of flow-through mesh bags containing activated coconut charcoal and deployed in a selected well, stream, or spring sites (Figure 52). The bugs absorb the dye and can be deployed for days or weeks before retrieval and analysis. These qualitative tests are almost always performed before a quantitative tracer test is conducted.

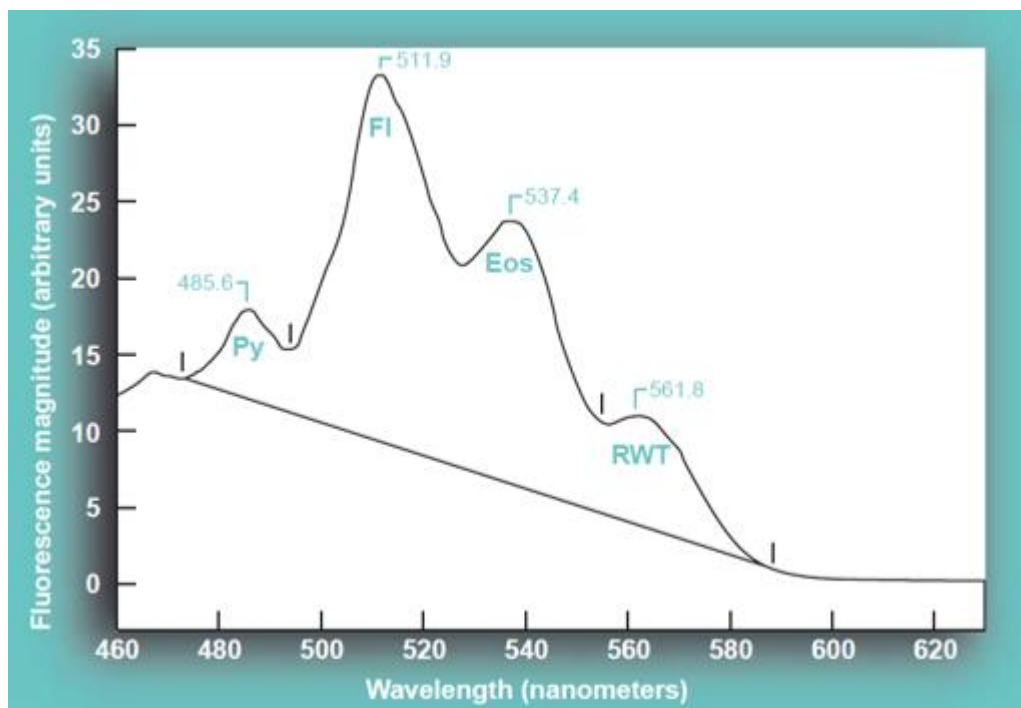


**Figure 52** - Photographs of J. Van Brahana setting a bug (dye absorbent material in a flow through mesh bag) at Tree Spring at the Savoy Experimental Watershed, Arkansas, USA. The bug is fixed in place (usually for days or weeks) to determine if dye passes that location, but the exact time of arrival cannot be determined. Photograph by Kuniansky (2017)

If bugs are retrieved and replaced with new bugs sub-daily, daily, or at weekly intervals, the approximate number of days or weeks for the dye to reach the outlet can be estimated. After bugs are collected in the field, and washed, samples of the charcoal are treated with a basic-alcohol eluant to expel any adsorbed tracer dyes, which are identified by running an aliquot sample of the resulting elutant through a fluorometer or spectrofluorophotometer. Various types of fluorometry instruments can be employed (an *eluant* is the liquid used to remove dye from the activated carbon bugs and results in the



*elutant*, which is the dye dissolved in the liquid eluant). An example of the graph resulting from spectrofluorophotometer analysis of an elutant is shown in Figure 53. The graph shows wavelength on the x-axis and relative excitation fluorescence on the y-axis for one sample from a given time.

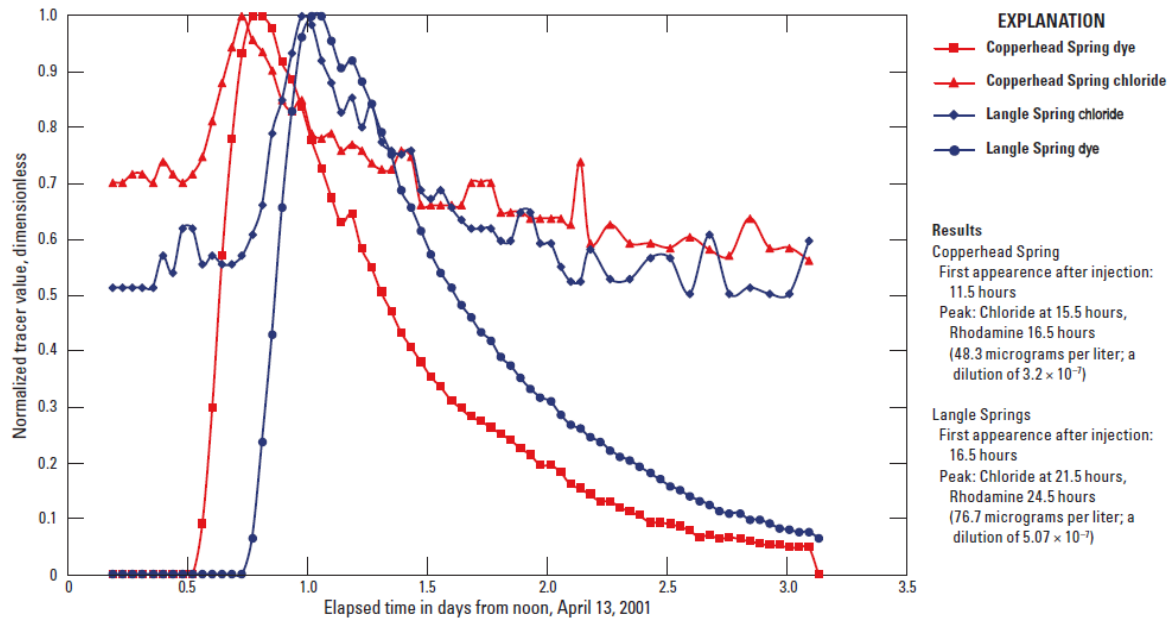


**Figure 53** - A graph of an activated carbon sampler elutant containing fluorescence peaks from pyranine, fluorescein, eosine, and rhodamine WT from a groundwater tracing study in British Columbia, Canada, from Aley (2002). A spectrofluorophotometer graph is a plot of wavelength on the x-axis and relative excitation fluorescence on the y-axis for one sample from a given time thus it identifies substances in the elutant. It is not a time series.

Quantitative tests can provide detailed information such as hydraulic conductivity and contaminant travel time for a conduit flow system, but are generally less commonly conducted than point-to-point tracer tests due to the need for more intensive monitoring and dye-analysis procedures. Quantitative tests require information on the amount of dye injected and the time series of concentration and groundwater discharge rate from the exit point (a spring or well). With fluorescent dye tracers, a field fluorometer and data logger typically are calibrated with standards in the field according to the manufacturer's instructions, and the equipment is installed at the discharge location. Grab samples are collected frequently and the grab samples are analyzed in the laboratory using a laboratory calibrated spectrofluorophotometer to verify the field fluorometer results. It is always advisable to collect and analyze grab samples even when a field fluorometer/data logger is deployed.

An example normalized breakthrough curve from a quantitative test in the Savoy Experimental Watershed at the University of Arkansas in the USA is shown in Figure 54. A normalized graph is created by taking the maximum concentration and dividing time

series concentration values by that concentration such that two different tracer breakthrough curves can be plotted on the same graph with the y-axis ranging from 0 to 1 and elapsed time starting at zero for the time the tracer was injected on the x-axis. For the tracer test shown in Figure 54, there was one sinking stream where a slug of dye and salt (NaCl) were injected and two springs that were known to be outlets of this sinking stream.



**Figure 54** - Normalized Rhodamine WT dye and chloride tracer-breakthrough curves for Copperhead and Langle Springs, Savoy, Arkansas, USA, April 13 to 17, 2001. Elapsed time begins at zero which is the time that tracer was introduced at noon on April 13. Chemical data collection began shortly after injection. Illustration provided by J.V. Brahana on November 13, 2017 from a University of Arkansas student, Tiong Ee Ting.

For successful quantitative water-tracer tests, it is critical to:

- consult local geology experts when selecting injection and discharge location(s);
- collect background samples of water to determine if there is background fluorescence or chemical that may interfere with the artificial tracer to be injected;
- select the dye, solute or particulate that is appropriate for the hydrogeologic setting and the study objective;
- use regression equations, once the appropriate dye is selected, to estimate the amount of dye required (Field, 2003; Worthington and Smart, 2003);
- run point-to-point tests to confirm the link(s) from the sink(s) to the discharge location(s);
- determine which method to use for collecting the time series of discharge and concentration (or fluorescence) data;
- determine the thickness of the unsaturated zone and if the tracer will be placed, rather than injected, into a sinking stream or well, determine



whether a tanker of deionized water is required to flush the tracer into the karst system;

- determine whether a pulse of tracer will be used or it will be continuously injected; and,
- for dyes, use dark sample bottles, or have a dark place to store the grab samples, because many organic dyes will lose fluorescence if exposed to sunlight.


[Exercise 19](#)  invites the reader to explore the relative behavior of the dye and the salt shown in Figure 54.

Of the eight fluorescent dyes, the five most useful are: Eosin (Eos), Uranine (Sodium Fluorescein) (Fl), Pyranine (Py), Rhodamine WT (RWT), and Sulforhodamine B (SRB), because all of these dyes are anionic compounds and thus, less subject to adsorption onto clays and similar materials than cationic dyes (Aley, 2002). Each of these five dyes has distinct characteristics and wavelength (for example, color) and are safe at low concentrations, but some may be better suited to one environment or another. For example, Uranine (fluorescein) is bright green, very soluble, safe and has a low detection limit, but will degrade in acidic or organic-rich waters. If one is trying to determine the outlet for several sinking streams and several springs in the same area, dyes of differing optical properties must be used at each sinking stream location to minimize optical interference in analysis of elutant from bugs used in a point-to-point test or grab samples of each spring. A spectrofluorophotometer analysis of one sample from a dye tracer study where four dyes made it to the outlet bug is shown in Figure 53. To summarize the use of fluorescent dyes as tracers, Taylor and Doctor (2017) write: *“Like any other hydrogeologic investigation technique, dye-tracing tests require good planning and implementation, proper interpretation of data, and understanding of the potential limitations and uncertainties associated with the technique. Dyes should be selected for conservative transport behavior, negligible toxicity, and unambiguous detection at low concentrations (Taylor and Greene, 2008). Successful use of dyes requires: (1) preinjection monitoring for substances present in the water that might interfere with detection of dye, (2) determination of the proper amount of dye to inject for the purpose of the test, (3) choosing the appropriate methods for dye monitoring and detection, (4) selection of sites to be monitored, and (5) determination of the duration of the test monitoring period. It is important to also consider the field or hydrologic conditions occurring at the start and over the duration of each dye-tracing test because groundwater flow directions and velocities can change drastically in karst between low-flow and high-flow conditions. These topics are discussed in detail by Smoot et al., (1987), Käss (1998), Goldscheider and Drew (2007), and Taylor and Greene (2008), among others.”*

Of the salts shown in Table 6, common table salt (sodium chloride, NaCl) is often used because it is inexpensive, and its concentration can be sensed by measuring specific conductance. The water-soluble salts split into cations and anions that increase electrical conductivity of water. Some samples can be chemically analyzed for the cation and/or anion concentration and compared with a time series of electrical conductance of the water

(which is inexpensive relative to chemical analysis). Goldscheider and others (2008) explain: “More specific chemical analysis allows use of lithium, potassium and strontium as cationic tracers, while bromide and iodide can be used as anionic tracers. Anions are generally more conservative than cations, which are prone to cation exchange and, thus, retardation. Variable natural background concentrations limit the use of salt tracers, and high concentrations may be harmful to biota”.

Non-toxic microspheres or particles are sometimes used in tracer studies for understanding of the transport of pathogens in the karst system (Harvey, 1997; Mahler et al., 1998 and 2000; Auckenthaler et al., 2002; Göppert and Goldscheider, 2008; Harvey et al., 2008).

[Exercise 20](#)  invites the reader to reflect on what a spectrofluorophotometer measures.

For readers that are interested in learning more about conducting tracing tests in karst, the following references are suggested: Behrens, 1986; Mull and others, 1988a; Aley, 1997, 2001 and 2002; Behrens and others, 2001; Field, 2002 and 2003; Worthington and Smart, 2003; and Goldscheider and others, 2008. A partial list of investigative reports that discuss applications of tracer testing include: Mull and others, 1988b; Mull, 1993a and 1993b; Bayless and others, 1994; Robinson, 1995; Pavlicek, 1996; Taylor, 1997; Kidd and others, 2001; Spangler and Susong, 2006; Kozar and others, 2007; Long and others, 2012; Spangler, 2012; Gouzie and others, 2014; and Kuniansky and others, 2019.

## 5.4 Aquifer Tests

An aquifer test is an experiment conducted at a well or piezometer to determine hydraulic properties of the aquifer. The hydraulic properties most frequently determined are transmissivity and storativity. As described by Darcy’s law, hydraulic conductivity ( $K$  in Equation 1) is the constant of proportionality related to discharge and head gradient. Thus,  $K$  is related to the ease with which water of a constant density and temperature can move through the aquifer. Table 2 has common ranges of  $K$  for all rock types. For relatively horizontal beds of uniform  $K$  and thickness, transmissivity ( $T$ ) is the horizontal hydraulic conductivity multiplied by the thickness of the bed. There is an extreme variation in range of hydraulic conductivity, with transmissivity for karst aquifers often spanning more than six orders of magnitude from 1 to  $1 \times 10^6$  m<sup>2</sup> per day. The variations in  $K$  can occur within a single geologic formation or within sub-layers.

Storativity ( $S$ ) is a measure of the volume of water an aquifer releases or takes into storage per unit surface area per unit change in water level. For confined aquifers, the storage coefficient is a function of the density and compressibility of water, the porosity and compressibility of the aquifer skeleton, and the thickness of the aquifer. Specific storage ( $S_s$ ) is the storativity divided by the thickness of the aquifer. Specific storage is defined by the expression shown as Equation 6.

$$S_s = \rho_w g(\alpha + n\beta) \quad (6)$$

where:

$S_s$  = specific storage ( $L^{-1}$ )

$\rho_w$  = density of water ( $ML^{-3}$ )

$\alpha$  = compressibility of the aquifer skeleton ( $T^2LM^{-1}$ )

$n$  = porosity (dimensionless)

$\beta$  = compressibility of water ( $T^2LM^{-1}$ )

In general, karst aquifers are composed of hard sound rock, so compressibility of the aquifer skeleton is small (Table 7). Thus, specific storage is generally small, on the order of  $1 \times 10^{-6} m^{-1}$ . The storativity for an unconfined (that is, water-table) aquifer is approximately equal to the specific yield ( $S_y$ ), which is related to the amount of water that can be released by gravity drainage. Often in unconfined zones of karst systems the competent carbonate rock may not have many large drainable fractures. Thus,  $S_y$  is often smaller than typical clastic aquifers; however, the specific yield is generally greater than  $10^{-3}$  and so the specific storage part of total storage remains negligible in unconfined karst aquifers.

**Table 7** - Range in values of bulk modulus of compressibility, typical porosity, and specific storage in  $m^{-1}$  and  $ft^{-1}$  (Modified from Jumikis, 1962).

Material	$\beta$ ( $m^2/N$ )	Porosity	$S_s$ ( $m^{-1}$ )	$S_s$ ( $ft^{-1}$ )
Plastic clay	$2.6 \times 10^{-7}$ to $2 \times 10^{-6}$	50.0%	$2 \times 10^{-2}$ to $3 \times 10^{-3}$	$8 \times 10^{-4}$ to $6 \times 10^{-3}$
Stiff clay	$1.3 \times 10^{-7}$ to $2.6 \times 10^{-7}$	40.0%	$3 \times 10^{-3}$ to $1 \times 10^{-3}$	$4 \times 10^{-4}$ to $8 \times 10^{-4}$
Medium-hard clay	$6.9 \times 10^{-8}$ to $1.3 \times 10^{-7}$	25.0%	$7 \times 10^{-4}$ to $1 \times 10^{-3}$	$2 \times 10^{-4}$ to $4 \times 10^{-4}$
Loose sand	$5.2 \times 10^{-8}$ to $1 \times 10^{-7}$	25.0%	$5 \times 10^{-4}$ to $1 \times 10^{-3}$	$2 \times 10^{-4}$ to $3 \times 10^{-4}$
Dense sand	$1.3 \times 10^{-8}$ to $2 \times 10^{-8}$	20.0%	$1 \times 10^{-4}$ to $2 \times 10^{-4}$	$4 \times 10^{-5}$ to $6 \times 10^{-5}$
Dense, sandy gravel	$5.2 \times 10^{-9}$ to $1 \times 10^{-8}$	20.0%	$5 \times 10^{-3}$ to $1 \times 10^{-4}$	$2 \times 10^{-5}$ to $3 \times 10^{-5}$
Rock, fissured	$3.3 \times 10^{-10}$ to $6.9 \times 10^{-10}$	0.1%	$3 \times 10^{-6}$ to $7 \times 10^{-6}$	$1 \times 10^{-6}$ to $2 \times 10^{-6}$
Rock, sound	$< 3.3 \times 10^{-10}$	0.1%	$< 3 \times 10^{-6}$	$< 1 \times 10^{-6}$
Water at 25°C	$4.6 \times 10^{-10}$	-	-	-

The most common tests are aquifer pumping tests and slug tests. Packers can be used for either aquifer pumping tests or slug tests to test short open intervals of a well bore. These tests stress the aquifer either by pumping a well (pumping test) or by suddenly changing the water level in a well (slug test), followed by measurement of the change in water level in and around the well through time. A slug test involves the sudden removal or insertion of an object into the well water which instantaneously raises or lowers the water level in the well. Single well tests, such as slug tests are inexpensive to conduct on existing wells. A multi-well aquifer test involves continuous pumping or injecting of water from/to a well which creates a cone of depression/impression respectively in the aquifer around the

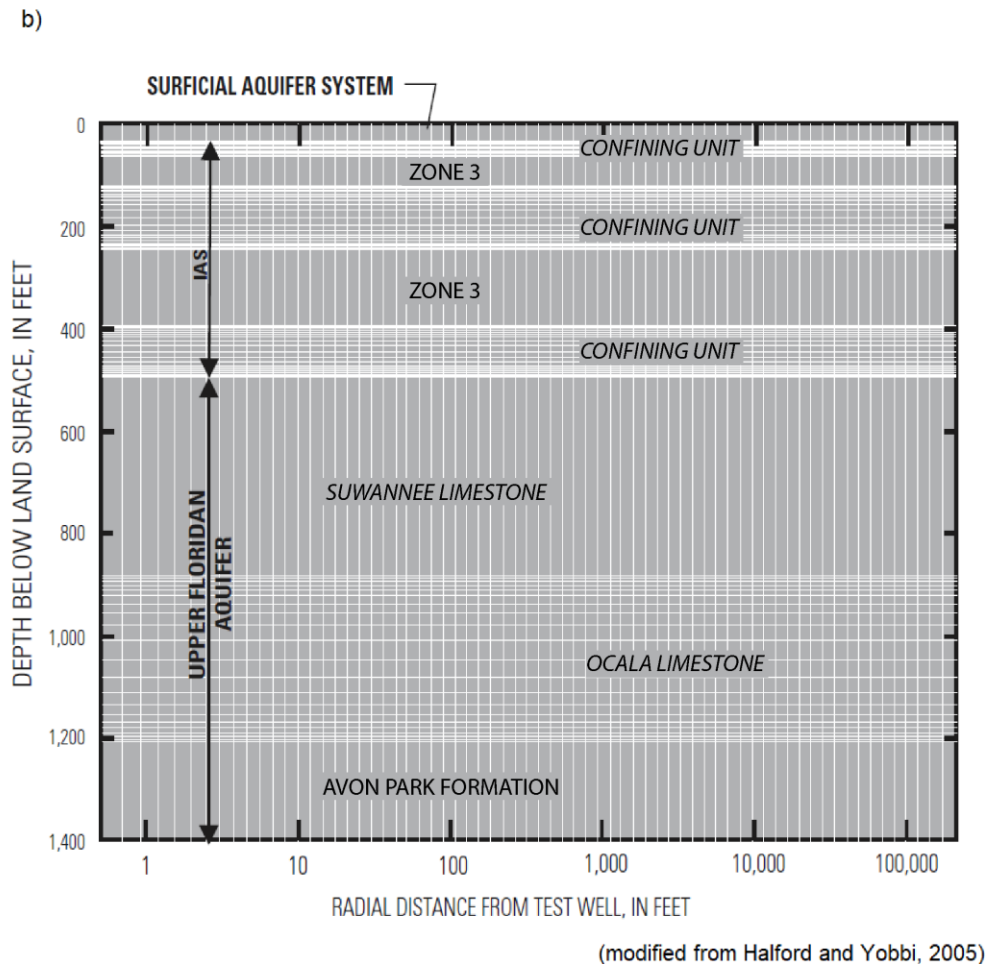
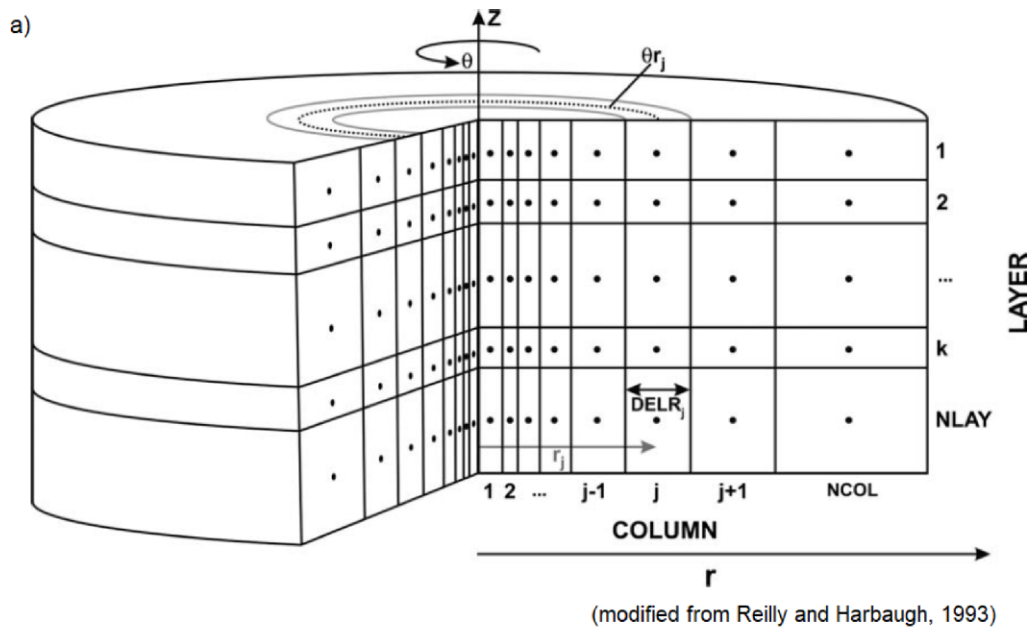
well, while water levels are measured in one or more observation wells at different distances from the pumping or injection well. Multiple-day aquifer pumping tests with multiple observation wells are much more expensive to conduct. Storage properties should not be estimated for single-well tests because single-well tests are not sensitive to aquifer-storage properties. Estimation of storage properties from single-well tests is also discouraged because single-well tests are affected by wellbore storage and well construction. These non-ideal effects frequently cause estimates of storage to be erroneous by orders of magnitude.

Analysis of most aquifer tests involve evaluating the time series of water level changes following a change in pumping or head. This is accomplished with the direct solution of the partial differential equation describing groundwater flow in simplified geometry with specified boundary conditions. This form of mathematical solution is called an analytical solution to a boundary value problem. Many different analytical solutions have been derived for both simple and complex geometries. Most are based on axisymmetric geometry such that the solution is defined in two-dimensional space on a radial plane extending from the well and is the same for every radial plane. The simplest transient solution for flow to a well is the Theis (1935) solution. It describes the head decline with time at any radial distance from a pumping a well. It is best to have several observation wells at varying radial distance from the pumping well. This simplest case assumes:

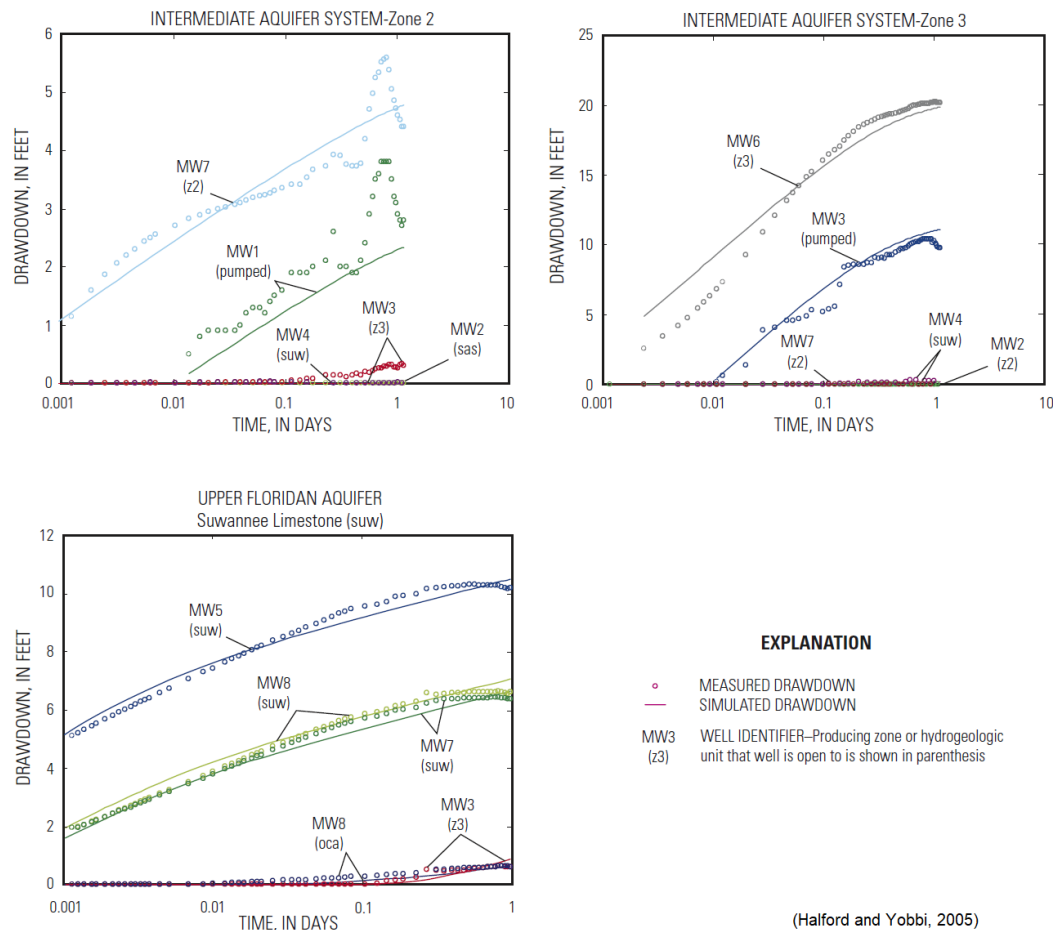
- a single homogeneous, isotropic, infinitely large, horizontal, confined aquifer of uniform thickness;
- discharge from the well is constant;
- the well fully penetrates the confined aquifer resulting in horizontal flow;
- the well has an infinitesimal diameter;
- the well fully penetrates the confined aquifer resulting in horizontal flow;
- flow to the well is constant and laminar;
- the initial potentiometric surface is horizontal; and,
- discharge is derived exclusively from storage in the aquifer and water removed from storage is discharged instantaneously with the associated instantaneous decline in head.

For multiple observation well tests, complex methods of analysis, such as, calibrating radial numerical models can provide better results than the analytical solutions in most cases. Figure 55 shows the schematic for radial axisymmetric model for a multi-observation well test in a carbonate aquifer and the results of fitting the model for one test are shown in Figure 56.





**Figure 55** - Radial axisymmetric models for simulation of aquifer tests: a) general schematic diagram for a radial axisymmetric model; and, b) specific diagram of the hydrogeologic units and radial model layering for aquifer tests conducted in west-central Florida, USA, within the Intermediate Aquifer System (IAS) and Upper Florida Aquifer (USA). Modified from Reilly and Harbaugh (1993) and Halford and Yobbi (2005).

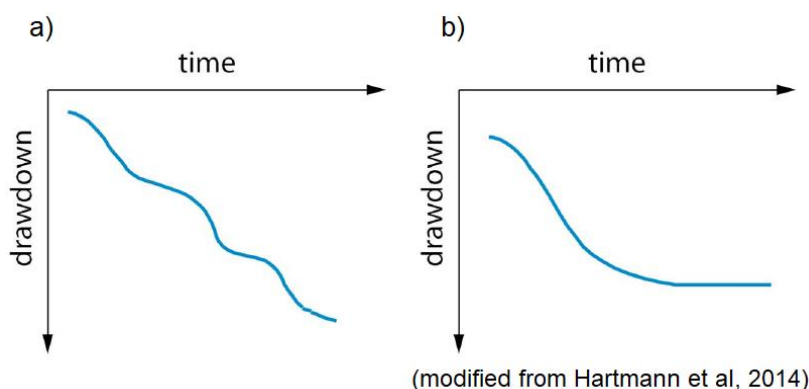


**Figure 56** - Simulated and measured drawdown for three, multi-observation-well aquifer pumping tests conducted at a karst aquifer system site in west-central Florida, USA. Drawdown is the difference between static water-level elevation before pumping and water level at the time shown on the x-axis. Circles indicate field measurements. The solid line represents calculated drawdown calculated in a simplified model of the system with the transmissivity and storativity adjusted to obtain a reasonably good fit to the field measurements. The relative positions of the aquifers and zones are illustrated in Figure 55. From Halford and Yobbi (2005).

For almost every type of hydrogeologic investigation, compilation of well locations and aquifer tests conducted in the study area is part of the literature review. Often these data are maintained by governmental agencies that regulate water-well drilling and water extraction. The types of data collected and stored varies by country and local governmental regulation. In the United States of America well drilling is regulated by state, and sometimes local, government. In some areas with no regulations, well-drilling organizations or companies may collect and store data as well logs that include basic lithology, well construction information, and aquifer tests conducted for the purpose of selecting the size of the pump. These are usually a step-drawdown test or specific capacity test, which are both single-well pumping tests and may provide estimates of transmissivity.

As with borehole geophysics, having more wells available and some wells with longer intervals of the well open to the formation is better for regional water supply studies. The dual or triple porosity nature of karst aquifers is so variable, that one well may not intersect any dissolution features while another well only a meter away may intersect a

major conduit. Compilation of all the water-well data available in a study area can be enlightening and is often critical to assessing characteristics such as the heterogeneity present in the aquifer. For example, water-level or potentiometric contour maps of highly heterogeneous karst aquifers often display sudden changes in gradient (that is, the contour interval divided by the distance between contours) over short distances, broad “U” shaped troughs in the contours that indicate the presence of highly transmissive areas, often dominated by major conduit flow. Wells in karst areas are often constructed like fractured rock aquifer wells which typically have a surface casing through the surficial material with the annular space between the casing and earth cemented down to the top of rock and below that, the borehole is uncased within the carbonate sequence. Borehole flowmeter logging and packer testing data will often indicate that only small zone of the borehole is contributing most of the flow to the well. Thus, it is best to use the transmissivity obtained from aquifer tests as qualitative data for understanding the location of the most transmissive parts of the aquifer. Traditional methods of aquifer test analysis, based on simplistic radial axisymmetric geometry using type-curve analysis may be successfully employed for some types of karst aquifers, however, the appropriate application of these methods must be carefully evaluated in light of the karst conceptual model and with an awareness of the potential effects of extreme heterogeneity and conduit-dominated hydraulic properties. Otherwise, misleading or erroneous interpretations may be obtained from the analysis of pump or slug test data. Curves showing drawdown or recovery of water level versus time obtained from well tests in karst aquifers may be difficult to analyze by traditional “curve-matching” techniques because of irregularities in the shape of the curves produced by dewatering of fractures, delayed release from storage in conduits and fractures, or other aquifer heterogeneities (Figure 57).



**Figure 57** - Illustrations of potential effects of pumping an open-borehole well in a fractured karst aquifer on resultant time-drawdown curves: a) irregular drawdown resulting from successive dewatering of multiple fractures and conduits; and, b) initial sharp drawdown caused by rapid dewatering of shallower-depth fractures and conduits, followed by stabilizing of drawdown due to groundwater held in storage in highly-transmissive conduits and fractures, at which time the system reaches steady-state. Modified from Hartmann and others (2014).

When a slug test is conducted in a high yielding karst well, the system is generally underdamped (that is, the water level will oscillate rapidly with sudden removal or insertion of the slug). This occurs because the transmissivity is large and storage is small for most karst systems, thus the diffusivity (transmissivity divided by storage) is large and slug tests are underdamped in all systems with large diffusivity (Butler, 1997). For underdamped slug tests, a data logger needs to record water level values more frequently than overdamped tests (that is, at least 5 measurements per second).

Many excellent textbooks and US Geological Survey reports provide more thorough discussions of aquifer and slug tests and include additional solutions for evaluating aquifer tests. Textbook discussions of analyzing hydraulic tests of formations and aquifers have been developed by: Lee, 1982; Driscoll, 1986; Dawson and Istok, 1991; Kruseman and de Ridder, 1994; Walton, 1996; Hall and Chen, 1996; Kasenow, 1997; and Butler, 1997. Some of the US Geological Survey reports related to hydraulic testing include: Ferris and others, 1962; Benthall, 1963; Stallman, 1971; Lohman, 1979; and Reed, 1980. The book by Lee (1982) discusses well testing from the perspective of petroleum engineering applications and is not commonly used by hydrogeologists. The book by Driscoll (1986) "Groundwater and Wells" is an excellent reference covering all aspects of well design, drilling, and hydraulic testing. The Kruseman and de Ridder (1994) book is popular as a textbook and covers most types of hydraulic tests in detail. The book by Butler (1997) is a good textbook for conducting and analyzing slug tests. Reports that provide examples of fitting aquifer test data to models of pumped aquifers include Garcia and others, 2016; Sepúlveda and Kuniansky, 2009; and Halford and Yobbi, 2005, 2006. The only reports specific to karst are those by Halford and Yobbi (2005, 2006). Many karst aquifers dominated by complex non-symmetric conduit networks defy the geometry of axisymmetric type-curve fitting analysis methods and may require more complex analysis for multi-well aquifer test data with either using analytical solutions with anisotropic capability or fully three-dimensional model fitting with the capability to incorporate laminar and turbulent flow (non-Darcian flow).

## 5.5 Use of Water Chemistry Data

A complete understanding of geochemistry is not a requirement for evaluating water-quality data to facilitate understanding karst aquifers. The main characteristic of karst aquifers is that they are composed of carbonate and evaporite rocks (rocks that can dissolve over time). Limestone is predominantly composed of calcite ( $\text{CaCO}_3$ ). Sand, clay and silt are commonly found in limestone as impurities but are not common in dolomite. If a limestone contains a lot of clay size particles or clay minerals, it is sometimes called a mudstone and generally forms a semi-confining unit with  $K < 0.1$  m/d. Dolomite ( $\text{CaMg}[\text{CO}_3]_2$ ) can be formed by dolomitization of limestone, where the calcite is recrystallized and magnesium (Mg) replaces some of the calcium (Ca). The exact processes



of dolomitization remains an area of research and is not completely understood. Most carbonates and evaporites are deposited in marine environments. One exception is tufa that forms when calcite precipitates out of freshwater often near mineral springs. Evaporites are a non-clastic sedimentary rock composed primarily of minerals produced from a saline solution as a result of extensive or complete evaporation of the water and often occur as layers of gypsum ( $\text{CaSO}_4 \cdot 2\text{H}_2\text{O}$ ), anhydrite ( $\text{CaSO}_4$ ) and halite ( $\text{NaCl}$ ) within a sequence of carbonate rocks. Evaporite minerals dissolve faster than limestone and thus, most evaporite rocks are found in more arid environments or at depth within carbonate sequences where freshwater has not flushed out the original seawater. Saline or hyper-saline water or  $\text{SO}_4$  within an aquifer system may indicate the presence of evaporite layers.

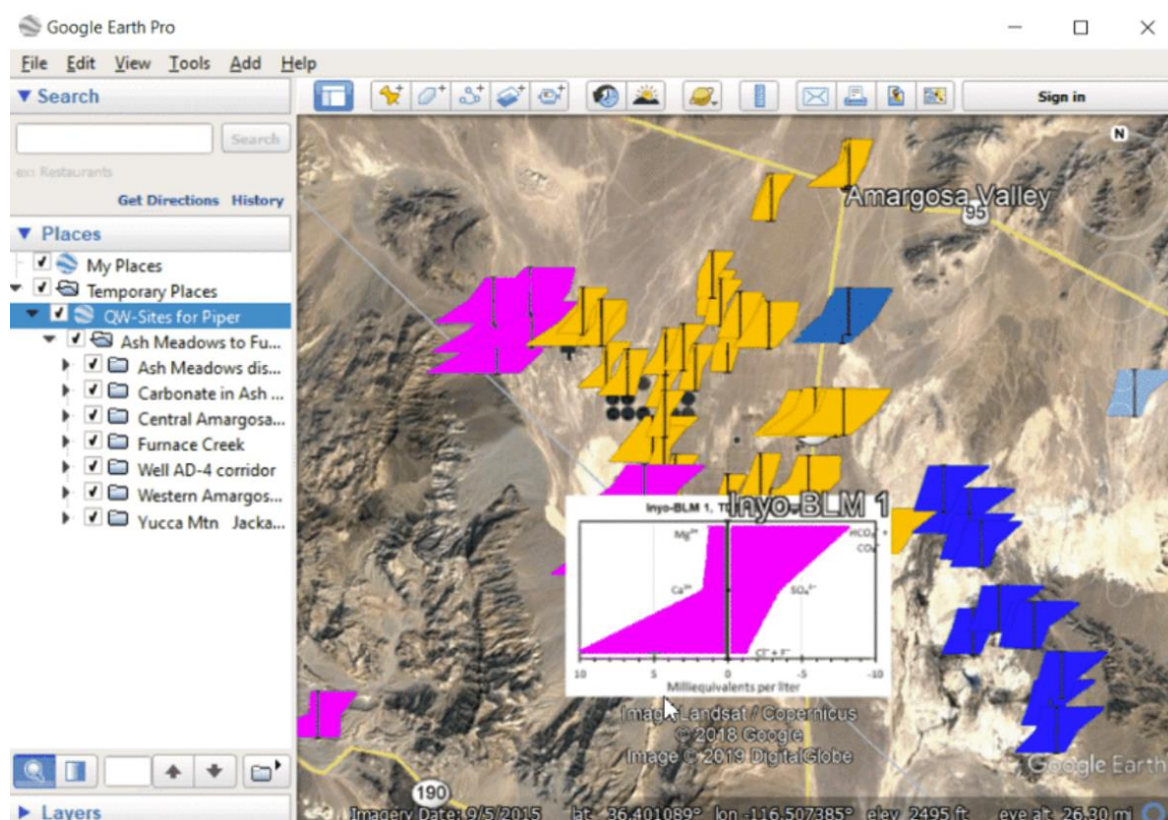
Rainwater can be slightly acidic, because carbon dioxide and water in the air react to form carbonic acid, a weak acid. As this acidic rainwater moves through carbonates and evaporites, it dissolves rocks until the dissolved rock minerals reach their saturation concentration in water. This process is called chemical weathering in many textbooks. Thus, dissolution begins in fractures and joints. It occurs at greater rates closer to land surface, or at the current base level of rivers, or at the base of sea cliffs. In confined zones, after large conduits or preferential flow layers have formed, new chemically under-saturated water may move through the system and dissolution will continue. In general, the longer time water remains in the carbonate rock, the higher the total *dissolved solids*. Thus, the collection of specific conductance data can be useful in karst aquifer studies. These data are presented as a chemograph and may indicate the presence of an evaporite layer at depth, seawater intrusion near the coast, or zones of slower diffuse flow versus faster conduit flow.

## Basic Water Quality Data

If basic water-quality data are available in a study area, contour maps of individual constituents can indicate the location of potable water. The simplest water-quality data to obtain is specific conductance, which can be used to estimate total dissolved solids (Hem, 1985). Often for drinking water supply studies, water-well samples are collected, and these can be compiled for the study area. Common standard inexpensive laboratory water quality analyses include acidity (pH), electrical conductance (EC), total dissolved solids (TDS), cations [calcium ( $\text{Ca}^{2+}$ ), magnesium ( $\text{Mg}^{2+}$ ), sodium ( $\text{Na}^+$ ) and potassium ( $\text{K}^+$ )] and anions [bicarbonate ( $\text{HCO}_3^-$ ), chloride ( $\text{Cl}^-$ ), sulfate ( $\text{SO}_4^{2-}$ ), nitrate ( $\text{NO}_3^-$ ) phosphate ( $\text{PO}_4^{2-}$ ) or orthophosphate ( $\text{PO}_4^{3-}$ )]. Common field parameters measured are pH, temperature, and EC (a surrogate for TDS).

If laboratory analyses are available, then more complex graphical water quality analyses will provide insight. The most common water quality diagrams used to evaluate the anion/cation chemistry are Stiff diagrams (Stiff, 1951) and trilinear diagrams (Piper, 1944).

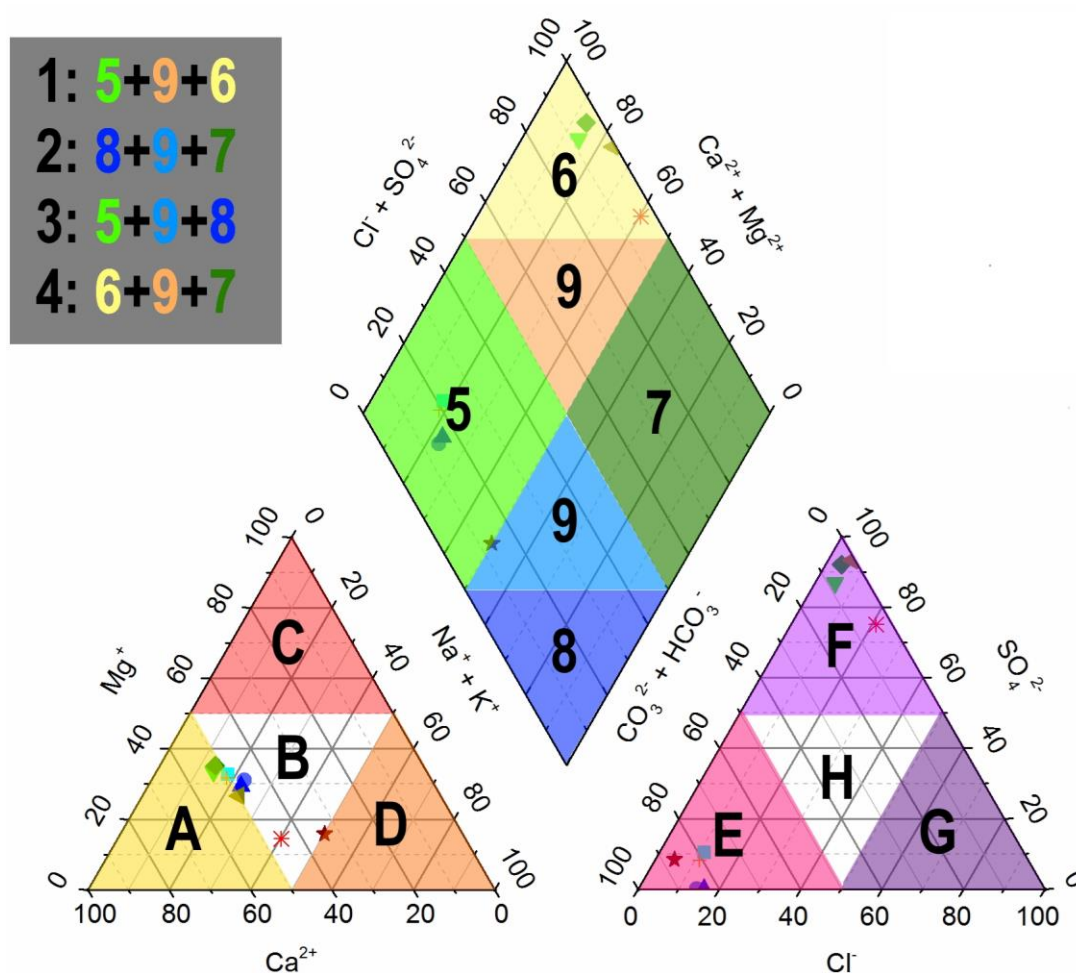
A Stiff diagram is a graph with four parallel horizontal axes extending on each side of a vertical zero axis. Concentrations of four cations and four anions are plotted on the left and right side of the vertical axis respectively. They are all plotted in the same sequence with concentration in milliequivalents per liter at the same scale. The plotted points are connected to create an irregular polygonal shape (Hem, 1985, page 175). Often the different water types in an aquifer show up as similar shaped polygons. Stiff patterns can be plotted on a map (Figure 58). The color coding on this map reflects the hydrogeologic unit the water sample was taken from. The Stiff diagrams within a unit do not all have a similar polygon shape indicating that the water quality depends on influences other than the formation chemistry.



**Figure 58** - Map of Stiff diagrams as presented with Google Earth. The colors on the diagram indicate samples from different hydrogeologic units. Note how the relative shape of the stiff diagrams from the same unit are fairly similar, indicating that there are water quality differences in different hydrogeologic units and demonstrating the usefulness of plotting the individual stiff diagrams on a map. Image created by Keith J. Halford and copied from free software available for [Piper and Stiff diagrams](#).

Trilinear plotting systems have been in use since the early 1900s. All cation and anion analyses are computed in terms of milliequivalents per liter and some are added together, such that the total number of lumped anion groups is three and cation groups is three. Then the values are calculated as a percentage of the total cation milliequivalents or anion milliequivalents. The simplest diagrams are two equilateral triangles of the same size with each side scaled from 0 to 100; one for the cation groupings and one for the anion groupings. Then a diamond shaped plotting area floats above and in the center of the cation


and anion equilateral triangle. The axes of the diamond are parallel to the triangles for cations (lower left) and anions (lower right), and are the same as the equilateral triangles. The upper left of the diamond is usually  $\text{SO}_4$  plus  $\text{Cl}$  and upper right  $\text{Ca}$  plus  $\text{Mg}$  (Figure 59). The diagram helps identify chemical facies and water types. All the sample analyses from wells in the study area are generally plotted together. On some trilinear diagrams the relative magnitude of total dissolved solids is shown by using different diameter circles (Hem, 1985, Figure 37). On others, the spatial nature is indicated by using a different symbol for each sample and having another map that indicates the location of each sample; still others use a number for each sample rather than symbol on both the trilinear diagram the map. The number can be used to link the full laboratory analysis provided in a database to the sample location.



**Figure 59** - The Piper diagram can be separated in hydrochemical facies. The letter and number labels are as follows: A - Calcium type; B - No dominant type; C - Magnesium type; D - Sodium and Potassium type; E - Bicarbonate type; F - Sulphate type; G - Chloride type; 1 - Alkaline earths exceed alkali metals; 2 - Alkali metals exceed alkaline earths; 3 - Weak acids exceed strong acids; 4 - Strong acids exceed weak acids; 5 - Magnesium bicarbonate type; 6 - Calcium chloride type; 7 - Sodium chloride type; 8 - Sodium bicarbonate type; 9 - Mixed type. Image by Kvgunten, 2017, [Hydrochemical facies in the Piper diagram](#) ↗ licensed under [CC BY-SA 4.0](#) ↗.

Plotting analyses of samples from wells that are successively down gradient from each other may reveal a linear chemical trend that indicates a mixing process. The graphs may lead to development of hypotheses that require more advanced research using various mixing models. The diagrams are a staple for evaluating natural-water chemistry of both surface and groundwater (Hem, 1985). The pros and cons of various diagrams used in geochemistry are discussed in Dauda and Habib (2015).

This section has not discussed concepts from basic inorganic chemistry or geochemistry. For readers who would like to know more about natural water chemistry, Hem (1985) provides an excellent free book (a link is provided in the reference section).

[Exercise 21](#)  invites the reader to consider the difference between alkaline earths and alkali metals.

### Use of End Member Mixing to Estimate Groundwater Contribution to Surface Water

Water quality data is often used in groundwater studies and particularly in karst systems for: understanding groundwater surface-water interactions; investigation of flow paths at contaminated sites; understanding the origins of groundwater and the formations the water has moved through; determining water age; and identifying mixture of waters of different age or from different formations.

Groundwater investigations for water supply in karst aquifers often need to characterize the groundwater discharge at springs or within a river reach (groundwater/surface-water interaction). If there is a chemical, an isotope, or a physical property present in the groundwater; but not present in the surface water (or is present at substantially different concentration or magnitude) that information can be used to develop a mixing model. The mixing model is used to determine the amount of groundwater in the surface water.

Radon-222 ( $^{222}\text{Rn}$ ) is one radioactive isotope of the inert radon gas that is used to directly estimate the groundwater discharge to a surface water. Radon-222 is a radioactive decay product from Uranium-Thorium minerals, which are within many rocks in varying amounts (Klepper and Wyant, 1957; René, 2017). Radon-222 is the longest-lived of the Rn isotopes with a half-life of 3.82 days, and is the most-studied isotope of Rn. Natural radon concentrations in the atmosphere are so low that surface waters in contact with the atmosphere will continually lose radon by volatilization so the  $^{222}\text{Rn}$  concentration in surface water is negligible. Consequently, where  $^{222}\text{Rn}$  is present in rocks of an area, groundwater has a higher concentration of  $^{222}\text{Rn}$  than surface water. Kraemer and Genereux (1998) provide a detailed discussion of  $^{222}\text{Rn}$  mixing models and the use of  $^{222}\text{Rn}$  to determine areas of groundwater discharge to streams. The use of  $^{222}\text{Rn}$  for this purpose has been applied to all aquifer types including karst aquifers.

If the concentration of a constituent in groundwater is constant and in large contrast to the concentration in surface runoff from precipitation and overland flow, then data describing continuous discharge of a stream and continuous concentration of the constituent of interest in the stream can be collected and groundwater discharge to the surface water body can be estimated. In short, one must know the two end member concentrations. In the case of  $^{222}\text{Rn}$ , it is assumed that the concentration in the surface runoff is zero, so all  $^{222}\text{Rn}$  measured in surface water is from local groundwater discharge to the surface water.

Assumptions/simplifications involved in estimating the groundwater discharge are:

- 100 percent surface runoff (precipitation plus overland flow) occurs after the largest storm event peaks;
- the constituent end member concentration of surface runoff,  $C_r$ , can be determined by measuring  $C$  of stream water after extremely wet periods (note in the case of Radon-222 the surface water end member is zero); and,
- the groundwater end member,  $C_g$ , can be determined from multiple groundwater samples.

Even if the groundwater concentration changes a small amount through time due to recharge events, if that concentration is measured and the surface-water end member concentration ( $C_r$ ) is stable, an estimate of the groundwater discharge can be made using the chemical mass balance of Equation 7 and the streamflow mass balance of Equation 8.

$$CQ = C_g Q_g + C_r Q_r \quad (7)$$

$$Q = Q_g + Q_r \quad (8)$$

where:

$C$  = concentration in the stream water ( $\text{ML}^{-3}$ )

$C_g$  = concentration in 100% groundwater ( $\text{ML}^{-3}$ )

$C_r$  = concentration in 100% surface runoff water ( $\text{ML}^{-3}$ )

$Q$  = total discharge of the stream ( $\text{L}^3\text{T}^{-1}$ )

$Q_g$  = groundwater portion of the total discharge of the stream ( $\text{L}^3\text{T}^{-1}$ )

$Q_r$  = surface runoff portion of the total discharge of the stream ( $\text{L}^3\text{T}^{-1}$ )

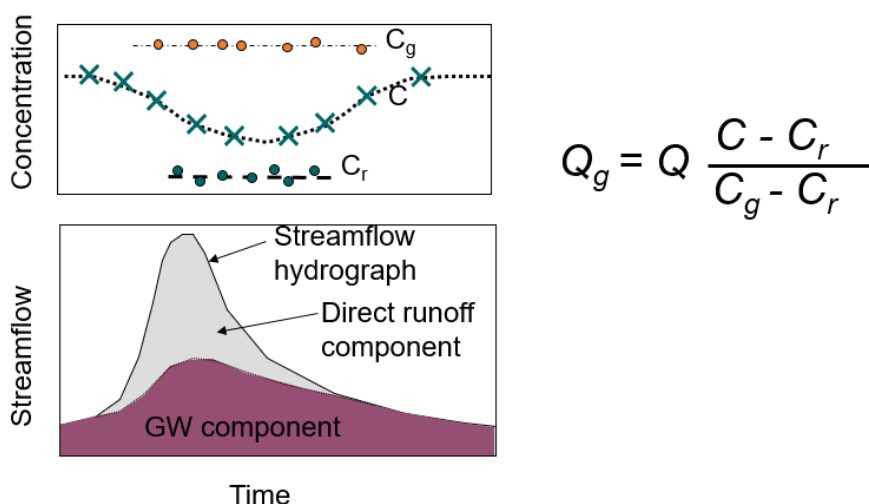
Figure 60 and Equation 9 show the relationship for calculating groundwater discharge to the stream ( $Q_g$ ).

$$Q_g = Q \frac{(C - C_r)}{(C_g - C_r)} \quad (9)$$



When the constituent is thought to only occur in groundwater, for example in the case of  $^{222}\text{Rn}$ , the concentration in surface runoff water  $C_r$  can be taken as zero, then Equation 9 simplifies to Equation 10.

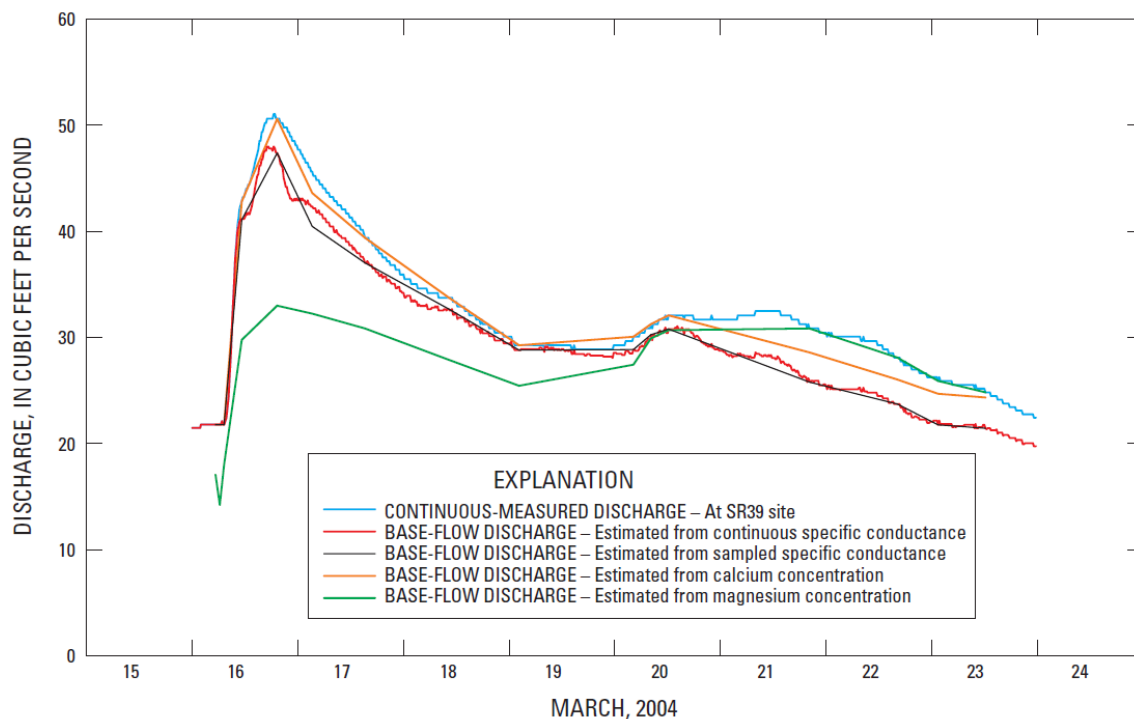
$$Q_g = Q \frac{C}{C_g} \quad (10)$$



**Figure 60** - Given the end-member concentration of groundwater ( $C_g$ ) and surface runoff ( $C_r$ ), the groundwater component ( $Q_g$ ) of total streamflow ( $Q$ ) is computed from the streamflow concentration ( $C$ ) time series.

An end-member mixing model can be used to calibrate traditional graphical hydrograph separation and thus, better estimate the groundwater component of stream flow. This component is called base flow. The procedure was developed by Stewart and others (2007) and applied to the Floridan aquifer system near Tampa by Kish and others (2010). Stewart and others (2007) used two years of continuous specific conductance data (a surrogate for total dissolved solids) and discharge measurements collected at 10 stream gages operated by the US Geological Survey to adjust the parameters of the automated hydrograph separation program HYSEP (Slotto and Krause, 1996) in order to calibrate the hydrograph-separation model to the conductance mass balance equation. The end member values for conductance were determined by measuring conductance of water samples from wells in the aquifer and conductance of stream water during dry periods to determine  $C_g$ , and measuring conductance of stream water after extremely wet periods to determine  $C_r$ . Calibration of the value of the  $2N^*$  parameter of HYSEP reduced the 10-station average error between HYSEP and conductance-mass-balance-derived cumulative base flow from 40 percent to 5 percent (Stewart et al., 2007). Calibration is the process of adjusting the value of model parameters until the values simulated by the model match the measured field observations. These calibrated HYSEP parameters can be used with historical daily streamflow records to estimate the groundwater component of total streamflow more accurately for that site with HYSEP.

Figure 61 shows a graph of base flow estimates from a storm event using the end-member mass balance approach with different physical and chemical data (Kish et al., 2010). Kish and others (2014) contend that the continuous specific conductance mass balance estimate of groundwater discharge is the most accurate because it is measured at 15-minute intervals as is stream discharge; whereas the estimates from sampled specific conductance, calcium, and magnesium concentration were sampled periodically, not conducted daily. Kish and others (2014) do not speculate why the estimate using magnesium is lower than using calcium. By connecting the groundwater contribution to total flow estimated from periodic sampling points of calcium concentration results in that line above the total discharge line, which is obviously not possible (Figure 61).



**Figure 61** - Observed storm hydrograph and groundwater discharge estimated by geochemical mass balance for selected major ions at the SR39 surface water gaging site near Tampa, Florida, USA, March 2004 storm. From Kish and others (2010).

Further information about hydro-geochemistry is discussed by Drever (1988), Clark and Fritz (1997) and Deutsch (1997). Additionally, the natural temperature variation between groundwater and surface water can be used as a tracer (Kurylyk et al., 2017).

### Use of Natural Stable Isotopes

Natural stable isotope chemistry has also been used for understanding diffuse versus conduit flow with other mathematical models. Isotopes are atoms of the same element that have different numbers of neutrons. Isotopes have the same number of protons (positive charge) and electrons (negative charge) but differ in molecular weight due to different numbers of neutrons (neutral charge). The previous section discussed


Radon-222 ( $^{222}\text{Rn}$ ), which is a naturally occurring radioactive isotope of radon gas and considered an unstable isotope owing to radioactive decay and subsequent transformation to a daughter product. There are many naturally occurring stable isotopes that are used in hydrology, such as Hydrogen-2 ( $^2\text{H}$ ), Oxygen-16 ( $^{16}\text{O}$ ), Oxygen-18 ( $^{18}\text{O}$ ), Carbon-12 ( $^{12}\text{C}$ ), and Carbon-13 ( $^{13}\text{C}$ ). The hydrogen and oxygen isotopes are frequently analyzed for hydrologic studies as these make up the water molecule. The natural abundance of these isotopes differs over time and climatic conditions. In groundwater studies, stable isotopes are often used to understand recharge. An excellent reference on the use of stable isotopes in hydrology edited by Kendall and McDonnell (1998) has a chapter devoted to the use of isotopes in groundwater hydrology. A Groundwater Project book by Cook (2020) introduces isotopes and environmental tracers as indicators of groundwater flow.

### Water Quality Issues for Water Supply

In the United States, private water-well permits are managed at the local or State level, however, minimum drinking water standards are set Nationally by the US Environmental Protection Agency (USEPA, 1991, 2001, 2009). When exploring karst aquifers for water supply its important to collect base line water chemistry data of cations and anions and, for shallow karst systems fed by sinking streams, bacteria.

If evaporite layers were deposited along with the carbonate rocks, often brackish or hypersaline groundwater is present. Evaporite rocks dissolve more readily than pure limestone and create areas of very high total dissolved solids within an aquifer system or deeper units where the original seawater is never replaced through freshwater circulation as in the Floridan aquifer system (Williams and Kuniansky, 2015). However, brackish water can be treated or mixed with fresher water to lower the total dissolved solids to potable levels (Stanton et al., 2017).

Karst aquifers can be especially vulnerable to contamination from human activity as noted in Section 3.7; thus, surface land-use can introduce toxic substances into these aquifers. In some cases, the substances are naturally present or can be mobilized from natural materials by introducing water of a differing chemistry. Aquifer storage and recovery efforts stalled in Florida because the chemistry of injected surplus surface water mobilized arsenic and other trace elements naturally occurring within the limestones (Cowart et al., 1998; Arthur et al., 2001, 2002, 2007; Williams et al., 2002).

[Exercise 22](#)  invites the reader to consider land use activities that might result in degradation of the water quality if conducted on the outcrop or near sinking streams of a karst aquifer.

## 6 Mathematical Model Applications in Karst

Understanding karst aquifers, for purposes of their management and protection, poses unique challenges. Since the 1960s, advances have been made in the development of modeling software and their use for characterization and management of karst aquifers. Modeling is applied to synthesize data related to the aquifer. The model represents the aquifer, and that representation is adjusted until the simulated model values match the equivalent field observations. The process of creating even simple models of the system helps investigators improve their understanding of observed data and the flow system within the karst aquifer.

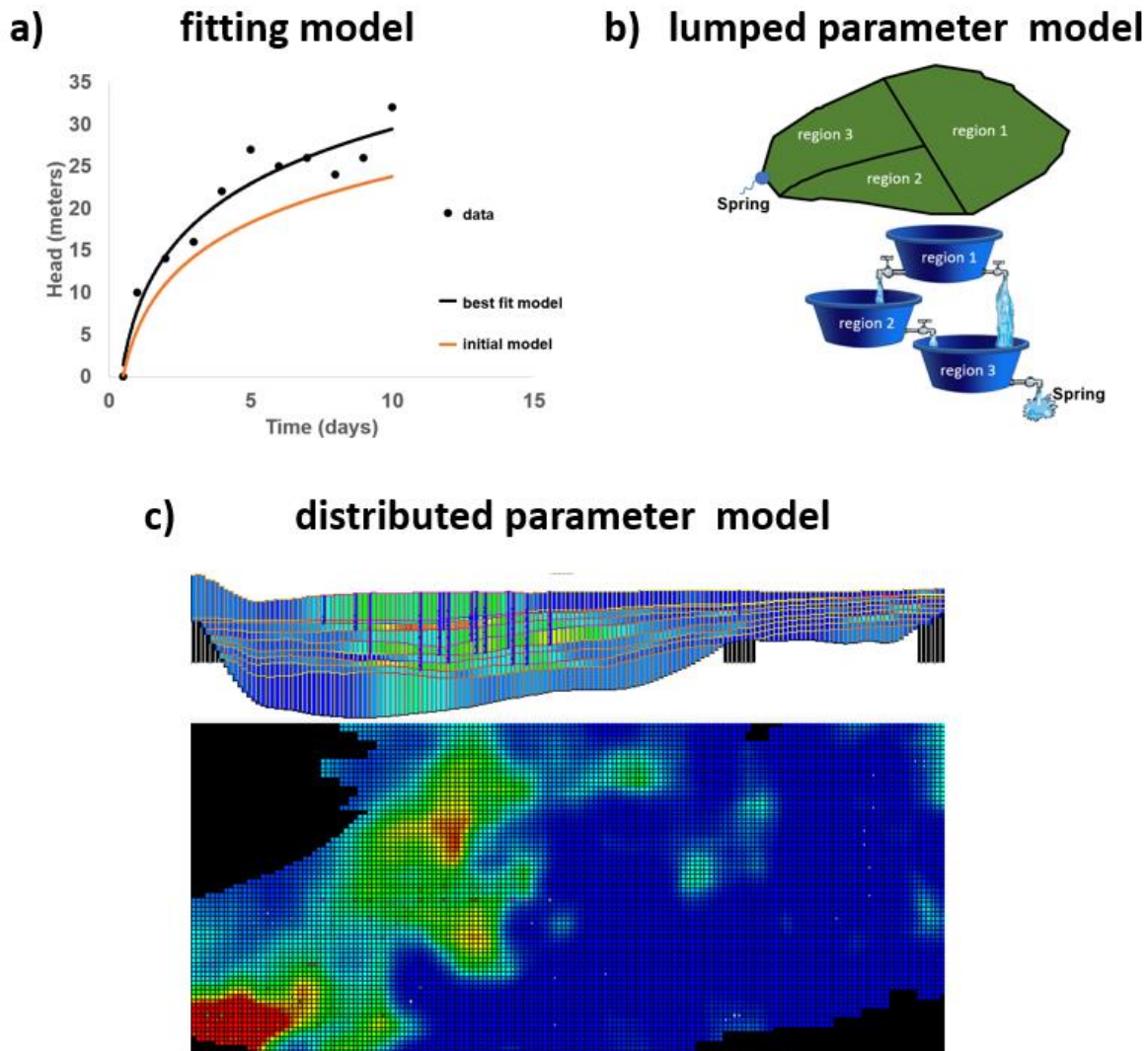
Different types of mathematical models can be applied to hydrologic and environmental problems in karst aquifers that have complex dual, or triple, porosity. The preferred mathematical techniques depend on the type of available data and the problems that need to be solved. Names of the types of mathematical models applied to karst aquifers can be confusing because terminology has not been used consistently in the literature. This section categorizes the mathematical approaches into three major groups based on the methods applied in the calculations: 1) fitting models; 2) lumped parameter models; and 3) distributed parameter models (Figure 62). There is some overlap in the mathematical methods employed in the categories of “lumped parameter models” and “fitting models” as both categories involve mathematical techniques that come from the fields of control theory (sometimes called operations research) or linear systems theory (Doo, 1973).

- The first category, fitting models, refer to mathematical methods that involve statistical regression, fitting shape functions, statistical transfer functions, or use of pattern recognition functions, such as artificial neural networks (ANN) to recreate field observations (Long and Putnam, 2002, 2007; Hu et al., 2007). These models have no physical basis and only require a known correlation between the system response (that is, the variable that will be predicted with the model) and system drivers or inputs (that is, independent variables used to define the shape function, neural network, or statistical transfer function). Most of the applications require pairs of observed data for dependent and independent variable(s) to calculate the coefficients for the function(s) and may not require detailed characterization of the karst aquifer.
- The second category, lumped parameter models, is based on mathematical methods that combine a physically based equation (an ordinary differential equation) with control theory or operations research techniques (Takahashi et al., 1972; Hillier and Lieberman, 1967; Dooge, 1973). This second category has some physical basis, but generally lumps the detailed properties of the karst aquifer into a few large basins for water management problems and is not meant to simulate details of flow in the system. A lumped parameter model does not distinguish between different system compartments and different flow processes. For example, many hydrogeochemical

mixing models that are used to estimate average age of water are based on simple expressions of physical flow, such as binary, piston, exponential, dispersion, or ordinary differential equations (Maloszewski, 2000; Katz, 2004; Jurgens et al., 2012). For water supply problems, some concept of the aquifer system is required, such as groundwater sub-basins (tanks) and their connection to each other.

- The third category, distributed parameter models are based on physical processes defined by partial differential equations describing water flow, which are solved numerically usually with finite-difference or finite-element methods (Anderson et al., 2015; Kresic, 2007). In these models, hydraulic properties are defined for many blocks of varying size that are joined together to represent every volume within the groundwater system at a level of detail defined by the modeler. Distributed parameter models are used to simulate all types of flow within karst aquifers as inferred from hydrogeologic investigations. This is the most-applied type of model for synthesizing all data from investigations in order to test concepts of how water moves into, through and out of the aquifer. Such modeling helps determine the most useful types and locations of additional data collection and can lead to adjustment of the conceptual model of the aquifer system. There are many numerical model approaches that use different formulations of the groundwater flow equations and techniques for solving the equations.





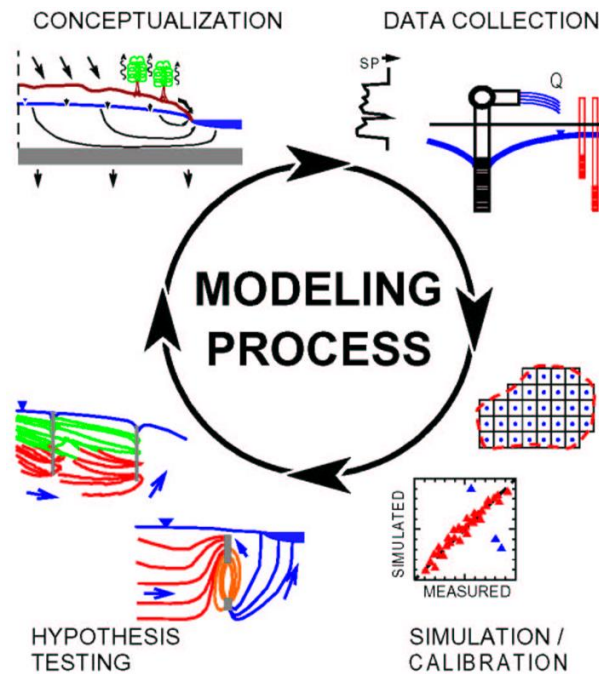
**Figure 62** - Examples of three categories of groundwater models: a) fitting models in which a mathematical function is used to express groundwater head variation with time (depending on the complexity of the fitting function, the software and computations can be simple and set up in a spreadsheet or can be more complex, involving many lines of computer code or use of statistical or custom software applications); b) lumped parameter models in which a series of ordinary differential equations for tanks are solved simultaneously to represent flow between and storage in subbasins as well as the final discharge to a spring given historical recharge, pumpage, and spring discharge data (often lumped parameter problems are solved with simple arithmetic in a spreadsheet); and, c) distributed parameter models showing the color-coded distribution of hydraulic conductivity in cells of one cross section and one layer for which the partial differential groundwater flow equations are solved using finite differences (the software codes for distributed parameter models are complex and requiring thousands of lines of code and large computers).

In this section, the general categories of modeling approaches are described with some examples. The mathematical methods are described in words and figures. The examples are intended to help non-mathematicians understand their application. Readers wishing to pursue mathematical modeling of aquifers are encouraged to study fluid mechanics and mathematics (including probability and statistics, calculus, differential equations, linear algebra, and numerical methods), as well as develop skills for manipulation of large geospatial datasets and computer programming.

To apply any mathematical model to a karst system, many of the characterization steps described in previous sections of this book need to be undertaken. Characterization provides the data needed to develop a conceptual model of the karst aquifer, create the mathematical model and calibrate the model to represent field conditions. A conceptual model of an aquifer is a description of 1) where water enters and exits the aquifer and 2) the hydrogeologic structure (that is, shape and size of geologic units and faults; and for karst, the location of dissolution features and porosity types). Distributed parameter models require the most complete data describing hydrogeologic framework and detailed definition of the quantity and location of water moving into and out of the system. A lumped parameter model requires less data. For example, many lumped parameter geochemical models for age dating require only environmental tracer data from a public supply well or spring for estimation of travel time and water age (Jurgens et al., 2012). A fitting model, such as a linear regression may use little data (for example, a few water levels in a well and spring discharge collected at the same time) to predict spring discharge given a measured well water level (Knochenmus and Yobbi, 2001). In order to use the model to estimate future spring discharge (dependent variable) from the water level in a nearby well (independent variable), the observed data used to develop the model needs to represent the full range of discharge to be estimated.

The steps involved in modeling are somewhat circular in that the model is developed, evaluated, revised and reevaluated numerous times before it is put to use (Figure 63). The process includes:

1. defining the purpose of the model (for example, what is to be learned or understood about the system);
2. compiling data available in the literature;
3. visiting the field area;
4. conceptualizing the aquifer framework and movement of water through that framework;
5. applying initial models to test hypotheses about the system in order to guide plans for data collection and model selection;
6. collecting data at the field site;
7. calibrating the model;
8. if the model does not acceptably match the field observations after calibration, then using what was learned from the process to return to step 4 and revising the conceptual model or to step 6 and collecting more data to develop a more complex model that better represents the system; and when ready;
9. putting the model to use.



**Figure 63** - The circular modeling process. First develop a conceptual model and compile all existing data about the karst aquifer. Then collect or compile more data if required for the problem at hand. Decide on a modeling approach and calibration strategy, then test your hypothesis. If model is adequate for the problem or proves the conceptual model is correct, then no further study is needed. If not and funding is available, revise the conceptual model, collect more data and incorporate the data into a more complex model, recalibrate, and test the new hypothesis.

Many distributed parameter model projects are started after years of aquifer studies including development of some fitting, lumped-parameter, and geochemical age-dating models. The distributed parameter model is then used to synthesize all the data and better understand the entire aquifer system.

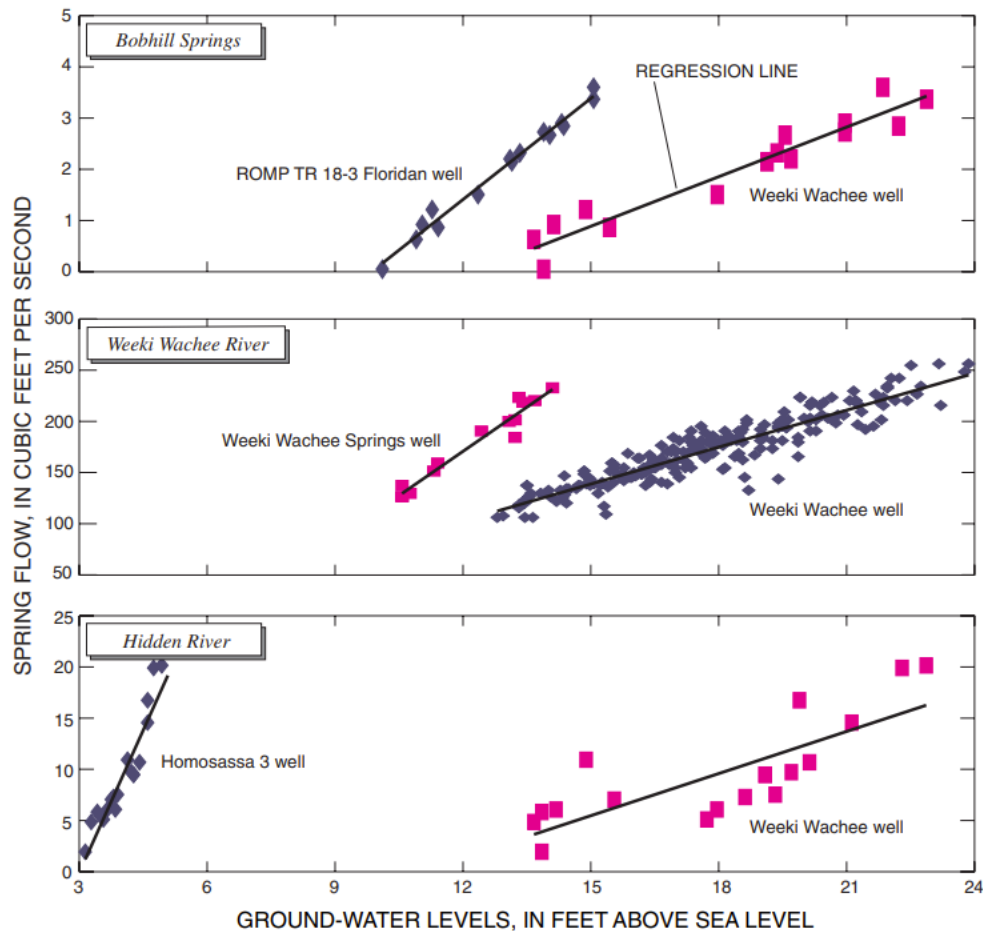
## 6.1 Fitting Models

Fitting models have been used in the field of hydrology for a long time. For this discussion, fitting models involve the matching of field data to either a statistical distribution function or a single- or multiple-linear regression equation. Additionally, the broad category includes other forms of linear systems modeling in which the karst aquifer is treated as a filter, in that complex mathematical functions (linear kernels) are used with inputs like recharge and pumpage in order to generate an output of spring flow. The simplest application of linear systems in hydrology has been in rainfall-runoff models that employ what is called the unit hydrograph method (Sherman, 1932). These and similar techniques have been applied to karst aquifers (Neuman and de Marsily, 1976; Dreiss, 1982; Wicks and Hoke, 2000). To some extent, these are considered “black-box” methods because

detailed knowledge about the physical system (for example, locations of conduits, transmissivity, and storage properties) is not required.

Fitting methods have advantages and disadvantages similar to those of lumped parameter models. In fact, statistical models are similar to the lumped parameter approach described in Section 6.2, except they lack a physically based differential equation to describe the aquifer. Instead, complex mathematical functions (sometimes based on statistical distributions) are used with time offsets and shape terms in order to take input(s) and create an output (response) that mimics the output (response) observed in the field. Another example of a fitting model is application of artificial neural networks, which is a form of pattern recognition, to karst aquifers (Hu et al., 2007; Trichakis et al., 2009). For neural network models, limited understanding of the karst aquifer system is needed for selection of appropriate inputs, such as recharge and pumpage, which are physically related to the outputs, such as spring flow(s) and/or water level(s).

Simple regression analysis has been used to predict spring discharge given water levels in a nearby well by developing a linear regression equation using historical data. This technique has also been used for tidally affected springs by developing a multiple-linear regression using both water levels at a nearby well and tidal stage data to estimate spring discharge (Wanakule, 1988; Knochenmus and Yobbi, 2001). Development of regression equations requires numerous spring discharge measurements over the full range of conditions that are anticipated to be simulated in predictive models, but does not involve time-series analysis. The discharge measurements must be paired with a water level in a nearby well (and if tides influence the system, then a tidal gage) from the same time as the discharge measurement. Figure 64, which is from Knochenmus and Yobbi (2001), shows the simplest form of a fitting model and their report presents the details of developing more complex multi-linear regressions for tidally affected springs. In this example, there is a known relationship between spring discharge and nearby groundwater level as well as tidal level at tidally effected springs, so the regression equations work well for accurately representing discharge at most of the springs.



**Figure 64** - Example of the simplest type of fitting model. The linear regression lines are developed for estimation of spring discharge from a groundwater level in a well in the Upper Floridan aquifer for each spring using the paired groundwater level for each discharge measurement at each spring location. These are non-tidally affected springs and the wells are close to the spring, such that the stage (groundwater level) to discharge relationship is linear through the range of discharge. This method is commonly applied for stable springs as it is less expensive than constructing a weir at the spring. Once the range of flow has been established and the stage-discharge measurements completed in order to create the regression equation, then fewer discharge measurements are required to establish that the regression equation remains accurate. Modified from Knochenmus and Yobbi (2001).

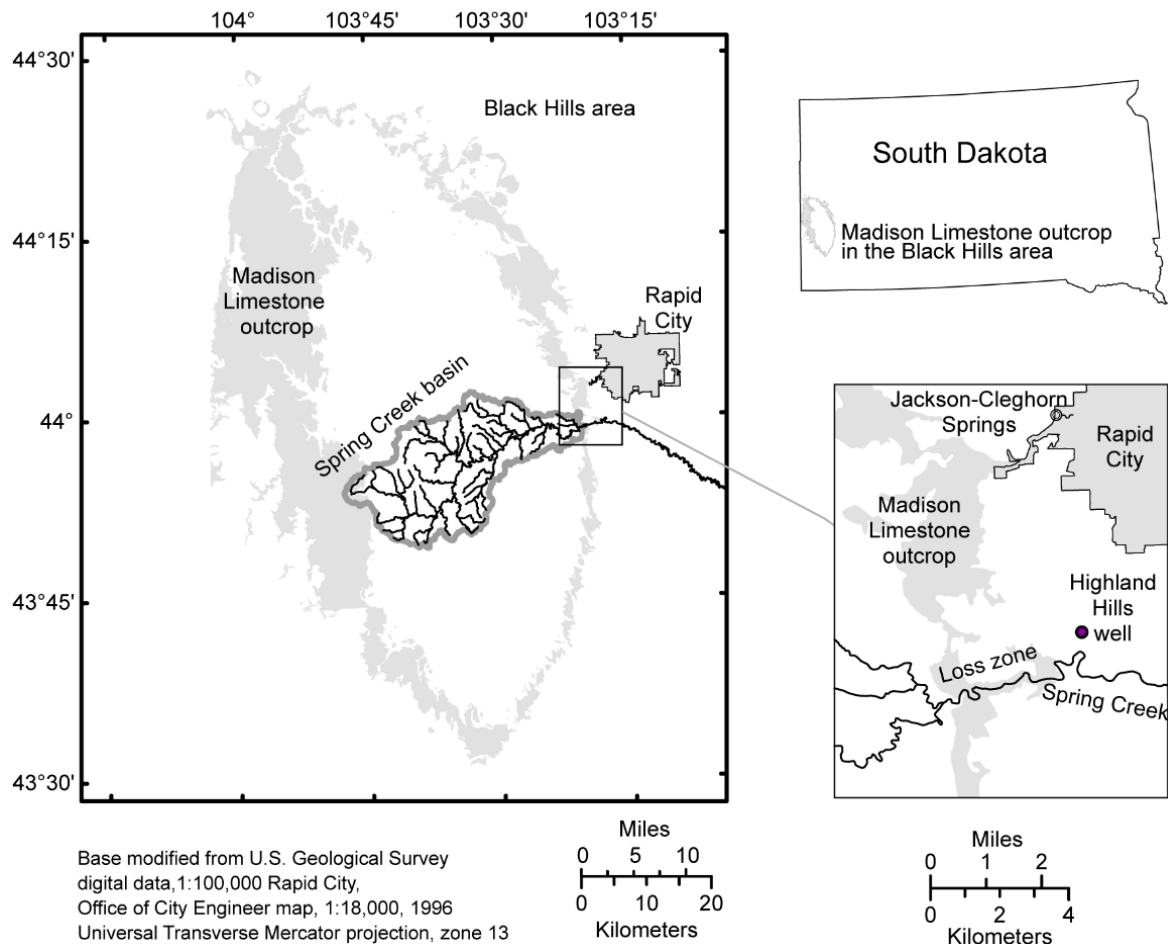
The advantage of fitting models is that they are easy to apply and calibrate. The disadvantage is that they are specific to the respective catchment and model results are highly uncertain if prediction simulations require input or output variables that exceed those of the historic calibration period.

### Example Application of Complex Fitting Model Using Stable Isotopes

Stable-isotope samples were collected at about 6-week intervals over a 6-year period at a streamflow-loss zone that recharges the karstic Madison aquifer in South Dakota (Figure 65) and at a nearby well located close to or within a main groundwater flow path (Long and Putnam, 2002, 2007). Time-series analysis of the isotope data indicates that the well responds rapidly to recharge from a sinking stream during wet periods. The hydraulic connection between the stream's loss zone and the well is primarily through karst conduits.

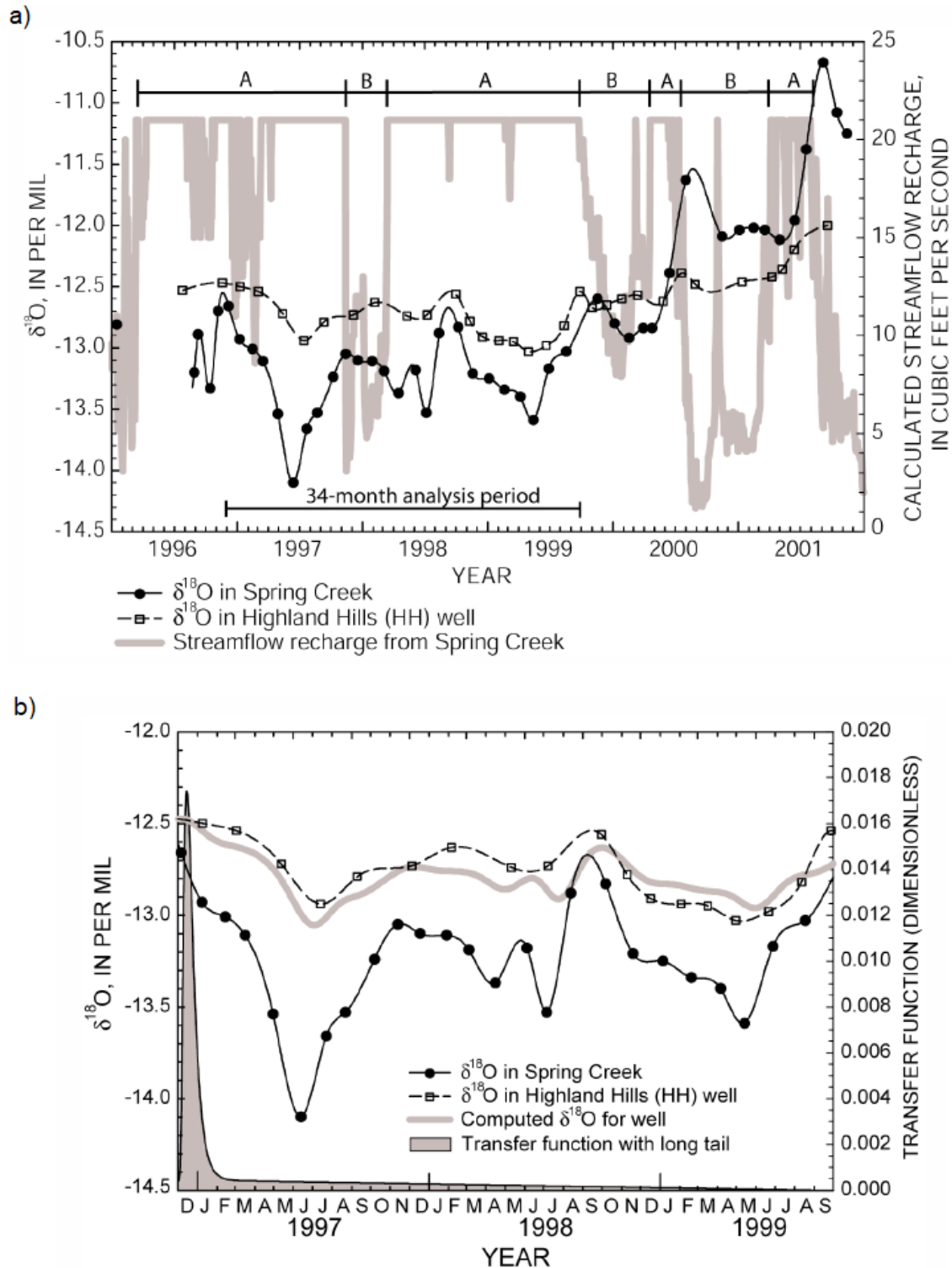


During dry periods when streamflow is low, isotopes in the well samples are primarily aquifer-matrix water that has been stored for months or years.



**Figure 65** - Location of the study area for collection of stable-isotope data in the karst Madison aquifer, South Dakota, USA. From Long and Putnam (2002).

The data were analyzed by correlation analysis and linear-systems analysis for a 34-month period of high recharge. The stable-isotope and water-level data sets exhibit the highest correlation when the data between the losing-reach of the stream and the well are lagged by 22 days, which may approximate the travel time from the loss zone to the well. Linear-systems analysis resulted in an estimated travel time to the well of about 15 days with a system memory of 2 to 3 years resulting from diffuse matrix flow. Based on these analyses, the conduit-flow velocity was estimated at 380 to 800 ft/day (120 to 240 m/day). The data used to develop the model are shown in Figure 66a. A log-normal distribution approximated the observed distribution of travel times for conduit flow. Figure 66b shows the final model and the log-normal distribution used as the transfer function for estimating the amount of stable oxygen-18 isotope in the spring discharge based on its presence in the stream water. The narrow peak of the transfer function reflects the roughly 2-week lag time.



**Figure 66** - Statistical regression model of stable oxygen-18 isotope. a)  $\delta^{18}\text{O}$  data and Spring Creek streamflow recharge to the Madison aquifer from 1996 to 2001. The A sections indicate periods of near-maximum recharge, whereas B sections indicate periods of lower recharge. The streamflow recharge has a maximum estimated rate of 21 ft<sup>3</sup>/s (~0.6 m<sup>3</sup>/s) (Hortness and Driscoll, 1998). b) Results of linear-systems analysis including the computed  $\delta^{18}\text{O}$  data for the sampled well and the transfer function used in the analysis. Unit conversions: 1 cubic foot per second ~ 0.03 m<sup>3</sup>/s. From Long and Putnam (2002, 2007).

## 6.2 Lumped Parameter Models

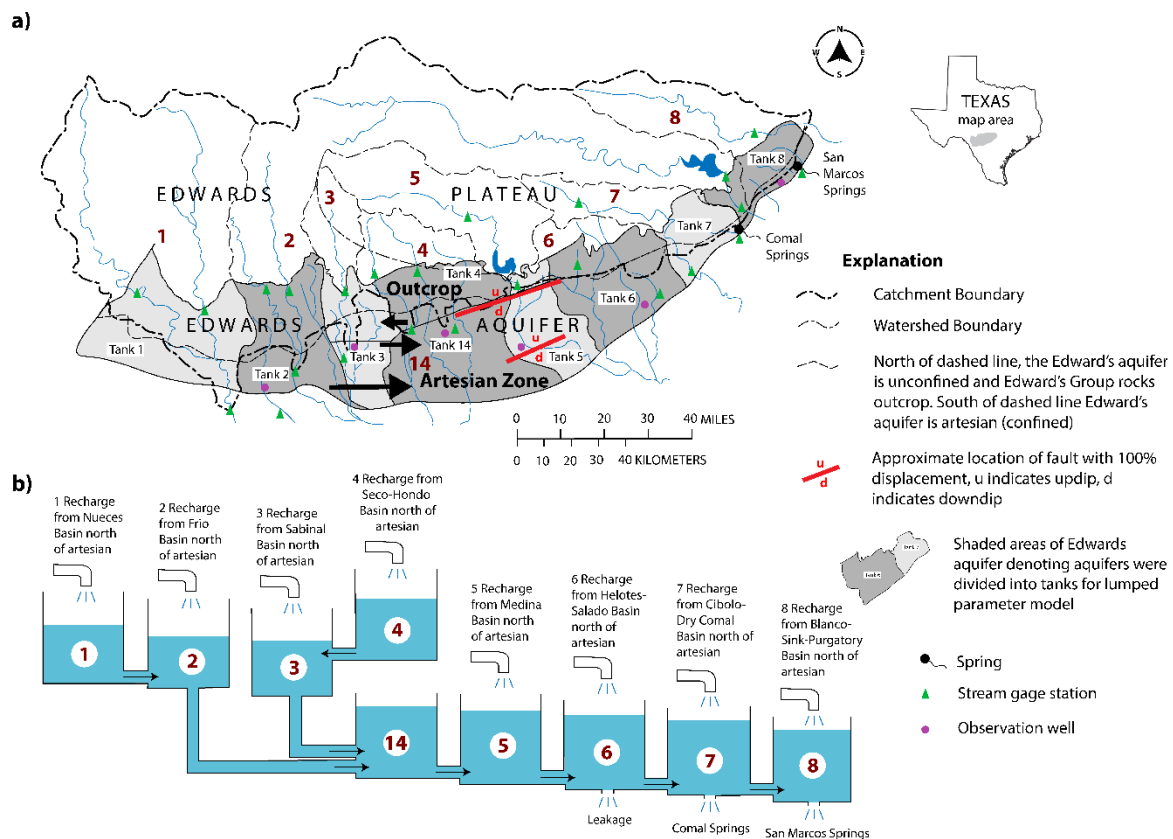
The control theory approach has been successfully applied to simulate karst aquifers using mathematical methods for solving sets of ordinary differential equations. For example, the control theory approach is used to evaluate the filling and mixing of water in a tank, or a network of tanks, and a karst basin can be conceptualized as a group of interconnected tanks. The tanks are not assigned spatial coordinates as is done for cells of distributed parameters models, rather flow between tanks is based only on connections assigned by the modeler. Coefficients (that is, lumped parameters) for each tank are developed by calibrating a system of equations describing the connections between tanks (Wanakule and Anaya, 1993; Hartmann et al., 2014). Data preparation for lumped parameter models is simpler than that required for distributed parameter models, and computational time is shorter. However, detailed representation of the aquifer is not possible using this approach.

Groundwater withdrawals and recharge are summed together for each tank which represents a geographic area (for example, a spring basin). Withdrawals from the model simulate spring discharge and inputs to the model may represent distributed infiltration, sink holes or sinking streams. Lumped parameter models may be adequate for providing gross estimates of the effects of changes in pumpage and/or recharge rates on spring discharge, as well as, for estimating recharge given natural discharge and pumpage. Mathematical filters can be applied to some of the input data, for example, to divide the annual basin recharge into varying recharge for each month, in order to achieve a better fit between observed and simulated spring discharge (Wanakule and Anaya, 1993; Dreiss, 1982). Many of the geochemical mixing models, such as piston flow, binary mixing, or exponential mixing models applied to atmospheric environmental tracers are also used for estimation of groundwater age. These are forms of lumped parameter models (Böhlke and Denver, 1995; Cook and Herzog, 2000).

### Example Application of a Lumped Parameter Model

The lumped parameter modeling method is demonstrated in a simulation of spring flow at Comal and San Marcos Springs, Texas. The model input and calibration data were based on annual estimates of recharge and pumpage in nine surface watershed basins and an index water level in each sub-basin of the San Antonio part of the Edwards Aquifer (Wanakule and Anaya, 1993). The lumped parameter model of Wanakule and Anaya (1993) was one of the earliest applications of such models to the Edwards Aquifer. Barret and Charbeneau (1997) applied the lumped parameter method to the Barton Springs part of the Edwards Aquifer, but it was simpler because there were fewer basins, so the earlier model is used as an example in this book. Conceptually, each of the nine watershed basins is treated as an interconnected tank. The lumped parameter mathematical relation was developed much like a statistical regression model where recharge and pumpage in each lumped parameter block (tank) were treated as input to a set of linked tanks that transport

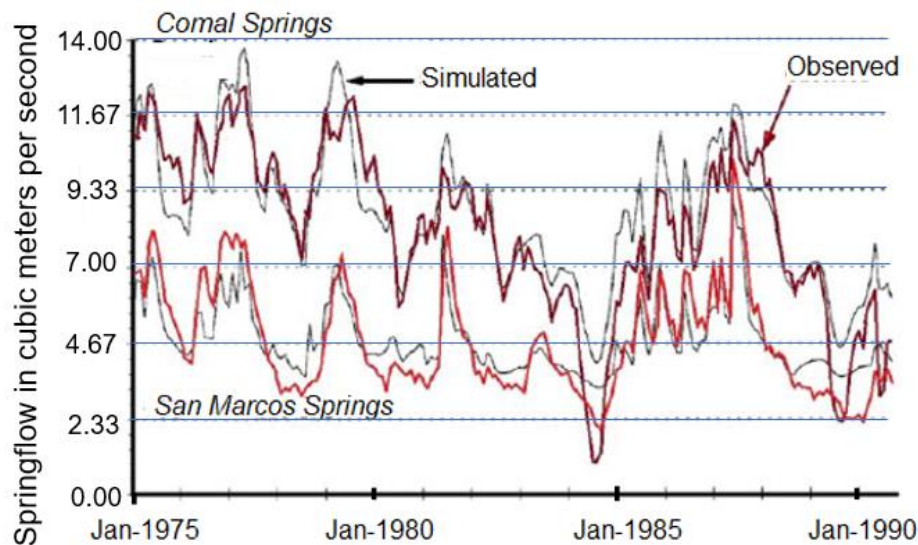
water to the major springs. The mathematical description of each tank was formulated with an ordinary differential equation. Figure 67 shows the Edwards Aquifer and catchment area as well as the conceptualized tanks.



**Figure 67 - a)** Map showing the Edwards Aquifer in Texas, USA, and its recharge zone in the Edwards Plateau. On the Edwards Plateau, the highly transmissive rocks of the Edwards Group are mostly eroded such that less permeable rocks outcrop on the plateau. En echelon faulting results in the narrow karst Edwards aquifer on the margin of the uplifted Edwards Plateau. Streams flowing on the plateau lose some, or all, of their flow through seepage to groundwater of the Edwards Aquifer. Stream gages, operated for decades, provide data for calculating this direct recharge to the aquifer. The two fault lines show where there is 100% vertical displacement of rocks within the Edwards Group causing groundwater recharged in basin 4 to move west on the north side of the fault before turning eastward toward major spring outlets. **b)** Schematic diagram of the lumped-parameter-model tanks and their connections. Each tank represents a basin where recharge and pumpage rates are known. Those volumetric rates were applied to each tank, then the size of the tank and discharge pipes were adjusted such that the water level in the tank matched the observed average groundwater level and leakage from the tank matched the estimated discharge from springs. (Modified from Wanakule and Anaya, 1993).

Surface runoff from the catchment area infiltrates the Edwards Aquifer across its outcrop. Wanakule and Anaya (1993) used the recharge and pumpage data as inputs to the system. They developed filters to break up the annual estimates of recharge into monthly estimates using stream gage data and annual recharge estimates. Additionally, the monthly pumpage by county was reapportioned to each sub-watershed (Wanakule and Anaya, 1993). These values were then matched to average monthly groundwater levels in each basin and to the historical spring discharge at Comal and San Marcos Springs by calibrating values of parameters related to storage and transmissivity for each tank. The filtering method for the disaggregation of recharge falls into category 1 (fitting models), which

includes time series techniques. Wanakule and Anaya (1993) were successful in refining estimates of monthly recharge and pumpage for each basin and simulating the spring discharge at Comal and San Marcos Springs (Figure 68) as well as water levels in each basin, which are not shown here, but were presented by Wanakule and Anaya (1993).



**Figure 68** - Simulated and observed spring flow at Comal and San Marcos Springs, Texas, USA. Modified from Wanakule and Anaya (1993).

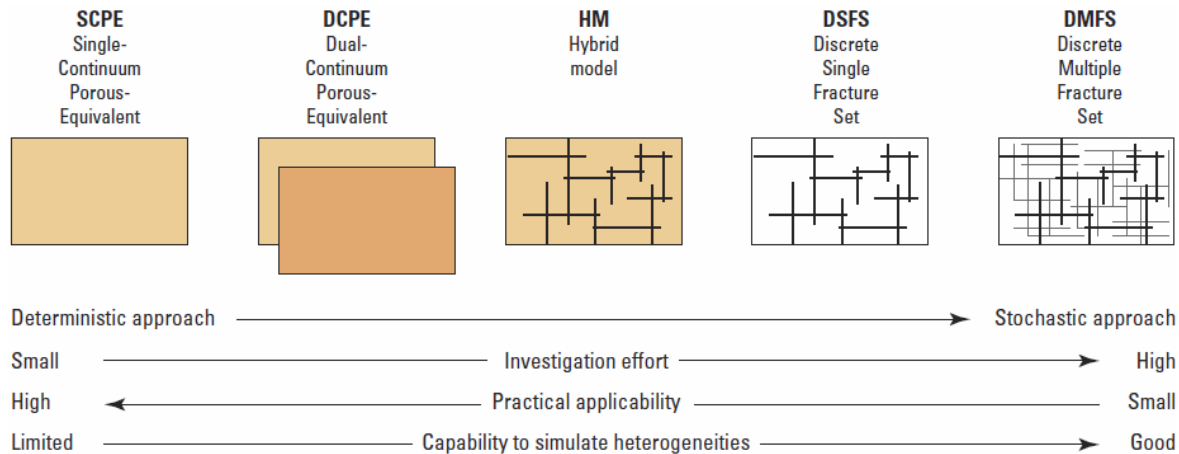
Schulman and others (1995) developed equations for stochastically generating recharge volumes for the watershed basins. The equations have the same statistical properties as the historical (since 1934) recharge data for each basin. The wellbeing of endangered species at the springs are a concern, and the courts have required minimum discharges to be maintained at both springs. Given these minimums, groundwater use is restricted at times during summer months even as the population continues to grow. Thus, water-resource planners recognize that water may need to be imported to maintain discharge at the springs. Because of its computational speed and simplicity, the calibrated lumped parameter model of Wanakule and Anaya (1993), combined with the generated recharge scenarios, were used to screen water-supply options for the Edwards Aquifer (Watkins and McKinney, 1999).

### 6.3 Distributed Parameter Models

Distributed parameter models may be deterministic or stochastic. For deterministic models, the output of the model is fully determined by the parameter values and the initial and boundary conditions. This is in contrast to stochastic models which have some type of inherent randomness (that is, the same input will lead to an ensemble of outputs because, for example, the input may specify statistics describing the frequency, size, and length of conduits, but not their exact size, length, or position, thus numerous realizations of the statistical distribution are generated to create individual deterministic simulations).



Various types of distributed parameter models have been applied to karst aquifers (Figure 69). The simplest approach is often referred to as the porous-equivalent media model approach (also called the single-continuum porous-equivalent [SCPE], heterogeneous-continuum, distributed-parameter, or smeared-conduit model). The SCPE assumes that flow in the aquifer system can be simulated with the potential flow equation of fluid mechanics which is the way typical porous aquifers are represented.



**Figure 69** - Approaches to karst modeling with distributed parameter models (numerical models) ranging from porous-media equivalents to fracture and conduit networks that are simulated with flow equations for fractures or conduits. Stochastic methods are commonly used for defining the nature and location of fractures and conduits. Modified from Teutsch and Sauter (1998).

Regardless of the distributed parameter modeling approach, field data are collected to: map the aquifers and confining units; determine the location and quantity of water entering and exiting the system; and, provide water-level and flow observations for calibration of the model. The data are used to define the hydrogeologic framework and develop a conceptual flow model for the application and finally for calibration of the site model. Calibration is the process of adjusting the value of model parameters until the values simulated by the model match the measured field observations. It is best if a basic model is developed early in the investigation because the process of building a model can reveal the type and location of data that should be collected during the rest of the investigation in order to improve the model. A common mistake is beginning the modeling task after the field work has been completed, at which time it is too late to use the model to inform the investigation process.

Most distributed parameter models have limitations in their use and application resulting from: simplifications of the system, inadequate calibration data, or poorly understood system geometry and boundary conditions. It is beyond the scope of this book to discuss the documentation of models such that their limitations are fully presented. However, good resources on this topic can be found in Anderson and others (2015) as well as in Reilly and Harbaugh (2004).

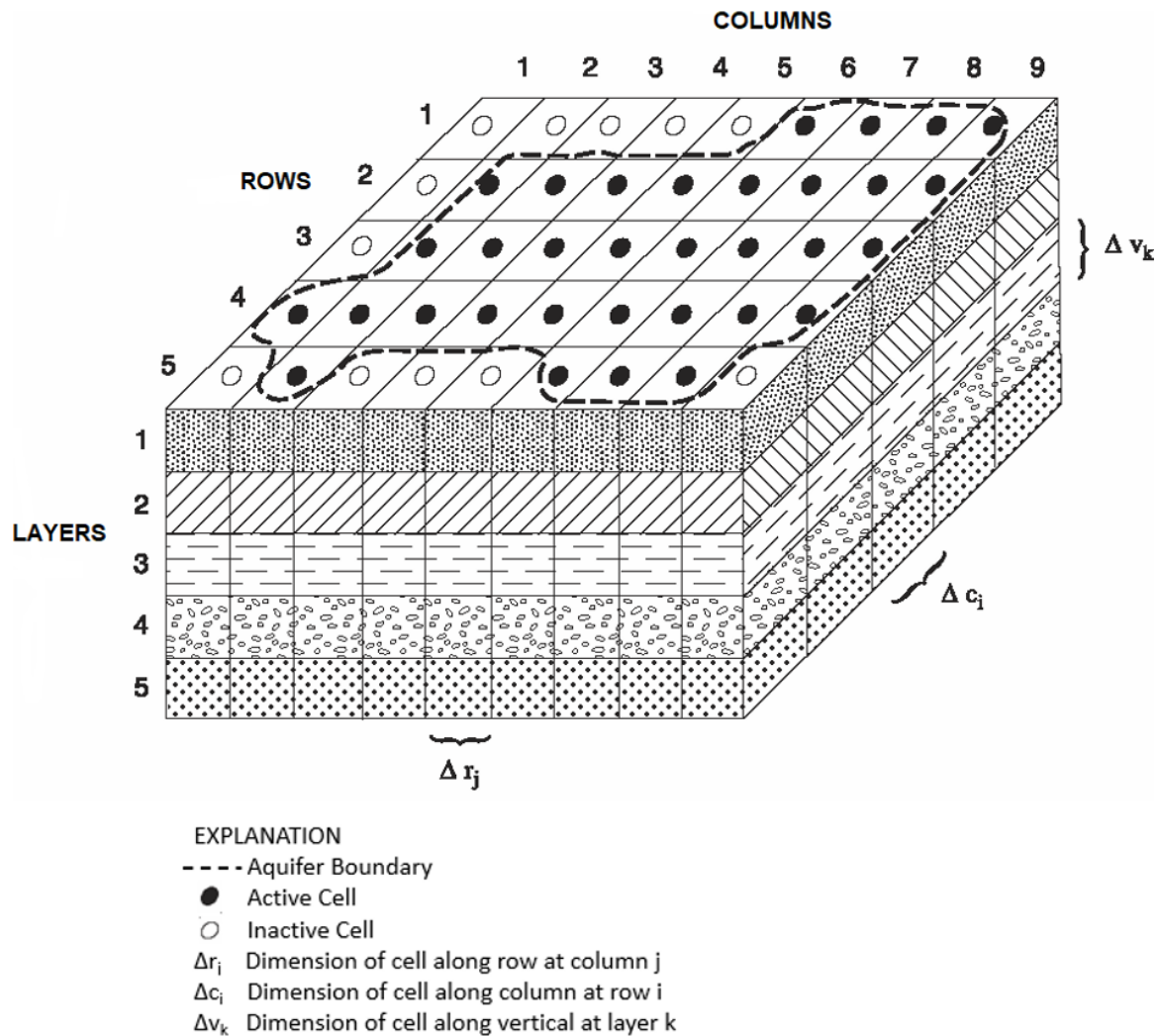
Distributed parameter models are frequently applied to karst aquifer systems (Kuniansky and Holligan, 1994; Teutsch and Sauter, 1998; Kuniansky et al., 2001; Kuniansky and Ardis, 2004; Scanlon et al., 2003). These types of models are process oriented, and the process can be represented by the Navier-Stokes equations that describe unsteady fluid flow in three dimensions. The Navier-Stokes equations are coupled sets of partial differential equations that describe how pressure, temperature, density and viscosity of a moving fluid are related. The equations were derived based on the underlying principles of conservation of mass, energy, and momentum and are the basis for almost all fluid mechanics problems (Daily and Harleman, 1966).

Unfortunately, all the forces described by these partial differential equations cannot be solved readily on the computers that are available at the time this book is being written due to speed, memory and storage limitations. Consequently, forces and processes that have negligible impact on the flow problem can be eliminated from the full set of Navier-Stokes equations such that a reduced equation (or set of equations) that includes the important physical process(es) is (are) applied. In groundwater problems, flow is typically dominated by potential energy as reflected by the hydraulic head gradient within an aquifer. The energy that would go into eddies or vortices within the water (kinetic energy losses from turbulence or non-laminar flow) is negligible for most groundwater flow problems as are differences in temperature, density, and viscosity for shallow groundwater systems. Thus, the potential-flow equation, used in groundwater model codes such as the basic version of the United States Geological Survey software called MODFLOW (McDonald and Harbaugh, 1988), assumes that flow is laminar and that temperature, density, and viscosity are constant over the model domain. Provided that the problem is reasonably well represented by these assumptions, the computational burden and time required to run the simulation can be greatly reduced with little loss of accuracy in the solution.

The potential-flow equation has also been used in aerodynamics for flow of air over a wing; in thermodynamics for heat flow; in hydrodynamics for flow around objects in a stream; for full pipe flow; and for flow of electrical current. Distributed parameter models require dividing (discretizing) the aquifer system into representative three-dimensional volumes, such as finite-difference cells or finite elements. Depending on the scale of the study, representation of the karst aquifer may also be greatly simplified due to limitations on the total number of cells or elements that can be solved in a reasonable time on a computer. Thus, the greater the area and thickness of the simulated karst system, the larger the number of cells or elements; which may be less representative of fine-scale features and require the use of composite hydraulic properties (Sepúlveda and Kuniansky, 2009). The physical aquifer properties (parameters), such as storage and hydraulic conductivity are distributed spatially and may have a different value in each model cell or element. Thus, the general name, distributed parameter model, is widely applied to these mathematical modeling approaches.

Other distributed parameter approaches shown in Figure 69 are the dual-continuum porous-equivalent model (DCPE), the hybrid model (HM), the discrete single fracture or conduit set model (DSFS), and the discrete multiple fracture or conduit set model (DMFS). The DCPE model links two flow regimes (two SCPEs) at each cell or element with a head-dependent water exchange term between sub-cells or sub-elements. In a DCPE the flow within each cell represents a physical volume of the aquifer with two, sub-cells exchanging flow with one another. One sub-cell represents the conduits and the other sub-cell represents flow in the rock matrix. The hybrid model (HM) couples a three-dimensional SCPE model with a discrete one-dimensional flowing fracture or conduit network (Figure 69, HM). The fracture-set or conduit-network modeling approaches shown in Figure 69 may involve the stochastic generation of fracture or conduit networks that are simulated with equations for conduit or fracture flow. The discrete, single-fracture or conduit network set (DSFS) and discrete multiple-fracture or multiple-conduit network set (DMFS) models are rarely applied to karst aquifers. The advantages and disadvantages of each modeling approach are described in the following sections.

Most distributed parameter models of karst systems have a large number of cells or elements used to subdivide the aquifers and confining units into discrete cell volumes (discretization). For illustrative purposes, Figure 71 shows the nomenclature for the division (discretization) of a five-layer aquifer system into cell volumes used by the block-centered finite-difference groundwater flow modeling code MODFLOW. Figure 71 is a simplified model diagram where all layers are constant thickness, and the number of rows and columns is small. Most site models have hundreds of rows and columns and the row and column dimensions are not constant.



**Figure 70** - Distributed parameter models divide (discretize) the aquifer system into representative three-dimensional volumes and define properties that represent the equivalent bulk properties of the volume of rock that the block represents. This diagram shows the convention for numbering block-centered, finite-difference cells for MODFLOW. In the illustrated case, each vertical layer has a different lithology as indicated by the shading pattern. Modified from McDonald and Harbaugh (1988).

### Single-Continuum Porous-Equivalent Models

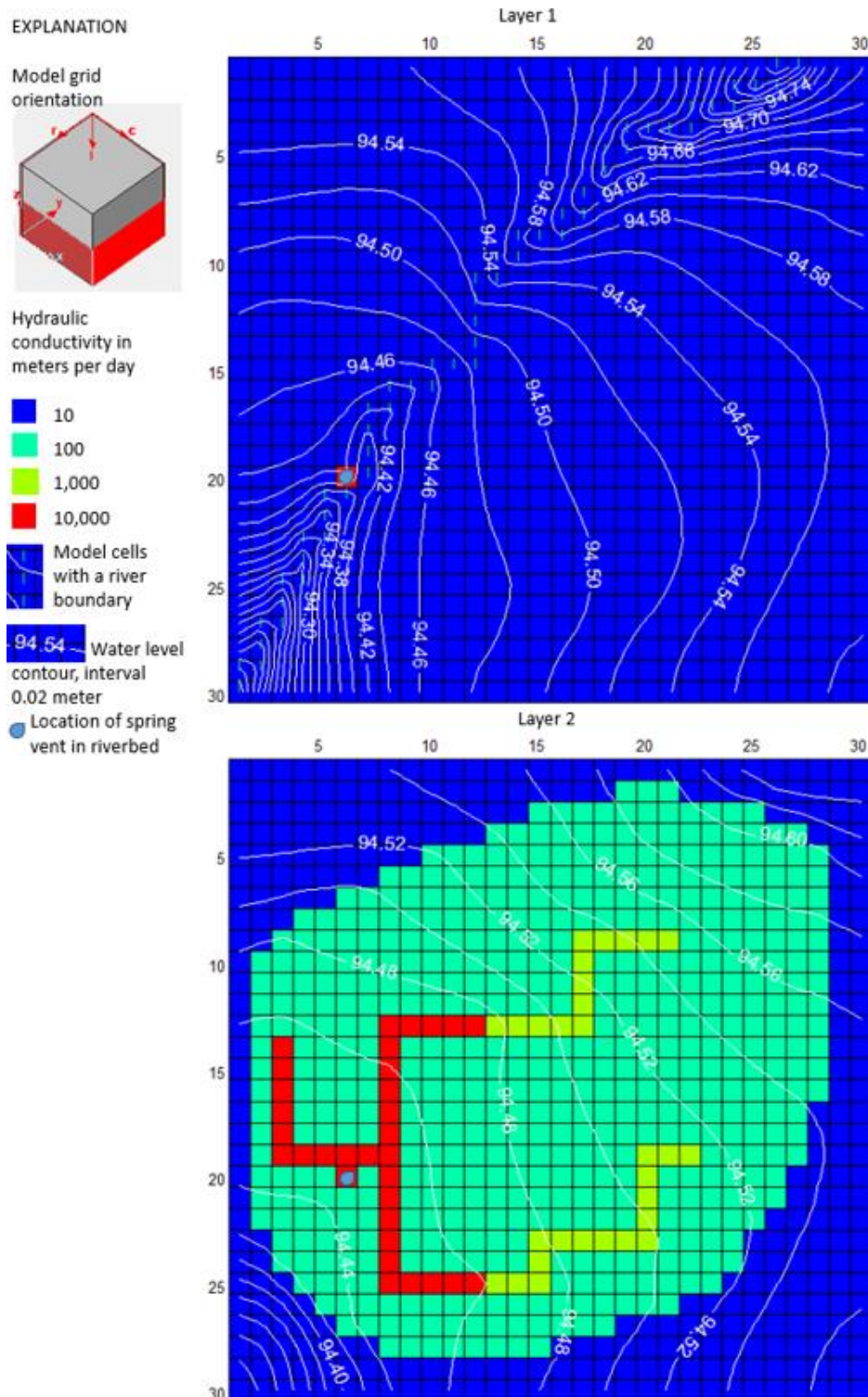
An SCPE approach using the potential-flow equation (which assumes laminar flow at constant temperature, density, and viscosity) is the simplest distributed parameter model to apply. Figure 72 displays a simple example of applying a SCPE to karst using MODFLOW. The model has two layers. The top layer is predominantly unconsolidated sand, and the bottom layer is a confined karst aquifer with mapped conduits that connect to an artesian spring that discharges in a reach of a perennial stream in the top layer. It is simplified by using high hydraulic conductivity cells to represent conduits.

The SCPE approach has been applied for regional, or sub-regional, flow in some karst aquifers because the scale of investigation is much greater than the scale of the heterogeneities in the rocks. In this case, heterogeneities refer to dissolution features or flow units with different water-transmitting properties. The SCPE approach has been successfully applied for water-resources investigations where the models are calibrated to

steady-state average conditions (generally representing one season- or annual-average recharge and pumpage conditions during the time period when the potentiometric mapping was conducted). The SCPE approach has also been applied for transient conditions using multiple stress periods that may represent monthly, seasonal, or annual flow. The models simulate head (water level) and provide a regional- or sub-regional-scale water budgets for water planning purposes. In general, the SCPE approach can simulate transient average monthly or annual spring flow, but generally cannot reproduce detailed storm-event hydrographs as well as other model types because non-laminar flow occurs during storms (Hill et al., 2010; Kuniansky et al., 2011; Gallegos et al., 2013; Saller et al., 2013; Kuniansky, 2014, 2016).

Simulations of advective transport using a single-continuum model are infrequently performed and have varying degrees of success. Advective transport modeling within karst aquifers has been able to match estimated geochemical age and travel times derived from tracer-tests for the Floridan Aquifer Systems in the USA by using effective porosity of less than 5 percent rather than the total porosity which ranges from 15 to 40 percent. These models have been documented by Knochemus and Robinson (1996) Kuniansky and others (2001), Merritt (2004), Renken and others (2005), as well as Davis and others (2010). In these studies, groundwater flow volume (Darcy flux) was mainly governed by the model cell hydraulic conductivity and model layer thickness. Effective porosity is used for calculation of a pore velocity that matches model simulated values to observed water age or time of travel determined by using field tracer tests. In some cases where conduit locations were known, the finite-difference cells or finite elements with conduits were assigned much greater hydraulic conductivity values than surrounding cells and were successful in reproducing transient spring discharge (annual, seasonal, and/or monthly averages) and matching tracer-test-derived times of travel (Davis et al., 2010). A similar attempt was not as successful within the Edwards Aquifer system in Texas, USA (Lindgren et al., 2004, 2009), but was successful in the Fort Payne aquifer in Tennessee, USA, which is a less permeable karst aquifer than the Edwards Aquifer system or the Florida Aquifer System (Haugh, 2006).





**Figure 71** - Example of a single-continuum porous equivalent model. This is a two-layer model with karst beneath a uniform, 100 m thick sand. All cells are 100 by 100 m on each side. Limestones are represented in layer 2 with cell hydraulic conductivity ranging from 100 to 10,000 m/d. Layer 2 is 200 m thick. Mapped conduits are located in cells with  $K$  of 1,000 and 10,000 m/d. The mapped conduit cells, shown in red and yellow, are mostly in layer 2, with one cell in layer 1 where the major spring outlet occurs and connects to the cell below in layer 2. A perennial stream flows across layer 1 with a stage of 95 m at row 1 column 30 and 94 m at row 30 column 1. The river cells are indicated with a light blue line within each cell in layer one and the river stage decreases linearly downstream. A constant rate of recharge is applied to the top of the model.

## Dual-Continuum Porous-Equivalent Models

The DCPE models link two, single-continuum, porous-equivalent models (SCPE) via a head-dependent flux term between the linked cells of the SCPEs. Thus, flow in each aquifer cell volume is represented by two, sub-cell properties of each SCPE within the dual porosity karst system, one represents flow in conduits and the other flow in the rock matrix. DCPE models were designed to help subdivide the flow within a block of aquifer between the conduits and the rock matrix by assigning different hydraulic properties to each, such that the faster flow in the extremely transmissive conduits and the slower flow in the rock matrix could result in better matches to observed spring flows.

In simple terms, a head-dependent flux means that flow between the two, sub-cells in the dual-continuum cell is controlled by the head difference between the two continuums and the hydraulic conductivity between them (water flows from the continuum with high head to the continuum with low head). One SCPE has large hydraulic conductivity and small storage, representing conduits, and the other SCPE has smaller hydraulic conductivity and larger storage, representing the rock matrix. The groundwater flow equations are solved iteratively for head at all SCPE sub-cells of the DCPE model for each step that the model takes through time until the solution converges. Most DCPE software codes look similar to a block-centered, finite-difference, numerical model for SCPE (Figures 70 and 71), but with two arrays of rock properties in the layer(s) that are defined as having dual porosity.

DCPE models have been applied successfully when the geometry of conduits is not known (Teutsch and Sauter, 1991; Sauter, 1993; Teutsch, 1993; Teutsch and Sauter, 1998; Painter et al., 2007). One advantage of using the DCPE approach is that the detailed geometry of the conduits is not required (Teutsch, 1993; Sauter, 1993; Lang, 1995). The main advantages of using a DCPE model are its capacity to simulate rapid variations in discharge and head following recharge events and its mathematical representation of both the conduit and rock matrix contribution to total flow through time. The required data for the model is relatively modest, and the effort required to construct the model is manageable for most projects. The DCPE model, however, generally does not have the ability to simulate transport processes on a small scale (Mohrlok, 1996). Application of this modeling approach is not common.

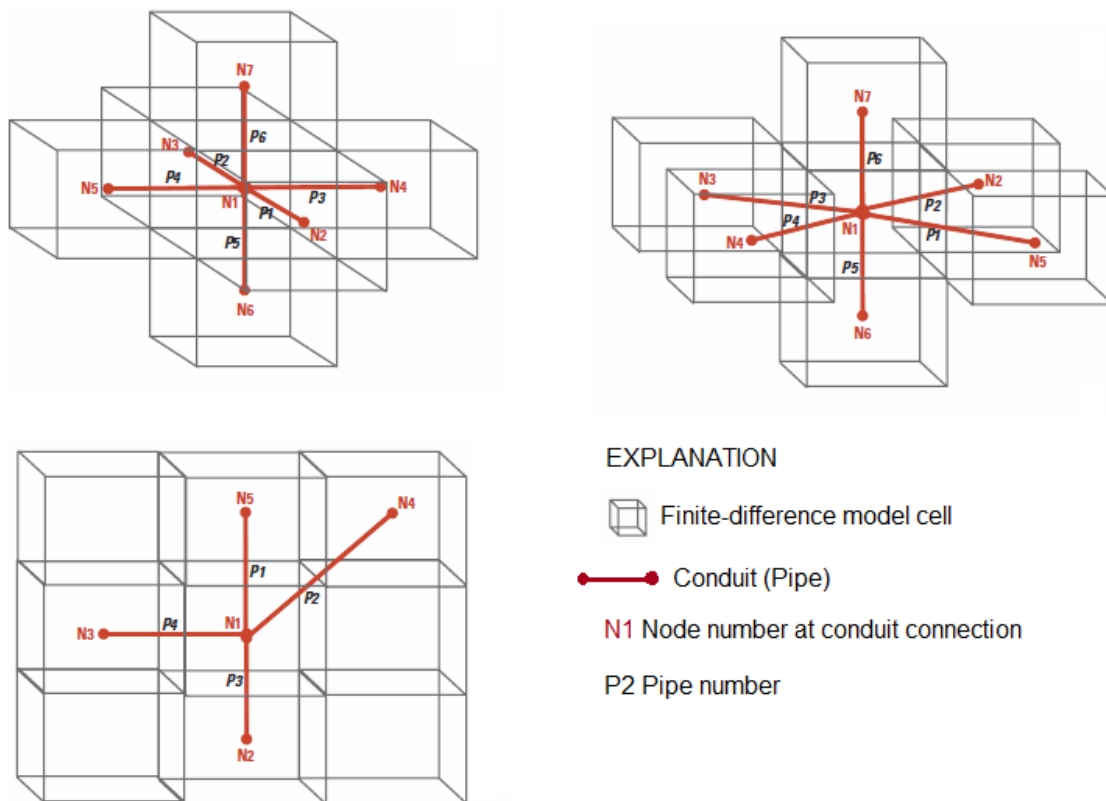
## Hybrid Models

A hybrid model (HM) is the coupling of an SCPE model with a discrete one-dimensional conduit network model (Kiraly, 1998; Teutsch and Sauter, 1998). The HM approach allows the integration of detailed information about conduits in areas where the geometry of major conduits is known, thus providing a more representative model of the physical system. The HM links a three-dimensional SCPE model for groundwater flow within the rock matrix with a one-dimensional conduit network model that can have laminar or turbulent flow. The conduit network geometry is specified by defining locations

within finite-difference cells where conduits are connected to other conduits (conduit network nodes). The SCPE model exchanges water between the conduit network and the porous matrix in cells containing conduit nodes by using head-dependent flux terms and iterates calculations between the two models until both converge to a solution for head, in a manner similar to the DCPE model.

The 2008 version of the MODFLOW-2005 conduit flow process (MODFLOW-CFP) (Harbaugh, 2005; Shoemaker et al., 2008) is based on the hybrid modeling approach developed in the Carbonate Aquifer Void Evolution (CAVE) software code (Clemens et al., 1996; Bauer et al., 2000; Bauer, 2002; Birk, 2002; Bauer et al., 2003; Liedl et al., 2003). The main advantage of this modeling approach is that it can simulate high transport velocities, under laminar and non-laminar flow, as observed in karst aquifer system conduits; while accounting for the presence of a lower hydraulic conductivity rock matrix. Most of the water storage occurs within the karst aquifer rock matrix. This approach has limited application for most studies due to the lack of geometric data for the entire conduit system (conduit location, diameter, roughness, and tortuosity) given that often only the largest conduits are mapped. The first release of the CFP has limitations in that the conduit network is intended for conduit-full flow where flow is controlled by the pressure gradient (potential flow but including turbulence) and does not account for free-surface flow in partially full conduits. For free-surface, open-channel flow, the free water surface is in equilibrium with atmospheric pressure and the forces driving flow are dominated by gravity. In this case, the gravity terms cannot be omitted from the Navier-Stokes equations because flow is predominantly controlled by open-channel slope, roughness, and channel shape. In short, the 2008 version of CFP should not be used for systems with large networks of partially full conduits. MODFLOW-CFP and research variants of the code have been applied to the Florida Aquifer System in several locations as discussed in the example for this section with respect to an application in the Woodville Karst Plain, Florida, USA.

The MODFLOW-CFP simulation code includes three modes. Mode 1 is the hybrid model described above. Mode 2 includes the capability to insert a high-conductivity flow layer that can switch between laminar and turbulent flow. Mode 3 allows for coupling a discrete one-dimensional conduit network in a high-conductivity flow layer that can switch between laminar and turbulent flow. Figure 72 shows how one-dimensional pipe conduit networks can be configured within the MODFLOW cells. A maximum of six pipes can be connected at a single node. Even if the mapped conduit is not at the centroid of a cell volume, the head-dependent flux term between the MODFLOW cell and the pipes is calculated between the pipe node and centroid of the cell. If the modeler wants to better locate the connection, then a finer grid needs to be defined. Additionally, the pipe leakage conductance is calculated using half of the surface area of the pipe between two nodes. Shoemaker and others (2008) provide more detailed discussion of MODFLOW-CFP.



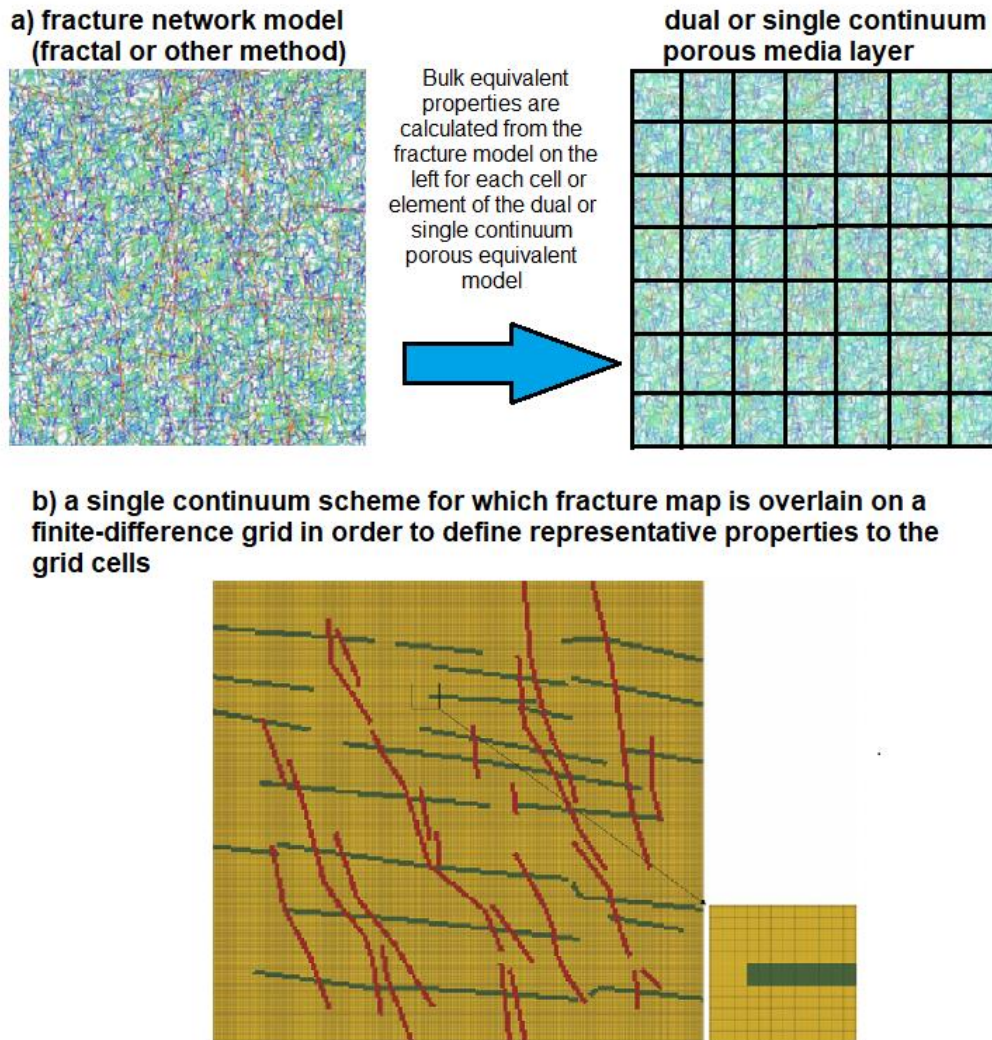
**Figure 72** - Three examples of how the one-dimensional conduit network could link to adjacent finite difference cells in MODFLOW-CFP. A maximum of six pipes can connect at a single node and flow exchange between the pipe and the model occurs at nodes within the specified finite-difference cell. Modified from Shoemaker and others (2008).

Models originally intended for surface-water systems have been used to represent karst aquifers. The Storm Water Management Model (SWMM) (Metcalf and Eddy Incorporated, 1971) was designed for simulation of sewer systems and was applied by Peterson and Wicks (2006) to simulate karst conduits, but no interchange with the rock matrix was simulated. The MODBRANCH code (Swain and Wexler, 1996) was modified for simulation of a karst system by Zhang and Lerner (2000). MODBRANCH was originally developed by coupling one-dimensional, free-surface, open-channel flow with the top layer of a three-dimensional groundwater flow model for simulation of interaction between groundwater and surface-water. Reimann and others (2011b) developed the ModBraC version of a hybrid model that couples the SCPE model with a conduit network model capable of simulating storage of the conduit system, conduit-full flow, and open-channel flow in the conduits. Accurate representation of conduit storage is essential in order to simulate the lag time between discharge changes and indicators of transport (for example, temperature, conductivity) after recharge events. Grubbs and Crandall (2007) applied MODBRANCH for simulation of groundwater and surface-water interactions in a karst aquifer.

## Discrete Single and Multiple Fracture or Conduit Network Models


The discrete fracture approach using a single fracture set (DSFS), or multiple fracture sets (DMFS) has been proposed for problems where transient solute-transport responses are desired for an aquifer system dominated by fractures or conduits (Adams and Parkin, 2002). Knowledge of the fracture network geometry is required for application of these models. Generally, data from mapping of the fracture network(s) are limited, thus stochastic methods are typically used to generate the single- or multiple-fracture network for individual, deterministic, numerical simulations of flow. The disadvantages of discrete multiple fracture networks are the requirement of detailed knowledge of a fracture network at multiple scales and the application of computationally intensive codes with long computer simulation time (days) and large memory requirements (Lang, 1995). Much effort is in the collection of data on fractures for stochastic generation of multiple fracture networks from the statistics based on fracture data from borehole imagery and processing of the images to estimate aperture size and orientation. Often fractures are planar features within low-permeability hard rock and borehole image processing is one of the best tools to delineate their orientation and gather the statistics for stochastic model simulations. Many different algorithms are used to generate the fractures and convert these to bulk cell-block properties. Lei and others (2017) provide an excellent overview of discrete fracture network modeling. Implementation of fluid-flow simulation is usually similar to that of SCPE or DCPE with rock properties assigned to cells based on the fracture network modeling (Figure 73); however other methods are applied in some cases. Application of this approach to field-scale problems is not common, so no examples are available. The petroleum industry has applied DSFS/DMFS, but model run times have not been published (McClure and Horne, 2013).





**Figure 73** - Examples of fracture network modeling. a) A network is stochastically generated for each unit, then a grid is overlain on that layer and bulk properties are calculated for each finite difference cell for dual or single continuum flow simulation. b) Fractures are mapped (those oriented vertically are in red and those oriented horizontally in green) and the cells of the finite-difference grid are assigned properties based on the mapped fractures that intersect most of the finite-difference grid. Modified from Lei and others (2017).

### Example Comparisons of Single-Continuum and Hybrid Models

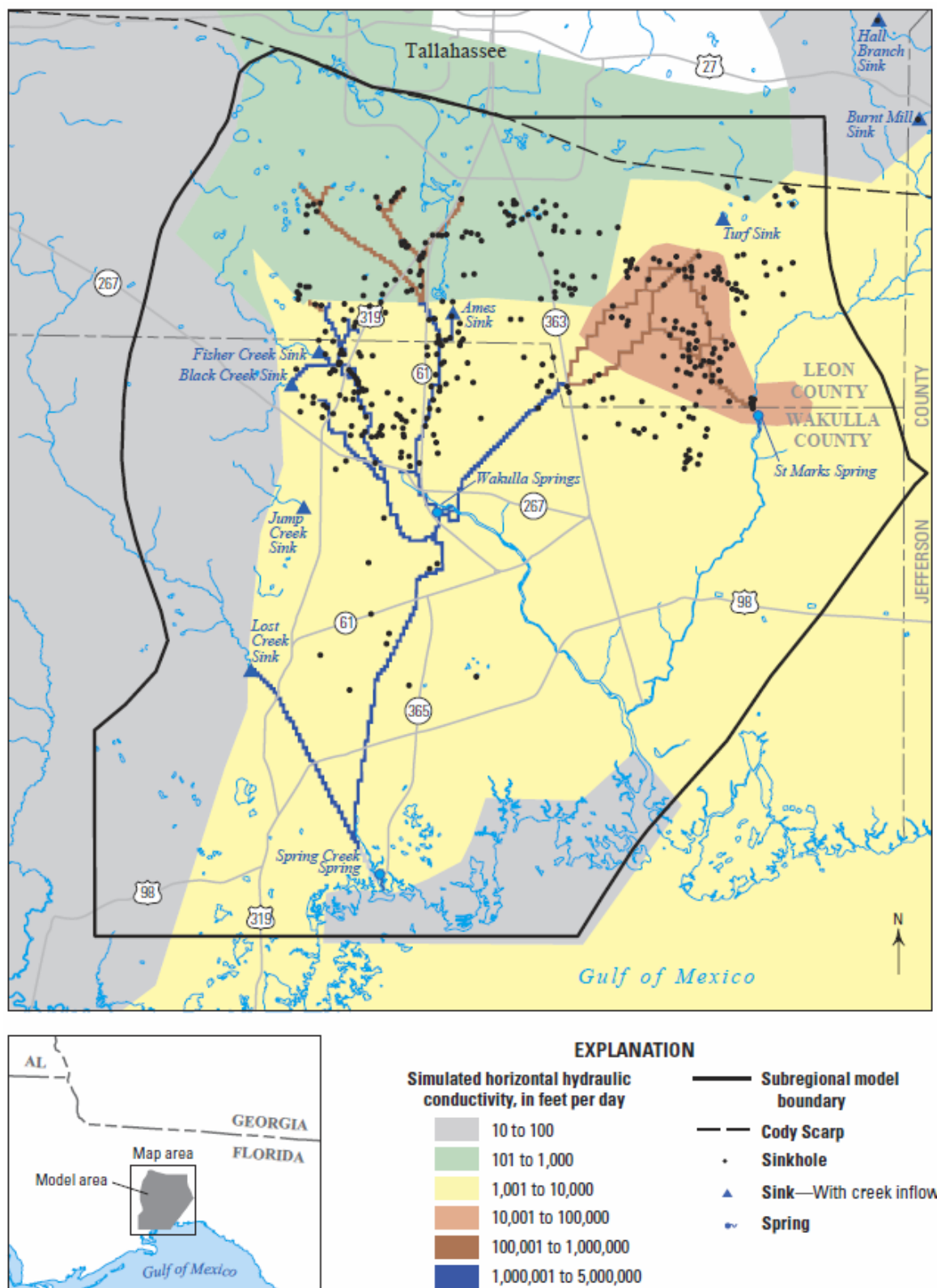
Extensive mapping of the sinks and submerged conduit system of the Wakulla Springs-Leon Sinks, Florida, USA, has been accomplished over the past 20 years by cave divers of the Global Underwater Explorers  as part of the Woodville Karst Plain Project (WKPP) as described by Kernagis and others (2008). As a result of their pioneering work, this karst drainage system is believed to be well characterized. The Woodville Karst Plain is 450 square miles ( $\sim 1200 \text{ km}^2$ ) and contains the Wakulla Springs-Leon Sinks system. Wakulla Springs is one of the largest first-magnitude springs in Florida, with average flows of approximately  $400 \text{ ft}^3/\text{s}$  (cubic feet per second;  $\sim 11 \text{ m}^3/\text{s}$ ). The spring occurs at a large vent opening of about 25 m by 15 m which forms a pool that is approximately 90 m in diameter and 55 m deep at the headwaters of the Wakulla River at Edward Ball Wakulla Springs

State Park, Florida, USA (Florida Department of Environmental Protection, 2016). A satellite image of Wakulla Springs is shown in Figure 1c. This area has been investigated for decades and several SCPE models have been developed and calibrated.

The Woodville Karst Plain Project (WKPP) maps were used by Davis and others (2010) to update an older SCPE model that had been developed and calibrated for a previous study (Davis and Katz, 2007). A hybrid model was developed and calibrated based on the model developed by Davis and others (2010) and published by Gallegos and others (2013). Ultimately, three modeling approaches were developed and their results were compared to examine the applicability of the approaches for this area.

### **Background on the Three Modeling Approaches**

Davis and others (2010) used a SCPE approach to simulate transient conditions in the area shown by the sub-regional model boundary in Figure 74. The simulation begins on January 1, 1966, when spray-field operations (irrigation using treated wastewater as part of municipal wastewater treatment processing) began, and ends in 2018, when operating system upgrades to the wastewater system were planned to take effect. Changing hydrologic stresses (for example, pumping and recharge) on the groundwater system were primarily represented in the model as average-annual conditions throughout the 1966–2018 model simulation period. For a 2.2-year period during 2006 and 2007 when tracer tests were conducted by Hazlett-Kincaid, Incorporated, hydrologic conditions were represented by average conditions over 10-day periods. Data describing the hydrologic stresses are listed in Davis and others (2010). Observations of water levels and spring discharge were available for November 1991 and May to early June 2006. These data were used to calibrate the model.



**Figure 74** – The extent of the sub-regional model of the Woodville Karst Plain, Florida, USA with colors indicating the hydraulic conductivity in model layer 2. Large hydraulic conductivities correspond to submerged conduits. Modified from Davis and others (2010).

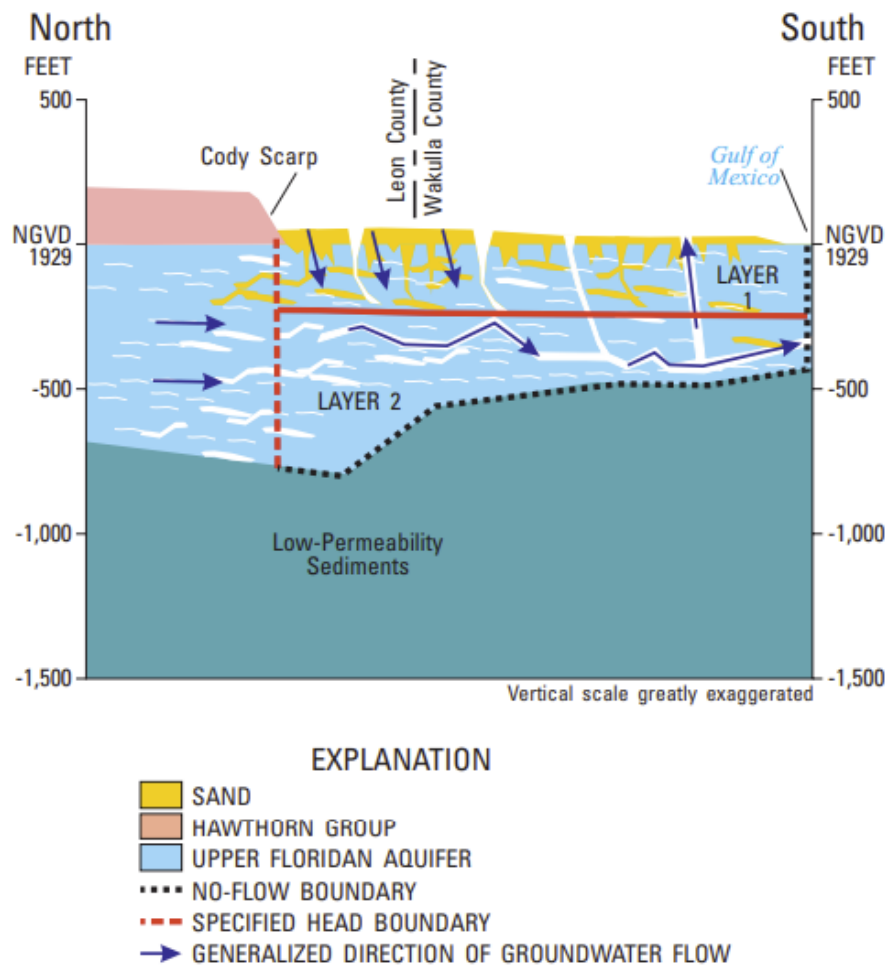
Two additional models were developed such that three approaches were used to represent the system. One, herein called Approach 2, was an SCPE model as used by Davis and others (2010), but with both laminar and turbulent flow in the SCPE for layer 2. The other, herein called Approach 3, was a hybrid model (HM) consisting of a single continuum as used in Approach 1 and 2 coupled to a one-dimensional, conduit-flow network capable of simulating laminar and non-laminar flow in the conduit network.

The three modeling approaches are summarized here to help the reader keep their differences in mind.

- Approach 1—SCPE model with only laminar flow using a previously calibrated model of Davis and others (2010). This model has high hydraulic conductivity (K) cells in mapped and inferred conduits.
- Approach 2—SCPE model as in Approach 1, but with both laminar and turbulent flow in the SCPE for layer 2. This is an application of MODFLOW-CFP using mode 2 (Shoemaker et al., 2008; Kuniansky et al., 2008; Davis et al., 2010; Kuniansky et al., 2011; Reimann et al., 2011a, b; Kuniansky, 2014, 2016). Groundwater flow can be laminar or non-laminar within a SCPE model layer for the MODFLOW-CFP mode-2 approach. Water temperature, average pore diameter, and critical Reynolds numbers for layer 2 are parameters that were not needed for Approach 1, but were required for Approach 2.
- Approach 3—HM model consisting of a single continuum coupled to a one-dimensional, conduit-flow network capable of simulating laminar and non-laminar flow in the conduit network. This is an application of MODFLOW-CFP using mode 1 (Shoemaker et al., 2008; Gallegos et al., 2013; Kuniansky, 2014, 2016). This model was developed from the Davis and others (2010) model with the hydraulic conductivity in their high-K cells decreased to the lower background-K values of surrounding cells and an interconnected pipe network was used to represent conduits.

More details about the hydrogeology of the area as well as the original model grid, boundary conditions, and calibration data, which were used as the basis for calibrating all three approaches, are discussed in Davis (1996), Davis and Katz (2007), Davis and others (2010), as well as Gallegos and others (2013). The simulation input and output files discussed herein are available as a data release (Kuniansky, 2016b).

The models for all three approaches have the same two-layer discretization (Figure 75). The top layer is the confined upper 60 m of the Upper Floridan aquifer, and the second layer is the confined lower part of the Upper Floridan aquifer, which is more than 300 m thick in the west, thins to 60 m in the east, and contains the submerged mapped conduits (Davis et al., 2010).



**Figure 75** - Generalized geologic cross section and model layers for the Woodville Karst Plain models, Florida, USA. From Davis and others (2010).

The calibrated  $K$  values used by Davis and others (2010) are shown in Figure 74, with hydraulic conductivity values greater than 10,000 ft/day (feet per day;  $> 3000$  m/d) assigned to cells that represent mapped and hypothesized conduits. The same values were used for SCPE Approach 2. The only additional parameter values required for Approach 2 were an average pore diameter of 0.75 ft (0.23 m), and lower and upper critical Reynolds numbers of 11 and 150, respectively. After Davis and others completed their project, head and spring flow data were collected for a 52-day storm event in 2008, so the pore diameter and critical Reynolds numbers were adjusted in a transient calibration of the SCPE Approach 2 model using average-daily hydrologic conditions. For model Approach 2, the average pore diameter and the upper and lower critical Reynolds number values were adjusted to improve the match of simulated and observed flows at Wakulla Springs for the daily transient simulation of the 52-day storm. The MODFLOW-CFP used for Approach 2 allows non-laminar flow, but is simplified by requiring only temperature, average pore diameter, and upper and lower Reynolds numbers for the entire layer so adjustments to improve the match at one spring impacts the simulated flow at other springs as well, thus the calibration strove to only match discharge at Wakulla Springs. Temperature was held constant at the average groundwater temperature (20.5 °C). In this original version of CFP



mode 2, the effect of non-laminar flow requires specification of parameters that represent large-pore porous media, not conduits. Reimann and others (2011a) developed a modification that allows for specification of Reynolds numbers more typical of large conduits. When the Reimann and others (2011a) form of CFP mode 2 was applied to this system, it reproduced similar spring flow as the calibrated model of Approach 2 by using higher values (an average pore diameter of 1 foot (~0.3 m), and lower and upper critical Reynolds numbers of 3,000 and 10,000, respectively).

Model Approach 3 is the HM with the one-dimensional, conduit-flow network representing the conduits. It was developed by replacing the higher  $K$  values of the SCPE model (those greater than 3,000 m/d) with the smaller  $K$  values of the surrounding cells and adding the mapped conduit network to those cells as one-dimensional circular pipe flow. Unlike the Approach 2 model, the Approach 3 model had to be calibrated because the initial parameter values used to describe the conduit properties did not produce an acceptable match to the calibration data. During the calibration process, the background  $K$ 's were not changed from those used in Approach 1 and 2, only the values of the pipe parameters were adjusted to obtain an acceptable fit to the calibration data.

The hybrid model is large with over 1000 interconnected pipes and nodes. The time required to run the HM transient model is ~100 times longer than the SCPE models. This makes calibration extremely difficult because the model needs to be run every time a parameter value is adjusted, and values need to be adjusted many times to obtain an acceptable fit to the field observations. Consequently, this model was not calibrated to the transient data used by Davis and others (2010). It was only calibrated to steady-state scenarios that approximated average conditions for two periods when both spring discharge and potentiometric data were available including:

- November 1991
- May-June 2006

Further calibration of pipe properties was accomplished by matching the times of travel along conduits from dye tracing tests conducted during 2006 using the steady-state data for May-June 2006 from the following sink-to-spring dye-trace times. Davis and others (2010) and Gallegos and others (2013) provide more details as both models were calibrated to match these dye-trace travel times:

- Fisher Sink to Wakulla Springs took 10 days;
- Ames Sink to Wakulla Springs took 20 days; and,
- Turf Sink to Wakulla Springs took 40 days.

Even steady-state HM simulation requires many iterations before the SCPE and the one-dimensional pipe network reach what is called convergence where the simulated heads and flows are not changing with additional iterations. Gallegos and others (2013) provide details about the pipe-network parameters and the calibration. Only the parameter values describing the pipe network were adjusted when calibrating the HM model.

The modelers defined criteria for the calibration, requiring that parameter values be adjusted until:

- simulated spring flows were within 10 percent of measured flows; and,
- simulated heads were within plus or minus 2 m of measured heads.

The SPCE models (Approaches 1 and 2) and the HM model (Approach 3) all simulated observed average spring discharge at Wakulla and Spring Creek Springs to be within the calibration criterion of 10 percent. For all three approaches, the difference between simulated heads and heads measured in the field were within  $\pm 2$  m (Davis et al., 2010; Gallegos, 2011; Gallegos et al., 2013). For average spring discharge, the three modeling approaches produce similar results, and all are considered acceptable representations of the system (Davis et al., 2010; Kuniansky et al., 2011; Gallegos et al., 2013; Kuniansky, 2014, 2016).

While all three modeling approaches met the water-level and flow calibration criteria, the simulated potentiometric maps for model layer 2 (the layer with submerged conduits) differed slightly between the HM (Approach 3) and the two SCPE models (Approach 1 and 2) in that, although the simulated heads were within  $\pm 2$  m of the measured heads, the simulated heads in layer 2 of the HM were nearly all lower than the measured heads. That is, the head differences were biased (Gallegos et al., 2013) thus, it was a less-than-acceptable representation of the system. Some decrease of all the hydraulic conductivities or perhaps only those of the matrix or the conduits is likely to resolve the bias, but that was not pursued in the study. The calibrated parameters would be different if the HM was rigorously calibrated to match the larger transient data sets rather than the steady-state average conditions, but transient calibration was not possible with the available computing power.

### Scenarios Simulated with the Calibrated Models

Three scenarios were simulated and compared using the various model approaches to examine applicability of the approaches for representing the Floridan Aquifer System in the vicinity of Wakulla Springs. The three scenarios represent the following conditions.

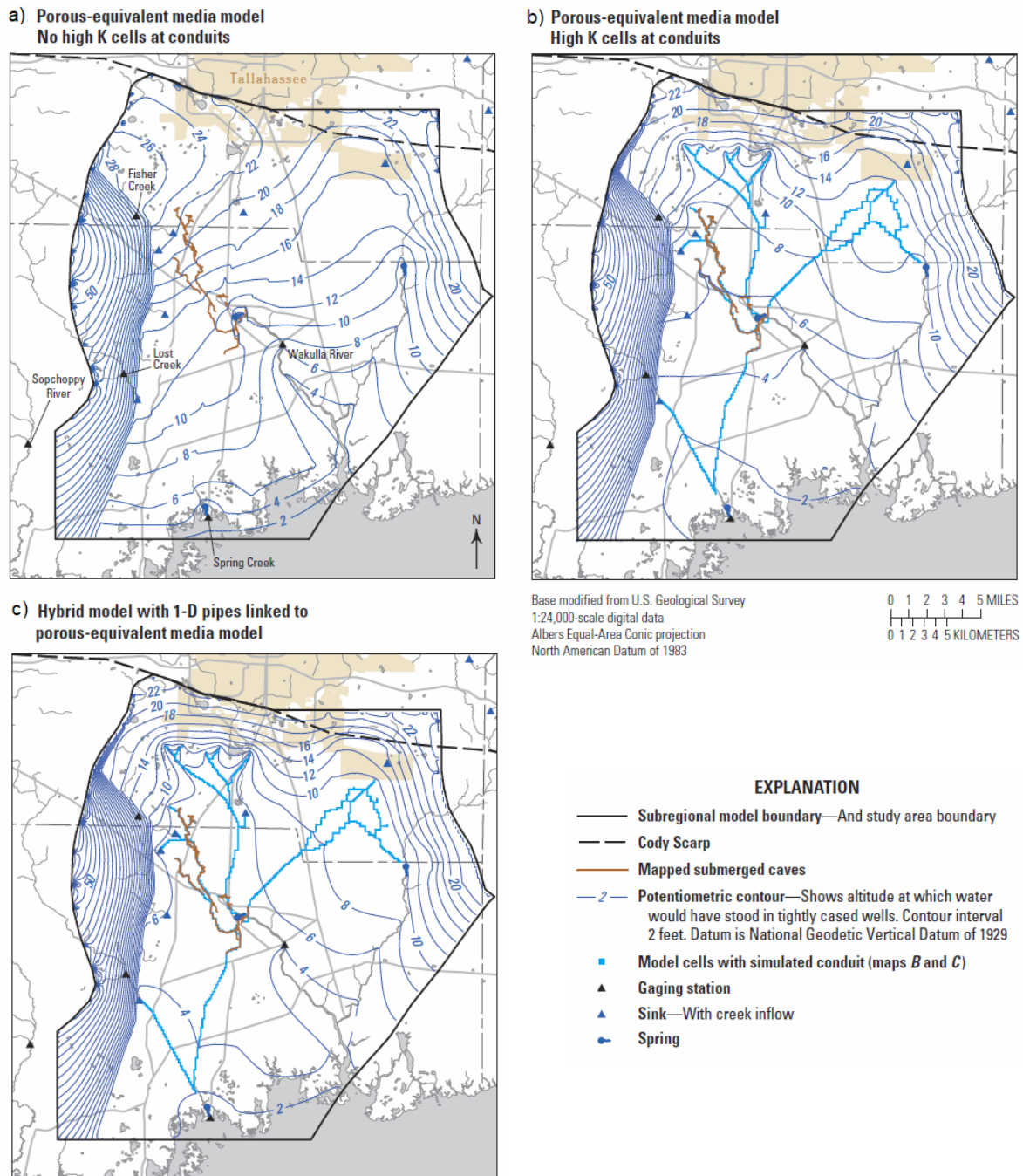
- Scenario 1 - transient representation of spray-field operations as presented by Davis and others (2010) for the 2.7-year period with 10-day averaging of hydrologic conditions (81 10-day average transient conditions beginning January 1, 1966 and extending 2.7 years).
- Scenario 2 - steady-state representation of average conditions for the entire period from 1966 to 2018.
- Scenario 3 - transient representation of a 52-day storm that occurred in 2008 using average-daily hydrologic conditions. This was a storm event that started on August 13, 2008 for which daily discharge was gaged at Wakulla Spring and daily recharge and groundwater pumpage was estimated for the simulations.

### Comparison of transient representation of spray-field operations

Scenario 1 used the calibrated model for Approach 1 (SCPE with high  $K$  cells in layer 2 where conduits are mapped or inferred) fully documented in Davis and others (2010). Scenario 1 was conducted with Approach 2 only (SCPE with turbulence allowed in layer 2 and same hydraulic conductivity and storage properties as Approach 1). Small differences occurred between heads and flows when turbulence was turned on with the average conditions used by Davis and others (2010). With annual and 10-day averaged recharge and pumpage, turbulence occurred in the high- $K$  model cells (cells with conduits) but did not change model head results enough to be noticed on potentiometric maps even with 5 ft (1.5 m) contour maps. For almost all the 10-day periods turbulence did not extend beyond the cells with conduits. For two of the 10-day periods with larger recharge (periods 44 and 66), turbulence occurred in the more cells than any other period and in a few adjacent to the cells with conduits. While it would be difficult to notice any difference in simulated water levels, there was a minor difference in the cumulative water budget from the comparison of Approach 1 and 2. The small amount of turbulence resulted in slightly less flow through the system for the 2.7-year period. The reduction was 8 percent, which is negligible given that the estimates of recharge and pumpage have more uncertainty than 8 percent.

### Comparison of Simulated Potentiometric Maps for Steady-State Average Conditions

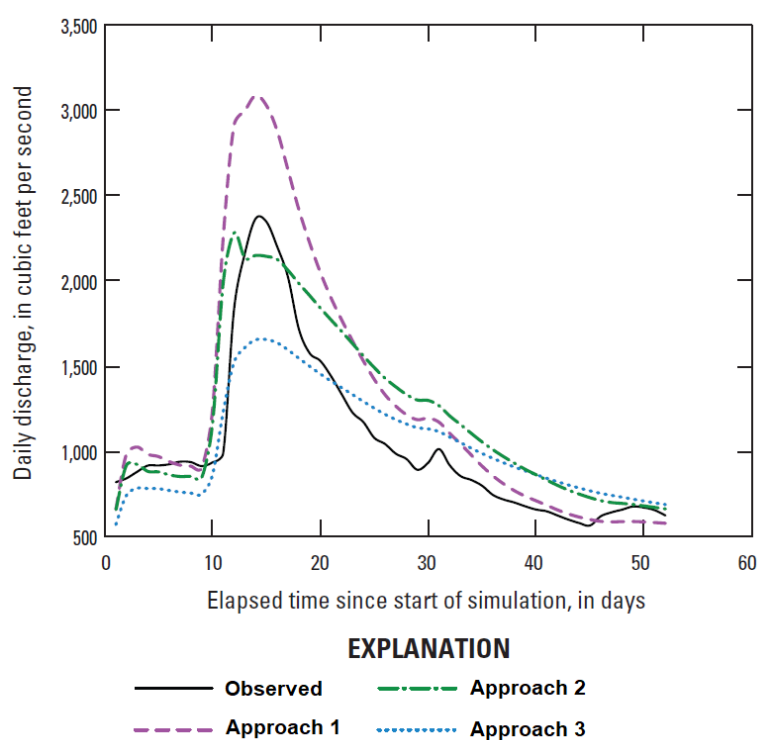
For illustration purposes, three simulated potentiometric maps are shown for model Layer 2, Scenario 2, which is a steady-state condition created by averaging the hydrologic stresses of recharge and groundwater withdrawals from 1966 to 2018 (Figure 76). The potentiometric map in Figure 76a shows a poor representation of the system with homogeneous  $K$  in layer 2 and no high hydraulic conductivity cells where conduits are mapped in an SCPE model. Figure 76b shows the essentially identical head distributions obtained from Approaches 1 and 2 which are SCPE models with high hydraulic conductivity cells where conduits are mapped (Figure 74 shows the high  $K$  cells with conduits). Figure 76c shows the simulated potentiometric map from the HM (Approach 3). The simulated potentiometric surfaces are similar when the conduits are represented in either an SCPE model or a hybrid model (Figure 76b and c). Thus, incorporation of conduits with very large hydraulic conductivity cells in an SCPE approach can mimic the HM approach. If high  $K$  cells are not used in areas of conduits, then the SCPE model will not approximate the water levels of an HM model. Turbulent conditions were not a factor for the average steady-state conditions. In general, scuba divers explore and map the submerged conduit system during low or base flows. Even though the low flow rates at Wakulla Spring are large, often over 100 ft<sup>3</sup>/s (3 m<sup>3</sup>/s), scuba divers do not enter these springs during storms and they have not observed turbulent conditions at these low or average flows. This can be observed in the video link associated with Figure 39 that shows scuba divers in the Weeki Wachee Spring conduit system.



**Figure 76** - Steady-state potentiometric maps of model layer 2 for simulation of average conditions from 1966-2018 in the Woodville Karst Plain, Florida, USA. a) Simulated potentiometric surface for an uncalibrated single-continuum porous-equivalent media model with no high hydraulic conductivity cells to represent conduits. b) Simulated potentiometric surface for the calibrated single-continuum porous-equivalent media model of Approach 1 with higher hydraulic conductivity in cells thought to contain conduits as indicated by small blue rectangles. There was no visible difference in heads between model Approaches 1 and 2 because, although turbulence could occur when using Approach 2, it did not occur for the simulated conditions. c) Simulated potentiometric surface for the calibrated hybrid model (model Approach 3) with low hydraulic conductivity values representing the rock matrix and a one-dimensional conduit network in cells with conduits. The equivalent porous media approaches (SCPE) produced a head distribution that was nearly identical to the distribution produced by the hybrid model approach (HM) as indicated by the similarity of contours in b) and c). Modified from Kuniansky (2016 a,b).

### Comparison of Transient Simulations of a Storm Event using Average-Daily Conditions

In order to observe larger differences between the SCPE and hybrid model approaches, a transient period with daily spring flow observations and a storm event (rising and falling of spring flow) was simulated without recalibrating the models to the storm event data (Kuniansky et al., 2011; Gallegos et al., 2013; Kuniansky, 2014). The 52-day period began August 13, 2008 and was simulated with daily stress conditions. Spring discharge rose rapidly on August 22 (10<sup>th</sup> day) as shown in Figure 77 and peaked on August 26 (14<sup>th</sup> day) at 2,363 ft<sup>3</sup>/s (cubic feet per second; ~67 m<sup>3</sup>/s) as indicated on Table 8. Only the Approach-2 model simulated the observed peak discharge within 10 percent of the measured discharge (Figure 77). The shape of the storm hydrograph for Wakulla Springs is best matched by model Approach 2, the SCPE model with turbulence (Figure 77).



**Figure 77** - Simulated and observed spring flow at Wakulla Springs, Florida, USA. Unit conversion: 1000 ft<sup>3</sup>/s (cubic feet per second; ~28.3 m<sup>3</sup>/s). Modified from Kuniansky (2014).

**Table 8** - Peak discharge at Wakulla Springs, August 26, 2008 during a storm event

	<i>cubic feet per second</i>	<i>cubic meters per second</i>	<i>percent difference from observed</i>	<i>comment</i>
Observed spring discharge	2,363	67		
Approach 1, SCPE no turbulence	3,085	87	-31	overshoots peak
Approach 2, SCPE allowing turbulence	2,149	61	9	reasonable match
Approach 3, Hybrid Model	1,653	47	30	undershoots peak



Model Approach 1 overestimated and model Approach 3 underestimated the peak daily discharge at Wakulla Spring and both were within 30 percent of the observed peak value. Model Approach 2 underestimated the peak but was within 9 percent of the observed peak daily discharge. When no turbulence is considered in the modeling approach then discharge remains a linear function of head gradient and thus Approach 1 overshoots the peak discharge. When turbulence is incorporated into the models, then discharge does not increase linearly with the head gradient and so the simulated peak discharge is not as high. In both Approach 2 and 3 the peak discharge is reduced by the turbulence. With a storm event and daily hydrologic stresses applied to the simulations, turbulence is a factor in both Approach 2 and 3 and reduces the peak discharge.

When the total volumes of measured and simulated discharges for the 52-day period at Wakulla Springs were compared, the following was found:

- Approach 1 (SCPE laminar) matched observed volume within 23 percent;
- Approach 2 (SCPE laminar and non-laminar) matched within 17 percent; and,
- Approach 3 (HM) matched within 0.01 percent.

Simulated fits to observed flow at Spring Creek Spring and Saint Marks Spring were worse than those at Wakulla Springs for all three modeling approaches and those results are not shown herein. Given that none of the approaches captured both the peak and the total volume, none of these models are satisfactory for simulation of this storm event. All require more calibration. When considering this, it is useful to remember that, with the exception of the average pore diameter and critical Reynolds numbers of Approach 2, the models were not calibrated using average-daily stresses to match the daily discharge data. Models of Approach 1 and 2 were calibrated to transient hydrologic conditions, but these were mostly annual-average conditions with only about 2 years of average 10-day conditions. The model of Approach 3 was only calibrated to steady state conditions because of computational limitations. Calibration to daily discharge data using average-daily stresses would improve predictive capability of the models.

The computation time required by the HM Approach 3 to simulate the 52-day transient period (about 12 hours in 2016) was more than 100 times longer than the time required for the SCPE model Approaches 1 and 2. Additionally, the run times for the hybrid model were long and thus it was not calibrated for the full transient conditions from 1966 to 2018 as used for model Approaches 1 and 2. This is a large hybrid model, with more than 1,000 simulated conduits and nodes. The hybrid approach requires that two models are solved iteratively until both converge for each 1-day step through time, requiring a lot of computation time. Practical model applications need to balance the rigor of the solution and the accuracy of the predictions.

Other studies have shown more success with HM. For example, Hill and others (2010) compared a hybrid model approach with a SCPE model approach for two other spring systems in Florida (Weeki Wachee and Twin Dees) and concluded that the hybrid

model more closely simulated observed transient spring discharge. Another study (Saller et al., 2013) converted a SCPE model to a hybrid model for a watershed in the Madison aquifer in South Dakota and found that the hybrid model better matched head observations at monitor wells, and both models simulated spring discharge within the calibration criteria.

Although other studies have found HM to provide better results, the Wakulla Springs example indicates that, for simulation of average conditions, none of the three approaches is distinctly better. However, the HM was manually calibrated with steady-state periods rather than the full transient simulation from 1966 to 2018 that was used for the SCPE models owing to long run times, which put the approach at a disadvantage (Gallegos et al., 2013). The HM is likely to have provided better results if it had been calibrated to the same transient conditions.

The SCPE model with turbulence (Approach 2) best matched peak spring daily discharge at Wakulla Springs for the 52-day storm, and the HM (Approach 3) best matched the total volume of spring flow. None of the model approaches had acceptable matches to the observed daily storm hydrographs at the springs in the model domain. The model of Davis and others (2010) was not intended for matching storm events. This illustrates the important concept that, if a project requires accurate simulation of daily storm events, then the model must be calibrated using storm event data.

It is unlikely that the extra effort required to use a hybrid model, both in data preparation and computation time, is justified for investigations not requiring site-scale transport or prediction of spring flow during storm events, because the simpler SCPE models adequately simulate groundwater-level and average fluid-mass-balance conditions. More recent ongoing work by Xu and others (2015) utilized a research version of CFP that includes transport between the conduit network and the SCPE (Reimann et al., 2013). It applied to a hybrid model of the Woodville Karst Plain for better simulation of long-term nitrate transport using the same long stress periods of Davis and others (2010) and improved on the HM developed by Gallegos and others (2013).

It would be useful to conduct additional tests of model approaches by comparing residence times of rapid (for example, storm event) flow components with slow flow matrix components, as derived from the use of geochemical mixing models with hydrograph separation techniques given time series data of chemistry and flow information. Unfortunately, no such time series data are currently (2022) available for the major springs within the Wakulla Springs-Leon Sinks area.

## 7 Summary

The term karst refers to a landscape or terrane underlain by soluble bedrock and characterized by unique hydrogeologic features, such as caves, sinkholes, sinking streams, and springs, that have been created mostly by the process of dissolution. Most karst is formed by near-surface percolation and circulation of fresh water and is an integral part of the active meteoric water cycle and local-to-regional scale hydrologic systems. The process of karst formation involving dissolution and re-precipitation of carbonate minerals accompanied by mass transfer of  $\text{CO}_2$  makes karst an important, though often under recognized, component of the natural global carbon cycle.

Karst aquifers are globally distributed and provide unique freshwater resources that are vitally important to human life, aquatic and terrestrial ecosystems, as well as local-to-global-scale hydrologic and biogeochemical systems. Karst aquifers typically possess extremely heterogeneous and highly complex internal structure, presenting many unique hydrogeological characteristics, such as the interconnected networks of subsurface conduits that are arguably a karst aquifer's most distinctive feature. In many karst areas, the surface and groundwater regimes are highly interconnected and function as a singular dynamic hydrologic unit. Subsurface groundwater drainage divides do not always coincide with topographic divides or groundwater divides defined by water table contours and directions of groundwater flow commonly changes with changing hydrologic conditions.

Karst aquifers can have three types of porosity.

- Small pores less than 1cm, in which flow is slow and is rarely turbulent (called rock matrix porosity).
- Pores greater than 1cm and less than 0.1m, called macro porosity and often the result of biological activity, in which flow is fast and the onset of turbulence occurs at relatively small Reynolds numbers similar to typical porous media.
- And, the most unique porosity, large conduits, often greater than 1 m, created by dissolution along fractures and bedding planes with fast, often turbulent, flow at large Reynolds numbers similar to pipe or open-channel flow.

For simplicity two terms are generally used for describing flow; matrix (slow flow) and conduit (fast flow). Within a karst aquifer system, the matrix and conduits exchange water. High-frequency monitoring of spring discharge and water quality along with analysis techniques such as hydrograph separation and hysteresis plot analysis, help to: 1) identify the relative proportions of water contributed by matrix and conduit flow under varying hydrologic conditions; and, 2) develop better understanding of the temporal variability of recharge, storage, and through-flow within an individual karst aquifer.

Karst aquifers present many challenges to investigating their character because they do not conform to ideal Darcian flow. As a consequence, traditional methods of

hydrogeologic investigation that rely on data collected from water wells may not provide sufficient data for proper interpretation of basic aquifer hydraulic properties and may lead to erroneous interpretations if not collected and analyzed with a proper conceptual understanding of karst aquifer structure and flow systems. Conventional methods of aquifer characterization based on well hydraulic tests are nevertheless useful, and often vital, for determining important aquifer properties—especially those related to assessing groundwater availability, effects of water withdrawals, and well sustainability. However, tracer tests, often conducted with fluorescent dyes, are required to positively identify groundwater flow directions, determine flow velocities and residence times, and to map groundwater basin and aquifer boundaries. Surface geophysical methods combined with borehole geophysics and structural mapping is useful, and sometimes critical, in delineation of conduit or preferential flow layers within the karst aquifer. More advanced hydraulic testing involving flow-meter logging under both ambient flow and pumping conditions is extremely beneficial along with hydraulic testing involving multiple wells when combined with numerical analysis.

Recent advances in computing technology and development of numerical groundwater modeling codes, have revolutionized the investigation, characterization, and understanding of karst aquifer behavior, and the management and protection of karst water resources. Modeling is now routinely used to synthesize karst aquifer data, analyze, and understand field observations and measurements, and simulate or forecast karst aquifer behavior under different natural conditions and human-induced changes or stresses. Karst aquifer modeling is often essential to understand, predict, and assess effects of climate change, water withdrawals, groundwater contamination, and effectiveness of natural attenuation or engineered contaminant remediation measures. Different mathematical modeling approaches can be applied depending on the model's intended purpose, the data available, and the types of hydrogeologic complexity present, especially the presence of multiple types of porosity and permeability components, including conduits, in the karst aquifer. These include fitting models, lumped parameter models, distributed parameter models including both single and dual continua, hybrid models that link continuum models with discrete models, and discrete fracture or conduit models.

The topics presented in this book introduce karst aquifers and foster better understanding of their unique characteristics, as well as the need for careful consideration of these characteristics when planning and implementing hydrogeological investigations. Although the topic of karst is extremely broad, the focus of this book is intentionally narrow, in order to address groundwater flow in karst aquifers and associated investigation methods.

Karst aquifers are not the mysterious hydrogeological entities that they are sometimes portrayed to be. They are complex aquifers that require careful consideration regarding the selection and use of hydrogeological investigative techniques for data collection and analysis. It is more difficult, time-consuming, and expensive, to collect and

interpret data for proper characterization, utilization, and protection of karst aquifers compared to aquifers of other rock types.

This book highlights the methods that have been most useful in karst aquifer studies conducted over many decades. The audience for this book is upper-level undergraduate science and engineering students, and one goal is to assist them in the selection of a major for a more focused advanced degree. The numerous references provide a head start on a literature review for advanced degree research. We strive to provide information that is 1) useful to students and researchers who are planning investigations of karst, and 2) stimulates interest and excitement in readers to learn more about karst aquifers and karst hydrogeology.

## 8 What is on the Horizon for Karst Aquifer Knowledge?

Karst aquifers are an important source of water supply for human activities in both urban and rural settings. They are globally distributed and, wherever they occur, provide unique freshwater resources that are vitally important to human life, as well as various aquatic and terrestrial ecosystems, and local-to-global-scale hydrologic and biogeochemical systems. The topic of Karst is extremely broad and there are many knowledge gaps that required further investigation.

Recent advances in computing technology and numerical groundwater modeling software, have revolutionized the investigation, characterization, and understanding of karst aquifer behavior, and the management and protection of karst water resources. Use of multidisciplinary and complementary field studies, such as water-tracing tests, analysis of spring discharge and water chemistry, advanced hydraulic testing in wells, geophysical methods, and geochemistry have advanced our knowledge of karst systems.

Yet, even with the use of the latest technology and multidisciplinary field methods, there are still numerous topics requiring further research to improve understanding of and assessing karst aquifers. Readers interested in undertaking graduate studies to enhance their ability to work in karst aquifer research may be interested in some of the following topics for future research:

- human impacts on karst aquifers;
- natural disasters related to groundwater processes in karst;
- groundwater development unique to karst areas, such as aquifer recharge via sinkhole flooding;
- relation between the ecosystems in karst areas with conservation and biodiversity maintenance how the restoration of plant communities provides better biosphere for soil microorganisms;



- controls on nitrate dynamics and associated water age in the different landscape units in karst catchments;
- relationship of epikarst to hydrologic (for example, recharge) and soil processes;
- development of better distributed parameter models which can be used to incorporate and synthesize the known information about the hydrogeologic framework of the karst aquifer and gain an understanding of the system through the calibration process;
- development and application of mathematical models for water resource management and incorporation of new game theory algorithms, economics, and optimization management algorithms;
- improvement of geophysical tools, surface and borehole tailored to karst aquifers; especially tools that help map large porosity and conduit features in the subsurface;
- development of educational material on karst terrane for communities and authorities; and,
- development of karst areas as natural laboratories for use in multi and transdisciplinary teaching.

Studying these topics offers opportunities for those who work in the groundwater arena to improve conditions for humankind and ecological systems by better managing karst systems.

## 9 Exercises

### Exercise 1

What is the composition of carbonate and evaporite rocks?

[Click here for solution to Exercise 1](#) ↓

[Return to where text linked to Exercise 1](#) ↑

### Exercise 2

The table below describes six types of sinkholes (Waltham et al., 2005). All occur in karst aquifers. Review the table and decide which types of sinkholes would:

- allow direct recharge from sinks to the saturated zone of the karst aquifers?
- allow more rapid movement of water to the saturated zone?
- slow movement or prevent movement of water into the saturated zone?

Types of sinkholes in karst aquifers (Waltham et al., 2005).

	<b>Formation process</b>	<b>Host rock type</b>	<b>Formation speed</b>	<b>Typical maximum size</b>	<b>Engineering hazard</b>	<b>Other names in use</b>
Solution sinkhole	Dissolutional lowering of surface	Limestone, dolomite, gypsum, salt	Stable landforms evolving over >20,000 years	Up to 1,000 m across and 100 m deep	Fissure and cave drains must exist beneath floor	Dissolution, cockpit, doline
Collapse sinkhole	Rock roof failure into underlying cave	Limestone, dolomite, gypsum, basalt	Extremely rare, rapid failure events, into old cave	Up to 300 m across and 100 m deep	Unstable breakdown floor; failure of loaded cave roof	Cave collapse, cenote
Caprock sinkhole	Failure of insoluble rock into cave in soluble rock below	Any rock overlying limestone, dolomite, gypsum	Rare failure events, evolve over >10,000 years	Up to 300 m across and 100 m deep	Unstable breakdown floor	Subjacent collapse, interstratal karst
Dropout sinkhole	Soil collapse into soil void formed over bedrock fissure	Cohesive soil overlying limestone, dolomite, gypsum	In minutes, into soil void evolved over months or years	Up to 50 m across and 10 m deep	The main threat of instant failure in soil-covered karst	Subsidence, cover collapse, alluvial
Suffosion sinkhole	Down-washing of soil into fissures in bedrock	Non-cohesive soil over limestone, dolomite, gypsum	Subsiding over months or years	Up to 50 m across and 10 m deep	Slow destructive subsidence over years	Subsidence, cover subsidence, alluvial
Buried Sinkhole	Sinkhole in rock, soil-filled after environmental change	Rockhead depression in limestone, dolomite, gypsum	Stable features of geology, evolved over >10,000 years	Up to 300 m across and 100 m deep	Local subsidence on soft fill surrounded by stable rock	Filled, compaction, paleo

[Click here for solution to Exercise 2](#) ↓

[Return to where text linked to Exercise 2](#) ↑

### Exercise 3

Look up the definition of porosity, permeability, and hydraulic conductivity and describe how hydraulic conductivity is related to permeability and porosity.

[Click here for solution to Exercise 3](#) ↓

[Return to where text linked to Exercise 3](#) ↑

### Exercise 4

Download [Williams and Kuniansky \(2016\)](#) ↑ and review Figure 13 of that report. The acoustic televiewer image from 2,100 to 2,200 feet (640 to 670 m) shows solution openings formed along bedding planes and in discrete zones near the base of the Oldsmar Formation of the Lower Floridan aquifer in well GA-GLY9, Brunswick, Georgia, USA. Next, download [Wacker and others \(2014\) plate 1](#) ↑ that shows visual borehole logs of the porosity in the upper Biscayne Aquifer.

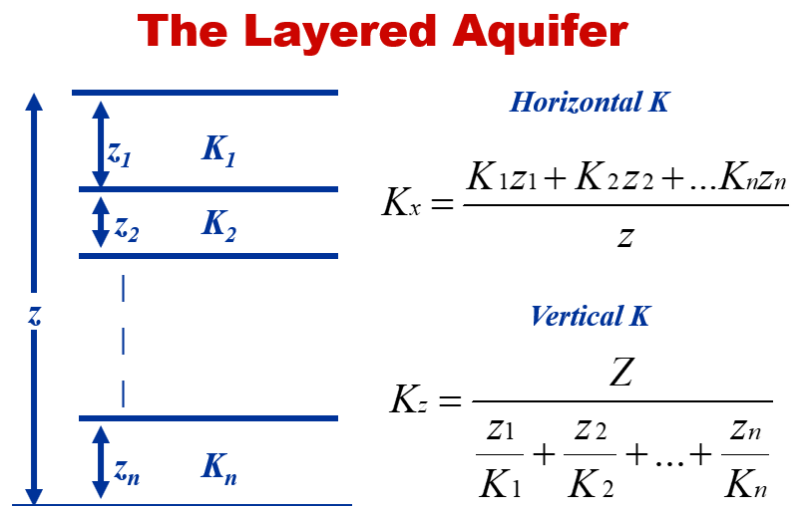
- a) What do you notice about the different dissolved openings?
- b) How do the older Floridan aquifer openings compare to the younger Biscayne Aquifer?
- c) How does this compare to the even older Paleozoic rock (541 to 252 million years ago) images of the telogenetic karst aquifer shown in Figure 17 of this book?

[Click here for solution to Exercise 4](#) ↓

[Return to where text linked to Exercise 4](#) ↑

## Exercise 5

The relative hydraulic conductivity of layers in an aquifer has a significant influence on the magnitude of flow in horizontal and vertical direction. The figure below shows the equation for calculation of the effective horizontal and vertical hydraulic conductivity of a flat lying sedimentary formation with different values of  $K$  in layers  $K_1$  and  $K_2$ , with thicknesses  $z_1$  and  $z_2$  (Bouwer, 1978).



Using the relationship illustrated above and described in detail in the equivalent hydraulic conductivity section of the Groundwater Project book "[Hydrogeologic Properties of Earth Materials and Principles of Groundwater Flow](#)", calculate the equivalent horizontal and vertical hydraulic conductivity of a two-layer aquifer system with each layer 10 m thick and with homogeneous, isotropic hydraulic conductivity of the shallow layer equal to 1000 m/d and the deep layer equal to 1 m/d.

[Click here for solution to Exercise 5](#) ↓

[Return to where text linked to Exercise 5](#) ↑

## Exercise 6

How does the scale of hydraulic conductivity heterogeneity influence advective transport in aquifers? The information below provides a tool for you to evaluate this.

The Particle Flow software (Hsieh, 2001) can be used to explore the influence of hydraulic conductivity heterogeneity on the movement of particles in groundwater. You can download and install a [Windows version of the software](#) or use the [online version](#).

Once you have the Windows software installed, launch the software by double clicking on the file pflow.exe and follow the straight-forward, step-by-step directions in the document that is provided with the software (that is, ofr01-286.pdf). Or, if you use the online version, read the website materials about the software and click on the ParticleFlow button to launch it.

Using the software, as described below for Model 1 and Model 2 below, set up two models of the same total area, but with different cell sizes. In both models choose to randomize the properties, solve for heads (notice the similarities), under flow choose particle movement with particles spaced 10 m apart and input to view 100 days of travel time in 1 second of real time, then draw a shape to indicate where particles will be added and click on the flow field to start the particles moving. These steps are described in detail where you access the software.

- Model 1: use a cell size of 10 m with 100 columns and 25 rows, and a gradient of 0.002. Place particles on upgradient side and release.
- Model 2: use a cell size of 50 m with 20 columns and 5 rows, and a gradient of 0.002. Place particles on upgradient side and release.

Rerun the simulation as many times as you want with different particle releases. Remember the differences are due to the size of zones with differing hydraulic conductivity. The zones are much larger in Model 2.

You may also wish to create your own patterns of heterogeneity. The instructions for the software will show you how to do that.

[Click here for solution to Exercise 6](#)

[Return to where text linked to Exercise 6](#)



## Exercise 7

What is the difference between hydraulic conductivity ( $K$ ) and intrinsic permeability ( $k$ )?

[Click here for solution to Exercise 7](#) ↴

[Return to where text linked to Exercise 7](#) ↴

## Exercise 8

Read “[Threat Down Below: Polluted Caves Endanger Water Supplies, Wildlife](#)” ↗.  
What were some of the common contaminants mentioned in numerous caves?

[Click here for solution to Exercise 8](#) ↴

[Return to where text linked to Exercise 8](#) ↴

## Exercise 9

### Part 1

What other aquifer types may have extremely large pores and high hydraulic conductivity, where water can flow at both laminar and turbulent flow conditions?

### Part 2

The average velocity,  $V$ , for flow to a pumped well at different radial distances would be computed from the following equation.

$$V = \frac{Q}{2\pi r b}$$

where:

$Q$  = pumping rate ( $L^3T^{-1}$ )

$r$  = radial distance (L)

$b$  = thickness of the aquifer (L)

The table below shows data for some pumping wells in different aquifers. Calculate the average velocity for radial distances of 0.25, 0.5, 1, 5, and 10 m. Just looking at the equation, can you guess what happens to the average velocity as the radial distance increases or the thickness increases?

Properties needed for calculation of average velocity for flow to a well and for calculation of the Reynolds Number.

Aquifer type and hydraulic conductivity	Pumping Rate ( $m^3/d$ )	Thickness (m)
Alluvial aquifer, $K=10$ m/d, and average pore diameter 0.005 m	300	10
same	300	50
same	300	100
Point Bar gravel aquifer, $K=100$ m/d and average pore diameter 0.02 m	1000	10
same	1000	50
same	1000	100
Sandstone $K=1$ m/d and average pore diameter 0.001 m	100	10
same	100	50
same	100	100

[Click here for solution to Exercise 9](#) ↓

[Return to where text linked to Exercise 9](#) ↑

## Exercise 10

### Part 1

Why did Reynolds try experiments with different temperatures of water with each pipe?

### Part 2

With the data from [Exercise 9](#)↑, calculate the Reynolds number at each radial distance. Note that the kinematic viscosity of water at 20 °C is approximately 1 centiStoke =  $1 \times 10^{-6}$  m<sup>2</sup>/s. You will need to multiply by 24×60×60 to convert m<sup>2</sup>/s to m<sup>2</sup>/day, 0.0864 m<sup>2</sup>/day. It is always important to pay attention to units and convert to consistent units when making calculations. Given that the pumping rate was given in m<sup>3</sup>/day, kinematic viscosity needs to be converted to length units of meters and time units of days. Which aquifers might have non-Darcian flow based on your calculations of average velocity?

[Click here for solution to Exercise 10](#)↓

[Return to where text linked to Exercise 10](#)↑

## Exercise 11

The Hagen-Poiseuille equation, also known as the Hagen-Poiseuille law, Poiseuille Law or Poiseuille equation, is a physical law that describes the pressure drop in an incompressible and Newtonian fluid in laminar flow flowing through a long cylindrical pipe of constant cross section. The assumptions of the equation are that the fluid is incompressible and Newtonian; the flow is laminar through a pipe of constant circular cross-section that is substantially longer than its diameter; and there is no acceleration of fluid in the pipe. For velocities and pipe diameters above a threshold, actual fluid flow is not laminar but turbulent, leading to larger pressure drops than calculated by the Hagen-Poiseuille equation as shown here.

$$\Delta p = \frac{8\mu L Q}{\pi R^4} = \frac{8\pi\mu L Q}{A^2}$$

where:

$\Delta p$  = pressure difference between the two ends ( $\text{ML}^{-1}\text{T}^{-2}$ )

$L$  = length of pipe (L)

$\mu$  = [dynamic viscosity](#) ↗ ( $\text{ML}^{-1}\text{T}^{-1}$ )

$Q$  = [volumetric flow rate](#) ↗ ( $\text{L}^3\text{T}^{-1}$ )

$R$  = pipe [radius](#) ↗ (L)

$A$  = [cross section](#) ↗ of pipe ( $\text{L}^2$ )

The equation does not hold close to the pipe entrance. The equation fails in the limit of low viscosity, wide and/or short pipe. Low viscosity or a wide pipe may result in turbulent flow, making it necessary to use more complex models, such as the [Darcy-Weisbach equation](#) ↗. The ratio of length to radius of a pipe should be greater than one forty-eighth (i.e.,  $> \frac{1}{48}$ ) of the [Reynolds number](#) ↗ for the Hagen-Poiseuille law to be valid.

- What are the assumptions associated with the Hagen-Poiseuille equation and the Poiseuille law?
- How does the viscosity of the fluid change the relationship between pressure gradient and flow?
- How is the equation for laminar flow in a full pipe similar to Darcy's law?

[Click here for solution to Exercise 11](#) ↴

[Return to where text linked to Exercise 11](#) ↴

## Exercise 12

Substitute  $64/Re$  and the equation for the Reynolds number into Equation 4 and prove to yourself that this results in the Hagen-Poiseuille equation for a circular pipe.

[Click here for solution to Exercise 12](#) ↴

[Return to where text linked to Exercise 12](#) ↴

## Exercise 13

Fully saturated dissolution features are not usually perfectly circular, smooth, or straight; how do these effect the onset of turbulent flow?

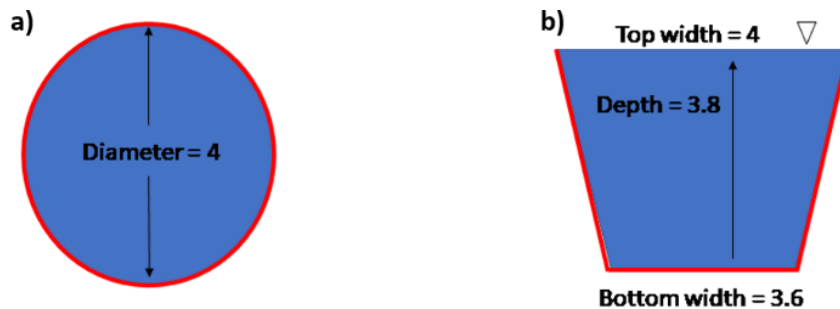
[Click here for solution to Exercise 13](#) ↴

[Return to where text linked to Exercise 13](#) ↴



## Exercise 14

- a) Calculate the hydraulic radius of the circular pipe and trapezoidal concrete channel shown below. Assume the concrete channel is symmetric and the length units are meters.



▽ Symbol for water surface, — Wetted perimeter, and ■ Saturated cross section

- b) If the flow is  $0.005 \text{ m}^3/\text{s}$ , what is the mean velocity for each conveyance?  
 c) What is the Reynolds number for each conveyance? Assume water temperature is  $20^\circ \text{C}$ .

*Hint:* The kinematic viscosity [ $\text{m}^2/\text{s}$ ] is the ratio between the dynamic viscosity of a fluid [(1 Pascal-second) = 1 kilogram/(meter-second)] and the density of a fluid [ $\text{kg}/\text{m}^3$ ]. The SI unit of the kinematic viscosity is  $\text{m}^2/\text{s}$ . Other units are:

- 1 St (Stoke) =  $1 \text{ cm}^2/\text{s} = 10^{-4} \text{ m}^2/\text{s}$ ;
- 1 cSt (centiStoke) =  $1 \text{ mm}^2/\text{s} = 10^{-6} \text{ m}^2/\text{s}$ ; and
- Water at  $20^\circ \text{C}$  has a kinematic viscosity of about 1 cSt.

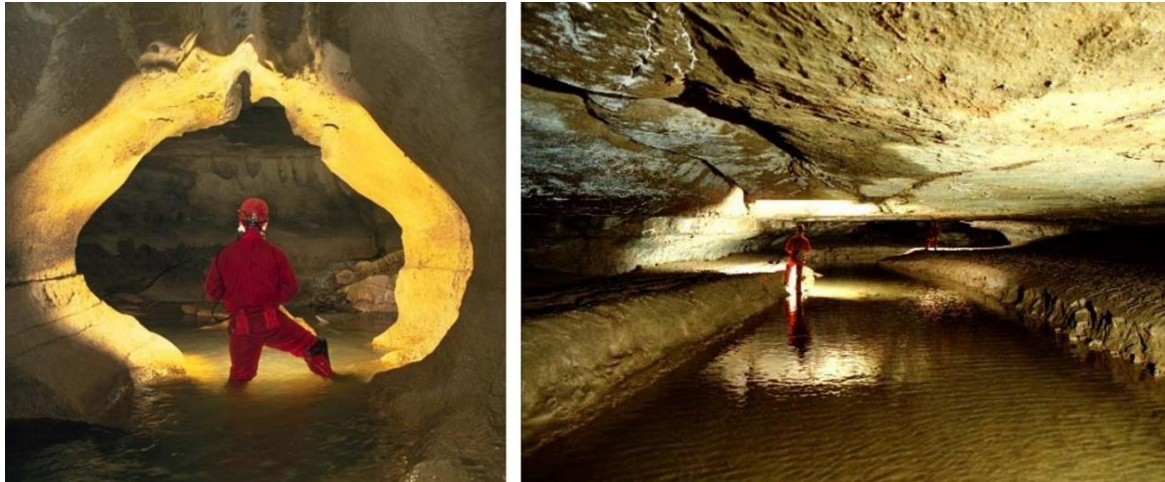
- d) Is flow laminar or turbulent in each conveyance?  
 e) If the flow is  $0.005 \text{ m}^3/\text{s}$ , what is the mean velocity for each conveyance?

[Click here for solution to Exercise 14](#) ↓

[Return to where text linked to Exercise 14](#) ↑

## Exercise 15

Considering the following photographs of Figure 38, repeated here for convenience:



- Conceptually, how would the wetted perimeter and the effective hydraulic radius of each of the two conduit passages be calculated at the flow condition shown?
- Conceptually, how would the wetted perimeter and the effective hydraulic radius of each of the two conduit passages would be calculated if the passages were completely water filled?
- How might wetted perimeter, flow velocities, and discharge progressively change for the passage on the left as it fills with water during a storm?
- How might wetted perimeter, flow velocities, and discharge progressively change for the passage on the right as it fills with water during a storm? *Hint:* Keep the presence of the rectangular open channel, the broad rounded sediment banks, and the flattened elliptical shape of the upper half of the conduit in mind.

[Click here for solution to Exercise 15](#) ↓

[Return to where text linked to Exercise 15](#) ↑

## Exercise 16

Why define three types of karst porosity, specifically with respect to the occurrence of laminar and turbulent flow?

[Click here for solution to Exercise 16](#) ↓

[Return to where text linked to Exercise 16](#) ↑

## Exercise 17

What is a hydrograph or chemograph?

[Click here for solution to Exercise 17](#) ↓

[Return to where text linked to Exercise 17](#) ↑

## Exercise 18

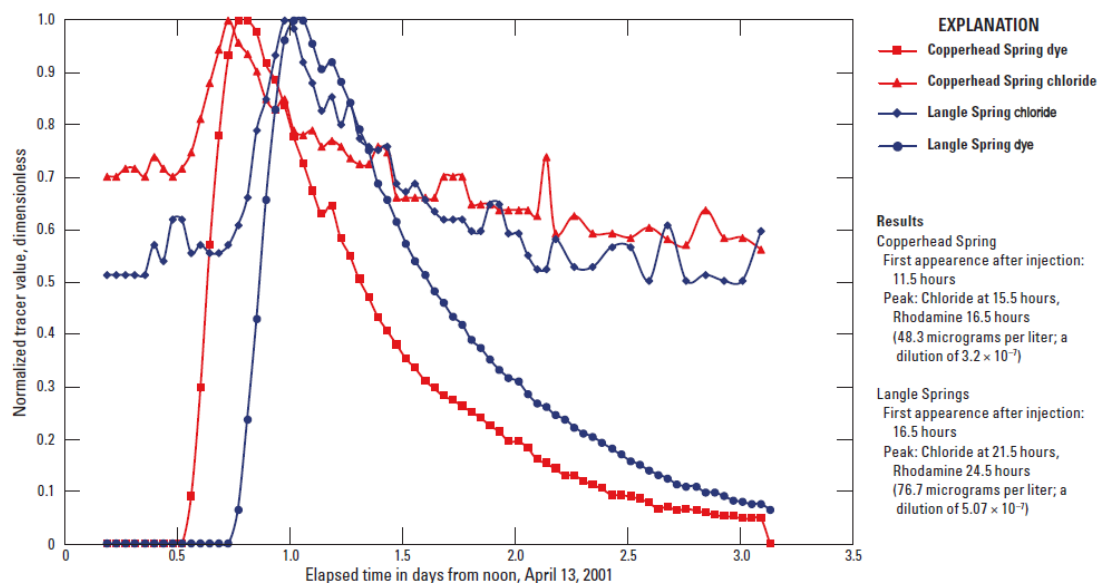
Table 4 and Table 5 of this book are helpful in understanding methods used in borehole geophysics. Look up words of the table that you do not understand in an applied geophysics textbook or other resource such as the [Environmental Geophysics page of the USEPA](#) ↑. Although the web page is no longer updated, the information it contains is valuable. The glossary is especially useful for this exercise.

[Click here for solution to Exercise 18](#) ↓

[Return to where text linked to Exercise 18](#) ↑

## Exercise 19

The image below is a repeat of Figure 54 showing normalized break-through curves for a dye and a salt. Which tracer appears to be more conservative?



[Click here for solution to Exercise 19](#) ↓

[Return to where text linked to Exercise 19](#) ↑

## Exercise 20

Search the internet to answer the question: What does a spectrofluorophotometer measure?

[Click here for solution to Exercise 20](#) ↴

[Return to where text linked to Exercise 20](#) ↴

## Exercise 21

Search the internet to answer the question: What is the difference between alkaline earths and alkali metals?

[Click here for solution to Exercise 21](#) ↴

[Return to where text linked to Exercise 21](#) ↴

## Exercise 22

List land use activities that might result in degradation of the water quality if conducted on the outcrop or near sinking streams of a karst aquifer.

[Click here for solution to Exercise 22](#) ↴

[Return to where text linked to Exercise 22](#) ↴

## 10 References

- Acosta, R.E., R.H. Muller, C.W. Tobias, 1985, Transport processes in narrow (capillary) channels. *American Institute of Chemical Engineers Journal*, volume 31, issue 3, pages 473-482, <https://doi.org/10.1002/aic.690310315>↗.
- Adams, R., and G. Parkin, 2002, Development of a surface-groundwater-pipe network model for the sustainable management of karstic groundwater. *Environmental Geology*, volume 42, issue 5, pages 513-517, <https://doi.org/10.1007/s00254-001-0513-8>↗.
- Aley, T., 1997, Groundwater tracing in the epikarst *in* Proceedings of the 6th Multidisciplinary Conference on Sinkholes and the Engineering and Environmental Impacts of Karst. A.A. Balkema, Rotterdam. Pp. 207 211.
- Aley, Thomas, 2001, Procedures and criteria for the analysis of fluorescein, eosine, rhodamine WT, sulforhodamine B, and pyranine dyes in water and charcoal samplers. Ozark Underground Laboratory, most recent publications accessed January 2022 is <https://www.ozarkundergroundlab.com//oul-documents.html>↗.
- Aley, T., 2002, Groundwater tracing handbook. Ozark Underground Laboratory, most recent publication accessed January 2022 is <https://www.ozarkundergroundlab.com//oul-documents.html>↗.
- Anderson, Christopher, 2021a, Photograph titled “Rumble River and the M.O.S. Borehole Rumbling Falls Cave, Van Buren County, TN”, Professional Photographer, Darklight Imagery, Kentucky, USA.
- Anderson, Christopher, 2021b, Photograph titled “Epitome Lake, Webster Avenue, Webster Cave Complex, Breckinridge County, KY”, Professional Photographer, Darklight Imagery, Kentucky, USA.
- Anderson, Christopher, 2021c, Photographs titled (left to right) “P Strange Falls Hawkins River, Mammoth Cave, Edmondson County, KY”, “First Falls In Flood Rumbling Falls Cave, Van Buren County, TN”, and “Shaft Freeman's Pit, IN”, Professional Photographer, Darklight Imagery, Kentucky, USA.
- Anderson, Christopher, 2021d, Photographs titled (left to right) “Stream Spring Mill Cave”, and “River Passage Cool Spring Cave, Trigg County, KY”, Professional Photographer, Darklight Imagery, Kentucky, USA.
- Anderson, M.P., 2005, Heat as a ground water tracer. *Groundwater*, volume 43, issue 6, pages 951-968, <https://doi.org/10.1111/j.1745-6584.2005.00052.x>↗.
- Anderson, M.P., W.W. Woessner, and R.J. Hunt, 2015, Applied groundwater modeling—simulation of flow and advective transport. Academic Press, 630 pages.
- Arthur, J.D., J.B. Cowart, J.B. and A.A. Dabous, A.A., 2001, Florida Aquifer storage and recovery geochemical study: Year three progress report. Florida Geological Survey, Open File Report, volume 83, 46 pages, <http://ufdc.ufl.edu/UF00094038/00001>↗.



- Arthur, J.D., A.A. Dabous., and J.B. Cowart., 2002, Mobilization of arsenic and other trace elements during aquifer storage and recovery, southwest Florida *in*. In: United States Geological Survey Artificial Recharge Workshop Proceedings, editors, G.R. Aiken, and E.L. G. R., and E.L. Kuniansky, 2002, United States Geological Survey Artificial Recharge Workshop Proceedings, pages 47-50,  
[https://water.usgs.gov/ogw/pubs/ofr0289/jda\\_mobilization.htm](https://water.usgs.gov/ogw/pubs/ofr0289/jda_mobilization.htm)↗.
- Arthur, J., H. Wood, A. Baker, J. Cichon, and G. Raines, 2007, Development and implementation of a Bayesian-based aquifer vulnerability assessment in Florida. *Natural Resources Research*, volume 16, issue 2, pages 93-107,  
<https://doi.org/10.1007/s11053-007-9038-5>↗.
- Auckenthaler, A., G. Raso, and P. Huguenberger, 2002, Particle transport in a karst aquifer: Natural and artificial tracer experiments with bacteria, bacteriophages, and microspheres. *Water Science and Technology*, volume 46, issue 3, pages 131-138,  
<https://doi.org/10.2166/wst.2002.0072>↗.
- Bakalowicz, M., 2005, Karst groundwater: A challenge for new resources. *Hydrogeology Journal*, volume 13, issue 1, pages 148-160, <https://doi.org/10.1007/s10040-004-0402-9>↗.
- Bandy, A.M., A. Fryar, K. Cook, J. Polk, K. McClanahan, and S. Macko, 2016, Mobility of *Escherichia coli* compared to traditional groundwater tracers within karst terrains. *Karst Waters Institute Special Publication*, volume 19, 13 pages.
- Barret, M.E., and R.J. Charbeneau, 1997, A parsimonious model for simulating flow in a karst aquifer. *Journal of Hydrology*, volume 196, pages 47-65,  
[https://doi.org/10.1016/S0022-1694\(96\)03339-2](https://doi.org/10.1016/S0022-1694(96)03339-2)↗.
- Bauer, S., 2002, Simulation of the genesis of karst aquifers in carbonate rocks. *Institut und Museum für Geologie und Paläontologie der Universität Tübingen*, volume 62.
- Bauer, S., R. Liedl., and M. Sauter, 2000, Modelling of karst development considering conduit-matrix exchange flow. *International Association of Hydrological Sciences Publication*, pages 10-15, <https://iahs.info/uploads/dms/16981.02-10-15-Bauer-et-al..pdf>↗.
- Bauer, S., R. Liedl, and M. Sauter, 2003, Modeling of karst aquifer genesis: Influence of exchange flow. *Water Resources Research*, volume 39, number 10, issue 1, 285 pages,  
<https://doi.org/10.1029/2003WR002218>↗.
- Bayless, E.R., P.J. Cinotto, R.L. Ulery, C.J. Taylor, G.K. McCombs, M.H. Kim, and H.L. Nelson Jr., 2014, Surface-water and karst groundwater interactions and streamflow-response simulations of the karst-influenced upper Lost River watershed, Orange County, Indiana. *United States Geological Survey, Scientific Investigations Report 2014-5028*, 39 pages, <https://doi.org/10.3133/sir20145028>↗.
- Bayless, E.R., C.J. Taylor, and M.S. Hopkins, 1994, Directions of ground-water flow and locations of ground-water divides in the Lost River watershed near Orleans, Indiana.

- United States Geological Survey, Water-Resources Investigations Report 94-4195, <https://doi.org/10.3133/wri944195>.
- Bear, J., 1979, *Hydraulics of groundwater*. McGraw-Hill, Incorporated, New York, USA, 567 pages.
- Behrens, H., 1986, Water tracer chemistry: A factor determining performance and analytics of tracers. *Proceedings of 5<sup>th</sup> International Symposium on underground water tracing*, Institute of Geology and Mineral Exploration, Athens, Greece, pages 121-133.
- Behrens, H., U. Beims, H. Dieter., G. Dietze, T. Eikmann, T. Grummt, H. Hanisch., H. Henseling, W. Käss, H. Kerndorff, C. Leibundgut, U. Müller-Wegener, I. Rönnefahrt, B. Scharenberg, R. Schleyer, W. Schloz, and F. Tilkes, 2001, Toxicological and ecotoxicological assessment of water tracers. *Hydrogeology Journal*, volume 9, issue 3, pages 321-325, <https://doi.org/10.1007/s100400100126>.
- Benischke, R., 2021, Review: Advances in the methodology and application of tracing in karst aquifers. *Hydrogeology Journal*, volume 29, pages 67-88, <https://doi.org/10.1007/s10040-020-02278-9>.
- Bentall, R., 1964, *Methods of determining permeability, transmissibility, and drawdown*. United States Geological Survey, Water-Supply Paper 1536-I, <https://doi.org/10.3133/wsp1536I>.
- Birk, S., 2002, Characterization of karst systems by simulating aquifer genesis and spring responses: Model development and application to gypsum karst. *Tübinger Geowiss. Arb., Reihe C*, Accessed February 2022 [https://www.researchgate.net/publication/289547236 Characterisation of karst systems by simulating aquifer genesis and spring responses Model development and application to gypsum karst](https://www.researchgate.net/publication/289547236_Characterisation_of_karst_systems_by_simulating_aquifer_genesis_and_spring_responses_Model_development_and_application_to_gypsum_karst).
- Böhlke, J.K., and J.M. Denver, 1995, Combined use of groundwater dating, chemical, and isotopic analyses to resolve the history and fate of nitrate contamination in two agricultural watersheds, Atlantic coastal plain, Maryland. *Water Resources Research*, volume 31, pages 2319-2339, <https://doi.org/10.1029/95WR01584>.
- Bouwer, Herman, 1978, *Groundwater Hydrology*. McGraw-Hill, New York, USA, 480 pages.
- Brahana, J.V., and E.F. Hollyday, 1988, Dry stream reaches in carbonate terranes: Surface indicators of ground-water reservoirs. *American Water Resources Association Bulletin*, volume 24, issue 3, pages 577-580 <https://doi.org/10.1111/j.1752-1688.1988.tb00907.x>.
- Bunnell, Dave, 2006, [Photo by Dave Bunnell showing the most common speleothems](#) by [Dave Bunnell](#) is licensed under [CC BY-SA 2.5](#).
- Butler, D.K., 1984, Microgravimetric and gravity gradient techniques for detection of subsurface cavities. *Geophysics*, volume 49, issue 7, pages 1084-1096, <https://doi.org/10.1190/1.1441723>.

- Butler, J.J., 2019, The design, performance, and analysis of slug tests. CRC Press, New York, USA, <https://doi.org/10.1201/9780367815509>.
- Cao, M., J. Lei, Q. He, Z. Zeng, X. Lü, and Y. Jiang, 2021, Rainfall-driven and hydrologically-controlled variations in cave CO<sub>2</sub> sources and dynamics: Evidence from monitoring soil CO<sub>2</sub>, stream flow and cave CO<sub>2</sub>. *Journal of Hydrology*, volume 595, article number 126060, <https://doi.org/10.1016/j.jhydrol.2021.126060>.
- Cao, J., D. Yuan, C. Groves, F. Huang, H. Yang, and L. Qian., 2012, Carbon fluxes and sinks: The consumption of atmospheric and soil CO<sub>2</sub> by carbonate rock dissolution. *Acta Geologica Sinica—English Edition*, volume 86, issue 4, pages 963-972, <https://doi.org/10.1111/j.1755-6724.2012.00720.x>.
- Cao, J., X. Wu, F. Huang, B. Hu, C. Groves, H. Yang, and C.L. Zhang, 2018, Global significance of the carbon cycle in the karst dynamic system: Evidence from geological and ecological processes. *China Geology*, volume 1, pages 17-27, <https://doi.org/10.31035/cg2018004>.
- Chen, Z., A.S. Auler, M. Bakalowicz, D. Drew, F. Griger, J. Hartmann, G. Jiang, N. Moosdorf, A. Richts, Z. Stevanovic, G. Veni, and N. Goldscheider, 2017, The world karst aquifer mapping project: Concept, mapping procedure and map of Europe. *Hydrogeology Journal*, volume 25, issue 3, pages 771-785, <https://doi.org/10.1007/s10040-016-1519-3>.
- Choquette, P.W., and L.C. Pray, 1970, Geologic nomenclature and classification of porosity in sedimentary carbonates. *American Association of Petroleum Geologists Bulletin*, volume 54, issue 2, pages 207-250, <https://doi.org/10.1306/5D25C98B-16C1-11D7-8645000102C1865D>.
- Clark, I.D., and P. Fritz, 1997, *Environmental isotopes in hydrogeology*. CRC Press, Boca Raton, Florida, USA, 328 pages, <https://doi.org/10.1201/9781482242911>.
- Clemens, T., D. Hückinghaus, M. Sauter, R. Liedl, and G. Teutsch, 1996, A combined continuum and discrete network reactive transport model for the simulation of karst development. *International Association of Hydrological Sciences Publication*, volume 237, pages 309-318, <https://iahs.info/uploads/dms/10509.309-318-237-Clemens.pdf>.
- Cook, Peter, 2020, [Introduction to Isotopes and Environmental Tracers as Indicators of Groundwater Flow](#). The Groundwater Project, Guelph, Ontario, Canada.
- Cook, P.G., and A.L. Herczeg, 2000, *Environmental tracers in subsurface hydrology*. Kluwer Academic Publishers, Boston, USA, 529 pages, <https://doi.org/10.1007/978-1-4615-4557-6>.
- Copeland, R., 2003, Florida spring classification system and spring glossary. Florida Geological Survey, Tallahassee, Florida, USA, Special Publication number 52, 17 pages, [https://www.lake.wateratlas.usf.edu/upload/documents/SP\\_52-Fla-Springs-Classification-Glossary-2003.pdf](https://www.lake.wateratlas.usf.edu/upload/documents/SP_52-Fla-Springs-Classification-Glossary-2003.pdf).

- Cowart, J.B., H.K. Williams, and J.D. Arthur, 1998, Mobilization of U isotopes by the introduction of surface waters into a carbonate aquifer. Geological Society of America Abstracts with Programs, volume 30, issue 7, page A-86.
- Cressler, A., 2005, Photograph of Upper Cueva Ventana, Ventana Entrance, Municipio de Arecibo, Puerto Rico, Dawn Ryan, Overlooking the Rio Grande de Arecibo Valley. Alan Cressler, Hydrologic Technician, United States Geological Survey, Norcross, Georgia, USA.
- Cressler, A., 2006, Field photographs of Dry Spring cave in Jackson County, Alabama, USA. Alan Cressler, Hydrologic Technician, United States Geological Survey, Norcross, Georgia, USA.
- Cressler, A., 2009, Photograph of Deer Cave, West Entrance Area, Gunung Mulu National Park, Borneo, Sarawak, Malaysia. Alan Cressler, Hydrologic Technician, United States Geological Survey, Norcross, Georgia, USA.
- Cressler, A., 2010, Field photograph of Alapaha River, river sink, Jennings Bluff-Avoca Tracts, Suwannee River Water Management District Lands, Hamilton County, Florida, USA. Allan Cressler, Hydrologic Technician, United States Geological Survey, Norcross, Georgia, USA.
- Cressler, A., 2011, Field photograph of Blue Hole Spring vent, Ichetucknee Springs State Park, Suwannee County, Florida taken by Alan Cressler, November 21, 2011, Hydrologic Technician, United States Geological Survey, Norcross, Georgia, USA.
- Cressler, A., 2013, Photograph of Putai Blowholes and Pancake Rocks, stylobedding, Dolomite Point, Paparoa National Park, Buller District, West Coast, New Zealand. Alan Cressler, January 3, 2013, Hydrologic Technician, United States Geological Survey, Norcross, Georgia, USA.
- Cressler, A., 2014, Field photograph of Waterslide Cave, Stephens Gap Callahan Cave Preserve, Southeastern Cave Conservancy, Jackson County, Alabama, Mississippian age Pennington Formation. Alan Cressler, November 22, 2014, Hydrologic Technician, United States Geological Survey, Norcross, Georgia, USA.
- Cressler, A., 2016, Field photograph of Ocala Limestone, Eocene Age, Ozello Archipelago, Gulf of Mexico, Citrus County, Florida taken by Alan Cressler, March 17, 2016, Hydrologic Technician, United States Geological Survey, Norcross, Georgia, USA.
- Cunningham, K.J., 2008, Photographs a and b, Research Hydrologist, United States Geological Survey, Davee, Florida, USA.
- Cunningham, K.J., and A. Aviantara, 2001, Characterization of the karstic Biscayne Aquifer in southeastern Florida using ground-penetrating radar, digital optical borehole images and cores *in* Proceedings of the 2001 United States Geological Survey, Karst Interest Group, Saint Petersburg, Florida, USA, February 13-16, editor, E. Kuniansky,  
[https://web.archive.org/web/20170602222911/https://water.usgs.gov/ogw/karst/kigcoference/kjc\\_characterization.htm](https://web.archive.org/web/20170602222911/https://water.usgs.gov/ogw/karst/kigcoference/kjc_characterization.htm)<sup>↗</sup>.

- Cunningham, K.J., S.D. Locker, A.C. Hine, D. Burky, J.A. Barron, and L.A. Guertin, 2001, Surface-geophysical characterization of ground-water systems of the Caloosahatchee River Basin, Southern Florida. United States Geological Survey, Water-Resources Investigations Report 2001-4084, <https://doi.org/10.3133/wri014084>.
- Cunningham, K.J., R.A. Renken, M.A. Wacker, M.R. Zygnerski, E. Robinson, A.M. Shapiro, and G.L. Wingard, 2006, Application of carbonate cyclostratigraphy and borehole geophysics to delineate porosity and preferential flow in the karst limestone of the Biscayne Aquifer, SE Florida. Geological Society of America Special Papers, volume 404, pages 191-208, [https://doi.org/10.1130/2006.2404\(16\)](https://doi.org/10.1130/2006.2404(16)).
- Cunningham, K.J., M.C. Sukop, H. Huang, P.F. Alvarez, H.A. Curran, R.A. Renken, and J.F. Dixon, 2009, Prominence of ichnologically influenced macroporosity in the karst Biscayne Aquifer: Stratiform “super-K” zones. Geological Society of America Bulletin, volume 121, numbers 1-2, pages 164-180, <https://doi.org/10.1130/B26392.1>.
- Currens, J.C., R.L. Paylor, and J.A. Ray, 2002, Mapped karst groundwater basins in the Lexington 30x60 minute quadrangle. Kentucky Geological Survey Map and Chart 35, Series XII, <https://doi.org/10.13023/kgs.mc35.12>.
- Dauda, M., and G.A. Habib, 2015, Graphical Techniques of Presentation of Hydro-Chemical Data. Journal of Environment and Earth Science, volume 5, issue 4, pages 65-75, <https://core.ac.uk/download/pdf/234664092.pdf>.
- Davis, J.H., 1996, Hydrogeologic investigation and simulation of ground-water flow in the Upper Floridan aquifer of north-central Florida and delineation of contributing areas for selected City of Tallahassee, Florida, water-supply wells. United States Geological Survey, Water-Resources Investigations Report 95-4296, <https://doi.org/10.3133/wri954296>.
- Davis, J.H., and B.G. Katz, 2007, Hydrogeologic investigation, water chemistry analysis, and model delineation of contributing areas for city of Tallahassee public-supply wells, Tallahassee, Florida. United States Geological Survey, Scientific Investigations Report 2007-5070, <https://pubs.usgs.gov/sir/2007/5070/>.
- Davis, J.H., B.G. Katz, and D.W. Griffin, 2010, Nitrate-N Movement in groundwater from the land application of treated municipal wastewater and other sources in the Wakulla Springs Springshed, Leon and Wakulla Counties, Florida, 1966-2018. United States Geological Survey, Scientific Investigations Report 2010-5099, <https://pubs.usgs.gov/sir/2010/5099/>.
- Day-Lewis, F.D., J.M. Harris, and S.M. Gorelick, 2002, Time-lapse inversion of crosswell radar data. Geophysics, volume 67, pages 1740-1752, <https://doi.org/10.1190/1.1527075>.
- De Rooij, R., and W. Graham, 2017, Generation of complex karstic conduit networks with a hydrochemical model. Water Resources Research, volume 53, number 8, pages 6993-7011, <https://doi.org/10.1002/2017WR020768>.



- Deutsch, W.J., 1997, Groundwater Geochemistry Fundamentals and Applications to Contamination. CRC Press, Lewis Publishers, Boca Raton, Florida, USA, 221 pages, <https://doi.org/10.1201/9781003069942> ↗.
- Doerfliger, N., P.Y. Jeannin, and F. Zwahlen, 1999, Water vulnerability assessment in karst environments: A new method of defining protection areas using a multi-attribute approach and GIS tools (EPIK method). *Environmental Geology*, volume 39, number 2, pages 165-176, <https://doi.org/10.1007/s002540050446> ↗.
- Domenico, P.A., and F.W. Schwartz, 1990, Physical and chemical hydrogeology. John Wiley and Sons, New York, USA, 824 pages.
- Dooge, J.C.I., 1973, Linear theory of hydrologic systems. United States Department of Agriculture, Agricultural Research Service, Technical Bulletin number 1468, 327 pages, [https://higherlogicdownload.s3.amazonaws.com/AGU/31ea296c-2c70-4dad-92ef-c4681bc6a288/UploadedImages/Dooge\\_LinearTheoryHydrology.pdf](https://higherlogicdownload.s3.amazonaws.com/AGU/31ea296c-2c70-4dad-92ef-c4681bc6a288/UploadedImages/Dooge_LinearTheoryHydrology.pdf) ↗.
- Dreiss, S.J., 1982, Linear kernels for karst aquifers. *Water Resources Research*, volume 18, number 4, pages 865-876, <https://doi.org/10.1029/WR018i004p00865> ↗.
- Drever, J.I., 1988, *The Geochemistry of Natural Waters*, 2<sup>nd</sup> edition. Prentice Hall, Englewood Cliffs, New Jersey, USA, 437 pages.
- Driscoll, F.G., 1986, *Groundwater and wells*, 2<sup>nd</sup> edition. Johnson Division, Saint Paul, Minnesota, USA, 1089 pages.
- Ewers, R.O., 2006, Karst aquifers and the role of assumptions and authority in science. *Geological Society of America Special Papers*, volume 404, pages 235-242, [https://doi.org/10.1130/2006.2404\(19\)](https://doi.org/10.1130/2006.2404(19)) ↗.
- Feist, S.K., J.C. Maclachlan, E.G. Reinhardt, and H.S. Skelding, 2020, Anthropogenic events captured within sediment in Hidden River Cave, Kentucky. *Quaternary Science Advances*, volume 1, article number 100001, <https://doi.org/10.1016/j.qsa.2020.100001> ↗.
- Ferris, J.G., D.B. Knowles, R.H. Brown, and R.W. Stallman, 1962, *Theory of aquifer tests*. United States Geological Survey, Water-Supply Paper 1536-E, 174 pages.
- Field, M.S., 1993, Karst hydrology and chemical contamination. *Journal of Environmental Systems*, volume 22, number 1, pages 1-26, [http://triggered.stanford.clockss.org/ServeContent?url=http%3A%2F%2Fbaywood.stanford.clockss.org%2FBWES%2FBAWOOD\\_BWES\\_22\\_1%2FX7MVC93E66GKBFH7.pdf](http://triggered.stanford.clockss.org/ServeContent?url=http%3A%2F%2Fbaywood.stanford.clockss.org%2FBWES%2FBAWOOD_BWES_22_1%2FX7MVC93E66GKBFH7.pdf) ↗.
- Field, M.S., 2002, The QTRACER2 program for tracer-breakthrough curve analysis for tracer tests in karstic aquifers and other hydrologic systems. United States Environmental Protection Agency, Office of Research and Development, National Center for Environmental Assessment, Washington Office, Washington, DC, USA, EPA/600/R-02/001, <https://cfpub.epa.gov/ncea/risk/recorddisplay.cfm?deid=54930> ↗.

- Field, M.S., 2003, A review of some tracer-test design equations for tracer-mass estimation and sample-collection frequency. *Environmental Geology*, volume 43, number 8, pages 867-881, <https://doi.org/10.1007/s00254-002-0708-7>.
- Field, M.S., 2004, Forecasting versus predicting solute transport in solution conduits for estimating drinking-water risks. *Acta Carsologica*, volume 33, number 2, 116 pages, <https://doi.org/10.3986/ac.v33i2.295>.
- Field, M.S., and S.G. Nash, 1997, Risk assessment methodology for karst aquifers (1): Estimating karst conduit-flow parameters. *Environmental Monitoring and Assessment*, volume 47, pages 1-21, <https://doi.org/10.1023/A:1005753919403>.
- Fitterman, D.V., and M. Deszcz-Pan, 1998, Helicopter EM mapping of saltwater intrusion in Everglades National Park, Florida. *Exploration Geophysics*, volume 29, pages 240-243, <https://doi.org/10.1071/EG998240>.
- Florea, L.L., and H.L. Vacher, 2006, Springflow hydrographs: Eogenetic vs. telogenetic kars. *Groundwater*, volume 44, number 3, pages 352-361, <https://doi.org/10.1111/j.1745-6584.2005.00158.x>.
- Folk, R., 1981, *Petrology of sedimentary rocks*. Hemphill Publishing Company, 2<sup>nd</sup> edition, Austin, Texas, USA, 182 pages, <http://hdl.handle.net/2152/22930>.
- Fong, D.W., D.C. Culver, G. Veni, and S.A. Engel, 2013, Carbon and Boundaries in Karst. Abstracts of the conference held January 7-13, 2013, Carlsbad, New Mexico, USA. Karst Waters Institute Special Publication 17, Karst Waters Institute, Leesburg, Virginia, 54 pages, [https://karstwaters.org/wp-content/uploads/2015/04/SP17\\_CarbonBoundaries.pdf](https://karstwaters.org/wp-content/uploads/2015/04/SP17_CarbonBoundaries.pdf).
- Ford, D., and P. Williams, 2007, *Karst Hydrogeology and Geomorphology*. Wiley, 576 pages, <https://doi.org/10.1002/9781118684986>.
- Ford, T.D., and C.H.D. Cullingford (editors), 1976, *The Science of Speleology*. Academic Press, London, New York, 594 pages.
- Freeze, A.R., and J.A. Cherry, 1979, *Groundwater*. The Groundwater Project, Guelph, Ontario, Canada, <http://gw-project.org/books/groundwater/>.
- Fu, S., Q. Fang, A. Li, Z. Li, J. Han, X. Dang, and W. Han, 2020, Accurate characterization of full pore size distribution of tight sandstones by low-temperature nitrogen gas adsorption and high-pressure mercury intrusion combination method. *Energy Science & Engineering*, volume 9, pages 80-100, <https://doi.org/10.1002/ese3.817>.
- Gallegos, J.J., B.X. Hu, and H. Davis, 2013, Simulating flow in karst aquifers at laboratory and sub-regional scales using MODFLOW-CFP. *Hydrogeology Journal*, volume 21, pages 1749-1760, <https://doi.org/10.1007/s10040-013-1046-4>.
- Garcia, C.A., T.R. Jackson, K.J. Halford, D.S. Sweetkind, N.A. Damar, J.M. Fenelon, and S.R. Reiner, 2017, Hydraulic characterization of volcanic rocks in Pahute Mesa using an Integrated Analysis of 16 multiple-well aquifer tests, Nevada National Security Site, 2009-14. United States Geological Survey, Scientific Investigations Report 2016-5151, <https://doi.org/10.3133/sir20165151>.

- Gary, M.O., D.F. Rucker, B.D. Smith, D.V. Smith, and K. Befus, 2013, Geophysical investigations of the Edwards-Trinity Aquifer system at multiple scales: Interpreting airborne and direct-current resistivity in karst. National Cave and Karst Research Institute Symposium 2, Proceedings of the 13<sup>th</sup> Sinkhole Conference, May 6-10, 2013, Carlsbad, New Mexico, USA, pages 195-206, [https://digitalcommons.usf.edu/cgi/viewcontent.cgi?article=1127&context=sinkhole\\_2013](https://digitalcommons.usf.edu/cgi/viewcontent.cgi?article=1127&context=sinkhole_2013).
- Glover, P.W.J., and E. Walker, 2009, Grain-size to effective pore-size transformation derived from electrokinetic theory. *Geophysics*, volume 74, number 1, pages E17-E29, [doi.org/10.1190/1.3033217](https://doi.org/10.1190/1.3033217).
- Goldscheider, N. and D. Drew, 2007, *Methods in Karst Hydrogeology*. International Association of Hydrogeologists: International Contributions to Hydrology 26, 1<sup>st</sup> edition, CRC Press, <https://doi.org/10.1201/9781482266023>.
- Goldscheider, N., J. Meiman, M. Pronk, and C. Smart, 2008, Tracer tests in karst hydrogeology and speleology. *International Journal of Speleology*, volume 37, number 1, pages 27-40, <https://doi.org/10.5038/1827-806X.37.1.3>.
- Göppert N., and N. Goldscheider, 2008, Solute and colloid transport in karst conduits under low and high flow conditions. *Groundwater*, volume 46, number 1, pages 61-68, <https://doi.org/10.1111/j.1745-6584.2007.00373.x>.
- Gouzie, D.R., K.L. Mickus, and M.V. Mayle, 2014, Challenges to a karst dye-tracing investigation in an urban brownfields area, Springfield, Missouri *in* United States Geological Survey Karst Interest Group Proceedings, Carlsbad, New Mexico, USA, April 29-May 2, 2014, editors, E.L. Kuniansky and Spangler. United States Geological Survey, Scientific Investigations Report 2014-5035, pages 45-54, <https://pubs.usgs.gov/sir/2014/5035/sir2014-5035.pdf>.
- Green, R.T., S.L. Painter, A. Sun, and S.R.H. Worthington, 2006, Groundwater contamination in karst terranes. *Water, Air, and Soil Pollution: Focus*, volume 6, pages 157-170, <https://doi.org/10.1007/s11267-005-9004-3>.
- Groves, C., 2007, Hydrologic methods *in* *Methods in Karst Hydrogeology*, International Association of Hydrogeologists: Contributions to Hydrology, editors, N. Goldscheider and Drew, CRC Press, pages 45-64, <https://doi.org/10.1201/9781482266023>.
- Grubbs, J.W., and C.A. Crandall, 2007, Exchanges of water between the Upper Floridan aquifer and the Lower Suwannee and Lower Santa Fe Rivers, Florida. United States Geological Survey, Professional Paper 1656-C, <https://pubs.usgs.gov/pp/pp1656c/>.
- Gunn, J., 1986, A conceptual model for conduit flow dominated karst aquifers *in* *Karst water resources*, Proceedings of the International Symposium, Ankara, Turkey, July 1985, editors, G. Gunay and Johnson. International Association of Hydrological Sciences Publication, volume 161, pages 587-596, <http://pascal-francis.inist.fr/vibad/index.php?action=getRecordDetail&idt=8335030>.

- Haeni, F.P., L. Halleux, C.D. Johnson, and J.W. Lane Jr., 2002, Detection and mapping of fractures and cavities using borehole radar. Fractured Rock Association, pages 13-15, [https://water.usgs.gov/ogw/bgas/publications/FracRock02\\_haeni/FracRock02\\_haeni.pdf](https://water.usgs.gov/ogw/bgas/publications/FracRock02_haeni/FracRock02_haeni.pdf).
- Hak, J., I. Hunyadi, I. Csigea, G. Géczy, L. Lénárt, and A. Várhegyi, 1997, Radon transport phenomena studied in karst caves-international experiences on radon levels and exposures. Radiation Measurements, volume 28, issues 1-6, pages 675-684, [https://doi.org/10.1016/S1350-4487\(97\)00163-7](https://doi.org/10.1016/S1350-4487(97)00163-7).
- Halford, K.J., and E.L. Kuniansky, 2002, Spreadsheets for the analysis of pumping-aquifer test and slug test data. United States Geological Survey, Open-File Report 02-197, <http://pubs.usgs.gov/of/2002/ofr02197/>.
- Halford, K.J., and D. Yobbi, 2005, Numerical simulation of aquifer tests, west-central Florida. United States Geological Survey, Scientific Investigations Report 2005-5201, <https://doi.org/10.3133/sir20055201>.
- Halford, K.J., and D. Yobbi, 2006, Estimating hydraulic properties using a moving-model approach and multiple aquifer tests. Groundwater, volume 44, issue 2, pages 284-291, <https://doi.org/10.1111/j.1745-6584.2005.00109.x>.
- Halihan, T., R.E. Mace, and J.M. Sharp Jr., 1999, Interpreting flow using permeability at multiple scales in Karst Modeling, Special Publication 5, Karst Waters Institute, [https://www.researchgate.net/publication/275832646\\_INTERPRETING\\_FLOW\\_United\\_StatesING\\_PERMEABILITY\\_AT\\_MULTIPLE\\_SCALES/link/5547e85d0cf26a7bf4da9a86/download](https://www.researchgate.net/publication/275832646_INTERPRETING_FLOW_United_StatesING_PERMEABILITY_AT_MULTIPLE_SCALES/link/5547e85d0cf26a7bf4da9a86/download).
- Halihan, T., J.M. Sharp Jr., and R.E. Mace, 2000, Flow in the San Antonio segment of the Edwards Aquifer: Matrix, fractures, or conduits? in Groundwater flow and contaminant transport in carbonate aquifers, editors, I.D. Sasowsky and Wicks, pages 129-146, A.A. Balkema, Rotterdam, Netherlands, [https://www.researchgate.net/publication/275832559\\_Flow\\_in\\_the\\_San\\_Antonio\\_segment\\_of\\_the\\_Edwards\\_aquifer\\_matrix\\_fractures\\_or\\_conduits](https://www.researchgate.net/publication/275832559_Flow_in_the_San_Antonio_segment_of_the_Edwards_aquifer_matrix_fractures_or_conduits).
- Hall, P., and J. Chen, 1996, Water well and aquifer test analysis. Water Resources Publication, <https://www.wrpllc.com/books/wwat.html>.
- Harbaugh, A.W., 2005, MODFLOW-2005, the United States Geological Survey modular ground-water model. United States Geological Survey Techniques and Methods 6-A16, [https://wwwbrr.cr.usgs.gov/hill\\_tiedeman\\_book/documentation/MODFLOW-MODPATH-ModelViewer/MF2005-tma6a16.pdf](https://wwwbrr.cr.usgs.gov/hill_tiedeman_book/documentation/MODFLOW-MODPATH-ModelViewer/MF2005-tma6a16.pdf).
- Hartmann, A., N. Goldscheider, T. Wagener, J. Lange, and M. Weiler, 2014, Karst water resources in a changing world: Review of hydrological modeling approaches. American Geophysical Union Reviews of Geophysics, volume 52, issue 3, pages 218-242, <https://doi.org/10.1002/2013RG000443>.

- Harvey, R.W., 1997, Microorganisms as tracers in groundwater injection and recovery experiments: A review. Federation of European Microbiological Societies Microbiology Reviews, volume 20, issues 3-4, pages 461-472, <https://doi.org/10.1111/j.1574-6976.1997.tb00330.x>.
- Harvey, R.W., D.W. Metge, A.M. Shapiro, R.A. Renken, C.L. Osborn, J.N., Ryan, K.J. Cunningham, and L. Landkamer, 2008, Pathogen and chemical transport in the karst limestone of the Biscayne Aquifer: 3. Use of microspheres to estimate the transport potential of *Cryptosporidium parvum* oocysts. Water Resources Research, volume 44, issue 8, 12 pages, <https://doi.org/10.1029/2007WR006060>.
- Haugh, C.J., 2006, Hydrogeology and simulation of ground-water flow at Arnold Air Force Base, Coffee and Franklin Counties, Tennessee, 2002. United States Geological Survey, Scientific Investigations Report 2006-5157, <https://pubs.usgs.gov/sir/2006/5157/>.
- Hem, J.D., 1985, Study and interpretation of the chemical characteristics of natural water, 3<sup>rd</sup> edition. United States Geological Survey, Water Supply Paper 2254, <https://pubs.usgs.gov/wsp/wsp2254/>.
- Henderson, R.D., F.D. Day-Lewis, E. Abarca, C.F. Harvey, H.N. Karam, L. Liu, and J.W. Lane, 2010, Marine electrical resistivity imaging of submarine groundwater discharge: Sensitivity analysis and application in Waquoit Bay, Massachusetts, USA. Hydrogeology Journal, volume 18, pages 173-185, <https://doi.org/10.1007/s10040-009-0498-z>.
- Hess, A.E., 1986, Identifying hydraulically conductive fractures with a slow-velocity borehole flowmeter. Canadian Geotechnical Journal, volume 23, issue 1, pages 69-78, <https://doi.org/10.1139/t86-008>.
- Hill, M.E., M.T. Stewart, and A. Martin, 2010, Evaluation of the MODFLOW-2005 Conduit Flow Process. Ground Water, volume 48, pages 549-559, <https://doi.org/10.1111/j.1745-6584.2009.00673.x>.
- Hillier, F.S., and G.J. Lieberman, 1967, Introduction to operations research. Holden-Day Series in Industrial Engineering and Management Science, San Francisco, 639 pages.
- Hortness, J.E., and D.G. Driscoll, 1998, Streamflow losses in the Black Hills of western South Dakota. United States Geological Survey, Water Resources Investigations Report 98-4116, <https://pubs.usgs.gov/wri/wri984116/>.
- Hsieh, P.A., 2001, Topodrive and particleflow—Two computer models for simulation and visualization of ground-water flow and transport of fluid particles in two dimensions. United States Geological Survey, Open-File Report 2001-286, <https://doi.org/10.3133/ofr01286>.
- Hu, C., Y. Hao, T.C.J. Yeh, B. Pang, and Z. Wu, 2007, Simulation of spring flows from a karst aquifer with an artificial neural network. Hydrological Processes, volume 22, issue 5, pages 596-604, <https://doi.org/10.1002/hyp.6625>.



- Hunt, B.B., B.A. Smith, S. Campbell, J. Beery, N. Hauwert, and D. Johns, 2005, Dye tracing recharge features under high-flow conditions, Onion Creek, Barton Springs Segment of the Edwards Aquifer, Hays County, Texas. *Austin Geological Society Bulletin*, volume 1, pages 70-86, [https://digital.lib.usf.edu/content/SF/S0/05/17/70/00001/K26-01321-Dye AGS Report 2005.pdf](https://digital.lib.usf.edu/content/SF/S0/05/17/70/00001/K26-01321-Dye%20AGS%20Report%202005.pdf).
- Istok, J., and K. Dawson, 1991, *Aquifer testing: Design and analysis of pumping and slug tests*. Lewis Publishers, 280 pages, <https://www.taylorfrancis.com/books/mono/10.1201/9781498710756/aquifer-testing-jonathan-istok-karen-dawson>.
- Johnson, C.D., 2008, Field photograph of Michael Wacker setting up borehole tool on a well near Miami, Florida. Carol D. Johnson, Hydrologist, United States Geological Survey, Branch of Geophysics, Storrs, Connecticut, USA.
- Jones, S.A., 1998, Data from United States Air Force Plant 4, Fort Worth, Texas, provided by Sonya Jones, Hydrologist, United States Geological Survey, Austin, Texas.
- Jumikis, A.R., 1962, *Soil Mechanics*: Van Nostrand Reinhold Incorporated, 824 pages, <http://hdl.handle.net/2027/uc1.b4532048>.
- Jurgens, B.C., J.K. Böhlke, and S.M. Eberts, 2012, *TracerLPM (Version 1): An Excel® workbook for interpreting groundwater age distributions from environmental tracer data*. United States Geological Survey, Techniques and Methods Report 4-F3, 60 pages, <https://pubs.usgs.gov/tm/4-f3/>.
- Kasenow, M., 1997, *Introduction to Aquifer Analysis*. Water Resources Publication, Limited Liability Company, 413 pages.
- Kastning, E.H., 1977, Faults as positive and negative influences on groundwater flow and conduit enlargement in Hydrologic problems in karst regions, editors, R.R. Dilamarter and S.C. Csallany, Bowling Green, Kentucky, Western Kentucky University, USA, pages 193-201, <http://pascal-francis.inist.fr/vibad/index.php?action=getRecordDetail&idt=PASCALGEODEBRGM7820204438>.
- Katz, B.G., 2004, Sources of nitrate contamination and age of water in large karstic springs of Florida, *Environmental Geology*, volume 46, pages 689-706, <https://doi.org/10.1007/s00254-004-1061-9>.
- Kendall, C., and J.J. McDonnell, 1998, *Isotope Tracers in Catchment Hydrology*. Elsevier Science B.V., Amsterdam, 839 pages, <https://www.rcamnl.wr.usgs.gov/isoig/isopubs/itchinfo.html>.
- Khang, P., 1985, The development of karst landscapes in Vietnam. *Acta Geologica Polonica*, volume 35, numbers 3-4, pages 305-319, <https://geojournals.pgi.gov.pl/agp/article/view/9412>.
- Kidd, R.E., C.J. Taylor, and V.E. Stricklin, 2001, Use of ground-water tracers to evaluate the hydraulic connection between Key Cave and the proposed industrial site near

- Florence, Alabama, 2000 and 2001. United States Geological Survey, Water-Resources Investigations Report 2001-4228, <https://doi.org/10.3133/wri014228>.
- Kindinger, J. L., J.B. Davis, and J.G. Flocks, 1999, Geology and evolution of lakes in North-Central Florida. *Environmental Geology*, volume 38, issue 4, pages 301-321, <https://doi.org/10.1007/s002540050428>.
- Kindinger, J. L., J.B. Davis, and J.G. Flocks, 2000, Subsurface characterization of selected water bodies in the St. Johns River Water Management District, Northeast Florida. United States Geological Survey, Open-File Report 2000-180, <https://doi.org/10.3133/ofr00180>, [https://web.archive.org/web/20170624084406/https://water.usgs.gov/ogw/karst/kigconference/jlk\\_subsurface.htm](https://web.archive.org/web/20170624084406/https://water.usgs.gov/ogw/karst/kigconference/jlk_subsurface.htm).
- Kindinger, J. L., J.B. Davis, and J.G. Flocks, 2001, Subsurface characterization of selected water bodies in the St. Johns River Water Management District, northeastern Florida *in* United States Geological Survey, Karst Interest Group: Proceedings, St. Petersburg, Florida, February 13-16, 2001, editor, E.L. Kuniansky, United States Geological Survey, Water-Resources Investigations Report 01-4011, pages 124-127, [https://www.researchgate.net/publication/240633478\\_Subsurface\\_Characterization\\_of\\_Selected\\_Water\\_Bodies\\_in\\_the\\_St\\_Johns\\_River\\_Water\\_Management\\_District\\_North\\_east\\_Florida](https://www.researchgate.net/publication/240633478_Subsurface_Characterization_of_Selected_Water_Bodies_in_the_St_Johns_River_Water_Management_District_North_east_Florida).
- Kinnaman, S., 2002, Slug test results from 1998-2001. Written communication by Kinnaman, Hydrologist. United States Geological Survey, Orlando, Florida, USA.
- Kiraly, L., 1998, Modelling karst aquifers by the combined discrete channel and continuum approach. *Bulletin d'Hydrogeologie*, volume 16, pages 77-98, [https://doc.rero.ch/record/260628/files/Kiraly L. - Modelling karst aquifers by the combined UNINE B.H. 16 1998.pdf](https://doc.rero.ch/record/260628/files/Kiraly_L._Modelling_karst_aquifers_by_the_combined_UNINE_B.H.16_1998.pdf).
- Kiraly, L., 2003, Karstification and groundwater flow. *Speleogenesis and Evolution of Karst Aquifers* 1, issue 3, pages 155-192, [http://doc.rero.ch/record/260704/files/Kiraly L. - Karstification and Groundwater SPELEOGENESIS S.E.K.A. 1 2003.pdf](http://doc.rero.ch/record/260704/files/Kiraly_L._Karstification_and_Groundwater_SPELEOGENESIS_S.E.K.A.1_2003.pdf).
- Kish, G.R., C.E. Stringer, M.T. Stewart, M.C. Rains, and A.E. Torres, 2010, A geochemical mass-balance method for base-flow separation, Upper Hillsborough River Watershed, West-Central Florida, volumes 2003-2005 and 2009. United States Geological Survey, Scientific Investigations Report 2010-5092, <https://pubs.usgs.gov/sir/2010/5092/pdf/sir2010-5092.pdf>.
- Klepper, M.R. and D.G. Wyant, 1957, Notes on the geology of uranium. United States Geological Survey Bulletin 1046-F, <https://pubs.usgs.gov/bul/1046f/report.pdf>.
- Klimchouk, A., 2015, The karst paradigm: Changes, trends and perspectives. *Acta Carsologica*, volume 44, issue 3, pages 289-313, <https://doi.org/10.3986/ac.v44i3.2996>.

- Knochenmus, L.A. and J.L. Robinson, 1996, Descriptions of anisotropy and heterogeneity and their effect on ground-water flow and areas of contribution to public supply wells in a karst carbonate aquifer system. United States Geological Survey, Water-Supply Paper 2475, <https://doi.org/10.3133/wsp2475>.
- Knochenmus, L.A. and D.A. Yobbi, 2001, Hydrology of the coastal springs ground-water basin and adjacent parts of Pasco, Hernando, and Citrus Counties Florida. United States Geological Survey, Water-Resources Investigations Report 2001-4230, <https://doi.org/10.3133/wri014230>.
- Konzuk, J.S., and B.H. Kueper, 2004, Evaluation of cubic law-based models describing single-phase flow through a rough-walled fracture. Water Resources Research, volume 40, issue 2, <https://doi.org/10.1029/2003WR002356>.
- Kozar, M.D., K.J. McCoy, D.J. Weary, M.S. Field, H.A. Pierce, W.B. Schill, and J.A. Young, 2007, Hydrogeology and water quality of the Leetown Area, West Virginia. United States Geological Survey, Open-File Report 2007-1358, <https://doi.org/10.3133/ofr20071358>.
- Kraemer, P.A., F. Anselmetti, and R. Curry, 2001, Geophysical characterization of pre-Holocene limestone bedrock underlying the Biscayne National Park reef *in* United States Geological Survey, Karst Interest Group: Proceedings, St. Petersburg, Florida, February 13-16, 2001, editor, E.L. Kuniansky. United States Geological Survey, Water Resources Investigations Report 01-4011, pages 128-133, <https://boris.unibe.ch/86797/>.
- Kraemer, T.F., and D.P. Genereux, 1998, Applications of Uranium- and Thorium-Series Radionuclides in Catchment Hydrology Studies *in* Isotope Tracers in Catchment Hydrology, editors, C. Kendall and J.J. McDonnell, Elsevier, Amsterdam, Netherlands, pages 679-722, <https://doi.org/10.1016/B978-0-444-81546-0.50027-6>.
- Kresic, N., 2007, Hydrogeology and Groundwater Modeling, 2<sup>nd</sup> edition, CRC Press, Boca Raton, Florida, USA, 808 pages, <https://doi.org/10.1201/9781420004991>.
- Kruseman, G.P., and N.A. de Ridder, 1994, Analysis and evaluation of pumping test data. International Institute for Land Reclamation and Improvement, The Netherlands, 372 pages, [https://www.hydrology.nl/images/docs/dutch/key/Kruseman\\_and\\_De\\_Ridder\\_2000.pdf](https://www.hydrology.nl/images/docs/dutch/key/Kruseman_and_De_Ridder_2000.pdf).
- Kuniansky, E.L., 2002, Field trip photograph of unnamed West Virginia spring taken by Eve Kuniansky, August 22, 2002, Southeast Region Groundwater Specialist, United States Geological Survey, Norcross, Georgia, USA.
- Kuniansky, E.L., 2006, Vacation photograph of forest karst towers from Li River, China near Guilin taken by Eve Kuniansky, November, 2006, taken by Eve Kuniansky, Southeast Region Groundwater Specialist, United States Geological Survey, Norcross, Georgia, USA.
- Kuniansky, E.L., 2008a, Vacation photograph on a trip to caves and karst of Slovenia and Croatia of tufa lakes at Plitvice Lakes World Heritage karst site, Croatia taken by Eve

- Kuniansky, Southeast Region Groundwater Specialist, United States Geological Survey, Norcross, Georgia, USA.
- Kuniansky, E.L., 2008b, Field trip photograph at Mammoth Cave National Park, Kentucky taken by Eve Kuniansky, Southeast Region Groundwater Specialist, United States Geological Survey, Norcross, Georgia, USA.
- Kuniansky, E.L., 2012, Vacation photograph on trip to caves and karst of Laos and Vietnam taken from a boat on the South China Sea, Vietnam by Eve Kuniansky, Southeast Region Groundwater Specialist, United States Geological Survey, Norcross, Georgia, USA.
- Kuniansky, E.L., 2014a, Field trip photograph of Sinkhole lakes near Carlsbad, New Mexico taken by Eve Kuniansky, Southeast Region Groundwater Specialist, United States Geological Survey, Norcross, Georgia, USA.
- Kuniansky, E.L., 2014b, Taking the mystery out of mathematical model applications to karst aquifers—A primer *in* United States Geological Survey, Karst Interest Group: Proceedings, Carlsbad, New Mexico, April 29-May 2, 2014, editors, E.L. Kuniansky and L.E. Spangler. United States Geological Survey, Scientific Investigations Report 2014-5035, pages 69-81, <https://pubs.usgs.gov/sir/2014/5035/sir2014-5035.pdf> ↗.
- Kuniansky, E.L., 2016a, Simulating groundwater flow in karst aquifers with distributed parameter models—Comparison of porous-equivalent media and hybrid flow approaches. United States Geological Survey, Scientific Investigations Report 2016-5116, <https://doi.org/10.3133/sir20165116> ↗.
- Kuniansky, E.L., 2016b, MODFLOW and MODFLOW Conduit Flow Process data sets for simulation experiments of the Woodville Karst Plain, near Tallahassee, Florida with three different approaches and different stress periods. United States Geological Survey data release, <https://doi.org/10.5066/F7PK0D87> ↗.
- Kuniansky, E.L., 2017, Field photograph of Van Brahana setting tracer test bugs in a spring at the Savoy Experimental Watershed, Savoy, Arkansas. Eve Kuniansky, Southeast Region Groundwater Specialist, United States Geological Survey, Norcross, Georgia, USA.
- Kuniansky, E.L., 2020, Satellite view of Wakulla Springs, Florida, United States, public domain image clipped from Google maps by Eve Kuniansky, Emeritus Scientist, United States Geological Survey, Norcross, Georgia, USA.
- Kuniansky, E.L., and J.C. Bellino, 2012, Tabulated transmissivity and storage properties of the Floridan aquifer system in Florida and parts of Georgia, South Carolina, and Alabama. United States Geological Survey Data Series 669, <https://pubs.usgs.gov/ds/669/> ↗.
- Kuniansky, E.L., J.M. Blackstock, D.M. Wagner, and J.V. Brahana, 2019, Interpretation of dye tracing data collected *in* Advanced Groundwater Field Techniques in Karst Terrains Course, Savoy, Arkansas, November 13-December 2, 2017, at the Savoy

- Experimental Watershed. United States Geological Survey, Scientific Investigations Report 2019-5016, <https://doi.org/10.3133/sir20195016>.
- Kuniansky, E.L., L. Fahlquist, and A.F. Ardis, 2001, Travel times along selected flow paths of the Edwards Aquifer, central Texas *in* United States Geological Survey, Karst Interest Group: Proceedings, St. Petersburg, Florida, February 13-16, 2001, editor, E.L. Kuniansky. United States Geological Survey, Water-Resources Investigations Report 2001-4011, pages 69-77, [https://web.archive.org/web/20170624084249/https://water.usgs.gov/ogw/karst/kigcoference/elk\\_traveltimes.htm](https://web.archive.org/web/20170624084249/https://water.usgs.gov/ogw/karst/kigcoference/elk_traveltimes.htm).
- Kuniansky, E.L., J.J. Gallegos, and J.H. Davis, 2011, Comparison of three model approaches for spring simulation, Woodville Karst Plain, Florida. United States Geological Survey, Karst Interest Group: Proceedings, St. Petersburg, Florida, February 13-16, 2001. United States Geological Survey, Water-Resources Investigations Report 2011-5031, pages 169-170, <https://pubs.usgs.gov/sir/2011/5031/pdf/sir20115031.pdf#page=177>.
- Kuniansky, E.L., K.J. Halford, and W.B. Shoemaker, 2008, Permeameter data verify new turbulence process for MODFLOW. Ground Water, volume 46, number 5, pages 768-771, <https://doi.org/10.1111/j.1745-6584.2008.00458.x>.
- Kuniansky, E.L., and S.T. Hamrick, 1998, Hydrogeology and simulation of ground-water flow in the Paluxy aquifer, in the vicinity of landfills one and three at United States Air Force Plant 4, Fort Worth, Texas. United States Geological Survey, Water Resources Investigations Report 98-4023, 34 pages, <http://pubs.usgs.gov/wri/wri98-4023/>.
- Kuniansky, E.L., and K.Q. Holligan, 1994, Simulations of flow in the Edwards-Trinity aquifer system and contiguous hydraulically units, west-central Texas. United States Geological Survey, Water-Resources Investigations Report 93-4093, [doi.org/10.3133/wri934093](https://doi.org/10.3133/wri934093).
- Kuniansky, E.L., D.J. Weary, and J.E. Kaufmann, 2016, The current status of mapping karst areas and availability of public sinkhole-risk resources in karst terrains of the United States. Hydrogeology Journal, volume 24, pages 613-624, [doi.org/10.1007/s10040-015-1333-3](https://doi.org/10.1007/s10040-015-1333-3).
- Kurylyk, B.L., D.J. Irvine, S.K. Carey, M.A. Briggs, D.D. Werkema, and M. Bonham, 2017, Heat as a groundwater tracer in shallow and deep heterogeneous media: Analytical solution, spreadsheet tool, and field applications. Hydrological Processes, volume 31, number 14, pages 2648-2661, <https://doi.org/10.1002/hyp.11216>.
- Kvgunten, 2017, Hydrochemical facies in the Piper diagram, licensed under [CC BY-SA 4.0](https://creativecommons.org/licenses/by-sa/4.0/), [https://commons.wikimedia.org/wiki/File:Hydrochemical\\_facies\\_in\\_the\\_Piper\\_diagram.jpg](https://commons.wikimedia.org/wiki/File:Hydrochemical_facies_in_the_Piper_diagram.jpg).














- Lage, J.L., and B.V. Antohe, 2000, Darcy's experiments and the deviation to nonlinear flow regime. American Society of Mechanical Engineers, Journal of Fluids Engineering, volume 122, pages 619-625, <https://doi.org/10.1115/1.1287722>.
- Lang, U., 1995, Simulation of regional flow and transport processes in karst aquifers using the double continuum approach: Stuttgart, Germany, method development and parameter study. Doctor of Philosophy dissertation, Institute for Hydraulic Engineering, University of Stuttgart (in German).
- Lee, J., 1982, Well Testing. Society of Petroleum Engineers of AIME, New York, USA, 159 pages.
- Lei, Q., J.P. Latham, and C.F. Tsang, 2017, The use of discrete fracture networks for modelling coupled geomechanical and hydrological behaviour of fractured rocks. Computers and Geotechnics, volume 85, pages 151-176, [dx.doi.org/10.1016/j.compgeo.2016.12.024](https://doi.org/10.1016/j.compgeo.2016.12.024).
- Liedl, R., M. Sauter, D. Hückinghaus, T. Clemens, and G. Teutsch, 2003, Simulation of the development of karst aquifers using a coupled continuum pipe flow model. Water Resources Research, volume 39, issue 3, <https://doi.org/10.1029/2001WR001206>.
- Lindgren, R.J., A.R. Dutton, S.D. Hovorka, S.R.H. Worthington, and S. Painter, 2004, Conceptualization and simulation of the Edwards Aquifer, San Antonio region, Texas. United States Geological Survey, Scientific Investigations Report 2004-5277, <https://pubs.usgs.gov/sir/2004/5277/>.
- Lindgren, R.J., C.J. Taylor, and N.A. Houston, 2009, Description and evaluation of numerical groundwater flow models for the Edwards Aquifer, south-central Texas. United States Geological Survey, Scientific Investigations Report 2009-5183, <https://pubs.usgs.gov/sir/2009/5183/>.
- Lohman, S.W., 1979, Ground-Water Hydraulics. United States Geological Survey. Professional Paper 708, 70 pages, <https://doi.org/10.3133/pp708>.
- Long, A.J., M.J. Ohms, and J.D.R.G. McKaskey, 2012, Groundwater flow, quality (2007-10), and mixing in the Wind Cave National Park area, South Dakota. United States Geological Survey, Scientific Investigations Report 2011-5235, <https://doi.org/10.3133/sir20115235>.
- Long, A.J., and L.D. Putnam, 2002, Evaluating travel times and transient mixing in a karst aquifer using time-series analysis of stable isotope data *in* United States Geological Survey, Karst Interest Group: Proceedings, Shepherdstown, West Virginia, August 20-22, 2002, editor, E.L. Kuniansky. United States Geological Survey, Water-Resources Investigations Report 02-4174, pages 66-73, <https://doi.org/10.3133/wri024174>, [https://web.archive.org/web/20170611102903/https://water.usgs.gov/ogw/karst/kig2002/ajl\\_travel.html](https://web.archive.org/web/20170611102903/https://water.usgs.gov/ogw/karst/kig2002/ajl_travel.html).
- Long, A.J., and Putnam, L.D., 2007, Characterization of ground-water flow and water quality for the Madison and Minnelusa aquifers in Northern Lawrence County,

- South Dakota. United States Geological Survey, Scientific Investigations Report 2007-5001, <https://pubs.usgs.gov/sir/2007/5001/> .
- Mahler B.J., P.C. Bennett, and M. Zimmerman, 1998, Lanthanide-labeled clay: A new method for tracing sediment transport in karst. *Ground Water*, volume 36, issue 5, pages 835-843, [doi.org/10.1111/j.1745-6584.1998.tb02202.x](https://doi.org/10.1111/j.1745-6584.1998.tb02202.x) .
- Mahler, B.J., L. Lynch, and P.C. Bennett, 1999, Mobile sediment in an urbanizing karst aquifer: Implications for contaminant transport. *Environmental Geology*, volume 39, issue 1, pages 25-38, <https://link.springer.com/content/pdf/10.1007/s002540050434.pdf> .
- Mahler, B.J., J.C. Personné, F.L. Lynch, and P.C. Van Metre, 2007, Sediment and sediment-associated contaminant transport through karst in *Studies of Cave Sediments*, editors, I.D. Sasowsky and J. Mylroie, pages 23-46, Springer, Boston, Massachusetts, USA, [https://doi.org/10.1007/978-1-4419-9118-8\\_2](https://doi.org/10.1007/978-1-4419-9118-8_2) .
- Mahler B.J., J.C. Personné, G.F. Lods, and C. Drogue, 2000, Transport of free and particulate-associated bacteria in karst. *Journal of Hydrology*, volume 238, issues 3-4, pages 179-193, [https://doi.org/10.1016/S0022-1694\(00\)00324-3](https://doi.org/10.1016/S0022-1694(00)00324-3) .
- Maloszewski, P., 2000, Lumped-parameter models as a tool for determining the hydrological parameters of some groundwater systems based on isotope data. *International Association of Hydrological Sciences Publication*, number 262, pages 271-276, <https://www.cabdirect.org/cabdirect/abstract/20013046080> .
- Mangin, A., 1975, Contribution to the hydrodynamic study of karst aquifers, 3<sup>rd</sup> part, Constitution and functioning of karst aquifers. *Annals of Speleology*, volume 30, issue 1, pages 22-124, (in French) <https://hal.archives-ouvertes.fr/tel-01575806> .
- Mathey, S.B., 1989, National Water Information System user's manual, Volume 2, Chapter 4, Ground-water site inventory system. United States Geological Survey, Open-File Report 89-587, <https://doi.org/10.3133/ofr89587> .
- McCann, M.R., and N.C. Krothe, 1992, Development of a monitoring program at a Superfund site in a karst terrain near Bloomington, Indiana. *Proceedings of the Third Conference on Hydrogeology, Ecology, Monitoring, and Management of Ground Water in Karst Terranes*, pages 349-372, <https://nepis.epa.gov/Exe/ZyPDF.cgi/9100NMJR.PDF?Dockey=9100NMJR.PDF> .
- McClure, M.W., and R.N. Horne, 2013, Discrete fracture network modeling of hydraulic stimulation-coupling flow and geomechanics. Springer, New York, USA, 90 pages, <https://doi.org/10.1007/978-3-319-00383-2> .
- Merritt, M.L., 2004, Estimating hydraulic properties of the Floridan aquifer system by analysis of earth-tide, ocean-tide, and barometric effects, Collier and Hendry Counties, Florida. United States Geological Survey, Water-Resources Investigations Report 03-4267, <https://doi.org/10.3133/wri034267> .
- Metcalf & Eddy, Incorporated, University of Florida, and Water Resources Engineers, Incorporated, 1971, Storm Water Management Model Volume I—Final Report.

- United States Environmental Protection Agency, EPA 11024DOC07/71, 353 pages, <https://nepis.epa.gov/EPA/html/DLwait.htm?url=/Exe/ZyPDF.cgi/9101OI3P.PDF?Dockey=9101OI3P.PDF>.
- Milanovic, P.T., 1981, Karst hydrogeology. Water Resources Publications, 434 pages.
- Miller, J.A., 1999, Ground water atlas of the United States: Introduction and national summary. United States Geological Survey, Hydrologic Atlas 730-A, <https://doi.org/10.3133/ha730A>.
- Mohrlok, U., 1996, Parameter identification in double continuum models using karst aquifers as an example. Tübingen, Germany, Series C. Institute and Museum for Geology and Paleontology of the University of Tübingen, Tübingen Geoscientific Work, volume 31, (in German) <https://ub01.uni-tuebingen.de/xmlui/handle/10900/48864>.
- Moore, G.W., and G. Nicholas, 1964, Speleology, The Study of Caves. Heath, Boston, 120 pages.
- Moore, C.H., and W.J. Wade, 2013, Chapter 4—The nature and classification of carbonate porosity, Developments in Sedimentology, volume 67, pages 51-65, <https://doi.org/10.1016/B978-0-444-53831-4.00004-5>.
- Morris, B., 2017, Field photograph of the outcrop of the middle portion of the Glen Rose limestone in Canyon Gorge, Texas, USA taken May 18, 2017 by Bob Morris, Hydrologist, United States Geological Survey, San Antonio, Texas, USA.
- Morris, D.A., and A.I. Johnson 1967, Summary of hydrologic and physical properties of rock and soil material as analyzed by the Hydrologic Laboratory of the U.S Geological Survey 1948-60. United States Geological Survey, Water-Supply Paper 1839-D, <https://doi.org/10.3133/wsp1839D>.
- Mull, D.S., 1993a, Use of dye tracing to determine the direction of ground-water flow from a Superfund waste-disposal site in karst terrane, near Auburn, Kentucky. United States Geological Survey, Water-Resources Investigations Report 92-4195, <https://doi.org/10.3133/wri924195>.
- Mull, D.S., 1993b, Use of dye tracing to determine the direction of ground-water flow in karst terrane at the Kentucky State University Research Farm near Frankfort, Kentucky. United States Geological Survey, Water-Resources Investigations Report 93-4063, <https://doi.org/10.3133/wri934063>.
- Mull, D.S., T.D. Liebermann, J.L. Smoot, and L.H. Woosley, 1988a, Application of dye-tracing techniques for determining solute-transport characteristics of ground water in karst terranes. United States Environmental Protection Agency, EPA 904/6-88-001, <https://nepis.epa.gov/Exe/ZyPDF.cgi/20013J3F.PDF?Dockey=20013J3F.PDF>.
- Mull, D.S., Smoot, J.L., and Liebermann, T.D., 1988b, Dye tracing techniques used to determine ground-water flow in a carbonate aquifer system near Elizabethtown,

- Kentucky. United States Geological Survey, Water-Resources Investigations Report 87-4174, <https://pubs.usgs.gov/wri/1987/4174/report.pdf>.
- National Research Council, 2000, Seeing into the Earth: Noninvasive Characterization of the Shallow Subsurface for Environmental and Engineering Applications. The National Academies Press, Washington, DC, USA, <https://doi.org/10.17226/5786>.
- Neuman, S.P., and G. de Marsily, 1976, Identification of linear systems response by parametric programming. Water Resources Research, volume 12, number 2, pages 253-262, <https://doi.org/10.1029/WR012i002p00253>.
- Neuzil, C.E., 1994, How permeable are clays and shales? Water Resources Research, volume 30, number 2, pages 145-150, <https://doi.org/10.1029/WR012i002p00253>.
- Nicholl, M.J., H. Rajaram, R.J. Glass, and R. Detwiler, 1999, Saturated flow in a single fracture: Evaluation of the Reynolds equation in measured aperture fields. Water Resources Research, volume 35, issue 11, pages 3361-3373, <https://doi.org/10.1029/1999WR900241>.
- Nimmo, J.R., 2013, Porosity and Pore Size Distribution. Reference Module in Earth Systems and Environmental Sciences, Elsevier, ISBN 9780124095489, <https://doi.org/10.1016/B978-0-12-409548-9.05265-9>.
- Paillet, F.L., 1998, Flow modeling and permeability estimation using borehole flow logs in heterogeneous fractured formations. Water Resources Research, volume 34, number 5, pages 997-1010, <https://doi.org/10.1029/98WR00268>.
- Paillet, F.L., 2000, A field technique for estimating aquifer parameters using flow log data. Groundwater, volume 38, number 4, pages 510-521, <https://doi.org/10.1111/j.1745-6584.2000.tb00243.x>.
- Paillet, F.L., 2001, Borehole geophysical applications in karst hydrogeology in United States Geological Survey, Karst Interest Group: Proceedings, St. Petersburg, Florida, USA, February 13-16, 2001, editor, E.L. Kuniansky. United States Geological Survey, Water-Resources Investigations Report 01-4011, pages 116-123, [https://web.archive.org/web/20170624084347/https://water.usgs.gov/ogw/karst/kigcoference/flp\\_borehole.htm](https://web.archive.org/web/20170624084347/https://water.usgs.gov/ogw/karst/kigcoference/flp_borehole.htm).
- Paillet, F.L., C. Barton, S. Luthi, F. Rambow, J.R. Zemanck, 1990, Borehole imaging and its application in well logging-an overview in Borehole Imaging. Society of Professional Well Log Analysts, Incorporated, volume 6001, pages 3-23.
- Paillet, F.L. and R.E. Crowder, 1996, A generalized approach for the interpretation of geophysical well logs in ground water studies—Theory and application. Groundwater, volume 34, number 5, pages 883-898, <https://doi.org/10.1111/j.1745-6584.1996.tb02083.x>.
- Paillet, F.L., A.E. Hess, and J.H. Williams, 1998, Design, operation, and data analysis for a wireline packer system in open boreholes, with field-test results from Belvidere, Illinois. United States Geological Survey, Open-File Report 98-413, <https://doi.org/10.3133/ofr98413>.

- Painter, S.L., A. Sun, and R.T. Green, 2007, Enhanced Characterization and Representation of Flow through Karst Aquifers—Phase II. Revision 1. Geosciences and Engineering Division, Southwest Research Institute, San Antonio, Texas, USA, [https://www.edwardsaquifer.org/science\\_docs/enhanced-characterization-and-representation-of-flow-through-karst-aquifers-phase-ii-revision-1/](https://www.edwardsaquifer.org/science_docs/enhanced-characterization-and-representation-of-flow-through-karst-aquifers-phase-ii-revision-1/) .
- Palmer, A.N., 1991, Origin and morphology of limestone caves. Geological Society of America Bulletin, volume 103, pages 1-21, [https://doi.org/10.1130/0016-7606\(1991\)103%3c0001:OAMOLC%3e2.3.CO;2](https://doi.org/10.1130/0016-7606(1991)103%3c0001:OAMOLC%3e2.3.CO;2) .
- Palmer, A.N., 1999, Patterns of dissolution porosity in carbonate rocks in Palmer. The Karst Waters Institute Special Publication, volume 5, pages 71-78, [https://www.researchgate.net/publication/26448037\\_Patterns\\_of\\_dissolutional\\_porosity\\_in\\_carbonate\\_rocks](https://www.researchgate.net/publication/26448037_Patterns_of_dissolutional_porosity_in_carbonate_rocks) .
- Pavlicek, D.J., 1996, Karst hydrogeology and hydrochemistry of the Cave Springs Basin Near Chattanooga, Tennessee. United States Geological Survey, Water-Resources Investigations Report 96-4248, <https://pubs.usgs.gov/wri/wri96-4248/#pdf> .
- Peano G., B. Vigna, E. Villavecchia, and G. Agnesod, 2011, Radon exchange dynamics in a karst system investigated by radon continuous measurements in water: First results. Radiation Protection Dosimetry, volume 45, issues 2-3, pages 173-177, <https://doi.org/10.1093/rpd/ncr053> .
- Perne, M., M. Covington, and F. Gabrovšek, 2014, Evolution of karst conduit networks in transition from pressurized flow to free-surface flow. Hydrology and Earth System Sciences, volume 18, pages 4617-4633, <https://doi.org/10.5194/hess-18-4617-2014> .
- Peterson, E.W. and C.M. Wicks, 2006, Assessing the importance of conduit geometry and physical parameters in karst systems using the storm water management model (SWMM). Journal of Hydrology, volume 329, issues 1-2, pages 294-305, <https://doi.org/10.1016/j.jhydrol.2006.02.017> .
- Piper, A.M., 1944, A graphic procedure in the geochemical interpretation of water analysis. Transactions American Geophysical Union, volume 25, pages 914-923, <https://doi.org/10.1029/TR025i006p00914> .
- Poeter, E., Y. Fan, J. Cherry, W. Wood, D. Mackay, 2020, Groundwater in our water cycle – getting to know Earth’s most important fresh water source. The Groundwater Project, Guelph, Ontario, Canada. <https://doi.org/10.21083/978-1-7770541-1-3> .
- Porter, A.J., J.S. Webber, J.W. Witt, and J.D. Jastram, 2020, Spatial and temporal patterns in streamflow, water chemistry, and aquatic macroinvertebrates of selected streams in Fairfax County, Virginia, 2007-18. United States Geological Survey, Scientific Investigations Report 2020-5061, <https://doi.org/10.3133/sir20205061> .
- Prudic, D.E., 1991, Estimates of hydraulic conductivity from aquifer-test data and specific-capacity data, Gulf Coast Regional Aquifer Systems, south-central United States. United States Geological Survey, Water-Resources Investigations Report 90-4121, <https://pubs.usgs.gov/wri/1990/4121/report.pdf> .



- Quinlan, J.F., and R.O. Ewers, 1989, Subsurface drainage in the Mammoth Cave area *in* Karst Hydrology, editors, W.B. White and E.L. White, Springer, Boston, Massachusetts, USA, [https://doi.org/10.1007/978-1-4615-7317-3\\_3](https://doi.org/10.1007/978-1-4615-7317-3_3).<sup>↗</sup>
- Quinlan, J.F., J.A. Ray, and G.M. Schindel, 1995, Intrinsic limitations of standard criteria and methods for delineation of groundwater-source protection areas (springhead and wellhead protection areas) in carbonate terranes—Critical review, technically-sound resolution of limitations, and case study in a Kentucky karst *in* Karst Geohazards Engineering and Environmental Problems in Karst Terrane, editors, B.F. Beck and F.M. Pearson. A.A. Balkema, Rotterdam, Netherlands, pages 165-176, <https://www.routledge.com/Karst-Geohazards-Engineering-and-Environmental-Problems-in-Karst-Terrane/Beck/p/book/9789054105350>.<sup>↗</sup>
- Quinn, P.M., J.A. Cherry, and B.L. Parker, 2011b, Quantification of non-Darcian flow observed during packer testing in fractured sedimentary rock. Water Resources Research, volume 47, issue 9, <https://doi.org/10.1029/2010WR009681>.<sup>↗</sup>
- Quinn, P.M., B.L. Parker, and J.A. Cherry, 2011a, Using constant head step tests to determine hydraulic apertures in fractured rock. Journal of Contaminant Hydrology, volume 126, pages 85-99, <https://doi.org/10.1016/j.jconhyd.2011.07.002>.<sup>↗</sup>
- Ray, J., 1999, A model of karst drainage basin evolution, interior low plateaus, United States *in* Karst modeling, editors, A.N. Palmer, M.V. Palmer, and L.D. Sasowsky. Karst Waters Institute Special Publication, volume 5, <https://karstwaters.org/publications/sp5-karst-modeling/>.<sup>↗</sup>
- Ray, J.A., 2001, Spatial interpretation of karst drainage basins *in* Geotechnical and Environmental Applications of Karst Geology and Hydrology, pages 235-244, <https://www.routledge.com/Geotechnical-and-Environmental-Applications-of-Karst-Geology-and-Hydrology/Beck-Herring/p/book/9789058091901>.<sup>↗</sup>
- Ray, J.A., 2012, Sinking streams and losing streams *in* Encyclopedia of Caves, 2<sup>nd</sup> edition, editors, D.C. Culver and W.B. White. Academic Press, Burlington, Massachusetts, USA, pages 707-712, <https://doi.org/10.1016/B978-0-12-383832-2.00104-3>.<sup>↗</sup>
- Reese, R.S. and K.J. Cunningham, 2000, Hydrogeology of the Gray Limestone Aquifer in southern Florida. United States Geological Survey, Water-Resources Investigations Report 99-4213, <https://doi.org/10.3133/wri994213>.<sup>↗</sup>
- Reilly, T.E., and A.W. Harbaugh, 1993, Simulation of cylindrical flow to a well using the U.S. Geological Survey Modular Finite-Difference Ground-Water Flow Model. Ground Water volume 31, issue 3, pages 489-494.
- Reilly, T.E. and A.W. Harbaugh, 2004, Guidelines for evaluating ground-water flow models. United States Geological Survey, Scientific Investigations Report 2004-5038, <https://doi.org/10.3133/sir20045038>.<sup>↗</sup>
- Reimann, T., S. Birk, C. Rehrl, and W.B. Shoemaker, 2011a, Modifications to the Conduit Flow Process Mode 2 for MODFLOW-2005. Groundwater, volume 50, issue 1, pages 144-148, <https://doi.org/10.1111/j.1745-6584.2011.00805.x>.<sup>↗</sup>

- Reimann, T., T. Geyer, W.B. Shoemaker, R. Liedl, and M. Sauter, 2011b, Effects of dynamically variable saturation and matrix-conduit coupling of flow in karst aquifers *Water Resources Research* volume 47, issue 11, <https://doi.org/10.1029/2011WR010446>.
- Reimann, T., R. Liedl, M. Giese, T. Geyer, J.C. Maréchal, N. Dörfliger, S. Bauer, and S. Birk, 2013, Addition and enhancement of flow and transport processes to the MODFLOW-2005 conduit flow process. National Ground Water Association Summit—The national and international conference on groundwater, <https://pdfs.semanticscholar.org/7d0e/4292819e24d8e0661900d48213e94c124aee.pdf>.
- René, M., 2017, Nature, sources, resources, and production of Thorium, Chapter 9 *in* Descriptive Inorganic Chemistry Researches of Metal Compounds, editor, T. Akitsu, IntechOpen, London, United Kingdom, pages 201-212, <https://doi.org/10.5772/intechopen.68304>.
- Renken, R.A., K.J. Cunningham, M.R. Zygnerski, M.A. Wacker, A.M. Shapiro, R.W. Harvey, D.W. Metge, C.L. Osborn, and J.N. Ryan, 2005, Assessing the vulnerability of a municipal wellfield to contamination in a karst aquifer. *Environmental and Engineering Geoscience*, volume 11, issue 4, pages 319-331, <https://doi.org/10.2113/11.4.319>.
- Revil, A., K. Koch, and K. Holliger, 2012, Is it the grain size or the characteristic pore size that controls the induced polarization relaxation time of clean sands and sandstones? *Water Resources Research*, volume 48, issue 5, [doi.org/10.1029/2011WR011561](https://doi.org/10.1029/2011WR011561).
- Reynolds, O., 1883, An experimental investigation of the circumstances which determine whether the motion of water shall be direct or sinous, and of the law of resistances in parallel channels. *Philosophical Transactions of the Royal Society of London*, volume 174, <https://doi.org/10.1098/rstl.1883.0029>.
- Robinson, J.L., 1995, Hydrogeology and results of tracer tests at the old Tampa well field in Hillsborough County, with implications for wellhead-protection strategies in west-central Florida. United States Geological Survey, Water-Resources Investigations Report 93-4171, <https://doi.org/10.3133/wri934171>.
- Rose, P.R., 1972, Edwards Group, surface and subsurface, central Texas. The University of Texas, Bureau of Economic Geology Report of Investigations, volume RI-74, 198 pages, <https://www.beg.utexas.edu/publications/edwards-group-surface-and-subsurface-central-texas>.
- Rupert F., and S. Spencer, 2004, Florida's sinkholes. Poster number 11, Florida Geological Survey, Tallahassee, Florida, USA.
- Saller, S.P., M.J. Ronayne, and A.J. Long, 2013, Comparison of a karst groundwater model with and without discrete conduit flow. *Hydrogeology Journal*, volume 21, number 7, pages 1555-1566, <https://doi.org/10.1007/s10040-013-1036-6>.
- Sauter, M., 1993, Double porosity models in karstified limestone aquifers: Field validation and data provision *in* Hydrogeological Processes in Karst Terranes (Proceedings of

- the Antalya Symposium and Field Seminar, October 1990). International Association of Hydrological Publication, volume 207, pages 261-279, <https://iahs.info/uploads/dms/8917.261-279-207-Sauter.pdf>.
- Scanlon, B.R., R.E. Mace, M.E. Barrett, B. Smith, 2003, Can we simulate regional groundwater flow in a karst system using equivalent porous media models? Case study, Barton Springs Edwards Aquifer, United States of America. *Journal of Hydrology*, volume 276, pages 137-158, [https://doi.org/10.1016/S0022-1694\(03\)00064-7](https://doi.org/10.1016/S0022-1694(03)00064-7).
- Schneebeli, G., 1955, Experiments on the limit of validity of Darcy's law and the occurrence of turbulence in a filtration flow (in French). *La Houille Blanche* (The White Coal), volume 10, pages 141-149, <https://www.shf-lhb.org/articles/lhb/pdf/1955/04/lhb1955030.pdf>.
- Schulman, A.E., D.C. McKinney, and P.W.M. John, 1995, Stochastic recharge model for Edwards Aquifer in central Texas. *Journal of Water Resources Planning and Management*, volume 121, number 6, pages 479-489, [https://ascelibrary.org/doi/abs/10.1061/\(ASCE\)0733-9496\(1995\)121:6\(479\)](https://ascelibrary.org/doi/abs/10.1061/(ASCE)0733-9496(1995)121:6(479)).
- Scoffin, T.P., 1987, An introduction to carbonate sediments and rocks. Chapman and Hall, New York, USA, 274 pages, <https://www.osti.gov/biblio/6755454>.
- Sepúlveda, N., and E.L. Kuniansky, 2009, Effects of model layer simplification using composite hydraulic properties. *Hydrogeological Journal*, volume 18, pages 405-416, <https://doi.org/10.1007/s10040-009-0505-4>.
- Sherman, L.K., 1932, Streamflow from rainfall by the unit-graph method. *Engineering News Record*, volume 108, pages 501-505, [https://www.scirp.org/\(S\(i43dyn45teexjx455qlt3d2q\)\)/reference/ReferencesPapers.aspx?ReferenceID=786190](https://www.scirp.org/(S(i43dyn45teexjx455qlt3d2q))/reference/ReferencesPapers.aspx?ReferenceID=786190).
- Shoemaker, W.B., E.L. Kuniansky, S. Birk, S. Bauer, and E.D. Swain, 2008, Documentation of a conduit flow process (CFP) for MODFLOW-2005. United States Geological Survey, Techniques and Methods, Book 6, Chapter A24, Reston, Virginia, USA, <https://pubs.usgs.gov/tm/tm6a24/pdf/tm6-A24.pdf>.
- Sloto, R.A., and M.Y. Crouse, 1996, HYSEP: A computer program for streamflow hydrograph separation and analysis. United States Geological Survey, Water Resources Investigations Report 96-4040. Washington, D.C., USA. United States Geological Survey, <https://doi.org/10.3133/wri964040>.
- Smith, B.D., M.J. Cain, A.K. Clark, D.W. Moore, J.R. Faith, and P.L. Hill, 2005, Helicopter Electromagnetic and Magnetic Survey Data and Maps, Northern Bexar County, Texas. United States Geological Survey, Open-File Report 05-1158, [https://pubs.usgs.gov/of/2005/1158/downloads/REPORTS/ofr\\_05\\_1158.pdf](https://pubs.usgs.gov/of/2005/1158/downloads/REPORTS/ofr_05_1158.pdf).
- Smith, B.D., D.V. Smith, P.L. Hill, and V.F. Labson, 2003, Helicopter Electromagnetic and Magnetic Survey Data and Maps, Seco Creek Area, Medina and Uvalde Counties,

- Texas. United States Geological, Survey Open-File Report 03-226, <https://pubs.usgs.gov/of/2003/ofr-03-226/OFR-03-226-508.pdf>.
- Spangler, L.E., 2012, Hydrogeology of the Mammoth Spring groundwater basin and vicinity, Markagunt Plateau, Garfield, Iron, and Kane Counties, Utah. United States Geological Survey, Scientific Investigations Report 2012-5199, <https://doi.org/10.3133/sir20125199>.
- Spangler, L.E., and D.D. Susong, 2006, Use of dye tracing to determine ground-water movement to Mammoth Crystal Springs, Sylvan Pass area, Yellowstone National Park, Wyoming. United States Geological Survey, Scientific Investigations Report 2006-5126, <https://doi.org/10.3133/sir20065126>.
- Stallman, R.W., 1971, Aquifer-test design, observation, and data analysis. United States Geological Survey, Techniques of Water-Resources Investigations 03-B1, <https://doi.org/10.3133/twri03B1>.
- Stanton, G.P., and T.P. Schraeder, 2001, Surface geophysical investigation of a chemical waste landfill in northwestern Arkansas *in* United States Geological Survey, Karst Interest Group: Proceedings, St. Petersburg, Florida, February 13-16, 2001, editor, E.L. Kuniansky. United States Geological Survey, Water Resources Investigations Report 01-4011, [https://web.archive.org/web/20170624084342/https://water.usgs.gov/ogw/karst/kigconference/gps\\_surfacegeophysical.htm](https://web.archive.org/web/20170624084342/https://water.usgs.gov/ogw/karst/kigconference/gps_surfacegeophysical.htm).
- Stanton, J.S., D.W. Anning, C.J. Brown, R.B. Moore, V.L. McGuire, S.L. Qi, A.C. Harris, K.F. Dennehy, P.B. McMahon, J.R. Degnan, and J.K. Böhlke, 2017, Brackish groundwater in the United States. United States Geological Survey, Professional Paper 1833, 185 pages, <https://doi.org/10.3133/pp1833>.
- Steeple, D.W., and R.D. Miller, 1987, Direct detection of shallow subsurface voids using high resolution seismic-reflection techniques *in* Karst Hydrogeology: Engineering and Environmental Applications, editors, B.F. Beck and W.L. Wilson, A.A. Balkema, Rotterdam, Netherlands, pages 179-183.
- Stevanović, Z., 2015, Karst Aquifers—Characterization and Engineering. Springer International Publishing, Switzerland, 692 pages, <https://doi.org/10.1007/978-3-319-12850-4>.
- Stevanović, Z., 2018, Global distribution and use of water from karst aquifers *in* Advances in Karst Research: Theory, Fieldwork and Applications, editors, M. Parise, F. Gabrovsek, G. Kaufmann, and N. Ravbar. Geological Society, London, Special Publications, volume 466, number 1, pages 217-236, <https://doi.org/10.1144/SP466.17>.
- Stewart, M., J. Cimino, and M. Ross, 2007, Calibration of base flow separation methods with streamflow conductivity. Groundwater, volumes 45, number 1, pages 17-27, <https://doi.org/10.1111/j.1745-6584.2006.00263.x>.

- Stiff Jr., H.A., 1951, The interpretation of chemical water analysis by means of patterns. *Journal of Petroleum Technology*, volume 3, issue 10, page 15, <https://doi.org/10.2118/951376-G>.
- Steater, Scott, 2009, Threat Down Below: Polluted Caves Endanger Water Supplies, Wildlife, *Scientific American*, accessed January 2022 at, [www.scientificamerican.com/article/pollution-caves-water-wildlife-trout/](http://www.scientificamerican.com/article/pollution-caves-water-wildlife-trout/).
- Sukop, M.C., H. Huang, P.F. Alvarez, E.A. Variano, and K.J. Cunningham, 2013, Evaluation of permeability and non-Darcy flow in vuggy macroporous limestone aquifer samples with lattice Boltzmann methods. *Water Resources Research*, volume 49, issue 1, pages 216-230, <https://doi.org/10.1029/2011WR011788>.
- Suwanee River Water Management District, 2008, Field photograph, Live Oak, Florida, United States.
- Swain, E.D., and E.J. Wexler, 1996, A coupled surface-water and groundwater flow model (Modbranch) for simulation of stream-aquifer interaction. United States Geological Survey, Techniques of Water-Resources Investigations 06-A6, <https://doi.org/10.3133/twri06A6>.
- Taborsi, D., and M. Kazmer, 2013, Erosional and depositional textures and structures in Coastal Karst Landscapes *in* Coastal Karst Landforms, editors, M. Lace and J. Mylroie. Coastal Research Library, volume 5, Springer, Dordrecht, Netherlands, pages 15-58, [https://doi.org/10.1007/978-94-007-5016-6\\_2](https://doi.org/10.1007/978-94-007-5016-6_2).
- Takahashi, Y., M.J. Rabins, and D.M. Auslander, 1972, Control and Dynamic Systems. Addison-Wesley Publishing Company, 800 pages, <https://doi.org/10.1002/aic.690170102>.
- Taylor, C.J., 1997, Delineation of ground-water basins and recharge areas for municipal water-supply springs in a karst aquifer system in the Elizabethtown area, northern Kentucky. United States Geological Survey, Water-Resources Investigations Report 96-4254, <https://doi.org/10.3133/wri964254>.
- Taylor, C.J., 2021a, Field photographs of karst overflow springs, Groundwater Hydrologist and Water Resources Section Head, Kentucky Geological Survey, University of Kentucky, Lexington, Kentucky, United States.
- Taylor, C.J., 2021b, Photographs depicting rock core, fractured limestone outcrop, and karst spring, Groundwater Hydrologist and Water Resources Section Head, Kentucky Geological Survey, University of Kentucky, Lexington, Kentucky, United States.
- Taylor, C.J., 2021c, Field photographs of well borehole in karstic limestone aquifer, Elizabethtown, Kentucky, Groundwater Hydrologist and Water Resources Section Head, Kentucky Geological Survey, University of Kentucky, Lexington, Kentucky, United States.



- Taylor, C.J., 2021d, Field photograph of rock outcropping showing karst features, Groundwater Hydrologist and Water Resources Section Head, Kentucky Geological Survey, University of Kentucky, Lexington, Kentucky, United States.
- Taylor, C.J., 2021e, Field photographs of fluorescent dye injections, Groundwater Hydrologist and Water Resources Section Head, Kentucky Geological Survey, University of Kentucky, Lexington, Kentucky, United States.
- Taylor, C.J., and E.A. Greene, 2008, Hydrogeologic characterization and methods used in the investigation of karst hydrology *in* Field techniques for estimating water fluxes between surface water and ground water, editors, D.O. Rosenberry and J.W. LaBaugh. United States Geological Survey, pages 71-114, <https://pubs.usgs.gov/tm/04d02/pdf/TM4-D2-chap3.pdf>.
- Taylor, C.J., and Doctor, D. 2017, Karst *in* Handbook of Applied Hydrology, editor, V.P. Singh, Second Edition, McGraw-Hill, pages 89-1 to 89-14.
- Taylor, C.J., and G.K. McCombs, 1998, Recharge-area delineation and hydrology, McCracken Springs, Fort Knox Military Reservation, Meade County, Kentucky. United States Geological Survey, Water-Resources Investigations Report 98-4196, over size map sheet, <http://pubs.er.usgs.gov/publication/wri984196>.
- Taylor, C.J., and H.L. Nelson Jr., 2008, A compilation of provisional karst geospatial data for the Interior Low Plateaus physiographic region, central United States. United States Geological Survey, Data Series 339, <https://pubs.usgs.gov/ds/339/>.
- Deutsch, G., 1993, An extended double-porosity concept as a practical modeling approach for a karstified terrain *in* Hydrogeological processes in karst terrains: Proceedings of the Antalya Symposium and Field Seminar, editors, J. Gultekin and W. Back. International Association of Hydrological Sciences, volume 207, pages 281-292, <http://www.speleogenesis.info/directory/karstbase/publication.php?id=8077>.
- Deutsch, G., and M. Sauter, 1991, Groundwater modeling in karst terranes-Scale effects, data acquisition, and field validation. Third Conference on Hydrogeology, Monitoring, and Management of Groundwater in Karst Terranes, Nashville, Tennessee, USA, pages 17-35, <https://nepis.epa.gov/Exe/ZyPDF.cgi/9100NMJR.PDF?Dockey=9100NMJR.PDF>.
- Deutsch, G., and M. Sauter, 1998, Distributed parameter modelling approaches in karst hydrological investigations. Bulletin d'Hydrogeologie, volume 16, pages 99-110, <http://pascal-francis.inist.fr/vibad/index.php?action=getRecordDetail&idt=6220844>.
- Theis, C.V., 1935, The relation between the lowering of the piezometric surface and the rate and duration of discharge of a well using ground water storage. Transaction of American Geophysical Union, volume 16, issue 2, pages 519-524, <https://doi.org/10.1029/TR016i002p00519>.
- Thraillkill, J., 1968, Chemical and hydrologic factors in the excavation of limestone caves. Geological Society of America Bulletin, volume 79, pages 19-46, [https://doi.org/10.1130/0016-7606\(1968\)79%5b19:CAHFIT%5d2.0.CO;2](https://doi.org/10.1130/0016-7606(1968)79%5b19:CAHFIT%5d2.0.CO;2).

- Toomey, R.S., H.H. Hobbs, and R.A. Olson, 2017, An orientation to Mammoth Cave and this volume *in* Mammoth Cave, editors, H. Hobbs III, R. Olson, E. Winkler, and D. Culver. Cave and Karst Systems of the World, Springer, Cham, [https://doi.org/10.1007/978-3-319-53718-4\\_1](https://doi.org/10.1007/978-3-319-53718-4_1) ↗.
- Toth, J., 1963, A theoretical analysis of groundwater flow in small drainage basins. *Journal of Geophysical Research*, volume 68, issue 16, pages 4795-4812, <https://doi.org/10.1029/JZ068i016p04795> ↗.
- Trcek, B., 2007, How can the epikarst zone influence the karst aquifer behavior? *Environmental Geology*, volume 51, pages 761-765, <https://doi.org/10.1007/s00254-006-0387-x> ↗.
- Trichakis, I.C., I.K. Nikolos, and G.P. Karatzas, 2009, Artificial neural network (ANN) based modeling for karstic groundwater level simulation. *Water Resources Management*, volume 25, issue 4, pages 1143-1152, <https://doi.org/10.1007/s11269-010-9628-6> ↗.
- Tucci, P., 2011, Field Trip photograph of a spring that flows out of base of cliff and forms a creek that flows into the Buffalo River, Arkansas taken in April 28, 2011. Retired Central Region Groundwater Specialist, United States Geological Survey, Denver, Colorado, United States.
- USEPA, 1991, United States Environmental Protection Agency, Secondary drinking water standards, EPA 570/9-91-019FS, <https://www.epa.gov/sdwa/secondary-drinking-water-standards-guidance-nuisance-chemicals> ↗.
- USEPA, 2002, United States Environmental Protection Agency, A lexicon of cave and karst terminology with special reference to environmental karst hydrology. Office of Research and Development, National Center for Environmental Assessment, Washington Office, Washington, DC, USA, <https://cfpub.epa.gov/ncea/risk/era/recordisplay.cfm?deid=54964> ↗.
- USEPA, 2009, United States Environmental Protection Agency, National primary drinking water regulations, <https://www.epa.gov/ground-water-and-drinking-water/national-primary-drinking-water-regulations> ↗.
- USEPA, 2021, United States Environmental Protection Agency, National primary drinking water standards, <https://www.federalregister.gov/documents/2001/01/22/01-1668/national-primary-drinking-water-regulations-arsenic-and-clarifications-to-compliance-and-new-source> ↗.
- USGS Website, 2021, Geology and Ecology of National Parks, Mammoth Cave National Park, United States Geological Survey, <https://www.usgs.gov/science-support/osqi/yes/national-parks/mammoth-cave-national-park> ↗.
- Vacher, H.L., and J.E. Mylroie, 2002, Eogenetic karst from the perspective of an equivalent porous medium. *Carbonates and Evaporites*, volume 17, number 2, pages 182-196, <https://doi.org/10.1007/BF03176484> ↗.

- Vennard, J.K., and R.L. Street, 1975, Elementary fluid mechanics. John Wiley, New York, USA, 740 pages.
- Vesper, D.J., C.M. Loop, and W.B. White, 2001, Contaminant transport in karst aquifers. *Theoretical and Applied Karstology*, issues 13-14, pages 101-111, <http://www.speleogenesis.info/journal/publication.php?id=4490>.
- Wacker, M.A., K.J. Cunningham, and J.H. Williams, 2014, Geologic and hydrogeologic frameworks of the Biscayne Aquifer in central Miami-Dade County, Florida. United States Geological Survey, Scientific Investigations Report 2014-5138, <http://dx.doi.org/10.3133/sir20145138>.
- Waltham, T., F.G. Bell, and M. Culshaw, 2005, Sinkholes and subsidence. *Karst and cavernous rocks in engineering and construction Book Series*, Springer-Praxis Books in Geophysical Sciences, Springer, Heidelberg, Germany, 384 pages, <https://doi.org/10.1007/b138363>.
- Wanakule, N., 1988, Regression analysis of the San Marcos Spring flows and water levels of the index well in San Antonio. Southwest Texas University, Edwards Aquifer Research and Data Center, 34 pages.
- Wanakule, N., and R. Anaya, 1993, A lumped parameter model for the Edwards Aquifer. Texas A&M University, Texas Water Resources Institute, Technical Report number 163, 84 pages, <https://hdl.handle.net/1969.1/6172>.
- Water Science School, 2021, How groundwater occurs. United States Geological Survey, Aquifers and Groundwater, accessed January 2022 at [https://www.usgs.gov/special-topic/water-science-school/science/aquifers-and-groundwater?qt-science\\_center\\_objects=0#qt-science\\_center\\_objects](https://www.usgs.gov/special-topic/water-science-school/science/aquifers-and-groundwater?qt-science_center_objects=0#qt-science_center_objects).
- Watkins Jr., D.W., and D.C. McKinney, 1999, Screening water supply options for the Edwards Aquifer region in central Texas. *Journal of Water Resources Planning and Management*, volume 125, issue 1, pages 14-24, accessed January 2022 at <https://ascelibrary.org/doi/10.1061/%28ASCE%290733-9496%281999%29125%3A1%2814%29>.
- White, W.B., 1988, *Geomorphology and hydrology of karst terrains*, Oxford University Press, Oxford, United Kingdom and New York, USA, 464 pages.
- White, W.B., 1993, Analysis of karst aquifers *in* Regional ground-water quality, editor, W.M. Alley. Van Nostrand Reinhold, New York, USA, pages 471-489.
- White, W.B., 1999, Conceptual models for karstic aquifers *in* Karst modeling, editors, A.N. Palmer, M.V. Palmer, and I.D. Sasowsky. Karst Waters Institute, Special Publication volume 5, pages 11-16, <https://apps.dtic.mil/sti/pdfs/ADA369937.pdf#page=19>.
- White, W.B., 2016, Groundwater Flow in Karst Aquifers *in* The Handbook of Groundwater Engineering, Third Edition, 25 November 2016, pages 563-595, <https://www.routledge.com/The-Handbook-of-Groundwater-Engineering/Cushman-Tartakovsky/p/book/9781498703048>.

- White, W.B., 2019, Hydrogeology of Karst aquifers *in* Encyclopedia of Caves, Third Edition, Chapter 64, editors, W.B. White, D.C. Culver, and T. Pipan. Academic Press, pages 537-545, <https://doi.org/10.1016/B9780128141243.000649>.
- White, W.B., and E.L. White, 1989, Karst hydrology: Concepts from the Mammoth Cave area. Van Nostrand Reinhold, New York, USA, 346 pages, <https://link.springer.com/book/10.1007/978-1-4615-7317-3>.
- White, W.B., J.S. Herman, E.K. Herman, and M. Rutigliano, 2018, Karst Groundwater Contamination and Public Health: Beyond Case Studies. Advances in Karst Science Series, Springer International Publishing, 347pages, <https://www.springer.com/gp/book/9783319510699>.
- Wicks, C.M., and J.A. Hoke, 2000, Prediction of the quality and quantity of Maramec spring water. Groundwater, volume 38, issue 2, pages 218-225, <https://doi.org/10.1111/j.1745-6584.2000.tb00333.x>.
- Williams, H., J.B. Cowart, and J.D. Arthur, 2002, Florida Aquifer Storage and Recovery (ASR) Geochemical Project: Year One and Two Progress Report. Florida Geological Survey, volume 100, 131 pages.
- Williams, L.J., and E.L. Kuniansky, 2016, Revised hydrogeologic framework of the Floridan aquifer system in Florida and parts of Georgia, Alabama, and South Carolina. United States Geological Survey, Professional Paper 1807, <https://pubs.usgs.gov/pp/1807/>.
- Winter, T.C., J.W. Harvey, O.L. Franke, and W.M. Alley, 1998, Ground water and surface water: A single resource. United States Geological Survey, Circular 1139, 87 pages, <https://pubs.usgs.gov/circ/circ1139/>
- Wolfe, W.J., C.J. Haugh, A. Webbers, and T.H. Diehl, 1997, Preliminary conceptual models of the occurrence, fate, and transport of chlorinated solvents in the karst regions of Tennessee. United States Geological Survey, Water-Resources Investigations Report 97-4097, <https://pubs.usgs.gov/wri/wri974097/new4097.pdf>.
- Wolff, R.G., 1982, Physical properties of rocks—Porosity, permeability, distribution coefficients, and dispersivity. United States Geological Survey, Open-File Report 82-166, <https://doi.org/10.3133/ofr82166>.
- Wong, C.I., B.J. Mahler, M. Musgrove, J.L. Banner, 2012, Changes in sources and storage in a karst aquifer during a transition from drought to wet conditions. Journal of Hydrology, volume 468-469, pages 159-172, <https://doi.org/10.1016/j.jhydrol.2012.08.030>.
- Wood, W.W., 1985, Origin of caves and other solution openings in the unsaturated (vadose) zone of carbonate rocks, a model for CO<sub>2</sub> generation. Geology, volume 13, issue 11, pages 822-824, [https://doi.org/10.1130/0091-7613\(1985\)13<822:OOCAS>2.0.CO;2](https://doi.org/10.1130/0091-7613(1985)13<822:OOCAS>2.0.CO;2).

- Wood, W.W., and J. Cherry, 2021, Written personal communication of a draft illustration for a book titled “Introduction to Groundwater Geochemistry” which is in preparation for The Groundwater Project, Guelph, Ontario, Canada.
- Wood, W.W., and M.J. Petraitis, 1984, Origin and distribution of carbon dioxide in the unsaturated zone of the Southern High Plains of Texas. *Water Resources Research*, volume 20, issue 9, pages 1193-1208, [doi.org/10.1029/WR020i009p01193](https://doi.org/10.1029/WR020i009p01193).
- Worthington, S.R.H., 1991, Karst hydrology of the Canadian Rocky Mountains: Hamilton, Ontario, Canada. McMaster University, unpublished Doctor of Philosophy dissertation, 380 pages, <http://hdl.handle.net/11375/8329>.
- Worthington, S.R.H., 2005, Evolution of caves in response to base-level lowering. *Cave and Karst Science*, volume 32, issue 1, pages 2-12, [https://www.researchgate.net/publication/282947188\\_Evolution\\_of\\_caves\\_in\\_response\\_to\\_base-level\\_lowering](https://www.researchgate.net/publication/282947188_Evolution_of_caves_in_response_to_base-level_lowering).
- Worthington, S.R.H., G.J. Davies, and D.C. Ford, 2000, Matrix, fracture and channel components of storage and flow in a Paleozoic limestone aquifer *in* Groundwater flow and contaminant transport in carbonate aquifers, editors, I.D. Sasowsky and C.M. Wicks, Rotterdam, Netherlands, A.A. Balkema, pages 113-128, <http://pascal-francis.inist.fr/vibad/index.php?action=getRecordDetail&idt=6190929>.
- Worthington, S.R.H., P.Y. Jeannin, E.C. Alexander Jr., G.J. Davies, and G.M. Schindel, 2017, Contrasting definitions for the term ‘karst aquifer’. *Hydrogeology Journal*, volume 25, pages 1237-1240, <https://doi.org/10.1007/s10040-017-1628-7>.
- Worthington, S.R.H., and C.C. Smart, 2003, Empirical determination of tracer mass for sink to spring tests in karst *in* Sinkholes and the engineering and environmental impacts on karst, editor, B.F. Beck. American Society of Civil Engineers, Geotechnical Special Publication number 122, pages 287-295, [doi.org/10.1061/40698\(2003\)26](https://doi.org/10.1061/40698(2003)26).
- Worthington, S.R.H., C.C. Smart, and W.W. Ruland, 2002, Assessment of groundwater velocities to the municipal wells at Walkerton. *Ground and Water: Theory to Practice*, pages 1081-1086, <https://www.researchgate.net/publication/282947211>.
- Zhang, B., and D.N. Lerner, 2000, Modeling of ground water flow to adits. *Groundwater*, volume 38, issue 1, pages 99-105, <https://doi.org/10.1111/j.1745-6584.2000.tb00206.x>.
- Zhou, W., 2007, Drainage and flooding in karst terranes. *Environmental Geology*, volume 51, pages 963-973, <https://doi.org/10.1007/s00254-006-0365-3>.
- Zimmerman, R.W., A. Al-Yaarubi, C.C. Pain, and C.A. Grattoni, 2004, Non-linear regimes of fluid flow in rock fractures. *International Journal of Rock Mechanics and Mining Sciences*, volume 41, supplement 1, pages 163-169, <https://doi.org/10.1016/j.ijrmms.2004.03.036>.

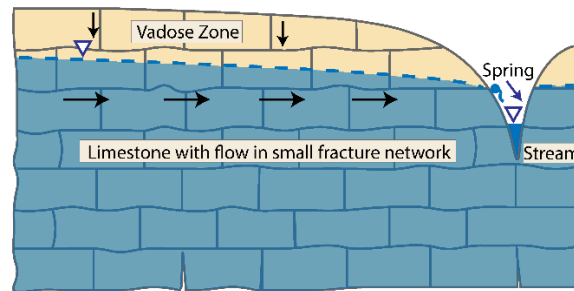


# 11 Boxes

## Box 1 Stages from Fracture Flow to Conduit Flow

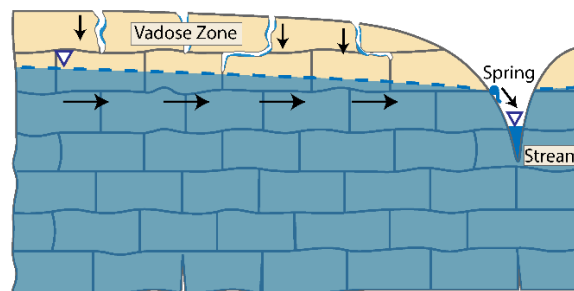
As mentioned in Section 2.3 and displayed in Figure 5, when the water table drops during short-term drought or longer-term minor changes in climate, the *vadose-zone* karstification processes function at greater depth and when the water table rises, groundwater flows in solution openings formed under the earlier saturated and unsaturated conditions. Erosion along stream channels also lowers the water table over time by opening spring outlets at lower elevations. Additionally, as the water table rises and falls seasonally, this results in more mixing of water and increases dissolution at that current relative position of the water table. The Stages of development are described in more detail in this Box.

### Stage 1



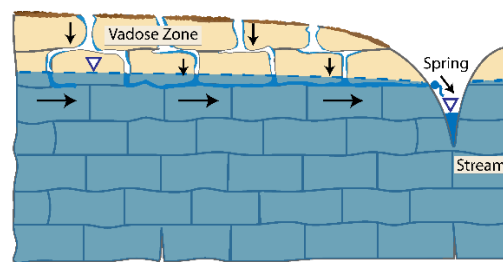
The evolution of the karst starts when the new limestone landscape is created from structural forces within the Earth's crust while a network of fractures forms with bedding plane fractures and vertical joints that provide pathways for an active, gravity driven groundwater flow system to develop. This example shows an established water table and a hill slope spring above the valley-bottom stream. Initially, water that infiltrates through the vadose zone has minimal geochemical aggressivity because the dissolved carbon dioxide ( $\text{CO}_2$ ) in the water is in equilibrium with the above ground atmospheric  $\text{CO}_2$  partial pressure ( $\text{pCO}_2 \sim 10^{-3.5}$  atmospheres). Additionally, groundwater flow is slow as the initial fractures are small and dissolution has not progressed.

### Stage 2



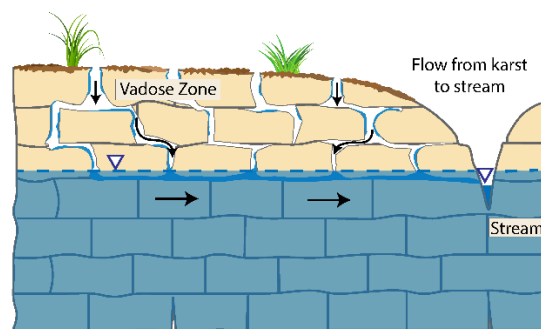
Soil and vegetation form at the surface converting the barren landscape into an active ecological system and dissolution is increasing fracture openings and through-flow. Henceforth  $\text{CO}_2$  is produced in the subsurface, both in the surficial organic soil zone and throughout the vadose zone as particulate and dissolved labile organic matter is dispersed throughout the vadose zone down to the water table. This partial pressure of  $\text{CO}_2$  is substantially elevated in the fracture network. Therefore, the water that infiltrates through the vadose zone becomes chemically aggressive with carbonic acid ( $\text{H}_2\text{CO}_3$ ) that dissolves the mineral calcite ( $\text{CaCO}_3$ ) which makes up the limestone. In this stage, solution channels begin to form and karstification is initiated, however until channels become connected to drainage outlets, the rate of karstification is minimal and the water table remains near the land surface.

### Stage 3



Solution channels at, or slightly below, the water table are connected to form a drainage outlet at a spring along the hill slope so that the spring feeds the stream. Less rainfall goes to the stream by surface runoff and more by subsurface channel flow and the water's capability to enlarge channels increases. As channel connectivity increases,  $\text{CO}_2$  emanating from the soil zone and the organic matter are transported deeper causing chemically aggressive water to spread farther and deeper. The water table declines nearly to the stream level because the bulk permeability in the channel network in the vadose zone is now so much larger than in the underlying fractured limestone.

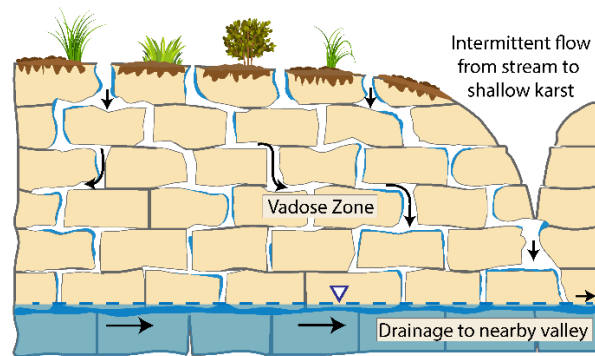
### Stage 4



The process of channel formation penetrates deeper and horizontal channels along bedding planes form with connections to the stream at which time the spring above the stream dries up. The volume of void space occupied by solution channels in the vadose

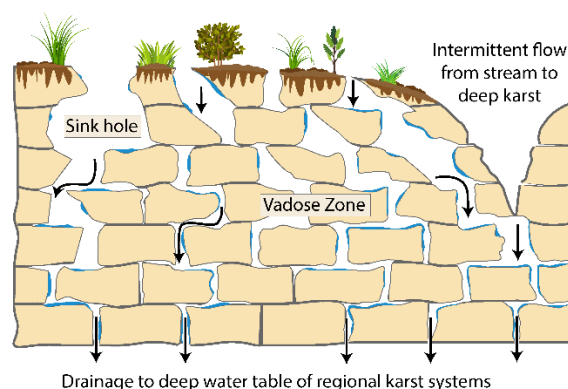
zone continues to increase because of the generation and spread of  $\text{CO}_2$  gas that immediately forms carbonic acid in the water wherever the  $\text{CO}_2$  spreads. The water discharging at the spring gives off  $\text{CO}_2$  into the atmosphere because the partial pressure of the  $\text{CO}_2$  in the subsurface water is much higher than that of the atmosphere. This off-gassing causes  $\text{CaCO}_3$  minerals to form at the spring. In this stage the water table drops to near stream level. If there were to be a relatively insoluble geologic stratum such as shale or mudstone at or near the elevation of the stream bed, then the karstification process would not penetrate deeper. However, in this illustrative example, there is only limestone and hence no stratigraphic constraint to the depth of penetration of this channel forming process over geologic time.

### Stage 5



The channel formation process continues deeper and eventually a channel pathway forms that drains all the local water to outlets beyond the stream valley and hence the local water table drops below the stream level and the stream changes from a gaining stream to a losing stream. The stream may have flow in response to surface runoff from rainfall events, but this water quickly disappears downward through vertical channels to flow to a deeper valley some distance away. This elevation of this distant valley now governs the karst flow system.

### Stage 6



The valley that now governs the depth of penetration of the karst flow system is at a lower elevation even farther away, hence outside of this field of view, such that this local karst flow system drains out the bottom of the figure to its primary drainage outlet in a distant valley at lower elevation. The process of karst deepening continues through geologic time so that some cave systems extend as deep as a kilometer or more. Nothing limits the depth of evolution of a cave system over geologic time except a geological stratum that is relatively insoluble such as shale, sandstone or granite or limits on the depths of valleys available to serve as the base level for the subsurface drainage system.

[Return to where text links to Box 1](#)↑

## 12 Abbreviated Glossary of Karst and Groundwater Terminology

This glossary includes terms used in this book. A more complete lexicon of karst terminology is provided by the United States Environmental Protection Agency (USEPA, 2002).

### Allogenic Recharge

Recharge contributed by surface runoff carried into the karst aquifer by sinking or disappearing streams, but which originates through precipitation falling on areas underlain by non-karstic bedrocks. Allogenic recharge contributions and the catchment areas they derive from must be included in the water budget for karst aquifers even though they are geographically and geologically outside the physical boundaries of the karst system.

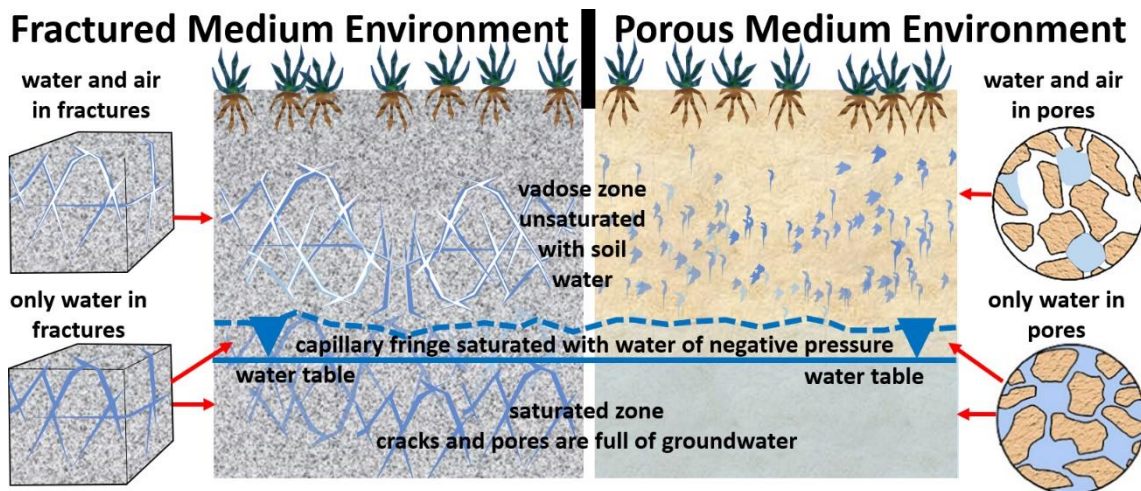
### Autogenic Recharge

Recharge originating from infiltration of precipitation that falls on the area directly underlain by the karst aquifer, or from underground diversion of surface runoff that accumulated within the geographic boundaries of the area underlain only by the karstified bedrock.

### Capillary Fringe

This is the saturated zone above a water table in which water pressure is less than atmospheric. The water table is defined by the surface below the capillary fringe where the water is at atmospheric pressure. Below the water table, pressure is greater than atmospheric. Where, in the capillary fringe, molecular forces between water molecules and the rock surface hold water via surface tension onto the pore walls. The thickness of the capillary fringe varies and decreases in thickness as pore diameters increase, but is generally less than 1 m thick. Figure Glossary-1 shows the vadose (unsaturated) zone and the phreatic (saturated) zone of a water table aquifer with insets showing the capillary zone in creviced rock and gravel rock.





**Figure Glossary-1** Illustration of the interface between the vadose and phreatic zones. Modified from Poeter and others (2020).

## Carbonates

Sedimentary rocks composed of at least 50 percent carbonate minerals that are often cemented. Carbonate minerals include calcite or aragonite (different forms of calcium carbonate), dolomite, many phosphate and sulfate minerals. The predominant mineral in limestones is calcium carbonate ( $\text{CaCO}_3$ ). The predominant mineral in dolostone formations is dolomite-calcium magnesium carbonate ( $\text{CaMg}(\text{CO}_3)_2$ ). These tend to be layered sedimentary rocks that accumulate from chemical precipitation of carbonate minerals or the accumulation of shells, reef and atoll structures in coastal or marine environments. Carbonates can also form by calcite precipitation from inland waters forming rocks called tufa.

## CO<sub>2</sub> Partial Pressure

Dalton's law of partial pressures states that in a mixture of non-reacting gases, the total pressure exerted is equal to the sum of the partial pressures of the individual gases if the independent gas alone occupied the entire volume of the original mixture at the same temperature. It is important to note that the gas pressure is a function of temperature. Additionally, in the earth's atmosphere the total pressure decreases with altitude.

$$\text{Dalton's Law of Partial Pressure: } P_{\text{Total}} = P_{\text{gas1}} + P_{\text{gas2}} + P_{\text{gas3}} \dots$$

The pressure exerted by an individual gas in a mixture of gasses is known as its partial pressure.

## Diagenetic Processes

The processes involved in the physical and chemical changes in sediments first caused by water-rock interactions, microbial activity and compaction after their deposition, but before lithification.

## Dissolved Solids (or TDS—Total Dissolved Solids)

It is a measure of the concentration of all organic and inorganic dissolved substances (like minerals, metals, and salts) present in a water. Generally reported in milligrams per liter (mg/L).

## Eogenetic Karst Aquifer

Karst aquifers composed of younger, near-surface carbonates that generally have higher matrix porosity and permeability than deeply buried carbonates. They were never deeply buried. Eogenetic karst could also be described as an epigene karst aquifer.

## Epigene Karst Aquifer

Shallower karst aquifers formed by aggressive recharge descending from the land surface, as a consequence of the infiltration of precipitation, subsurface diversion of stormwater runoff and surface stream flow via sinks, and the subsequent movement of groundwater via karst features. These processes can occur with eogenetic and telogenetic karst aquifers as telogenetic refers to a carbonate that was buried, its porosity reduced and then uplifted to expose the aquifer to surface processes that may increase dissolution along fractures and bedding planes. An eogenetic karst aquifer has never been compacted via burial.

## Epikarst

The uppermost weathered zone of carbonate rocks that possesses substantially enhanced porosity and permeability relative to the deeper parts of the rock mass. Epikarst stores and intermittently distributes infiltrated recharge water to the underlying karst aquifer's unsaturated zone. It is an important water storage system that functions as a perched, leaky aquifer. Some studies suggest that water storage in the epikarst can be more significant than storage in the saturated zone of the karst aquifer.

## Estavelle

An open ground orifice that supports flow both into and out of the groundwater system. It can be a sink hole that is not along a stream or can occur beneath a stream channel.

## Evaporites

Layered crystalline sedimentary rocks that form from brines generated in areas where the amount of water lost by evaporation exceeds the total amount of water from rainfall and influx via rivers and streams. The mineral composition includes carbonates (especially calcite, dolomite, magnesite, and aragonite), sulfates (anhydrite and gypsum), and chlorides (particularly halite, sylvite, and carnallite), as well as various borates, silicates, nitrates, and sulfocarbonates. All evaporitic rocks are water soluble to varying degree.

## Geomorphic Period

Geomorphology is the study of the origin and evolution of topography and bathymetry. Sometimes described as the study of landforms and landscapes. A period predominated by erosion over decades or centuries could be described as a geomorphic period.

## Hydraulic Conductivity

In groundwater, a constant of proportionality, symbolized by the letter  $K$ . It is a coefficient in Darcy's law as shown here:

$$Q = -KA(\Delta h/\Delta L)$$

where:

$Q$  = rate of water flow ( $L^3T^{-1}$ )

$K$  = hydraulic conductivity ( $LT^{-1}$ )

$A$  = column cross-sectional area ( $L^2$ )

$\Delta h/\Delta L$  = head gradient across the column of length  $L$  (dimensionless)

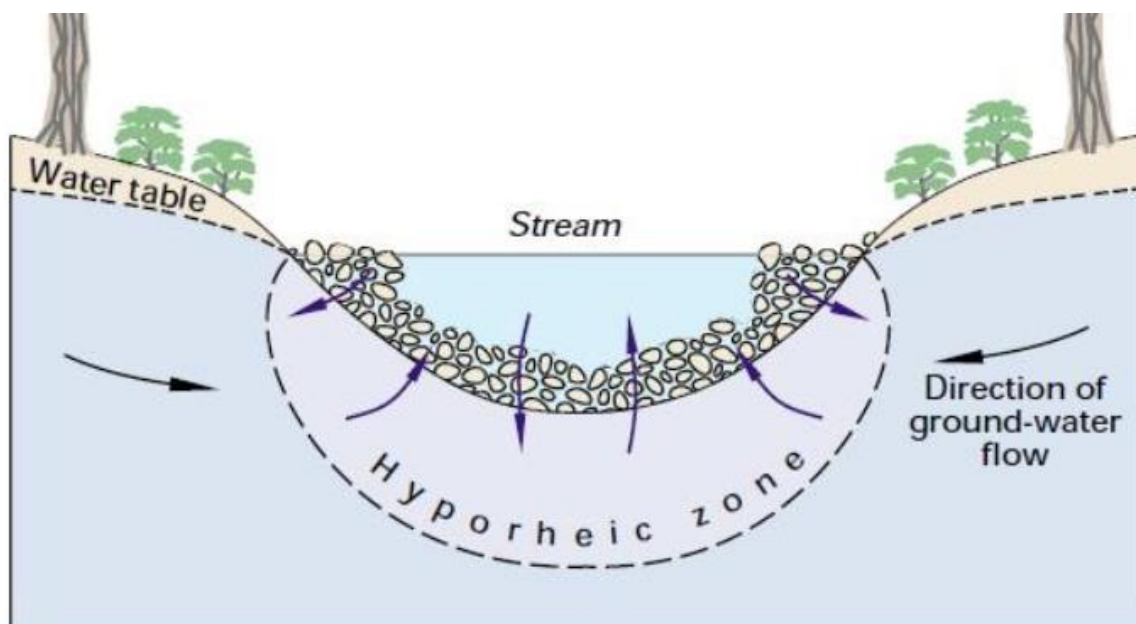
This is illustrated by Figure 33 and discussed in Section 4.1 of this book.

## Hypogene Karst Aquifer

Deeper karst aquifers formed in the subsurface by aggressive recharge moving upward from ground water under artesian conditions. Hypogene karst is generally located in, or near, regions of tectonic, volcanic, or high-temperature geothermal activity past or present.

## Hyporheic Zone

The layer of streambed where exchange or cycling occurs between groundwater and surface water and considered important in stream nutrient cycling, in moderating stream temperature regimes, and in creating unique habitats within streams (Figure Glossary-2).

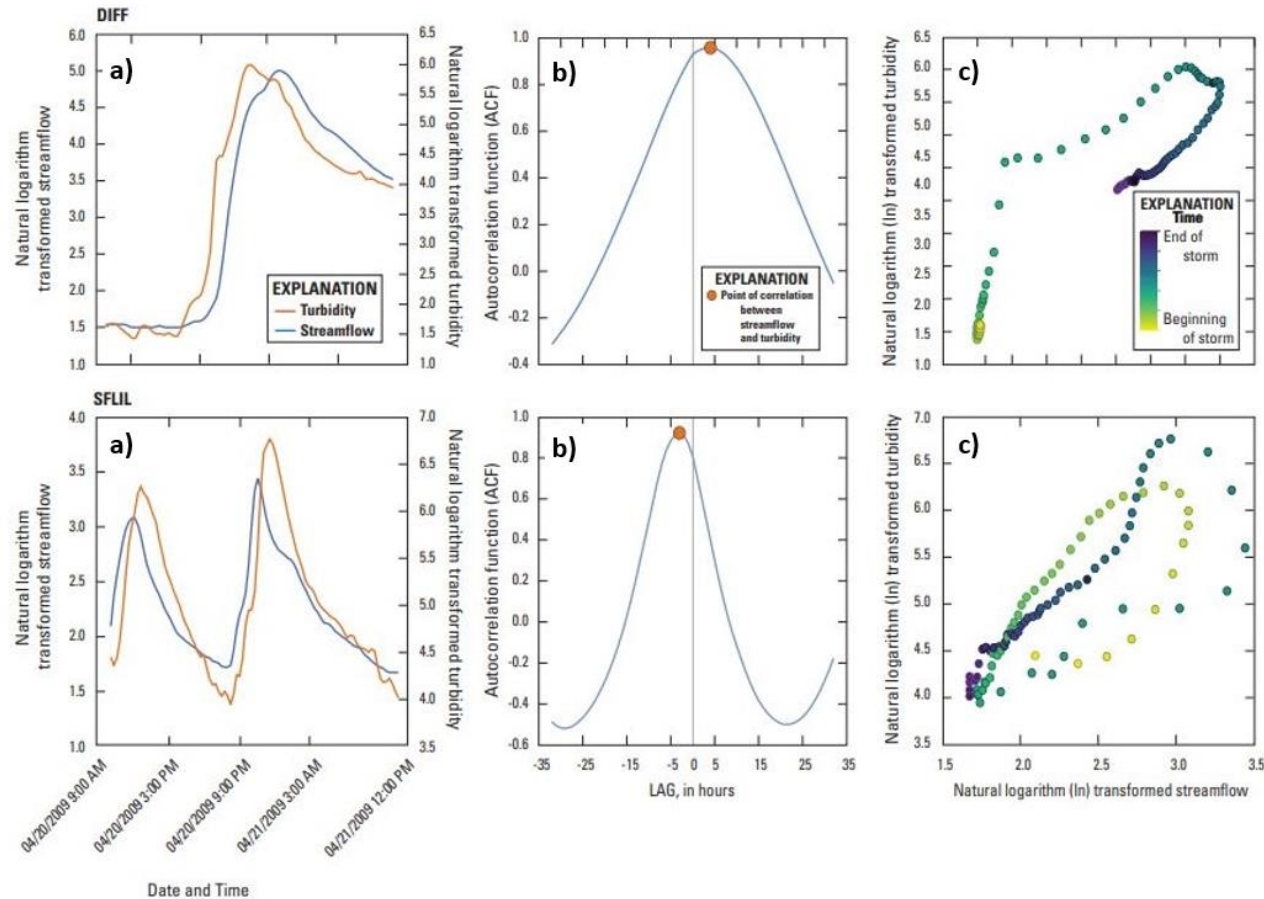


**Figure Glossary-2** – Hyporheic zone, from Winter and others (1998).

## Hysteresis

Hysteresis occurs when a system's output is based on its history. For example, concentration of a chemical constituent increases more rapidly during the increase of discharge from a storm (rising limb) and decreases more slowly during the recession period (falling limb) at a spring or river. There are many definitions of hysteresis as the phenomenon is noted in many natural and engineered systems and the definition is often context dependent. In hydrology soil moisture tension, river discharge, and suspended sediment concentration exhibit hysteresis. Hysteresis plots have different forms that depend on their context. In the example above, a hysteresis plot of the chemical-concentration time series will form a loop.

Figure Glossary-2 shows an example of hysteresis with turbidity and streamflow data. These data are not from a karst area, but this is illustrative by using a) a natural-logarithm, transformed streamflow and turbidity time series; then b) a plot of an autocorrelation function indicating time lags between the streamflow and turbidity; and finally, c) the hysteresis loop when the log streamflow (y-axis) and log turbidity (x-axis) are plotted together. The data comes from two sites (DIFF and SFLIL), but the sites are not important—rather it is important to understand that the DIFF site has a clockwise hysteresis loop from beginning to end of the storm and the SFLIL site has two storm events plotted together on one graph and two counterclockwise loops. These two sites behave quite differently with respect to the relationship between time lag between rising storm peak and turbidity peak.



**Figure Glossary 3** - Example of hysteresis with turbidity and streamflow data from two different stream sites labeled DIFF and SFLIL: a) natural logarithm, transformed streamflow and turbidity time series; b) autocorrelation function indicating time lags between the streamflow and turbidity; and, c) hysteresis loop with log turbidity (y-axis) and log streamflow (x-axis). For the DIFF site, turbidity peaks before streamflow peaks (top a); autocorrelation (top b) indicates a positive time lag; and hysteresis (top c) loops in a clockwise manner. Thus, for the DIFF site, in-channel material and streambank erosion are the dominant sources of suspended solids. Two storms are shown for the SFLIL site (bottom a) and turbidity peaks after the streamflow peak for both storms indicating the same negative time lag for both storms (bottom b); the hysteresis loops are counterclockwise (bottom c). Thus, for the SFLIL site, upland material and erosion of upper streambanks are important components of the suspended solids. From Porter and others (2020).



## Karst Window

A large surface opening that allows the aquifer to be directly exposed to land surface. Generally formed by the collapse of the ground surface into a conduit forming a sink hole which is a window to underground flow in the karst aquifer.

## Mesogenetic Karst Aquifer

Aquifers generally composed of deeply buried older carbonate rocks that experienced karstification before burial with matrix porosity and permeability reduced during burial.

## Newtonian Fluid

Newtonian fluids are named after Isaac Newton, who first used the differential equation describing the relation between the shear strain rate and shear stress for such fluids. This differential equation is the simplest mathematical model of fluids that accounts for viscosity. While no fluid fits the definition perfectly, many common liquids and gases, such as water and air, can be assumed to be Newtonian for practical calculations under ordinary conditions. A Newtonian fluid has a constant viscosity tensor that does not depend on the stress state and velocity of the flow. If the fluid is also isotropic (that is, its mechanical properties are the same along any direction), the viscosity tensor reduces to two coefficients, describing the fluid's resistance to continuous shear deformation and continuous compression (or expansion), respectively.

## Non-Point Source

A source of contaminants that comes from widely distributed or pervasive environmental elements, such as the diffuse source of bacteria and nutrients from pastures, or fertilizers and pesticides applied over agricultural fields or golf courses.

## Phreatic Zone (Zone of Saturation or Saturated Zone)

Part of an aquifer below the water table in which pores and fractures are saturated with water. Immediately above the water table is the capillary fringe (a saturated zone of negative pressure owing to surface tension between the solid matrix and water molecules). Above the capillary fringe is the vadose zone. The phreatic zone size and depth may fluctuate with changes of season, and during wet and dry periods. See Figure Glossary-1.

## Point Source

A source of contamination that comes from a fixed-point location, such as a sewage outfall to a stream or a leaking oil or gas well.

## Post-Depositional Structural Deformation

Sedimentary rocks tend to be deposited in horizontal layers and can be deformed after deposition (post-depositional). Any changes to the layering of the rock are termed deformation. Deformation can be caused by desiccation causing cracks; or by dewatering or volcanic/tectonic events causing faulting and folding.

## Sinkhole

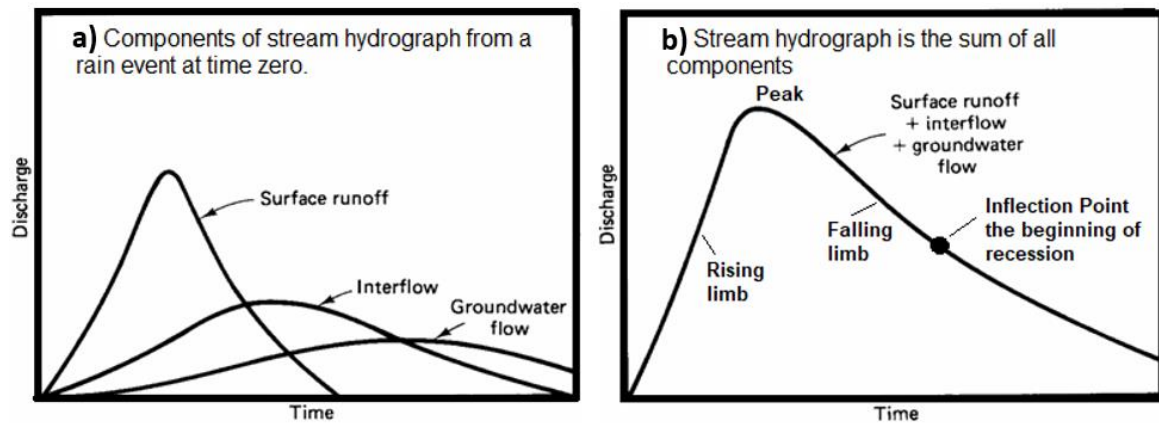
An area of ground that has no natural external surface drainage — when it rains, the water stays inside the sinkhole and typically drains into the subsurface. Sinkholes can vary from a few meters across to hundreds of kilometers and are typically between 1 and 30 m deep. Some are shaped like shallow bowls or saucers whereas others have vertical walls; some hold water and form natural ponds. Some allow surface runoff to directly enter a karst conduit system. Sink holes can be a *Karst Window* or *Swallet (Throat or Swallow Hole)*.

## Swallet (Throat or Swallow Hole)

A place in a limestone stream channel where water disappears underground into a small sinkhole that may be called a snake hole. Swallets are generally smaller than most sinkholes or karst windows. In the latter, all streamflow diverts underground during times of minimal overland runoff.

## Stream Discharge Hydrograph

A graph showing the rate of flow (volumetric discharge) versus time past a specific point in a river, channel, or conduit (Figure Glossary-4). The components contributing to a stream hydrograph are surface runoff, interflow, and groundwater flow. Surface runoff is the overland runoff that occurs when the rate of rainfall exceeds the infiltration capacity of the soil and surface depressions are full. Interflow is the lateral flow of water occurring in the unsaturated zone that returns to the surface or a streambed without reaching the saturated zone. Groundwater flow is the component of streamflow that moves into the streambed from the saturated zone of an aquifer.



**Figure Glossary-4** – Example of a stream discharge hydrograph for a single storm with a) showing the flow components that sum together to form the total streamflow as shown in b). The inflection point shown on b) is the beginning of what is called the recession limb of the hydrograph when surface overland flow has ceased, interflow is beginning to recede, and the majority of flow entering the stream is from groundwater.

### Telogenetic Karst Aquifers

Aquifers generally composed of long-buried carbonate rocks now uplifted to near the surface with matrix porosity and permeability reduced owing to deep burial, and/or diagenetic changes (for example, interstitial cementation—a process that can occur without deep burial) that are exposed to weathering and subaerial and subaqueous erosion, creating porosity from dissolution along fractures, joints, and bedding planes. These could also be described as epigene karst aquifers.

### Thermodynamically Saturated

Term used in chemistry for chemical or gas dissolution in water. At a specific temperature and pressure, a gas, for example Oxygen, has a maximum concentration and that is the saturation concentration. For a mineral such as calcite, there is a maximum concentration that can be dissolved into a solution at a specific temperature or pressure.

### Thermodynamically Undersaturated

More gas or chemical can be dissolved into the water at a given temperature and pressure.

### Vadose Zone

Also termed the unsaturated zone, is between the land surface and the top of the phreatic zone, the position at which the groundwater is at atmospheric pressure. Hence, the vadose zone extends from the top of the ground surface to the water table. See Figure Glossary-1.

### Water Salinity

Natural waters contain dissolved solids. The ranges of total dissolved solids (TDS) used for defining the salinity of water in the USA (Stanton et al., 2017) is as follows:

- Fresh: < 1,000 mg/L (milligrams per liter);
- Brackish: 1,000 to 10,000 mg/L; and
- Saline: > 10,000 mg/L of dissolved solids.

Seawater generally has a dissolved-solids concentration of 35,000 mg/L. The secondary maximum contaminant level, a nonmandatory standard that only applies to public water systems in the USA, advises a level of 500 mg/L for dissolved solids (USEPA, 1991), although numerous water supplies exceed this level. Water with dissolved solids levels exceeding 1,000 mg/L is generally considered undesirable for human consumption.

## 13 Exercise Solutions

### Exercise 1 Solution

Carbonate sediments and rocks are composed of greater than 50 percent carbonate minerals ( $\text{CO}_3$ ) and the predominant carbonate mineral is calcium carbonate or limestone ( $\text{CaCO}_3$ ) and next dolomite or dolostone ( $\text{CaMg}(\text{CO}_3)_2$ ). Evaporites are considered sedimentary rocks that form when seawater or lake water evaporates and precipitate out minerals; most commonly gypsum ( $\text{CaSO}_4 \cdot 2\text{H}_2\text{O}$ ) and halite ( $\text{NaCl}$ ), plus other minerals depending on the dissolved chemical composition of the source water. Both rock types can dissolve over time when exposed to water. Often carbonates are deposited in a marine environment, thus, it is common for layers of evaporites to be found within carbonate rock sequences. Evaporite rocks dissolve much more rapidly than carbonate rocks and so are found intact above ground in very arid environments or in layers beneath land surface in saline or hypersaline groundwater (brines).

[Return to Exercise 1](#) ↑

[Return to where text linked to Exercise 1](#) ↑

### Exercise 2 Solution

- a) Solution sinkhole, collapse sinkhole, caprock sinkhole, dropout sinkhole.
- b) Solution sinkhole, collapse sinkhole.
- c) Suffosion sinkhole, buried sinkhole.

[Return to Exercise 2](#) ↑

[Return to where text linked to Exercise 2](#) ↑



## Exercise 3 Solution

*Porosity* is the ratio of pore void volume divided by total volume of a rock and is always less than 1. The term effective porosity refers to the ratio of interconnected void volume to total rock volume and is always smaller than total porosity. In general, the larger the porosity and effective porosity, there is the potential of greater water flow through a rock. Exceptions can occur as in a pure clay mineral, where the sheet minerals of clay have slight electric charge and the slightly charged molecules of water stay trapped within the clay mineral sheets and so the porosity created by the space between mineral sheets actually traps water.

*Permeability* also called intrinsic permeability ( $k$ ) is related to the hydraulic conductivity ( $K$ ) but is a function of only the properties of the porous medium and not the fluid properties.

$$k = K \frac{\mu}{\rho g}$$

where:

$k$  = permeability,  $\text{m}^2$

$K$  = hydraulic conductivity,  $\text{m/s}$

$\mu$  = dynamic viscosity of the fluid, Pascal·s, that is,  $\text{kg}/(\text{ms})$

$\rho$  = density of the fluid,  $\text{kg}/\text{m}^3$

$g$  = acceleration due to gravity,  $\text{m}/\text{s}^2$

*Hydraulic conductivity* is usually calculated from aquifer tests or permeameter tests and based on Darcy's law. It is not uncommon for people use the term permeability when they mean hydraulic conductivity because both relate to how easy a fluid can move through porous media, but it is important not to confuse people and to correctly use the terms.

[Return to Exercise 3](#) ↗

[Return to where text linked to Exercise 3](#) ↗

## Exercise 4 Solution

- There are similar porous zones of rock matrix porosity and zones with larger scattered solution openings that may or may not be from biological activity in Figure 13 of Williams and Kuniansky (2016). Most features and layering of the rocks in both logs are horizontal.
- The greatest difference between the older Floridan aquifer rocks in Figure 13 of Williams and Kuniansky (2016) is the more numerous horizontal bedding plane openings where the entire layer has been dissolved with some a meter thick; whereas the younger Biscayne Aquifer beds (Figure 14 of this book) haven't completely dissolved.
- The unit (Figure 17 of this book) has practically no rock matrix porosity but does have some porosity in solution-enhanced vugs and solution modified fractures and brecciated zones. One concludes that both age of the rock and the length of near surface exposure to meteoric water have a large impact on karstification. Additionally, the depositional environment [shallow sea or deeper sea]; fluid energy at deposition [wave action or fluvial influence near shore or further off shore]; biological activity [reef versus burrowing creatures or shell deposition in large layers]—all of which have a great impact on the relative amount of clays and sands or other impurities within the carbonate or evaporite units, the original porosity at deposition, and their subsequent ability to be dissolved or develop joints after deposition. The subject of carbonate rock formation is a field all its own and there is an excellent textbook on the subject by Scoffin (1987).

[Return to Exercise 4](#) ↑

[Return to where text linked to Exercise 4](#) ↑

## Exercise 5 Solution

$$\text{horizontal } K = \frac{1000 \frac{\text{m}}{\text{d}} (10 \text{ m}) + 1 \frac{\text{m}}{\text{d}} (10 \text{ m})}{20 \text{ m}} = \frac{100010 \frac{\text{m}^2}{\text{d}}}{20 \text{ m}} = 5000.5 \frac{\text{m}}{\text{d}}$$

$$\text{vertical } K = \frac{20 \text{ m}}{\frac{10 \text{ m}}{1000 \frac{\text{m}}{\text{d}}} + \frac{10 \text{ m}}{1 \frac{\text{m}}{\text{d}}}} = \frac{20 \text{ m}}{0.01 \text{ d} + 10 \text{ d}} = 1.98 \frac{\text{m}}{\text{d}}$$

For a three-order of magnitude difference in hydraulic conductivity, horizontal flow is through the more permeable layer and the equivalent  $K$  is dominated by the more permeable layer, while in the vertical direction flow must pass through the low conductivity layer so the equivalent  $K$  is much lower. This is equivalent to the phenomenon of electrical current flowing through resistors in parallel and in series.

[Return to Exercise 5](#) ↑

[Return to where text linked to Exercise 5](#) ↑

## Exercise 6 Solution

When the size of zones with different hydraulic conductivity are small relative to total area, the particles move more evenly, in a manner that is similar to movement in a homogeneous system.

[Return to Exercise 6](#) ↑

[Return to where text linked to Exercise 6](#) ↑

## Exercise 7 Solution

"Intrinsic permeability" or permeability ( $k$ ) is a quantitative property of porous material and is controlled solely by pore geometry. Unlike saturated hydraulic conductivity, intrinsic permeability is independent of fluid viscosity and density. It can be calculated as hydraulic conductivity ( $K$ ) multiplied by the fluid viscosity and divided by fluid density and the gravitational constant. Permeability ( $k$ ) has the dimension of area ( $L^2$ ).

Differences between hydraulic conductivity and intrinsic permeability.

Saturated Hydraulic Conductivity ( $K$ )	Intrinsic Permeability ( $k$ )
Temperature dependent	Temperature independent
Fluid viscosity dependent	Fluid viscosity independent
Changes with change in soil structure	Changes with change in soil structure
Dimensions ( $LT^{-1}$ )	Dimensions ( $L^2$ )
Only applicable under Darcian flow conditions	Independent of flow conditions

[Return to Exercise 7](#) ↑

[Return to where text linked to Exercise 7](#) ↑

## Exercise 8 Solution

Caves and karst systems are very susceptible to contamination. Sediment transport even if not contaminated from human activity can result in poor water quality. However, the article specifically mentions contaminants from land use activities, such as industrial chemicals, pesticides, nutrients, bacteria, and pathogens from raw sewage.

[Return to Exercise 8](#) ↑

[Return to where text linked to Exercise 8](#) ↑

## Exercise 9 Solution

### Part 1

Aquifer types that may have extremely large pores and high hydraulic conductivity, where water can flow at both laminar and turbulent flow conditions include:

- volcanic aquifers with large lava tubes;
- clean well-sorted large gravel point bar deposits (4 cm diameter or greater); and,
- fractured rock with large fracture aperture openings.

### Part 2

Average velocity for radial distances of 0.25, 0.5, 1, 5, and 10 m.												
Aquifer type	Pumping Rate (m <sup>3</sup> /d)	Thickness (m)	Radial Distance in Meters									
			0.25	0.5	1	5	10	0.25	0.5	1	5	10
Area m <sup>2</sup>								Velocity m/d				
Alluvial, K=10 m/d, and average pore diameter 0.005 m	300	10	16	31	63	314	628	19.1	9.55	4.77	0.95	0.48
same	300	50	79	157	314	1571	3142	3.82	1.91	0.95	0.19	0.1
same	300	100	157	314	628	3142	6283	1.91	0.95	0.48	0.1	0.05
Point Bar gravel, K=100 m/d and average pore diameter 0.02 m	1000	10	16	31	63	314	628	63.66	31.83	15.92	3.18	1.59
same	1000	50	79	157	314	1571	3142	12.73	6.37	3.18	0.64	0.32
same	1000	100	157	314	628	3142	6283	6.37	3.18	1.59	0.32	0.16
Sandstone, K=1 m/d and average pore diameter 0.001 m	100	10	16	31	63	314	628	6.37	3.18	1.59	0.32	0.16
same	100	50	79	157	314	1571	3142	1.27	0.64	0.32	0.06	0.03
same	100	100	157	314	628	3142	6283	0.64	0.32	0.16	0.03	0.02

Based on the equation alone, the average velocity is inversely and linearly correlated to both radial distance and thickness as both are used to calculate the cross-sectional surface area perpendicular to flow to the pumping well in a homogeneous aquifer of constant thickness. The cross-sectional area is provided in the answer at each radial distance along with the average velocity. As the thickness increases the area increases and so velocity decreases. Note, hydraulic conductivity is not used in any of the equations.

However, the pumping rate selected is based on knowing typical pumping rates that are possible for these types of confined aquifers, such that there is not too much drawdown at the pumping well.

[Return to Exercise 9](#) ↗

[Return to where text linked to Exercise 9](#) ↗



## Exercise 10 Solution

### Part 1

Temperature changes the viscosity and density of water. Thus, Reynolds did experiments at different temperatures.

### Part 2

The table below shows the calculated Reynolds number for the different aquifer types and at different radial distances from the production wells from [Exercise 9](#).

How to convert centistokes to square meters per second (cSt to m<sup>2</sup>/s):

$$v \text{ m}^2/\text{s} = 1.0 \times 10^{-6} \times v \text{ cSt}$$

*Hint* regarding conversion of units for kinematic viscosity, consider how many square meters per second are in a centistoke: If,  $v \text{ cSt} = 1$ , then  $v \text{ m}^2/\text{s} = 1.0 \times 10^{-6} \times 1 = 1.0 \times 10^{-6} \text{ m}^2/\text{s}$ .

*Note:* a centistoke is a centimeter-gram-second (CGS) unit of kinematic viscosity. Square meter per second (m<sup>2</sup>/s) is a metric unit of kinematic viscosity. At 20° C, water has a kinematic viscosity of approximately 1 centiStoke. To convert “per second” to “per day”, remember 24×60×60 seconds in a day. So, 1 centiStoke is approximately 0.0864 m<sup>2</sup>/d.

Calculated Reynolds number for different aquifer types at different radial distances from production wells.

Aquifer type	Pumping Rate (m <sup>3</sup> /d)	Thickness (m)	Radial Distance in Meters				
			0.25	0.5	1	5	10
Reynold's Number							
Alluvial, K=10 m/d, and average pore diameter 0.005 m	300	10	1.11	0.55	0.28	0.06	0.03
same	300	50	0.22	0.11	0.06	0.01	0.01
same	300	100	0.11	0.06	0.03	0.01	0.003
Point Bar gravel, K=100 m/d and average pore diameter 0.02 m	1000	10	14.74	7.37	3.68	0.74	0.37
same	1000	50	2.95	4.09	2.05	0.41	0.2
same	1000	100	4.09	2.05	1.02	0.2	0.1
Sandstone, K=1 m/d and average pore diameter 0.001 m	100	10	0.074	0.037	0.018	0.004	0.002
same	100	50	0.015	0.007	0.004	0.001	0.0004
same	100	100	0.007	0.004	0.002	0	0.0002

Shaded in blue are any estimated Reynolds numbers greater than one. A value >1 was chosen because when rock samples are tested in a lab, rather than glass spheres, the onset of divergence from Darcy's law often occurs at Reynolds numbers >1. The sandstone

never has an estimated Reynolds number greater than one, so flow is probably never non-Darcian in the sandstone aquifer. The alluvial aquifer may have non-Darcian flow very close to the well bore, but only for a small distance from the well where the velocity is highest. The largest hydraulic conductivity is associated with clean gravel in a large point bar deposit with a  $K$  of 100 m/day and this material may have non-Darcian flow further out into the formation from the well. This exercise reveals that it is possible for non-Darcian or even turbulent flow to occur near water supply wells in rock formations with a hydraulic conductivity  $>10$  m/d. However, this non-Darcian flow will not extend far into the formation unless the hydraulic conductivity is 100 m/d or greater. These are estimated Reynolds numbers because for groundwater it is not easy to know the average pore diameter within a hydrogeologic unit. For granular aquifers, grain-size distribution via sieve analysis and total porosity estimates are commonly conducted. In sieve analysis, the notation,  $D_{xx}$ , refers to the size  $D$ , in mm, for which  $xx$  percent of the sample by weight passes a sieve mesh with an opening equal to  $D$ . The  $D_{10}$ , sometimes called the effective grain size, is the grain diameter for which 10 percent of the sample (by weight) is finer and is sometimes used as an estimate of effective average pore diameter. Others have used the  $D_{50}$  size. In some cases, the height of the capillary fringe is used in calculations of effective pore diameter in soil physics and for intact rock samples measurements of fracture aperture are used or when samples are not available, aperture is estimated from photos of borehole walls are used to estimate the average effective pore diameter. The following materials discuss methods of estimating effective pore diameter: Nimmo, 2013; Glover and Walker, 2009; Revil and others, 2011; Fu and others, 2020.

[Return to Exercise 10](#) ↗

[Return to where text linked to Exercise 10](#) ↗

## Exercise 11 Solution

- The assumptions of the equation are that the fluid is incompressible and Newtonian; the flow is laminar through a pipe of constant circular cross section that is substantially longer than its diameter; and there is no acceleration of fluid in the pipe.
- If  $\mu$  increases, then the gradient increases in order to drive the same mean volumetric flow rate of a more viscous fluid through the same opening. That is, the more viscous fluid presents more resistance to flow. This makes sense because a more viscous fluid is “thicker” like syrup compared to water, so the fluid does not flow as easily thus requiring more pressure to push the fluid through the pipe.
- The specific velocity is linearly proportional to the pressure gradient if the viscosity of the fluid is constant.

[Return to Exercise 11](#) ↑

[Return to where text linked to Exercise 11](#) ↑

## Exercise 12 Solution

Substituting  $64/Re$  and the equation for the Reynolds number into Equation 4 proves that this results in the Hagen-Poiseuille equation for a circular pipe.

$$\text{Reynolds Number: } Re = \frac{VD\rho}{\mu} = \frac{VD}{\nu}$$

$$\text{Equation 4: } \frac{\Delta p}{L} = f_D \frac{\rho V^2}{2D}$$

*Hint:* Remember that the radius of a circle is one half the diameter.

$$\frac{\Delta p}{L} = \frac{64\mu \rho V^2}{VD\rho 2D}$$

$$\frac{64\mu \rho V^2}{VD\rho 2D} = \frac{32\mu V}{D^2}$$

$$\frac{32\mu V}{D^2} = \frac{32\mu V}{2^2 r^2}$$

$$\frac{32\mu V}{2^2 r^2} = \frac{8\mu V}{r^2}$$

[Return to Exercise 12](#) ↑

[Return to where text linked to Exercise 12](#) ↑

## Exercise 13 Solution

It is impossible to know the exact value of  $Re_c$  for a conduit system because fully saturated dissolution features are not usually perfectly circular, smooth, or straight. However, increased roughness, curved passages and irregular conveyance shape would all reduce the  $U_R$  and  $L_R$ .

[Return to Exercise 13](#) ↑

[Return to where text linked to Exercise 13](#) ↑

## Exercise 14 Solution

- a) The hydraulic radius for image a) is

$$\frac{\text{Area}}{\text{Circumference}} = \frac{\pi r^2}{2\pi r} = \frac{r}{2} = \frac{2}{2} = 1 \text{ meter}$$

for image b) the hydraulic radius is

$$\frac{\text{Area}}{\text{Wetted perimeter}} = \frac{(3.6)(3.8) + (0.2)(3.8)}{3.6 + 2\sqrt{0.2^2 + 3.8^2}} = \frac{13.68 + 0.76}{3.6 + 2\sqrt{14.48}} = \frac{14.44}{3.6 + 7.61} = 1.29 \text{ meter}$$

- b) For image a)  $(0.005 \text{ m}^3/\text{s}) / (12.57 \text{ m}^2) = 0.000398 \text{ m/s}$

and for image b)  $(0.005 \text{ m}^3/\text{s}) / (14.44 \text{ m}^2) = 0.000346 \text{ m/s}$

- c)

$$Re = \frac{VD\rho}{\mu} = \frac{VD}{\nu}$$

For the pipe (a)  $D$  is equal to the pipe diameter of 4 m, but for the open channel (b), we would use the equation for a pipe diameter that has the same hydraulic radius  $r = 2(1.29) = 2.58$ , then  $D = 2r = 5.16 \text{ m}$

for image a)  $Re = (0.000398 \text{ m/s})(4 \text{ m}) / (10^{-6} \text{ m}^2/\text{s}) = 1600$

and for image b)  $Re = (0.000346 \text{ m/s})(5.16 \text{ m}) / (10^{-6} \text{ m}^2/\text{s}) = 1800$

- d) for image a) Most likely laminar as  $Re < 2100$

for image b) Most likely turbulent as  $Re > 500$

[Return to Exercise 14](#) ↑

[Return to where text linked to Exercise 14](#) ↑

## Exercise 15 Solution

- a) A string could be stretched across the channel in both images and a line level used to ensure the string is level. Then the depth of water measured at constant widths from the edge of each side. This could be transferred to drafting paper and used to calculate both the cross sectional area and the wetted perimeter.
- b) A tape measure could be used to measure the perimeter of the conduit cross-section for the wetted perimeter at full flow in both channels, much like the above exercise, but more measurements required, and the string stretched across the widest space.
- c) The wetted perimeter increases as the conduit fills but remains constant once full. Higher discharge must occur to completely fill the conduit. All three would increase. However, this channel is more like a circle shape.
- d) Like the above channel all three would be increasing. However, since this channel seems to have a small rectangle that is cut into the wider channel. As the water tops that first smaller downcut channel the wetted perimeter will suddenly increase and it will take much more discharge to raise the water level over this even wider channel, also the cross-sectional area divided by wetted perimeter will not change at the same rate as for the smaller channel at the lower flow.

[Return to Exercise 15](#) ↗

[Return to where text linked to Exercise 15](#) ↗

## Exercise 16 Solution

It is useful to define three types of karst porosity because there are karst aquifers of differing ages that have one, two or all three types of porosities and these zones support laminar or turbulent flow at different velocity ranges. Some carbonate layers can be confining units having no dissolution features, large fractures or joints and limited water transmitting interconnected rock matrix porosity. Other carbonate rocks have some rock matrix porosity that transmits water and large conduits with no interconnected macropores. Others have all three types of porosity that are shown in Figure 16. Most carbonate rock matrices have hydraulic conductivity that ranges from very low values to large values on the order of 0.01 to 10 m/d and rarely have turbulent flow under natural conditions. For the permeable macro porosity layers of interconnected macropores (Figure 16b), turbulent flow is possible, but the onset occurs at very small Reynolds numbers (1 to 60). Whereas for the large submerged fully flowing dissolution features (Figure 16c) laminar flow occurs with lower critical Reynolds numbers up to 2,000.

[Return to Exercise 16](#) ↗

[Return to where text linked to Exercise 16](#) ↗



## Exercise 17 Solution

Using an internet search, learn that a hydrograph is a chart of the time series of water level or flow (that is, water level in a well, streamflow, stream gage height, spring flow). A chemograph is a chart of the time series of changing water chemistry (that is, groundwater chemistry, spring or stream water chemistry). Often a time series of discharge is used in conjunction a times series of water chemistry to assess diffuse versus rapid flow of water to a spring, or to estimate the groundwater discharge component of streamflow.

[Return to Exercise 17](#) ↗

[Return to where text linked to Exercise 17](#) ↗

## Exercise 18 Solution

The answer varies depending on the items of interest to each individual reader. Information can be found at [Environmental Geophysics page of the USEPA](#) ↗. The glossary is an excellent source of term definitions.

[Return to Exercise 18](#) ↗

[Return to where text linked to Exercise 18](#) ↗

## Exercise 19 Solution

Chloride is more conservative. Neither plot is a perfect bell curve in time, which indicates mixing of tagged groundwater with other water along the path. The normalized chloride graph is more symmetric and closer to a bell-shaped curve. It is likely that background chloride is present, which is why the chloride graphs from both springs never show zero values. The dye doesn't have a symmetric normalized curve and has what is called a long tail before returning to zero. This indicates the dye is being delayed in the system, perhaps because it is temporarily sorbed to the surface of aquifer minerals or stored in dead-end pores, then released with passing groundwater and thus concentration declines slower than the rise in concentration. Neither the dye nor the salt is perfectly conservative, but the normalized chloride curve is always greater than zero because some dissolved solids including chloride were in the system before salt is added, whereas the normalized dye curves have a starting value of zero. The normalized chloride curves at both springs are more symmetric than the normalized dye curves, which indicates the chloride is a more conservative tracer (that is, it is not getting sorbed onto aquifer minerals or being delayed by other processes).

[Return to Exercise 19](#) ↗

[Return to where text linked to Exercise 19](#) ↗

## Exercise 20 Solution

“A [spectrofluorometer](#)<sup>↗</sup> is an instrument which takes advantage of fluorescent properties of some compounds in order to provide information regarding their concentration and chemical environment (that is, redox [oxidation-reduction] state and acidity/basicity) in a sample. A certain excitation wavelength is selected, and the emission is observed either at a single wavelength, or a scan is performed to record the intensity versus wavelength, also called an emission spectrum. The instrument is used in fluorescence spectroscopy.”

[Return to Exercise 20](#)<sup>↗</sup>

[Return to where text linked to Exercise 20](#)<sup>↗</sup>

## Exercise 21 Solution

Using an internet search, it was determined that all the alkali metals have one electron in their outermost shell and all the alkaline earth metals have two outer electrons. Alkali metals tend to form singly charged positive ions while alkaline earth metals tend to form cations with a +2 charge. To achieve the inert noble gas configuration, alkali metals need to lose one electron (valence is “one”), whereas alkaline earth metals need to lose two electrons (valence is “two”). Thus, alkali metals tend to form singly charged positive ions while alkaline earth metals tend to form cations with a +2 charge. If this is confusing, it will be useful to review an inorganic chemistry textbook (or other source of basic inorganic chemistry information) and to learn how the periodic table of elements is organized.

[Return to Exercise 21](#)<sup>↗</sup>

[Return to where text linked to Exercise 21](#)<sup>↗</sup>

## Exercise 22 Solution

This list is only a sample of activities that might degrade water quality if conducted on the outcrop of a karst aquifer.

1. Any activity that involves application of pesticides or fertilizer, such as golf courses, agriculture, or urban lawn maintenance.
2. Industrial activities that involve the use of chemicals, especially liquids, when spills may occur.
3. Poorly maintained tanks, such as in a tank farm or gasoline station.
4. Activities that store waste liquids in lined ponds, such as Confined Animal Feeding Operations (pig or chicken farms for example).
5. Neighborhoods built with septic tanks for each residence rather than a sewer system feeding a wastewater treatment plant.

[Return to Exercise 22](#)<sup>↗</sup>

[Return to where text linked to Exercise 22](#)<sup>↗</sup>

## 14 Notation

$A$	cross-sectional area perpendicular to flow ( $L^2$ )
$\alpha$	compressibility of the aquifer skeleton ( $T^2LM^{-1}$ )
$\beta$	compressibility of water ( $T^2LM^{-1}$ )
$C$	concentration in the stream water ( $ML^{-3}$ )
$C_g$	concentration in 100% groundwater ( $ML^{-3}$ )
$C_r$	concentration in 100% surface runoff water ( $ML^{-3}$ )
$D$	in Equation 2, mean pore size diameter for porous media or the pipe diameter ( $L$ )
$D$	in Equation 4, hydraulic diameter of the pipe ( $L$ ) (for circular pipe it is the pipe diameter, but for a non-circular pipe $D = 2$ times the square root of $(A/\pi)$ ; where $A$ is the cross-sectional area)
$\Delta h$	measured head difference ( $L$ )
$\Delta l$	length over which the head difference is measured ( $L$ )
$\Delta p$	pressure difference between two ends of the pipe ( $ML^{-1}T^{-2}$ )
$f_D$	Darcy friction factor (dimensionless)
$g$	local acceleration due to gravity or gravity constant ( $LT^{-2}$ )
$K$	hydraulic conductivity of the porous medium ( $LT^{-1}$ )
$L$	pipe length ( $L$ )
$\mu$	absolute or dynamic viscosity of water ( $ML^{-1}T^{-1}$ )
$n$	porosity (dimensionless)
$\nu$	kinematic viscosity of water ( $L^2T^{-1}$ )
$Q$	volumetric discharge ( $L^3T^{-1}$ )
$q$	specific discharge ( $LT^{-1}$ )
$Q_g$	groundwater portion of the total discharge of the stream ( $L^3T^{-1}$ )
$Q_r$	surface runoff portion of the total discharge of the stream ( $L^3T^{-1}$ )
$r$	pipe radius ( $L$ )
$Re$	Reynolds number (dimensionless)
$\rho$	density of water ( $ML^{-3}$ )
$S_s$	specific storage ( $L^{-1}$ )
$V$	$Q/A$ and is the mean flow velocity ( $LT^{-1}$ ) across a cross sectional area (also called Darcy velocity), which is equal to the volumetric flow, $Q$ ( $L^3T^{-1}$ ), divided by the cross-sectional area perpendicular to the direction of flow, $A$ ( $L^2$ )

## 15 About the Authors



**Eve Louise Kuniansky** pursued a dual degree program graduating with a degree in Physics from Franklin and Marshall College in 1978; a Bachelor in Civil Engineering with highest honors from Georgia Institute of Technology, 1981; and Master of Science in Civil Engineering from Georgia Institute of Technology, specializing in Hydrology/Hydraulics, 1982. In January 1983, she began a career with the United States Geological Survey (USGS) and gained experience in surface-water modeling, project management, borehole geophysics, geologic mapping, field data collection, groundwater flow and transport simulation, Geographic Information Systems, karst hydrology, and aquifer hydraulics. Eve has been interested in karst aquifers since 1986 when she encountered the Edwards-Trinity aquifer system and coordinated the USGS Karst Interest Group (2000-2017). In 1998, she was promoted to Southeastern Region Groundwater Specialist providing technical assistance to groundwater projects throughout the southeastern USA, Puerto Rico, and the Virgin Islands. Because of her expertise she was frequently selected for short term international assignments by the USGS International Water Resources Branch (China, Israel, Cyprus, Ethiopia, Kenya, and South Africa). One of the last courses she coordinated and helped teach was the first ever USGS GW2227, Advanced Groundwater Field Techniques in Karst, in November 2017 at the Savoy Experimental Watershed on the University of Arkansas campus. After 35 years with the USGS, she retired December 2017, but continued to work part time on the USGS Floridan Aquifer System Groundwater Availability Study (another major karst aquifer). She is currently in emeritus status with USGS. This book is part of her USGS emeritus work along with continued work with the USGS Karst Interest Group.



**Charles J. (Chuck) Taylor** is a groundwater hydrologist and heads the Water Resources Section of the Kentucky Geological Survey (KGS), a research institute of the University of Kentucky. Chuck joined the KGS after a 21-year career with the United States Geological Survey where he conducted a variety of karst and other hydrogeological studies in Kentucky, Indiana, Alabama, Tennessee, and other states. In his present position, Chuck supervises the research projects and data-collection activities of the Water Resources Section, including the Kentucky Groundwater Data Repository and the Kentucky Groundwater Observation Network. His main research interests are characterization of karst and fractured-sedimentary aquifers, water-tracer tests, groundwater monitoring, low-temperature geochemistry, and groundwater and

surface water interaction. He holds undergraduate and graduate degrees in Geology from the University of Kentucky.



**John H. Williams** has a Bachelor of Arts in Geology from Colgate University, and a Master of Science in Geosciences from Pennsylvania State University. John currently is the Groundwater Specialist for the United States Geological Survey (USGS) Water Science Center in New York and is responsible for technical oversight of the Survey's groundwater program in the State. John has provided technical assistance to the United States Environmental Protection Agency, Army Corp of Engineers, and United States Nuclear Regulatory Commission on investigations of contaminated fractured-bedrock aquifers. He has worked with the Geological Survey of Canada in the investigation of transboundary aquifers in New York and Quebec. In addition, John is an integral part of the geophysical training and technology transfer program of the Hydrogeophysics Branch of the Earth System Processes Division of the USGS. He has provided support in borehole geophysics to USGS offices throughout the USA and in the United Arab Emirates. He recently co-taught a borehole geophysics workshop in northern Iraq for the Iraqi Central and Kurdish Regional Governments that was supported by the United States Department of Defense. Over the past several years, John has made presentations on water-resource issues related to shale-gas development to the United States Department of Energy, United States Environmental Protection Agency, National Ground Water Association, North American Energy Marketers Association, Empire State Water Well Drillers Association, New York State Department of Environmental Conservation, Pennsylvania Department of Environmental Protection, professional associations, universities, and environmental groups. He also has provided testimony to the New York State Assembly and New York City Council on these issues.



**Fred Paillet** is Adjunct Professor of Geosciences at the University of Arkansas and Emeritus Research Scientist with the United States Geological Survey (USGS). He served as Chief of the USGS Borehole Geophysics Research Project in Denver from 1983 until his retirement in 2002. Since then, he has had temporary appointments at the University of Maine (Orono), The University of Rennes (France) and the University of Queensland (Australia). His work in karst aquifer characterization includes studies in Minnesota, Wisconsin, Illinois, Texas, Tennessee, and Arizona in the USA, and in Egypt and Kuwait overseas. During this time, he has written numerical codes for the analysis of geophysical well logs, including applications for



acoustic waveform, high-resolution flowmeter, and fluid-column resistivity measurements in both single-hole and cross-borehole experiments.

Please consider signing up to the Groundwater Project mailing list and stay informed about new book releases, events and ways to participate in the Groundwater Project. When you sign up to our email list it helps us build a global groundwater community. [Sign-up](#)<sup>↗</sup>.



# Modifications to Original Release

## Changes included in Modifying from Original Version to Version 2 and Version 3

Page numbers refer to page numbers in the original pdf where the introduction section began with page number 12. This version begins the Introduction with page number 1.

### **General changes:**

Several formatting changes were made such as: adjustment of margin width in some sections; removal of blank spaces and lines; small adjustments of the width of some captions, figures, and tables; insertion of metric equivalent units in a few places; change of % to percent, capitalization of some words, correction of minor typographical errors, and the addition of title, author and copyright pages to the table of contents.

pages 117 through 147, corrected figure numbers and their cross references from the text

### **Specific changes:**

page iii, changed number of pages from 225 to 216

page v, moved Preface to follow Foreword

page xii, added Acknowledgments

page 12, page numbering revised to begin the Introduction as page number 1

page 100, changed order of dimensions for compressibility to be consistent with other Groundwater Project books

page 110, changed  $Q_g$  = surface runoff portion to  $Q_r$  = surface runoff portion to

page 157, added dimensions to variables in Exercise 9 Part 2

pages 158 159, 203, and 210, removed equation numbers from equations 11, 12, 13 and 14 to be consistent with other Groundwater Project books that do not number equations in exercises and glossary

page 159, added dimensions to variables in Exercise 11

page 201, replaced Figure Glossary-1 with a figure that better illustrates the nature of the capillary fringe

A

page 222, added a Notation section after Exercise Solutions

## Changes from Version 3 to Version 4

### General changes:

Changed all occurrences of chemo-graph and chemo graph to chemograph.

### Specific changes:

page ii, added Version 4

page iii, updated copyright format and enhanced copyright information

page iii, citation, implemented the link to the book webpage

page 21, 5th line from bottom. changed “Section of 4.1” to “Section 4.1”

page 24, line 11, changed “Vacher and Mylorie, 2002,” to “Vacher and Mylorie (2002)”

page 25, added closing parenthesis on 2nd line of caption to Figure 15, i.e., (2008)

page 28, last line, removed apostrophe after Milanovic

page 53, changed  $\Delta L$  to  $\Delta l$  in Figure 33 and in line 3 of the figure caption

page 53, in parameter list, “A” changed to italic font

page 55, paragraph 1, line 6. replaced Newtons with N

page 56, in parameter list, second  $Q$  in the definition of  $V$  changed to italic font

page 56, paragraph after parameter list, capitalized first e of exercise 6, Exercise 6

page 57, Figure 36 caption, line 4, Figure 35b changed to Figure 34b

page 60, line 2, subscript of  $f_D$  changed to italic font,  $f_D$

page 84, replaced Figure 52 with a version that has separators between the three photos

page 89, changed  $n$  in equation 6 to italic font,  $n$

page 89, Table 7, second to last row,  $3.3 * 10^{-10}$  changed to  $3.3 \times 10^{-10}$

page 91, replaced Figure 55 with a version that has sharper text

page 113, replaced Figure 67 with a version that has sharper text and color to clarify features

page 142, corrected the link for "Click here for solution to Exercise 4"

page 143, 1st paragraph, variables  $K$  and  $z$  changed to italic font

page 146,  $K$  in first column of table at the bottom of page changed to italic

page 148, paragraph after parameter definitions. "i.e.," changed from italic to roman font

page 149. Reynolds number change from  $R_e$  to  $Re$

page 190, Carbonates definition, line 5, added an opening parenthesis before  $\text{CaMg}(\text{CO}_3)_2$

page 192, Hydraulic Conductivity definition, explanation of variable  $A$ , added "area" after "cross-sectional"

page 201, Exercise 5 solution, the units  $m$  and  $d$  changed from italic to roman font

page 203,  $K$  in first column of table at the bottom of page changed to italic

page 206, line 13, subscripted  $xx$  of  $D_{xx}$ ,  $D_{xx}$

page 207, Exercise 12 solution, removed subscript font from  $R_e$ ,  $Re$

page 208, line 1m, changed subscript  $c$  of  $Re_c$  to italic,  $Re_c$

page 208, 2nd equation, added a “)” after the first 3.8, removed  $x$ ’s that represented multiplication and used parentheses where needed, with following items adjusted (3.6)(3.8), (0.2)(3.8), 2 before the square root

page 212, parameter  $A$  (cross-sectional area) changed to italic, second occurrence of  $\Delta p$  removed and  $p$  given italic font, The second  $Q_g$  changed to  $Q_r$ , deleted definition of  $\rho_w$